Pulsed plasma discharge for CVD of carbon thin films and atmospheric pressure plasma jet

by

Md Abdullah Al Mamun

Student ID Number: 1198005

A dissertation submitted to the
Engineering Course, Department of Engineering
Graduate School of Engineering
Kochi University of Technology
Kochi, Japan

in partial fulfilment of the requirements for the degree of

Doctor of Engineering

Assessment committee:

Supervisor: Akimitsu Hatta
Co-supervisor: Hiroshi Furuta
Co-supervisor: Hisao Makino
Committee Member: Masayoshi Tachibana
Committee Member: Mamoru Furuta

September 2018

(This page is intentionally left blank)

Abstract

Plasma technologies attract great attention owing to fast growing interests in variety of plasma-based applications in research and industry with consideration for the sustainable development of humankind. In this work, systematic research and development in designing novel pulsed power generators for energy efficient pulsed plasma discharge methods at both low-pressure and atmospheric-pressure have been carried out. The main purpose of this study is to design novel pulsed power generator circuits with high energy conversion efficiency and wide range of controllable parameters with examining how they perform in actual application to pulsed DC plasma chemical vapour deposition (CVD) of carbon thin films and to atmospheric-pressure plasma jet (APPJ).

In the first part of research, low-pressure pulsed plasma discharge for the synthesis of carbon thin films was investigated. A pulsed DC plasma chemical vapour deposition (CVD) system with a compact vacuum chamber using a simple configured pulsed DC power supply was developed. The first pulsed DC power supply was a conventional half-bridge circuit consisting of a couple of metal-oxide-semiconductor field-effect transistors (MOSFETs) for switching a high voltage direct current (HVDC) like as a push-pull amplifier. The pulsed DC discharge was examined with variation of operation parameters as well as source gas materials. Diamond like carbon (DLC) films, as an example of carbon thin films, were deposited on silicon (Si) substrates from acetylene (C_2H_2) or carbon-monoxide (CO) at two distinct temperatures. The fabricated films were characterized by Raman spectroscopy, FTIR spectroscopy, and scanning electron microscopy (SEM). The results reveal that the films prepared from CO gas exhibited soft conductive DLCs with a large number of graphite like structures whereas mostly insulating hydrogenated amorphous carbon DLCs were obtained from C_2H_2 gas. The deposition rate from CO was lower than from C_2H_2 due to etching by oxygen produced from the source gas. As the substrate temperature increased, progressive graphitization was incorporated to the films deposited from both gases. By using the developed pulsed DC plasma CVD system, the energy efficiency for CVD as the ratio of growth volume to energy consumption was dramatically improved with some distinctive differences in film properties as compared to our previous RF plasma CVD. While the results showed many advantageous features of pulsed DC plasma CVD for replacing conventional RF plasma CVD, it was confirmed that the push-pull operation for the capacitive load such as an electrode caused loss of energy at every pulsed discharge with resulting in limitation of operation frequency.

A novel pulsed-DC generator for capacitively coupled plasma (CCP) discharge was developed to improve energy conversion efficiency and operation frequency for further

advanced pulsed plasma discharge processes. The circuit design, the system assembly, and the operating tests of the high-frequency and HV pulsed DC generator (PDG) for CCP discharge have been investigated. For such the capacitive loads, it is challenging to obtain sharp rectangular pulses with fast rising and falling edges, requiring intense current for quick charging and discharging. In addition, the loss of energy usually occurs from the capacitive loads at every termination of pulse. The requirement of intense current and loss of energy generally limit the pulse operation frequency. To overcome these constraints, a new type of PDG consisting of a pair of half- resonant converters and a constant current-controller circuit connected with high-voltage solid-state power switches was developed that could deliver almost rectangular high voltage pulses with fast rising and falling edges for capacitively coupled plasma discharge. A prototype of the PDG was assembled to modulate from a HVDC input into a pulsed HVDC output, following an input pulse signal and a set current level. The pulse rise time and fall time are less than 500 ns and 800 ns, respectively, and the minimum pulse width is 1 μs. The maximum voltage for a negative pulse is 1000 V, and the maximum repetition frequency is 500 kHz. During the pulse on time, the plasma discharge current is controlled steadily at the set value. The half-resonant converters in the PDG perform recovery of the remaining energy from the capacitive load at every termination of pulse discharge. The PDG performed with high energy efficiency of 85% from the HVDC input to the pulsed DC output at a repetition rate of 1 kHz, and with stable plasma operation in various discharge conditions. The results suggest that the developed PDG can be considered to be more efficient for plasma processing by CCP.

To examine the performance of novel pulsed-DC discharge system consisting of the developed PDG and the custom-made compact vacuum chamber, hydrogenated amorphous carbon (a-C:H) films were deposited on silicon (Si) substrates using a high-repetition microsecond-pulsed DC plasma chemical vapor deposition (CVD) from acetylene (C_2H_2) at a gas pressure of 15 Pa. The plasma discharge characteristics, hydrocarbon species, and the microstructure of the resulting films were examined at various pulse repetition rates from 50 to 400 kHz and a fixed duty cycle of 50%. The optical emission spectra confirmed the increase in electron excitation energy from 1.09 to 1.82 eV and the decrease in the intensity ratio of CH/C_2 from 1.04 to 0.75 with increasing pulse frequency, indicating the enhanced electron impact dissociation of C_2H_2 gas. With increasing pulse frequency, the deposition rate gradually increased, reaching a maximum rate of 60 nm/min at 200 kHz, after which a progressive decrease was noted, whereas the deposition area was almost uniform for all the prepared films. Clear trends of increasing sp^3 content (amorphization) and decreasing hydrogen (H) content in the films were observed as the pulse repetition rate increased, while most of the hydrogen atoms bonded to carbon atoms by sp^3 hybridization rather than by sp^2 hybridization.

For further evaluation of the novel pulsed-DC discharge system, argon (Ar) gas discharge experiments were performed under a variety of discharge conditions, and plasma conditions were evaluated using optical emission spectroscopy (OES). The developed system can perform glow discharge by employing nearly rectangular, unipolar, and high-voltage negative pulses with a wide variation of voltage amplitudes and a set discharge current, pulse repetition rate, and duty cycle. Plasma conditions could also be tuned by varying the pulse parameters. Diamond-like carbon (DLC) films were deposited on silicon (Si) substrates from acetylene (C_2H_2) with a variation of gas pressure, applied voltage, and discharge current. The Raman spectra confirmed the DLC properties of the deposited carbon films. All DLC films demonstrated highly insulating properties, and the amorphization increased with a decrease in gas pressure, voltage, and discharge current. With intention of applying the develop system to growth of graphene, ultrathin pyrolytic carbon (PyC) films have been produced on glass substrates using nano-thickness metal catalysts from C_2H_2. While graphene growth has not been confirmed at the examined conditions, the ultrathin PyC films exhibited conductive and semitransparent properties. These results revealed that the developed pulsed-DC discharge system for plasma CVD is applicable for the synthesis of insulating hard DLC coating as well as soft-conducting ultrathin carbon thin films.

The experimental results of the first part are summarized as follows. The original developed pulsed DC plasma CVD system with a compact vacuum chamber and a simple half-bridge pulsed power supply was advantageous due to energy-efficient deposition. However, the original system had the limitation of the modulation of pulse parameters such as high repetition rate, fast rise and fall time, and wide control of pulse width. A novel pulsed plasma discharge system was successfully developed which was more versatile and favorable for the operation of high frequency with fast rising and falling edges. Plasma discharge characteristics, the deposition of films and its properties can be widely modified by the developed novel system, which may open new possibilities in etching, ion implanting, and sputtering applications for the material processing.

In the second part of research, atmospheric-pressure pulsed plasma discharge for plasma jet was investigated. Atmospheric-pressure plasma jet (APPJ) is a kind of small dielectric barrier discharge (DBD) device that can be run under atmospheric-pressure in the ambient air also with various gases and it is technically simple and low-cost process because no vacuum systems is required. In the APPJ system, the power supply is considered one of the significant components, as it plays a key role on the discharge characteristics of the APPJ. Among various types of power supplies, pulsed generator is considered as it can deliver high instantaneous power with respect to low average power, offer fast rise time and high repetition rate which are advantageous to control the production of high electron density and more active plasma species.

For operation of APPJ, alternative current (AC) HV power sources of sinusoidal wave at lower frequency than a several 10s of kHz are widely used because it is easy to boost the voltage by using a transformer. In most cases, the APPJ is operated at a fixed frequency and a fixed voltage. For research and development of APPJ technology, however, it is important to examine the effects of operation frequency and waveforms on the plasma properties and processed results. For operation of DBD, the voltage increasing rate, decreasing rate, pulse width and pulse interval are crucial parameters. For control of APPJ process induced in gas jet, the operation frequency is also an important parameter. In the case of conventional sinusoidal wave ACHV, with the variation of operation frequency and peak voltage, the voltage increasing rate, decreasing rate, pulse width and pulse intervals automatically varies. Because of the sinusoidal property, it is impossible to control the important discharge parameters intentionally. For advancing research on APPJ, it is necessary to develop a novel pulse power source which enables independent control of frequency, voltage, and waveforms.

A high-voltage high-frequency impulse generator (IG) for atmospheric-pressure plasma jet (APPJ) was developed using dual resonance pulse transformer (DRPT) and solid-state switches. The DRPT performs not only to boost the voltage from the primary circuit to the secondary circuit but to recover the energy from the secondary circuit to the primary circuit. At the appropriate condition, the energy conversion efficiency is dramatically improved and it enables high frequency operation with a same pulse waveform. It has been revealed, in this work, that the conditions for total transfer of energy (neglecting dissipation) from primary capacitor to secondary capacitor are: the resonant frequency of the primary circuit for open secondary circuit should be equal to the resonant frequency of secondary circuit for open primary, and the transformer coupling coefficient should be 0.6. Under these conditions, the two normal modes of frequencies of the coupled primary-secondary circuits have in the ratio of 2:1. In the optimized DRPT, the high voltage is not proportional to the number of turns ratio as in an ordinary transformer but formed by resonance. If the capacitance of the secondary circuit is very small compared to the primary capacitor and the inductance of secondary coil is very large compared to the primary coil, the primary voltage is stepped up to a high value in secondary.

The developed generator is compact and has convenient control for voltage and frequency selection. It can deliver high-voltage impulses (peak to peak) up to 11 kV from a DC voltage of 500 V. The pulse operating frequency range is 0.5-100 kHz. The fixed pulsed width is approximately 4 μs with the pulse rise-time and fall-time are almost 2 μs. The DRPT-IG is tested by producing a stable room-temperature atmospheric pressure plasma plume using helium (He) gas flow in a plasma jet device designed as cylindrical configuration of DBD with single electrode configuration. It is probable that this work may stimulate the further development of pulsed generators for atmospheric-plasma discharge processes.

Atmospheric-pressure plasma jets designed as cylindrical configuration of DBD was operated using the developed DRPT-IG and the plasma was examined by means of electrical and optical characteristics using He as working gas. The power source is connected to two different types of single-electrode configurations such as strip-electrode and wire-electrode for the production of plasma jet with various experimental conditions. Wire-electrode configuration shows a strong impact on plasma jet operation with the variation of frequency at a fixed voltage and gas flow rate rather than strip-electrode. The optical spectral analysis for wire-electrode APPJ confirmed the existence of active species such as NO, N_2, N_2^+, He, O and OH in the plasma plume. The spectral intensities of these species increase with the pulse frequency and become most dominant at 100 kHz. This results reveal that the high frequency operation of plasma jet by the developed DRPT-IG is preferable for generation of more reactive species.

Reactive oxygen and nitrogen species (RONS) in plasma-activated water (PAW) are considered to be the key elements that can destroy bacteria and cancer cells. Therefore, it is significant to control the production of RONS in PAW for achieving preferred effects in particular biological or medical applications. PAW was produced from deionized water (DIW) employing plasma treatment by the developed pulsed-APPJ system and UV absorption spectroscopy method was applied to evaluate the RONS compositions and their concentrations in PAW. In this work, mainly the dependency of pulse operating frequency and polarity on plasma jet characteristics and RONS production in PAW were investigated. A higher frequency operation of pulse-plasma jet enhances the plasma density as well as the plasma-water interaction, which introduces to produce higher concentration of RONS and dissolved O_2 in PAW. The concentration ratio of reactive oxygen species (ROS) and reactive nitrogen species (RNS) also varies with the pulse operating frequency. In contrast, the positive pulse operated plasma jet shows the cylindrical shape and intense appearance, whereas negative pulse operated plasma jet displays conical and less intense. The plasma jet driven under positive pulse introduces higher electric field, leads to a higher speed of ionization rate, generates a higher density of excited species in plasma, accordingly a higher concentration of RONS production in PAW than that of negative pulse.

These results reveal that the plasma jet characteristics and the production of RONS can be significantly controlled by varying both pulse frequency as well as polarity during the operation of the developed pulsed-APPJ system. Hence, in the future, the developed pulsed-APPJ system can offer an effective and low cost method to control of RONS composition for specific biomedical applications.

Table of contents

Abstract……. ..... **i**

Table of contents… ..... **vi**

List of figures…… ..... **ix**

List of tables…….. ..... **xiv**

Abbreviations…… ..... **xv**

Disclaimer……. ..... **xvii**

Acknowledgements ..... **xix**

Chapter 1. Introduction **1-6**

1.1. Background 1

1.2. Motivation and research issue 1

1.3. Research objectives 3

1.4. Outline of the thesis 4

References 5

Chapter 2. Research background **7-29**

2.1. Plasma 7

2.1.1. What is plasma? 7

2.1.2. Generation of plasma by electric gas discharge 8

2.1.3. Classification of plasma 10

2.2. Pulsed power 12

2.2.1. What is pulsed power? 12

2.2.2. Pattern of pulsed power 13

2.2.3. Pulsed power supply topologies 14

2.2.4. Power electronics in pulsed power generation 15

2.3. General processes in pulsed plasma discharge 17

2.4. Carbon materials 19

2.5. Diamond-like carbon 21

2.5.1. Introduction 21

2.5.2. Classifications of DLC 22

2.5.3. Synthesis of DLC films 23

2.5.3.1. Growth mechanism 24

2.5.3.2. Deposition methods of DLC 24

References 27

Research Part-I: Pulsed plasma discharge for low-pressure synthesis of carbon thin films…….....……30-110

Chapter 3. Pulsed DC Plasma CVD system for the synthesis of DLC films 30-50

3.1. Introduction 30

3.2. Objective.....31

3.3. Experimental procedures 32

3.3.1. Development of pulsed DC plasma CVD system 32

3.3.2. Substrate preparation, films deposition and characterization techniques.....37

3.4. Results and discussions 39

3.4.1. Gas discharge characteristics.....39

3.4.2. Deposited films properties.....40

3.4.3. Comparison of films properties.....46

3.5. Conclusion.....48

References.....48

Chapter 4. Novel pulsed DC generator for capacitively coupled plasma discharge ..51-73

4.1. Introduction 51

4.2. Objective.....52

4.3. Design and construction of the pulsed DC generator 53

4.3.1. Design architecture.....53

4.3.2. Topology of LC resonant converter.....54

4.3.3. Circuit layout and description.....56

4.3.4. Control system and operation modes.....59

4.4. Experimental setup.....63

4.5. Results and discussion.....64

4.6. Conclusion.....71

References.....71

Chapter 5. Deposition and characterization of a-C:H films using a high-repetitive microsecond -pulsed DC capacitive-couple plasma CVD system.....74-92

5.1. Introduction 74

5.2. Objective.....76

5.3. Experimental and methods 76

5.4. Results and discussion.....78

5.4.1. Discharge Characteristics.....78

5.4.2. Characterization of a-C:H films 81

5.5. Conclusion.....89

References.....89

Chapter 6. Investigation of pulsed plasma characteristics and deposition of carbon thin films with a variation of discharge conditions.....93-110
6.1. Introduction 93
6.2. Objective.....94
6.3. Experimental setup 94
6.4. Gas discharge characteristics.....96
6.5. Optical emission spectral analysis of plasma 97
6.6. Carbon film deposition 101
6.6.1. DLC films.....102
6.6.2. Ultrathin PyC films 104
6.7. Conclusion.....106
References.....107

Research Part-II: Pulsed plasma discharge for atmospheric-pressure plasma jet ..111-153
Chapter 7. An impulse generator for atmospheric-pressure plasma jet (APPJ).....111-129
7.1. Introduction 111
7.2. Objective.....112
7.3. Dual resonance pulse transformer (DRPT) principles.....112
7.4. Design and construction of the DRPT impulse-generator (IG).....116
7.4.1. Design consideration 116
7.4.2. Design layout and circuit diagram.....117
7.4.3. Construction of the DRPT 120
7.4.4. Control Module and operation modes 121
7.5. Test of impulse generator 125
7.6 Conclusion.....127
References.....127
Chapter 8. Investigation of pulsed plasma discharge characteristics for APPJ.....130-153
8.1. Introduction 130
8.2. Objective.....131
8.3. Experimental setup 131
8.4. Experimental results and discussions 132
8.4.1. Discharge characteristics.....132
8.4.2. Spectral characteristics 138
8.4.3. Production of RONS in plasma-activated water (PAW) 140
8.4.4. Typical observations - APPJ operated by positive and negative pulses.....146
8.5. Conclusion.....150
References.....151
Chapter 9. Summary 154-157

List of Figures

Figure 2.1. Generation of plasma from a solid material with increase of temperature/energy.

Figure 2.2. Typical application areas of plasma.

Figure 2.3. (a) A schematic of electric gas discharge (b) The current-voltage characteristic of electric gas discharge. The values on the current scale are only illustrative, the exact values depend on the details of the discharge configuration.

Figure 2.4. (a) Low-pressure plasma discharge system (b) Atmospheric-pressure plasma discharge system (c) Paschen graph for the evaluation of breakdown voltage at low and high pressure.

Figure 2.5. Power delivered to load by continuous and pulse power at identical energy content.

Figure 2.6. Typical current-voltage waveforms of basic two patterns of pulsed power (a) pulsed-DC (b) high-impulse.

Figure 2.7. Typical pulsed power topologies (a) Marx generator (MG) (b) magnetic pulse compressor (MPC) (c) pulse forming network (PFN) (d) pulse transformer (PT).

Figure 2.8. Current/Voltage/switching frequency domains of the main power electronics switches.

Figure 2.9. Scenario of (a) hard switching and (b) soft/zero crossing switching.

Figure 2.10. (a) Regime of processes in pulsed-DC plasma discharge (b) Advantageous processes of pulsed-DC discharge in the synthesis of materials over continuous discharge.

Figure 2.11. Allotropes of carbon: (a) diamond, (b) graphite, (c) graphene, (d) fullerene, (e) carbon nanotube, and amorphous carbon.

Figure 2.12. Ternary phase diagram of amorphous carbons. The three corners correspond to diamond, graphite, and hydrocarbons, respectively.

Figure 2.13. Schematic diagram of a subplantation process; direct penetration and relaxation mechanism of a densified region.

Figure 2.14. Schematics of various deposition systems for DLC.

Figure 3.1. Picture of the developed pulsed DC plasma CVD system

Figure 3.2. Schematic view of developed pulsed DC plasma CVD system.

Figure 3.3. A view of substrate heater arrangement.

Figure 3.4. (a) Detail circuit diagram (b) image of the Half-Bridge Pulsed DC power supply.

Figure 3.5. Schematic drawing for the pulsed DC power supply.

Figure 3.6. Timing sequence of the pulsed DC power supply.

Figure 3.7. (a) Top view of electrode (b) Deposited film of entire deposition window (c) Arrangement of Si substrate and dummy substrate.

Figure 3.8. Illustration of Si substrate cleaning by Ar Plasma.

Figure 3.9. Gas discharge experiment (a) simplified schematic (b) discharge mechanism (c) discharge current and voltage waveforms at various working pressure of Ar gas (d) glow discharge characteristics.

Figure 3.10. Photographs of typical pulsed plasma discharges of Ar, C_2H_2 and CO gas.

Figure 3.11. Photographs for deposited DLC films from C_2H_2 (a) and CO (b) at room temperature.

Figure 3.12. Raman spectra for DLC films deposited from (a) C_2H_2 (samples 1 and 3) and (b) CO (samples 2 and 4).

Figure 3.13. Peak analysis on the Raman spectrum for sample.

Figure 3.14. Plots of (a) G peak position, (b) FWHM of the G peak and (c) intensity ratio of the D and G peaks (I_D/I_G) as a function of substrate temperature.

Figure 3.15. FTIR spectra for DLC films deposited from C_2H_2 (sample 1) and CO (sample 2) at ambient temperature (25 ^{0}C).

Figure 3.16. SEM cross section micrographs of the interface between Si substrate and DLC films, (a) sample 1 (deposited from C_2H_2) and (b) sample 2 (deposited from CO).

Figure 3.17. Comparison of energy consumption for a unit deposition of DLC film between our conventional RF plasma CVD system and developed pulsed DC plasma CVD.

Figure 3.18. Evaluation of films properties prepared from RF and pulsed DC plasma CVD system (a) Raman Spectra (b) FT-IR spectra.

Figure 4.1. Pulsed dc plasma discharge scenario. (a) Basic scheme (b) Proposed topology (c) Expected voltage and current waveforms.

Figure 4.2(a) Circuit diagram and (b) voltage and current waveforms of a typical *LC* resonant circuit, (c) circuit diagram and (d) voltage and current waveforms of a typical *LC* half-resonant converter.

Figure 4.3 Structure diagram of the PDG.

Figure 4.4 Detail circuit diagram of PDG (a) LC resonant charging-discharging circuit with pulsed constant current controller (b) gate pulse control system.

Figure 4.5. Simplified circuit layout of the pulsed dc generator (PDG).

Figure 4.6. Block diagram of the control system with control signals.

Figure 4.7. Timing sequence of the control signals.

Figure 4.8. Operation modes of the PDG with the active circuit loop indicated as colored solid thick lines, and current as dotted lines. (a) Mode 1 (S2, S3, D1 on; S1, S4, S5, D2 off) (b) Mode 2 (S2, S3 on; S1, S4, S5, D1, D2 off) (c) Mode 3 (S4, D2 on; S1, S2, S3, S5, D1 off) (d) Mode 4 (S1, S5 on; S2, S3, S4, D1, D2 off).

Figure 4.9. (a) Experimental setup and (b) equivalent circuit of the pulsed dc CCP system.

Figure 4.10. Image of the fabricated Pulsed DC Generator (PDG).

Figure 4.11. Discharge waveforms of (a) voltage, (b) total current, and (c) plasma discharge current for Ar plasma at 5 Pa, 100 kHz, 50% duty, and 5 mA set discharge current.

Figure 4.12. Discharge voltage waveform of Ar plasma (5 Pa) at 500 kHz, 50% duty cycle.

Figure 4.13. Discharge voltage waveforms of Ar plasma (15 Pa, 20 kHz, set discharge current 20 mA) with a variation of pulse width.

Figure 4.14. Efficiency of PDG with variation of pulse frequency with and without energy recovery operation for each pulse.

Figure 4.15. Pulse rising edge for a CCP load by the improved PDG and the half-bridge PDG.

Figure 4.16. Efficiency of improved PDG and half-bridge PDG with variation of pulse frequency.

Figure 5.1. Schematic view of experimental setup of the pulsed DC plasma glow discharge system.

Figure 5.2. Discharge current-voltage waveforms of the deposited films (a) a typical individual pulse at 100 kHz (b) pulses of different frequency vertically placed within a time frame of 45μs.

Figure 5.3. (a) Optical emission spectra of the C_2H_2 in pulsed DC plasma CVD at different pulse frequency. Each spectrum was normalized using the CH emission intensity. (b) Electron excitation energy and intensity ratio of CH/C_2 in C_2H_2 plasma with a variation of pulse operating frequency.

Figure 5.4. (a) Deposition rate of the films as a function of pulse frequency and (b) radial profiles of thickness of the deposited films.

Figure 5.5. Raman spectra of the a-C:H films prepared at different pulse frequency where the spectra are set vertically for clarity.

Figure 5.6. Hydrogen content of the a-C:H films evaluated using the Raman spectra as a function of the pulse frequency.

Figure 5.7. Raman spectral parameters (a) G peak position (b) I(D)/I(G), and (c) FWHM of G peak all as function of pulse frequency.

Figure 5.8. Amorphization evaluation diagram of the film prepared at the highest pulse frequency (400 kHz) compared to some previous works based on Robertson's three stage model.

Figure 5.9. FT-IR spectra of the a-C:H films deposited by varying pulse frequency from 50 to 400 kHz.

Figure 5.10. An expected model of C_2H_2 electron impact dissociation and film growth at lower and higher electron excited energy.

Figure 6.1. Schematic diagram of the experimental setup for pulsed-DC discharge.

Figure 6.2. Pulsed-DC discharge with a variation of working argon (Ar) gas pressure and steady discharge current. (a) typical current-voltage waveforms (b) photographs of steady discharge current waveforms and glow plasma.

Figure 6.3. (a) Typical OES spectrum of Ar plasma obtained by pulsed-DC glow discharge at gas pressure: 40 Pa, flow rate: 100 sccm, input DC voltage: -800 V, set discharge current: 40 mA, pulse on (T_{on}): 100 μs, pulse off (T_{off}): 400 μs. (b) Expanded view of the Ar(I) 750.39 nm and 811.53 nm emission lines of spectrum in (a) employed for the evaluation of T_{exc} in this study.

Figure 6.4. Evaluation of electron excitation temperature, T_{exc} with a variation of discharge conditions such as (a) pulse off time (T_{off}) (b) pulse on time (T_{on}) (c) applied negative voltage (d) controlled discharge current (e) precursor gas pressure and (f) gas flow rate.

Figure 6.5. Deposited DLC films: (a) physical appearance of a typical DLC film (S1) and (b) Raman spectra.

Figure 6.6. Intensity ratio of D peaks to G peaks [I(D)/I(G)], FWHM of G peaks, and G peak positions for different samples.

Figure 6.7. Deposited thin carbon films. (a) Raman spectra (b) physical appearance and structure of a typical ultrathin PyC film (500 ^{0}C, 2 s).

Figure 7.1. Pulse transformer coupled capacitor charger (a) circuit diagram and (b) its equivalent circuit.

Figure 7.2. Equivalent input impedance model.

Figure 7.3. Theoretical voltage waveforms at dual resonance condition (a) primary capacitor (b) secondary capacitor.

Figure 7.4. Design considerations for DRPT-IG.

Figure 7.5. Architectural block diagram of DRPT impulse generator.

Figure 7.6. Circuit layout of the proposed impulse generator (a) detail (b) simplified.

Figure 7.7. (a) Design model of the DRPT (b) Dependence of the coupling coefficient with the variation of air gap distance.

Figure 7.8. Schematic diagram of pulse control system.

Figure 7.9. Timing diagram of control signals and expected voltage waveforms across the C1 and load.

Figure 7.10. Operation modes of the DRPT impulse generators: (a) mode 1, for the energy transfer to the load (b) mode 2, for the energy recover from the load (c) mode 3, for the off-state. Solid colored lines are the indication of active circuit loops in each mode.

Figure 7.11. Arrangement of secondary circuit to produce both positive and negative impulse

Figure 7.12. (a) Photo of the developed DRPT-IG, (b) schematic of test setup for APPJ using DRPT-IG.

Figure 7.13. APPJ operation (a) typical voltage waveforms and (b) photograph of plasma plume.

Figure 8.1. Experimental setup of atmospheric-pressure pulsed plasma jet device with APPJ load model.

Figure 8.2. Two different HV single electrode configurations of plasma jet.

Figure 8.3. Equivalent circuit diagram of the APPJ device.

Figure 8.4. Typical waveforms of applied voltage $V_{p,}$ total current I_t, displacement current I_d and plasma conduction current I_p and discharge image of the strip-electrode type APPJ.

Figure 8.5. Dependency of the peak applied voltage on the characteristics of the strip-electrode type APPJ (a) Voltage and total current waveforms, (b) DC power consumption and (c) plasma jet photos.

Figure 8.6. Dependency of the impulse frequency on the characteristics of the strip-electrode type APPJ (a) Voltage and total current waveforms, (b) DC power consumption and (c) plasma jet photos.

Figure 8.7. Dependency of the impulse frequency on the characteristics of the wire-electrode type APPJ (a) Voltage and total current waveforms, (b) DC power consumption and (c) plasma jet photos.

Figure 8.8. Optical emission spectral analysis of wire-electrode type APPJ.

Figure 8.9. Selective killing effect of cancer cells by RONS in PAW.

Figure 8.10. (a) Experimental setup of PAW, (b) photographs of plasma treatment of DIW at various frequencies, and (c) measurement of transmittance by UV absorption spectroscopy.

Figure 8.11. Method to evaluate the UV absorption spectrum of PAW.

Figure 8.12. UV absorption spectra of PAW with the variation of pulse operating frequency.

Figure 8.13. Fitting of a typical UV absorption spectrum.

Figure 8.14. Evaluated absolute concentration of the RONS in PAW with the variation of pulse operating frequency. H_2O_2 is denoted as reactive oxygen species (ROS), whereas NO_2- and NO_3- are together denoted as reactive nitrogen species (RNS).

Figure 8.15. Evaluated concentration of dissolved O_2 in PAW with the variation of frequency.

Figure 8.16. The concentration ratio of ROS and RNS with the variation of frequency.

Figure 8.17. A probable model of bulk plasma interaction with bulk liquid (water).

Figure 8.18. Schlieren image of He plasma jet interaction with DIW.

Figure 8.19. (a) Photographs of plasma jet-water medium interaction and (b) voltage waveforms under positive and negative pulse.

Figure 8.20. Probable model of APPJ discharge characteristics by (a) positive pulse and (b) negative pulse. I and II denote initial and propagation phase of the steamers, respectively.

Figure 8.21. Optical emission spectra taken near the nozzle end of APPJ operated by positive and negative pulse of 8 kV at 50 kHz. The spectra were acquired at different exposure time in both polarities and were then normalized for comparison.

Figure 8.22. The concentrations of RONS in PAW by the plasma jets operated under positive and negative pulse. The operation conditions were as voltage amplitude of 8 kV (peak-peak), pulse frequency of 50 kHz, treatment time of 5 min, and treatment distance of 10 mm respectively.

List of Tables

Table 2.1. Pulse parameters between pulsed-DC and high-impulse power.

Table 2.2. General processes take place in each regime of pulsed plasma discharge

Table 2.3. Summary of properties and applications of diamond-like carbon films.

Table 3.1. Films deposition conditions.

Table 4.1. Specification of the developed PDG.

Table 5.1. Plasma CVD conditions for deposition of a-C:H films.

Table 5.2. Main species of OES spectra in C_2H_2 plasma.

Table 6.1. Deposition Conditions of DLC Films

Table 7.1. Specification of the developed DRPT-IG.

Table 8.1. Pulse polarity-induced properties for APPJ

Abbreviations

AC – Alternating Current

a-C – Amorphous Carbon

a-C:H – Hydrogenated Amorphous Carbon

APPJ – Atmospheric Pressure Plasma Jet

CCP – Capacitively Coupled Plasma/ Capacitive-coupled plasma

CNT– Carbon Nanotube

DBD – Dielectric Barrier Discharge

DC – Direct Current

DIW- De-Ionized Water

DLC – Diamond-Like Carbon

DLCH – Diamond-Like Hydrogenated Amorphous Carbon

DRPT – Dual Resonance Pulse Transformer

FCVA – Filtered Cathodic Vacuum Arc

FE-SEM – Field Emission Scanning Electron Microscope

FNS- First Negative Band System

FT-IR – Fourier Transform Infrared

FWHM – Full Width at Half Maximum

GLCH – Graphite-Like Hydrogenated Amorphous Carbon

HV– High-Voltage

HVDC – High-Voltage Direct Current

IG – Impulse Generator

IGBT – Insulated-Gate Bipolar Transistor

MG – Marx Generator

MOSFET – Metal Oxide Semiconductor Field Effect Transistor

MPC – Magnetic Pulse Compressor

OES – Optical Emission Spectroscopy

PAW- Plasma-Activated Water

PC – Personal Computer

PDG – Pulsed DC Generator

PDPS – Pulsed DC Power Supply

PECVD – Plasma Enhanced Chemical Vapour Deposition

PFN – Pulse Forming Network

PLCH – Polymer-Like Hydrogenated Amorphous Carbon

PLD – Pulsed Laser Deposition

PT – Pulse Transformer

PWM – Pulsed Width Modulation

PyC – Pyrolytic Carbon

RF – Radio Frequency

RLC – Resistor-Inductor-Capacitor

RNS- Reactive Nitrogen Species

RONS-Reactive Oxygen and Nitrogen Species

ROS-Reactive Oxygen Species

SCR – Silicon Controlled Rectifier

SLM- Standard Liters per Minute

SPS- Second Positive Band System

SSU – Solid-State Switching Unit

ta-C – Tetrahedral Amorphous Carbon

ta-C:H – Hydrogenated Tetrahedral Amorphous Carbon

TTL – Transistor-Transistor Logic

UV– Ultra-Violate

VIS – Visible

ZCS – Zero-Current Switching

ZVS – Zero-Voltage Switching

Disclaimer

The study stated in this dissertation has not been previously submitted to meet the requirements for any award of degree. To my best knowledge and belief, the dissertation contains no materials previously published or written by other person except where due reference is applied. The passages in some chapters in this dissertation have been quoted *verbatim* from the previous publications and works which were originally written by the author, listed as following.

Journal Papers:

1) Md Abdullah Al Mamun, Hiroshi Furuta, Akimitsu Hatta, "Pulsed DC plasma CVD system for the deposition of DLC films", *Materials Today Communications, **14**, 40-46, (2017).*
2) Md Abdullah Al Mamun, Hiroshi Furuta, Akimitsu Hatta, "Novel high-frequency energy-efficient pulsed-dc generator for capacitively coupled plasma discharge", *Review of Scientific Instruments, **89,** 033506, (2018).*
3) Md Abdullah Al Mamun, Hiroshi Furuta, Akimitsu Hatta, "Preparation of a-C:H films using a microsecond pulsed DC capacitive-coupled plasma CVD system operated at high frequency up to 400 kHz", *Japanese Journal of Applied Physics, **57**, 06JF02, (2018).*
4) Md Abdullah Al Mamun, Hiroshi Furuta, Akimitsu Hatta, "Pulsed-DC Discharge for Plasma CVD of Carbon Thin Films", *IEEE Transactions on Plasma Science, **46,** (2018) (Early access: DOI:10.1109/TPS.2018.2853717).*

Conference Publications:

1) Md Abdullah Al Mamun, Hiroshi Furuta, Akimitsu Hatta, "Pulsed DC plasma CVD system for DLC film deposition", *Nanotechnology Symposium, Kochi University of Technology, Eikokuji, Kochi, Japan, November 12, 2016.*
2) Md Abdullah Al Mamun, Shun Nagano, Hiroshi Furuta, Akimitsu Hatta, "High Frequency Pulsed DC Plasma CVD for DLC Films", *Proceeding of the 34th symposium on Plasma Processing (SPP34) / the 29th Symposium on Plasma Science for Materials (SPSM29), Hokkaido University, Hokkaido, Japan, January 16-17, 2017, 18pB2 (93).*
3) Md Abdullah Al Mamun, Hiroshi Furuta, Akimitsu Hatta, "Pulsed DC plasma discharges for deposition of diamond like carbon films from carbon-monoxide", *Book of Abstracts*

of the 11th New Diamond and Nano Carbons Conference, Cairns, Queensland, Australia, April 28- June 1, 2017, (080).

4) Md Abdullah Al Mamun, Hiroshi Furuta, Akimitsu Hatta, "Synthesis of DLC films using pulsed DC plasma CVD", *Proceedings of 6th International Symposium on Frontier Technology, Kochi University of Technology, Kami, Kochi, Japan, November 5-6, 2017, pp. 217-220.*

5) Md Abdullah Al Mamun, Hiroshi Furuta, Akimitsu Hatta, "A high frequency pulsed-DC power supply for capacitive coupled plasma CVD of DLC films, Proceeding *of 39th International symposium on Dry Process, Tokyo Institute of Technology, Tokyo, Japan, November 16-17, 2017, pp.123-124.*

6) Md Abdullah Al Mamun, Hiroshi Furuta, Akimitsu Hatta, "Pulsed-DC discharge for plasma CVD of carbon thin films", *Proceeding of the PLASMA2017 conference, Himeji, Japan, November 20-24, 2017, 24P-44.*

Author

September, 2018

Acknowledgements

First of all, I would like to show respect to my supervisor *Prof. Akimitsu Hatta* for having faith in my abilities and giving me the chance to study at Kochi University of Technology. I would like to express my gratitude to him for guiding me, providing me with valuable feedback that helped me deal with many challenging problems as well as for encouragement and support during my study.

I would like to express my very sincere gratitude to *Assoc. Prof. Hiroshi Furuta* and *Assoc. Prof. Hisao Makino* for being very good advisors during the course of study. Their ideas and comments very indispensable and allowed me to improve my work many times. I am also thankful to *Prof. Masayoshi Tachibana and Prof. Mamoru Furuta,* for their great help, advice, and valuable feedback during the carrying out of this study.

I am grateful to all the members of the Hatta-Furuta laboratory for their assistance during my research. I am especially thankful to *Dr. Jun-Seok Oh,* for his countless advice, ideas, and guidance. I appreciate *Yuki Yasuoka, Kotaro Ogawa and Hideki Yajima* for their cooperation in the experiments. Big appreciation to my fellow doctoral students *Udorn Junthorn, Adam Pander,* and *Vladislav Gamaleev* for being great friends during the last years. Their presence in the laboratory always introduced a spark of happiness to my daily life. I'm also thankful to some of my Japanese friends namely *Shun Nagano, Hiroki Miyaji, Keisuke Noguchi, Hiroyuki Ichii, Keigo Nomura, and Yusaku Magari* for many interesting discussions and relaxing times.

I am also very thankful to the staff members of International Relations Division for their support, hard work and commitment. I'm especially grateful to *Mikako Takataru, Miki Okauchi, Saki Hamamura* and *Yoko Morio* for being great help and support during my study. Nevertheless, I am also grateful to *Prof. Shinichiro Sakikawa* for his time, guidance, big help and countless advice regarding Japanese and university life. I am very thankful to *Prof. Gordon Bateson* for his help and support to enhance the skills in English language.

Big thanks to my friend, *S. G. Mehadi Aman* for his continuous supports both in the moments of happiness and trouble.

Finally, I take this opportunity to express my profound gratitude to *my family* for supporting me in my decisions, for the unconstrained encouragement, and truthful love they have shown me all these years.

"The author would like to dedicate this dissertation to his family and teachers"

Chapter 1
Introduction

This chapter introduces the main motivation and issues regarding to the research works presented in the thesis. The requirements for the current research are revealed and explained. The research objectives are also demonstrated. Furthermore, an outline of thesis is exhibited.

1.1. Background

Plasma technology plays a huge role in industrial, medical, domestic applications, due to the unique and outstanding features of plasma [1]. Chemically reactive plasma discharges are broadly used to modify the surface properties of materials. Particularly, low-pressure plasmas are widely used in surface treatment and material processing applications, since the plasma can be delivered in large area with uniformity on the surface of substrates [2-3] whereas, atmospheric-pressure cold plasmas are generally used for medical and biological applications, for example, sterilization, cancer treatment, healing wounds and so on [4-5]. Hence, the generation of plasma discharges with broad controllability in both cases has appealed a much attention.

1.2 Motivation and research issues

The most common method for generation of plasma is the electrical breakdown of a neutral gas by an external electric field. The electric field accelerates the charge particles that couples their energies in the plasma via collisions with other particles. A variety of plasma generators are used based on the requirements of applications [6] such as direct current (DC), alternating current (AC), radio frequency (RF), microwave and pulsed. However, a vital challenge is the necessity of coupling energy into a plasma. When plasma is operated under DC and low-frequency AC, this becomes comparatively straightforward. While coupling energy in a plasma, at high-frequencies becomes more crucial. In fact, where the energization of plasma is the central of the process, the optimal selection and proper operation of the power generators are critical to the achievement of research or industrial processes. Thus, an understanding of both the plasmas and its connection with the generators, is important in the study for optimum applications.

Recently, pulsed power technology shows huge potential in the field of plasma processing. It is reported that pulsed generators can deliver high instantaneous power with respect to low average power, offer fast rise time and high repetition rate which are advantageous to control

the production of high electron density and more active plasma species [7-8]. The present developments in power electronics improve the high speed solid-state switching techniques [9] and enable to produce high–frequency pulsed generators that advances the plasma-based materials processing.

A very popular method of low-pressure plasma-based thin-films processing for industrial applications is plasma enhanced chemical vapour deposition (PECVD) due to the advantages, as the source gas molecules can easily be stimulated, dissociated, and even ionized at a considerably low gas temperature [10-11]. However, RF power is mostly used in PECVD, particularly depositing diamond-like carbon (DLC) films of highly insulating properties, because the substrates were required to be powered with an alternating current [12]. In RF PECVD, the intentional control of CVD conditions, however, the substrate bias voltage, one of important parameters for deposition as it influences the ion energy falling on the growing film, is not independent of other conditions but mostly determined by RF power density. Therefore, it is expected to be controlled independently the ion energy impinge on the substrate for the growth of films.

Accordingly, pulsed DC plasma CVD can be considered as an alternative to the RF PECVD and supposed to be a simple and cost effective deposition system that can be used to improve film properties as compared to widely used RF system [13]. In a pulsed DC PECVD system, pulsed DC generator is a significant component for the reason that it may possible to change the gas phase chemistry, energy of ions bombardment on substrate, electron density, electron temperature to meet the requirements of highly selective deposition process by varying the pulse parameters such as pulse frequency, duty ratio and amplitude [12-15].

Therefore, the development of wide controllability of pulsed-DC discharge system and the study of its impact on the low-pressure plasma properties as well as deposited films properties, have appealed extensive attention.

Besides, the operation of plasma at low pressure includes vacuum systems, which are expensive and need precautions. Recently, the development of plasmas on the micro-sale at atmospheric pressure [16], especially generated by dielectric barrier discharge (DBD), has attained much interest to provide economical processing solutions by omitting the vacuum systems. Atmospheric pressure plasma jet (APPJ) is a popular DBD device for generation of cold plasma. It is technically simple, low-cost, environment-friendly and usefulness of small size in treating localized regions and widely used in surface modification, sterilization and biomedical treatment [17-19]. For operation of APPJ, alternative current (AC) HV power sources of sinusoidal wave at lower frequency than a several 10s of kHz are widely used because it is easy to boost the voltage by using a transformer. In most cases, the APPJ is

operated at a fixed frequency and a fixed voltage. For research and development of APPJ technology, however, it is important to examine the effects of operation frequency and waveforms on the plasma properties and processed results. Moreover, it is expected that pulsed generator with high repetition rate with fixed pulse shape becomes more attractive owing to control the generation of non-thermal plasmas and their chemical and physical properties.

Henceforth, the development of a compact high-voltage, high-repetition and energy efficient pulse generator for atmospheric-pressure plasma applications, is of a great interest.

1.3. Research objectives

The main objective of this dissertation is the development of pulsed plasma discharge system for low-pressure CVD of carbon thin films and atmospheric-pressure plasma jet (APPJ). For this purpose, it is important to perform the following studies:

- Study of the pulsed plasma discharges at low-pressure— understanding of the pulse plasma generation mechanism through gas discharge at low pressure, development of pulsed-dc power supplies using new techniques with broad controllability of pulse parameters, test of the power supplies for low-pressure discharges, investigation of plasma parameters with the variations of discharge conditions, reproducible generation of the plasma and optimized parameters for reproducible discharge.
- Study of the deposited carbon thin-films— understanding the growth mechanism of carbon thin-films, analysis of the effect of the experimental conditions (substrate, temperature, precursor gas) on deposited films, investigation the films properties and their dependency on pulsed power parameters such voltage, current, pulse frequency and duty ratio.
- Study of the pulsed plasma discharges at atmospheric-pressure— understanding of the plasma generation mechanism at atmospheric-pressure, development of high-voltage impulse generator with new topology, test of generator for atmospheric pressure plasma discharge.
- Study of the characteristics of APPJ— understanding of the phenomena of APPJ, investigation of pulsed plasma discharge of APPJ, observation of the effects of pulse amplitude, repetition rate and electrode configurations on the plasma plume length and discharge characteristics, investigation of the production of reactive oxygen and nitrogen species (RONS) in plasma-activated water (PAW) by APPJ.

1.4. Outline of the thesis

The thesis is organized as follows:

Chapter 1 introduces the main motivation and issues regarding to the research works presented in thesis. The requirements for the current research are revealed and explained. The research objectives are also demonstrated. Furthermore, an outline of thesis is exhibited.

Chapter 2 introduces the comprehensive background of the presented research. The introduction of plasma, low and atmospheric pressure plasma, pulsed power, carbon thin films and its deposition methods are presented. A literature review of the most relevant experimental and theoretical studies in those fields is demonstrated.

Research Part-I: Pulsed plasma discharge for low-pressure synthesis of carbon thin-films

Chapter 3 presents the development of pulsed DC plasma CVD system using a simple pulse power supply and customized CVD apparatus and the investigation of the growth of DLC films on silicon substrates from two different precursor gases with the variation of deposition temperature. The introduction, objectives, experimental methods and results are described. Lastly, discussions and conclusions are drawn based on the experimental results.

Chapter 4 presents a novel pulsed DC generator (PDG) for capacitively coupled plasma discharge inside a vacuum chamber employing solid-state switches that can operate in pulsed dc mode with continuous power within a pulse, controllable pulse duration, and wide controllable frequency. Introduction, objectives, experimental methods, and results are described. The details of the fabrication and evaluation of the high-frequency PDG are reported. To end, discussions and conclusions are drawn based on the experimental results.

Chapter 5 presents the investigation of the growth of hydrogenated amorphous carbon (a-C:H) films on silicon substrates with the variation of pulse repetition rate using a developed high-frequency pulsed DC capacitive-couple plasma CVD system. The introduction, objectives, and experimental methods are described. The study of the influence of the pulse repetition rate on the plasma characteristics is performed. Furthermore, the deposition rate and films properties are presented as a function of pulse operating frequency. Finally, discussions and conclusions are drawn based on the experimental results.

Chapter 6 provides the investigation of pulsed plasma characteristics with the variation of discharge conditions using optical emission spectroscopy (OES). A trial deposition of carbon thin films is also examined by the developed novel pulsed discharge system, following the results obtained from the optimization process. Introduction, objectives, and used methods are described. The deposited films properties are characterized. Finally, conclusions are drawn based on the experimental results.

Research Part-II: Pulsed plasma discharge for atmospheric-pressure plasma Jet (APPJ)

Chapter 7 presents the development of a high-voltage high-frequency impulse generator for atmospheric-pressure plasma jet (APPJ) using dual resonance pulse transformer (DRPT). The principle, design and construction of DRPT are demonstrated. Introduction, objectives, operations and results are described accordingly. A conclusion is drawn based on the experimental results.

Chapter 8 presents the investigation of pulsed plasma discharge characteristics for APPJ by the developed impulse generator based on DRPT. The brief introduction, experimental methods and results are described. The effects of pulse amplitude, repetition rate and electrode configurations on the plasma plume length and characteristics of APPJ are discussed by means of electrical and optical properties. Furthermore, the dependency of pulse operating frequency and polarity on plasma jet characteristics and RONS production in PAW are also presented.

Chapter 9 summarizes the main achievements drawn from the research and discusses future research recommendations, which could open new dimensions in the research of pulsed plasma discharge applications.

References

[1] J. Harry, *Introduction to Plasma Technology: Science, Engineering and Applications,* Wiley-VCH, Germany, 2010.

[2] M. A. Lieberman, *Principles of plasma discharges and materials processing* (Wiley, New Jersey, 2005)

[3] Th. Lampe, S. Eisenberg, and E. Rodríguez Cabeo, "Plasma surface engineering in the automotive industry—trends and future prospectives" *Surf. Coat. Technol.* 174-175, 1 (2003).

[4] H. Tanaka, M. Hori, "Medical applications of non-thermal atmospheric pressure plasma", *J. Clin. Biochem. Nutr.,* 60(1), 29-32, (2017).

[5] M. Laroussi, "Plasma Medicine: A Brief Introduction", *Plasma,* 1(1), 5(1-14), 2018.

[6] H. Conrads and M. Schmidt, "Plasma generation and plasma sources", *Plasma Sources Sci. Technol.* 9, 441–454, (2000).

[7] J. Laimer, M. Fink, T. A. Beer, H. Störi, "Plasma dynamics as a key to successful upscaling of pulsed plasma processes", *Surf. Coat. Technol.,* 174−175 118 (2003).

[8] T. Shao, W. Yang, C. Zhang, Z. Fang, Y. Zhou, and E. Schamiloglu, "Temporal evolution of atmosphere pressure plasma jets driven by microsecond pulses with positive and negative polarities", *EPL (Euro-physics letters)* 107, 65004 (2014).

[9] W. Jiang, K. Yatsui, K. Takayama, M. Akemoto, E. Nakamura, N. Shimizu, A. Tokuchi, S. Rukin, V. Tarasenko, and A. Panchenko, "Compact solid-state switched pulsed power and its applications," *Proc. IEEE*, 92(7), 1180–1195, (2004).

[10] J. R. Roth, *Industrial Plasma Engineering* (Institute of Physics, University of Reading, Berkshire, Vol. 2. 2001).

[11] Daniel Lundin, Jens Jensen and Henrik Pedersen, "Influence of pulse power amplitude on plasma properties and film deposition in high power pulsed plasma enhanced chemical vapor deposition", *J. Vac. Sci. Technol. A*, 32(3), 030602 (2014).

[12] C. Corbella, M. Vives, G. Oncins, C. Canal, J. L. Andújar, and E. Bertran, "Characterization of DLC films obtained at room temperature by pulsed-dc PECVD," *Diamond Relat. Mater*. 13 (4–8), 1494 (2004).

[13] R. A. Scholl, "Asymmetric bipolar pulsed power: a new power technology", *Surf. Coatings Technol.* 98, 823 (1998).

[14] S. Samukawa and T. Mieno, "Pulse-time modulated plasma discharge for highly selective, highly anisotropic and charge-free etching", *J. Plasma Sources Sci. Technol.* 5, 132 (1996).

[15] M. A. Lieberman and S. Ashida, "Global models of pulse-power-modulated high-density, low-pressure discharges", *J. Plasma Sources Sci. Technol.* 5, 145 (1996).

[16] K. Tachibana, "Current status of microplasma research", *IEEJ Trans. Electr. Electron. Eng.* 1, 145 (2006).

[17] E. J. Szili, A. S. Al-Baraineh, P. M. Bryant, R. D. Short, J. W. Bradley, and D. A. Steele, "Controlling the spatial distribution of polymer surface treatment using atmospheric-pressure microplasma jets" *Plasma Process. Polym.* 8, 38 (2011).

[18] K. Lee, K-H. Paek, W-T. Ju, and Y. Lee, "Sterilization of bacteria, yeast, and bacterial endospores by atmospheric-pressure cold plasma using helium and oxygen", *J. Microbiol. 44*, 269 (2006).

[19] X. Zhang, D. Liu, R. Zhou, Y. Song, Y. Sun, Q. Zhang, J. Niu, H. Fan, and S. Yang, "Atmospheric cold plasma jet for plant disease treatment", *Appl. Phys. Lett.* 104, 043702 (2014).

[20] J. S. Oh, Y. Aranda-Gonzalvo, and J. W. Bradley, "Time-resolved mass spectroscopic studies of an atmospheric-pressure helium microplasma jet," *J. Phys. D. Appl. Phys.* 44, 365202 (2011).

Chapter 2

Research background

This chapter introduces the comprehensive background of the presented research. The introduction of plasma, low and atmospheric pressure plasma, pulsed power, carbon thin films and its deposition methods are presented. A literature review of the most relevant experimental and theoretical studies in those fields is demonstrated.

2.1. Plasma

2.1.1. What is plasma?

Plasma is partially or fully ionized gas, consisting of neutral atoms (or molecules) and charged particles (ions and electrons). The most significant feature of plasma is quasi-neutrality, in which the volume concentration of positive and negative charged particles of plasma are almost same. If some of gas atoms (or molecules) will lose one or more electrons due to some external impact, gas becomes plasma. If neutral particles remained in the gas, plasma is called partially ionized, whereas if no neutral particles remained in the gas, plasma is called fully ionized [1].

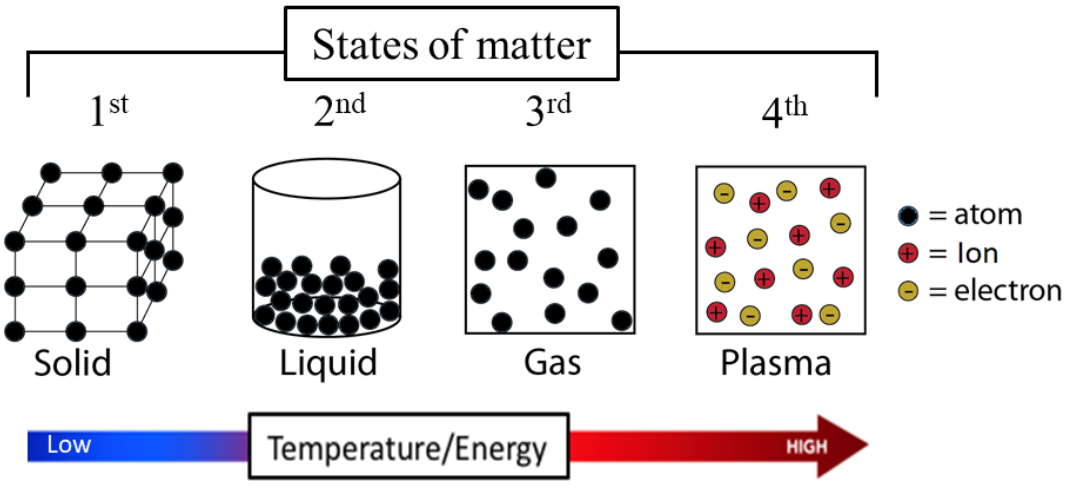

Figure 2.1. Generation of plasma from a solid material with increase of temperature/energy.

Figure 2.1 shows the process of generation plasma from a solid material by adding more temperature/energy. Generally, with increase of temperature, a solid material begins to melt and lastly evaporates (goes to the gas phase). In the case of molecular gas (such as H_2, N_2), with further increase of temperature, gas molecules start to dissociate to single atoms. Further increase of temperature, gas becomes ionized by the formation of positive ions and free

electrons and turns into plasma. In plasma, free electrons can easily move and producing electric current, that's why plasma is also called "conductive gas" [1]. However, plasma follows most of the principles of the gas physics, it acts different in some of the cases. One of the major differences in behavior of plasma, compared to gas, could be observed when plasma interacts with electric or magnetic field. It could be explained by existence of charged particles in the plasma. Owing to extraordinary behavior of plasmas in electric and magnetic fields, plasma is also called 4th state of matter.

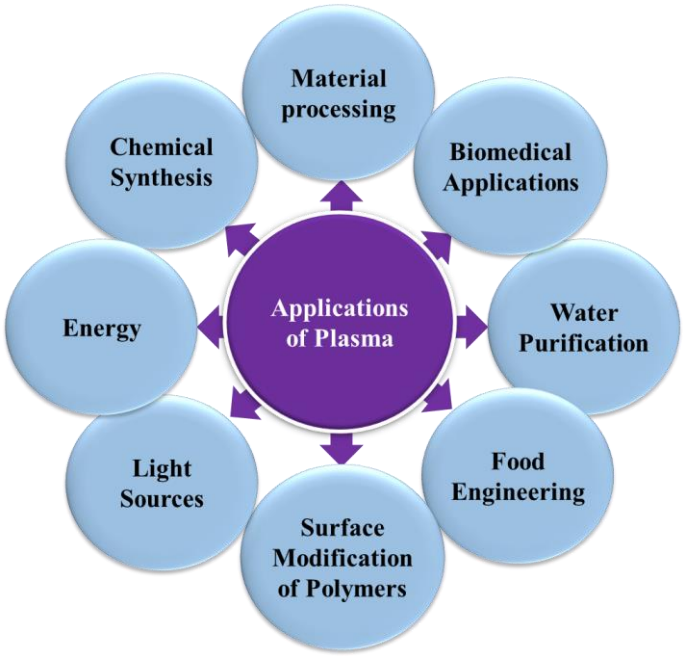

Figure 2.2. Typical application areas of plasma.

Plasma is used in areas where it matters; to bond materials together, or to change their surface properties to suit our needs. It is possible to modify virtually any surface with this pioneering technology. Therefore, in recent times, plasma technologies are widely used in various fields and having huge impact in our daily life, as demonstrated in Figure 2.2. Almost all microelectronic devices are produced using plasma processes (plasma-based deposition and etching). Plasma technologies are taking growing role in biomedical sector in such applications as plasma coating (coating of prostheses, such as artificial hips or knee), sterilization of equipment by plasma, plasma treatment of drugs and plasma medicine (treatment of cancer and wounds by non-thermal plasmas).

2.1.2. Generation of plasma by electric gas discharge

The generation of plasma by ordinary heating of the substance stated above, is not the most common method. The most common method of generating plasma in laboratory and industry is the use of an electric gas discharge rather than by ordinary heating of the substance stated above. For generation of the gas discharge, usually, two electrodes should be connected to a

power source and placed inside the glass tube, which could be filled by various gasses under various pressure as shown in Figure 2.3(a). This simple device is already used for more than 150 years and allows to produce various types of plasma discharge. The crucial parameters of electrical gas discharge are gas pressure (P), applied voltage (V) and inter-electrode distance (d).

The current-voltage characteristic of the electric gas discharge generated is presented in Figure 2.3(b). When a low voltage is applied to an electrode gap containing neutral gas, an extremely small current (about 10^{-15} A) is observed passing through the gap. It could be explained by existence of charged particles in the gas formed by natural sources of radiation (e.g. cosmic rays or a nearby UV lamp). The applied voltage is not high enough to cause ionization of atoms by electron impact. In this case, discharge is formed only due to external ionization sources or due to emission of electrons and ions from the cathode. Such a discharge maintained by external sources is called *non-self-sustaining discharge* (Figure 2.3, region a-b).

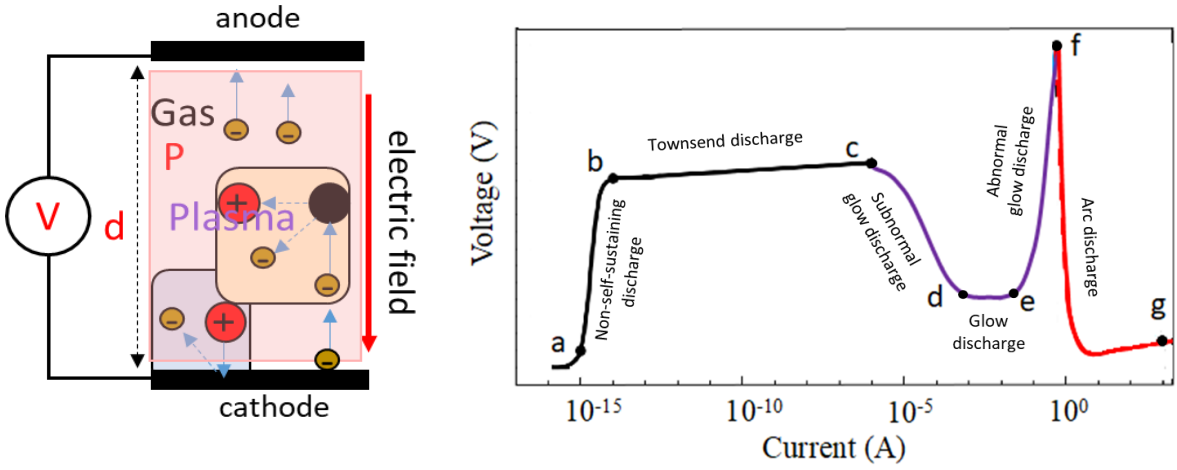

(a) (b)

Figure 2.3. (a) A schematic of electric gas discharge (b) The current-voltage characteristic of electric gas discharge. The values on the current scale are only illustrative, the exact values depend on the details of the discharge configuration.

The increasing voltage results in a higher electric field inside the discharge gap. The field becomes high enough such that electrons gain enough energy to cause ionization of neutral atoms in the gap by electron impact. As a result, release of new free electron happens after a random collision. The original ionization event releases one electron, and each subsequent collision releases a further electron, causing so-called cascade multiplication of carriers or avalanche multiplication. This type of discharge is called the *Townsend discharge* (Figure 2.3,

region b-c), which is also known as *dark discharge* as there is no significant amount of light emission [1-2].

A further increase of voltage, current starts to grow rapidly and breakdown of the gas occurs, which is one of the most significant processes in the gas discharges. The voltage at which breakdown happens is known as the *breakdown voltage.* The potential drop across the cathode fall is almost equal to the potential difference across the electrodes. The result is that the total voltage needed to sustain the discharge can be reduced. This discharge mode is known as *subnormal glow discharge* (Figure 2.3, region c-d), as emission of light from the gas can be observed. However, this discharge phase stage is often unstable and leads towards a glow discharge [1-2].

In a *glow discharge* (Figure 2.3, region d-e), the voltage needed to sustain the discharge is at its minimum. A further increase in current does not lead to a decrease of voltage, but to spreading of the discharge over the electrode surfaces, keeping the current density constant [1-2]. In this discharge mode, plasma is weakly ionized and not equilibrium. Emission of light form glow discharge is produced by excitation of atoms and often employed to investigate plasma-generated species by optical atomic emission spectroscopy (OES).

With further increase of voltage, current density starts to increase rapidly and *abnormal glow discharge* (Figure 2.3, region e-f) appears. The electrodes are fully covered by the discharge and a further current increase leads to an increase of voltage across the electrodes. When the current is further increased, abnormal glow discharge turns into an *arc discharge* (Figure 2.3, region f-g). Typically, the arc discharge is characterized by high currents (more than 1 A) and low voltages (tens of volts) and high pressure of the gas comparing to glow discharge. Different processes such as gas heating and thermionic electron emission from the electrodes become important.

2.1.3. Classification of plasma

Plasma can be classified in several ways, such as-

i) Low pressure and atmospheric pressure plasma —based on pressure in plasma chamber.
ii) Hot and cold plasma —based on degree of ionization and temperature of plasma.
iii) DC and AC plasma (Microwave, RF, Pulse) —based on the frequency of power generator.

❖ *Low pressure and atmospheric pressure plasma*

In low pressure plasma, gas is excited by energy supplied in a vacuum as shown in Figure 2.4(a). This results in energetic ions and electrons, as well as other reactive particles, which constitute the plasma. The effect of the plasma can be altered by varying the process parameters such as pressure, power, process time, gas flow and composition. Several effects can therefore

be achieved in a single process step and material surfaces can then be effectively modified. Generally, low pressure plasma has wide applications in materials processing and play a vital role in semiconductor devices [3] owing to the advantages such as high concentrations of reactive species that can etch and deposit thin films, uniform glow discharge, low gas temperature that cannot damage the thermally sensitive substrates, low breakdown voltage [Figure 2.4(c)] and a stable operational window between spark ignition and arcing. However, low pressure plasma has some drawbacks: expensive vacuum systems are required to reduce the gas pressure, the size of the sample to be treated is constrained by the size of the vacuum chamber and electrode configurations, and direct processing or treatments of biological samples with liquid phase.

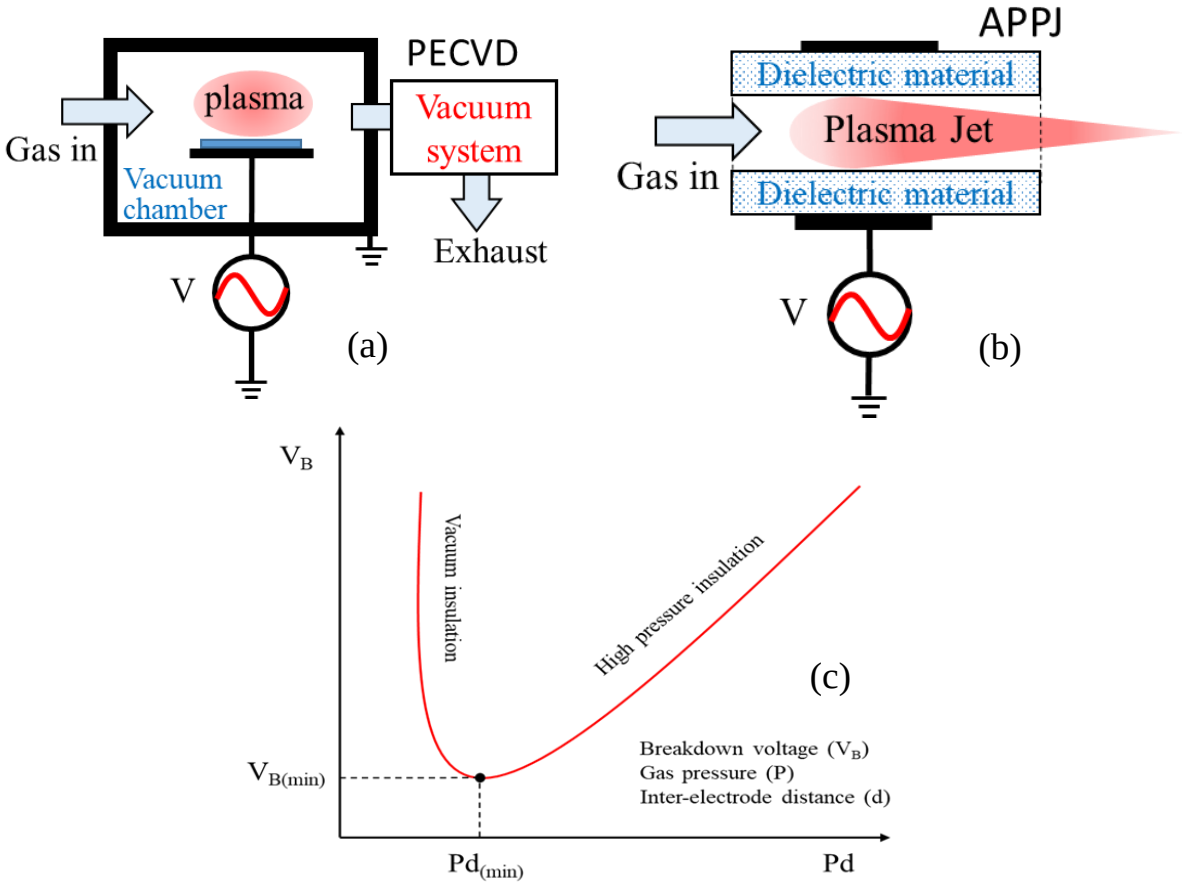

Figure 2.4. (a) Low-pressure plasma discharge system (b) Atmospheric-pressure plasma discharge system (c) Paschen graph for the evaluation of breakdown voltage at low and high pressure.

In atmospheric pressure plasma, gas is excited by means of a high voltage (several kV) under atmospheric pressure, such that a plasma is ignited. Atmospheric pressure plasmas overcome the disadvantages of vacuum operation as shown in Figure 2.4 (b). It is useful in a verity of materials processes at ambient and plays a vital role in biomedical applications [4]. However, difficulty of sustaining a glow discharge, higher breakdown voltage [Figure 2.4(c)],

and non-uniform plasma discharge are the drawbacks of atmospheric pressure plasma. Corona discharge, dielectric barrier discharge, and plasma jet are the examples of atmospheric pressure plasma.

❖ *Hot and cold plasma*

Hot plasma occurs when the degree of ionization is high and the temperature of electrons, atomic and molecular species becomes extremely high. Hot plasma is nearly fully ionized. For example, the sun and stars in the universe consist completely of hot plasma. Hot plasma is generally used in production of light sources and atomic emission spectroscopy measurements. In contrast, cold plasma occurs when the atomic and molecular species are almost at ambient temperature, whereas the electrons are at high temperatures. A small fraction of gas molecules is ionized. Cold plasma can be used to treat surfaces or to deposit thin films onto organic and inorganic substrates.

❖ *DC and AC plasma*

Plasma is usually carried out by DC (0 Hz) power and a variety of AC generators such as, microwave (2.4 GHz), radio frequency (13.56 MHz), pulsed power (adjustable frequency range Hz to kHz). In a DC discharge, charge particles from the plasma can accumulate on the substrate surface causing unwanted charging effects. Compared to DC discharge, AC discharges are preferred in plasma systems for a number of reasons. Firstly, the energy transfer into the discharge becomes more efficient by AC discharge, as the frequency increases. Moreover, by altering the direction of current flow rapidly, the charging effects on the substrate can be reduced. Among these AC-driven discharges, definitely, plasma discharge by *pulsed power* introduces substantial advance in the stability and controllability of plasma properties.

2.2. Pulsed Power

2.2.1. What is pulsed power?

Pulsed power is referred to the science and technology of accumulating energy over a relatively long period of time and releasing it very quickly, thus increasing the instantaneous power. Steady accumulation of energy and its quick release can deliver a larger amount of instantaneous power over a short period of time although the total energy content is identical, as shown in Figure 2.5. Typically, energy is stored within electrostatic fields (capacitors), magnetic fields (inductors, transformers). The release of the stored energy over a very short interval (known as energy compression), a vast amount of peak power can be delivered to a load. For example, if 1 J of energy is stored within a capacitor and released to a load over 1 s,

the peak-power delivered to the load would be 1 W. However, it is totally released to the load within 1μs, the peak-power would be 1 MW (a million times larger).

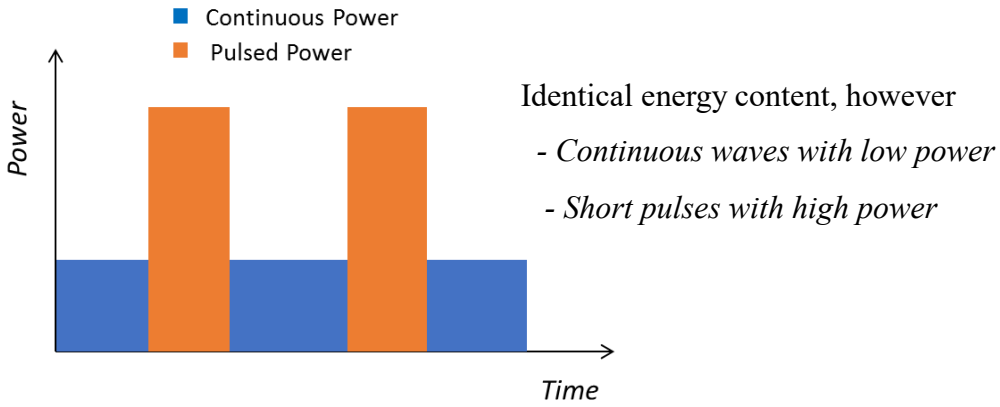

Figure 2.5. Power delivered to load by continuous and pulse power at identical energy content.

2.2.2. Pattern of pulsed power

The pulse attributes differ based on the demand of various applications. In general, the pulsed high voltage generators have variation of pulse duration from few nanoseconds to few hundred microseconds and voltage level from several hundred volts to several mega-volts. Pulse repetition rate also depends on the applications, however, demand of highly repetitive pulses has further increased recently. The methods for forming pulse pattern appeal the scientific and applied interest. It links with understanding of physical processes and increasing of efficiency for pulsed generators. Basic two patterns of pulsed power are widely used which are pulsed-DC (*preferred for research part I)* and high-impulse *(preferred for research part II).* The typical current-voltage characteristic waveforms of these two patterns of pulsed power are shown in Figure 2.6. A comparison of pulse parameters between pulsed-DC and high-impulse power can be presented in the Table 2.1.

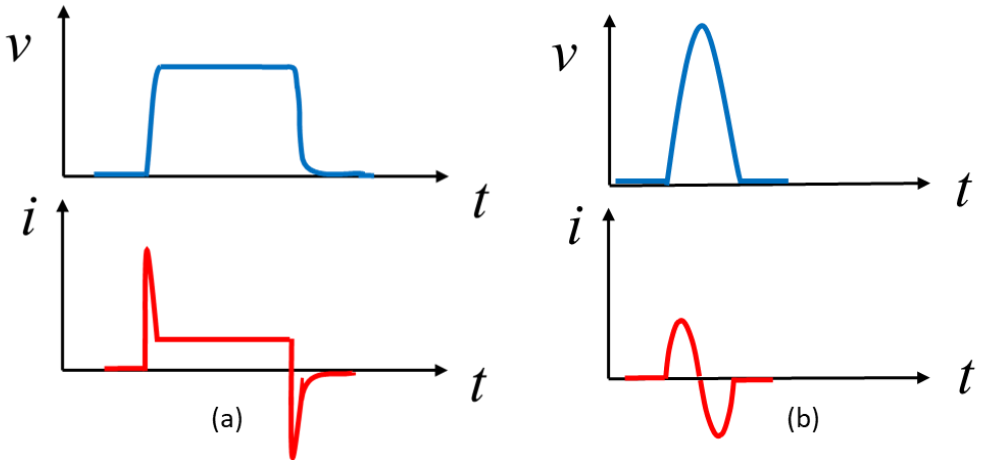

Figure 2.6. Typical current-voltage waveforms of basic two patterns of pulsed power (a) pulsed-DC (b) high-impulse.

Table 2.1. Pulse parameters between pulsed-DC and high-impulse power

Pulse parameters	Pulsed-DC	High-impulse
Peak pulse power	Low (continuous within a pulse)	High
Pulse width	Controllable (several ms to μs)	Short (several μs to ns)
Pulse shape	Controllable	Mostly fixed
Pulse repetition rate	High (up to several hundreds of kHz)	Low (up to several kHz)
Pulse steady on-state	Yes	No

2.2.3. Pulsed power supply topologies

Owing to progressive demand of pulsed power in industrial and environmental applications, several pulsed power topologies using various techniques have been reported [5-14]. Among these topologies, some typical topologies are sated below.

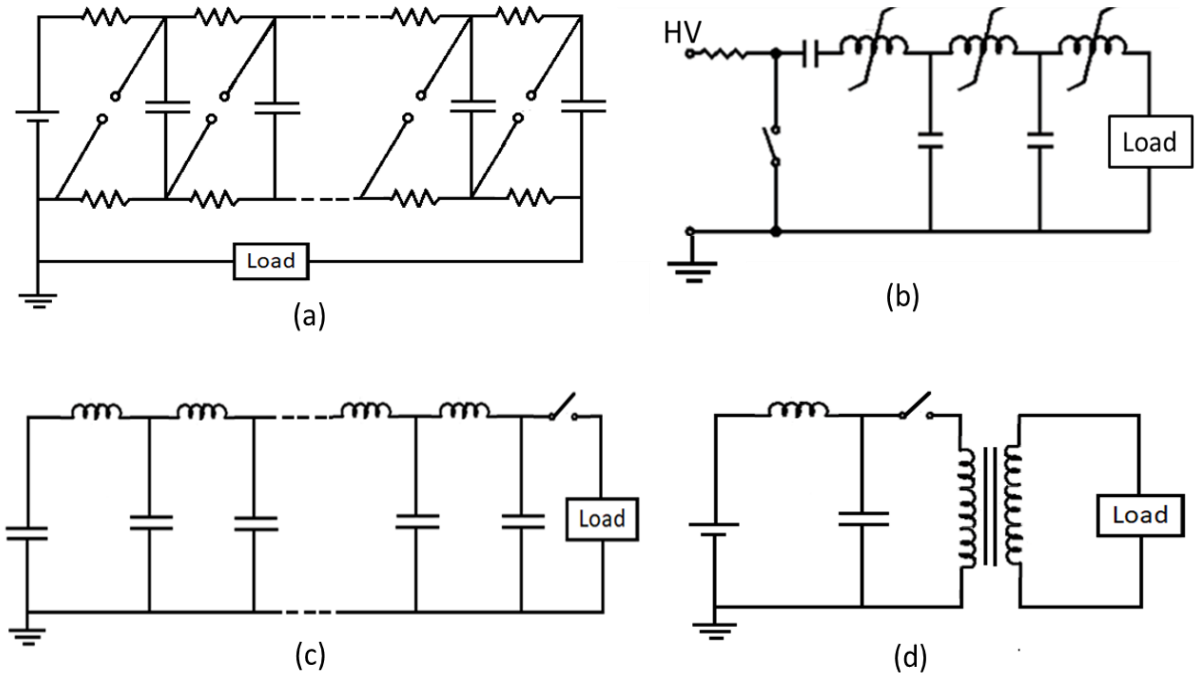

Figure 2.7. Typical pulsed power topologies (a) Marx generator (MG) (b) magnetic pulse compressor (MPC) (c) pulse forming network (PFN) (d) pulse transformer (PT).

❖ *Marx generator (MG):*

Marx generator is first introduced by Erwin Otto Marx in 1924. It is a type of electrical circuit whose purpose is to generate a high-voltage pulse from a low-voltage DC supply. A

number of capacitors are charged in parallel to a given input voltage, V_{in} and then connected in series by spark gap switches to produce ideally a high-voltage pulse of nV_{in} to the load, where n is the number of capacitors (stages). Due to some practical constraints, the output voltage is usually somewhat less than the ideal value. A basic circuit of MG is shown in Figure 2.7(a).

❖ *Magnetic pulse compressor (MPC)*

Magnetic pulse compressor is the technology employed for decades to produce high-voltage pulses for many applications, specifically in laser systems. The idea is to generate a relatively long pulse by a switch and to compress it in the time domain using resonant charge transfer through saturable inductors. The saturable inductors consist of a ferro-magnetic core and act as a magnetic switch by utilizing the nonlinearity of the magnetization curve of ferro-magnetic materials. Figure 2.7(b) shows a basic circuit of MPC.

❖ *Pulse forming network (PFN)*

A pulse forming network is an electric circuit that accumulates electrical energy over a comparatively long time, then releases the stored energy in the form of a relatively square pulse of comparatively brief duration for various pulsed power applications. In a PFN, energy storage components such as capacitors, inductors or transmission lines are charged by means of a high voltage power source, then rapidly discharged into a load via a high voltage switch. A number of resonant units are connected in ladder shapes compressing the electric fields through magnetizing energy. A basic circuit of PFN is shown in Figure 2.7(c).

❖ *Pulse transformer (PT)*

Pulse transformer refers to high power pulse transformer which generally works in step-up mode and can produce a high-voltage from a low-voltage. In this topology, the switching is at considerably low voltage and the difficulties of using very high voltage switches can be avoided. In this topology, the energy is primarily stored in the intermediate energy storage system (capacitor). The switching unit controls the pulse transformer to pulse shaping and compression, and then, a desired pulse is obtained on the load. However, in order to ensure the reliability of pulse transformer, it is necessary to measure the relevant parameters of magnetic core. Figure 2.7(d) shows a basic circuit of PT.

2.2.4. Power electronics in pulsed power generation

Spark gap or magnetic switches were conventionally used as switching devices in pulsed power generation as they have high blocking voltage as well as high current-carrying capabilities. However, they have some undeniable disadvantages such as bulky in size, low efficiency, short life span, and low operational frequency. Usually, the output power rating,

output pulse shape, repetition frequency, lifetime, and compactness of a pulsed power generator depend on the performance of the switching devices. Recently developed solid-state technology demonstrates many favorable switches with high voltage ratings and switching frequency, making them suitable candidates for pulsed power generation. Insulated-gate bipolar transistors (IGBTs), metal–oxide–semiconductor field- effect transistors (MOSFETs), silicon controlled rectifiers (SCRs) (Thyristors), and gate turn-off thyristors (GTOs) are examples of main semiconductor switches [15] that can be utilized as reasonable replacements for existing switches. A scheme of current, voltage and switching frequency domains of these power switches are shown in Figure 2.8.

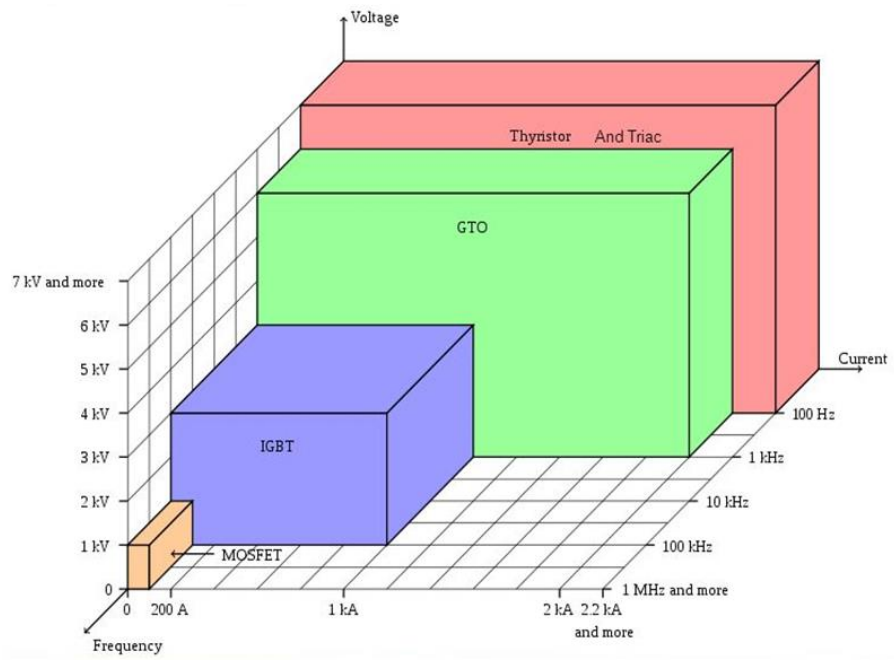

Figure 2.8. Current/Voltage/switching frequency domains of the main power electronics switches [16].

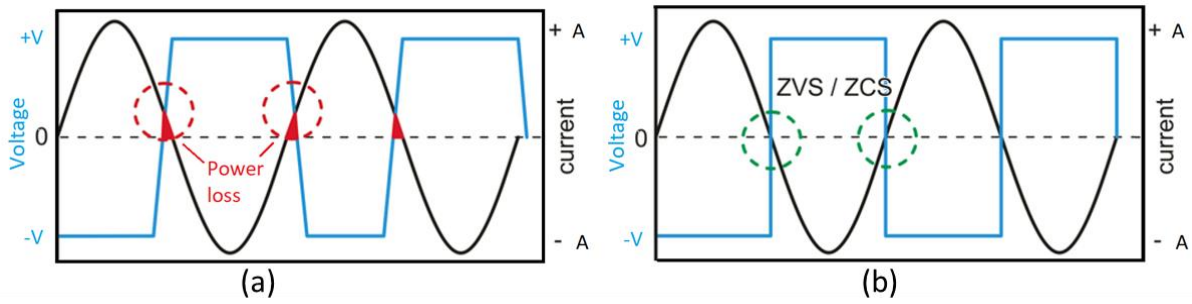

Figure 2.9. Scenario of (a) hard switching and (b) soft/zero crossing switching.

Moreover, power electronics converters offer attractive advantages for pulsed power applications. Although there are various types of power electronics converters, resonant converters are popular due to zero crossing switching capability. In conventional pulse-width

modulation (PWM) methods for power converters, the power flow is controlled by chopping at high frequency using power switches with sudden changes of voltages and currents. Owing to the hard switching [Figure 2.9(a)], substantial switching power loss and noise occurs.

In *resonant converters*, resonance occurs among capacitive and inductive elements in the circuit and the power flow can be controlled in a sinusoidal manner, introducing zero-current crossing (ZCS) or zero-voltage crossing (ZVS). The switching at zero-current or zero-voltage crossing is known as zero-current switching (ZCS) or zero-voltage switching (ZVS). These type switching are called soft switching [Figure 2.9(b)], markedly eliminates the switching losses in power switches. Moreover, the power interchange scheme between inductive and capacitive elements of resonant circuits is also advantageous for reducing current ripples and noises of high voltage power generators.

2.3. General processes in pulsed plasma discharge

A variety of processes occur in each regime of pulsed plasma discharge as shown in Figure 2.10(a). Generally, it has four regimes: turn on, steady state, turn off and late afterglow as also noticed in ref. [17]. The common processes of these regimes are listed briefly in the following Table 2.2. However, turn on and turn off regime are very crucial and become more dominating in plasma discharge, especially in high frequency operation.

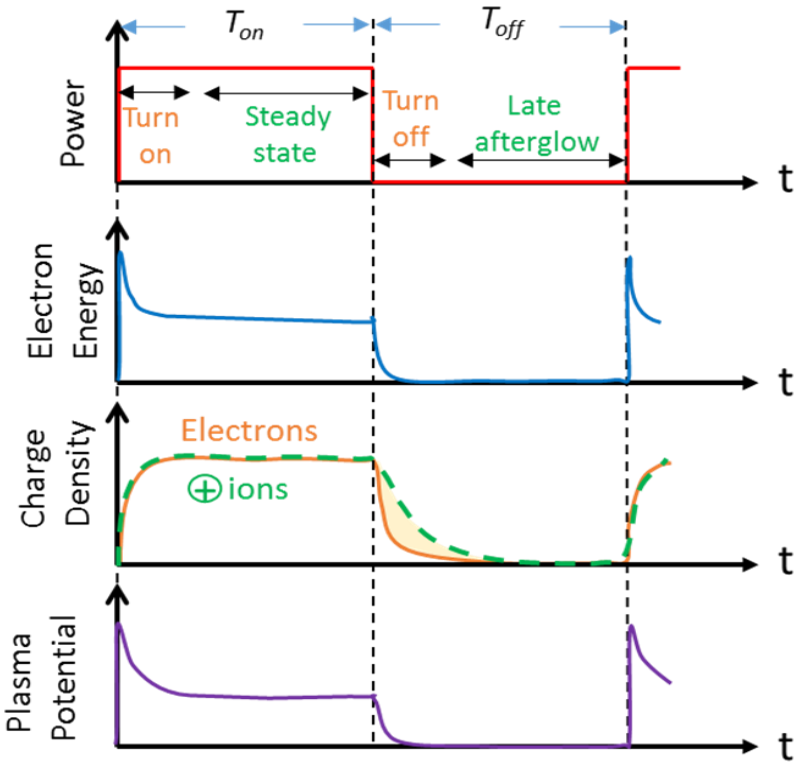

(a)

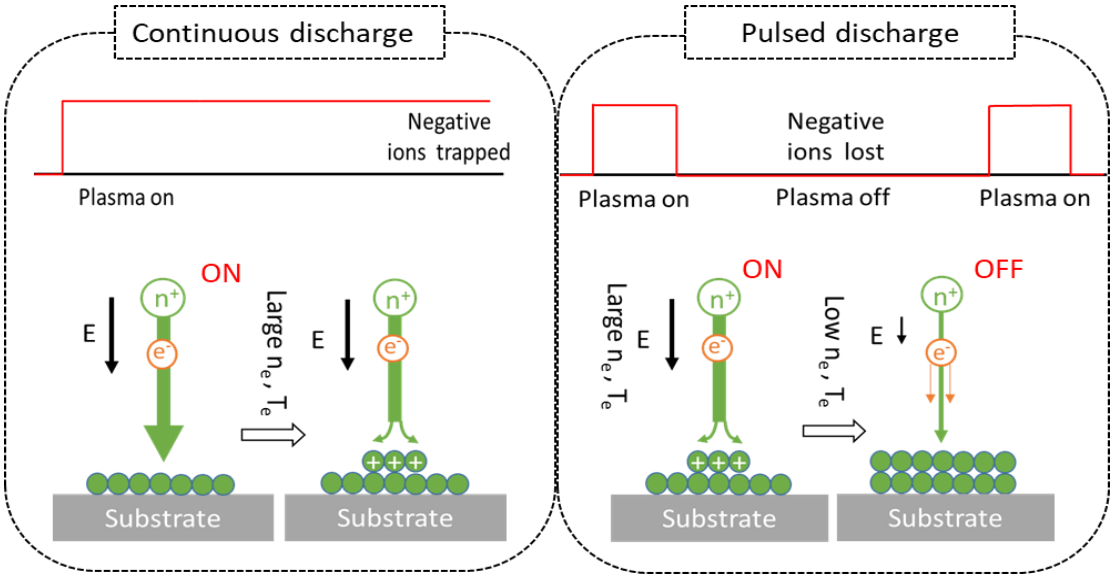

(b)

Figure 2.10 (a) Regime of processes in pulsed-DC plasma discharge (b) Advantageous processes of pulsed-DC discharge in the synthesis of materials over continuous discharge.

Table 2.2. General processes take place in each regime of pulsed plasma discharge

Regimes	Processes
Turn on	Larger electron energy, rising electron density, rising ion density, forming plasma sheath, power not well-matched, larger plasma potential
Steady state	Medium electron energy, large & almost constant electron density, large positive ion flux density, power well-matched to about constant impedance, medium plasma potential
Turn off	Quickly decreasing electron energy, fast-falling electron density, rapidly falling ion density, falling power and plasma potential
Late afterglow	Near thermal electron average energy, small electron density, small ion density, disintegrate plasma sheath, zero power and plasma potential

Moreover, there are some advantageous processes of pulsed discharge in the synthesis of materials over continuous discharge as schematically demonstrated in Figure 2.10(b). In case of continuous discharge, the sheaths of plasma do not disintegrate, so negative ions are trapped for long times and can polymerize to produce dust particles. On the other hand, the sheaths of plasma disintegrate periodically in case of pulsed discharge. As a consequence, negative ions can be lost before they polymerize. In case of insulating films, surface charge can build up on the substrate during a continuous discharge due to large electron density (n_e) and electron energy (T_e). This can deflect the ions and introduce surface damage of the samples. Besides, the surface charge build-up can be reduced in pulsed discharges because of the low n_e and T_e in the afterglow regime that allows more negative ions and electrons to be pulled to the surface and neutralize the positive charges.

2.4. Carbon materials

Carbon is one of the most abundant elements the Earth's crust. Carbon materials have attracted much attention, because of their low cost and various characteristics. It is well known of their applications in environmental, thermal and biomedical fields. Another important field is the electrical applications, including electrodes, electronic devices, and so on. The wonder feature of carbon is its unique atomic structure and capability of combining with other elements. Carbon ($^{12}_{6}C$) is a polyatomic non-metal chemical element which belongs to group 14 of the periodic table. Carbon atoms have four valence electrons forming the $1s^2\ 2s^2\ 2p^2$ electron configuration which allows to build of covalent chemical bonds. Two main properties of carbon elements are: — firstly, it shows the possibility of forming simple and complicated compounds which are built only from carbon atoms, and the high durability of such compounds is related to high bonding energy between carbon atoms, and secondly, the ability of creating double and triple bonds between carbon atoms which increases the number of possible reactions.

When carbon atoms move close to other adjacent atoms, a phenomenon called hybridizations occurs and build multi-atomic structures in various physical forms— known as allotropes. Allotropes are constituted of carbon atoms bonded by sp^2, sp^3 and combinations of both hybridizations. There are many types of carbon allotropes depending on various covalent chemical bonds with the neighboring carbon atoms as stated below.

❖ *Diamond*

Diamond is famous for its very high hardness and dispersion of light. In diamond, each carbon atom forms tetrahedral bond to four other carbon atoms by covalent bonds in the sp^3 hybridization of the electron configuration, forming the diamond lattice as a variation of the face-centered cubic structure [Figure 2.11(a)]. Diamond exhibits the highest hardness of all known materials, very high thermal conductivity of 900 – 2320 $Wm^{-1}K^{-1}$, wide bandgap of 5.5 eV, high optical dispersion, and insulating electric properties.

❖ *Graphite*

Graphite shows a stable trigonally bonded crystal structure [Figure 2.11(b)], where carbon atoms are bonded by sp^2 hybridizations. The atoms are arranged in parallel and single-atom planes, called graphene. Carbon atoms from adjacent planes are bonded by weak dispersion van der Waals forces. Due to altered structure, graphite shows different properties. This material is soft, optically opaque, chemically active, and is a good electric conductor.

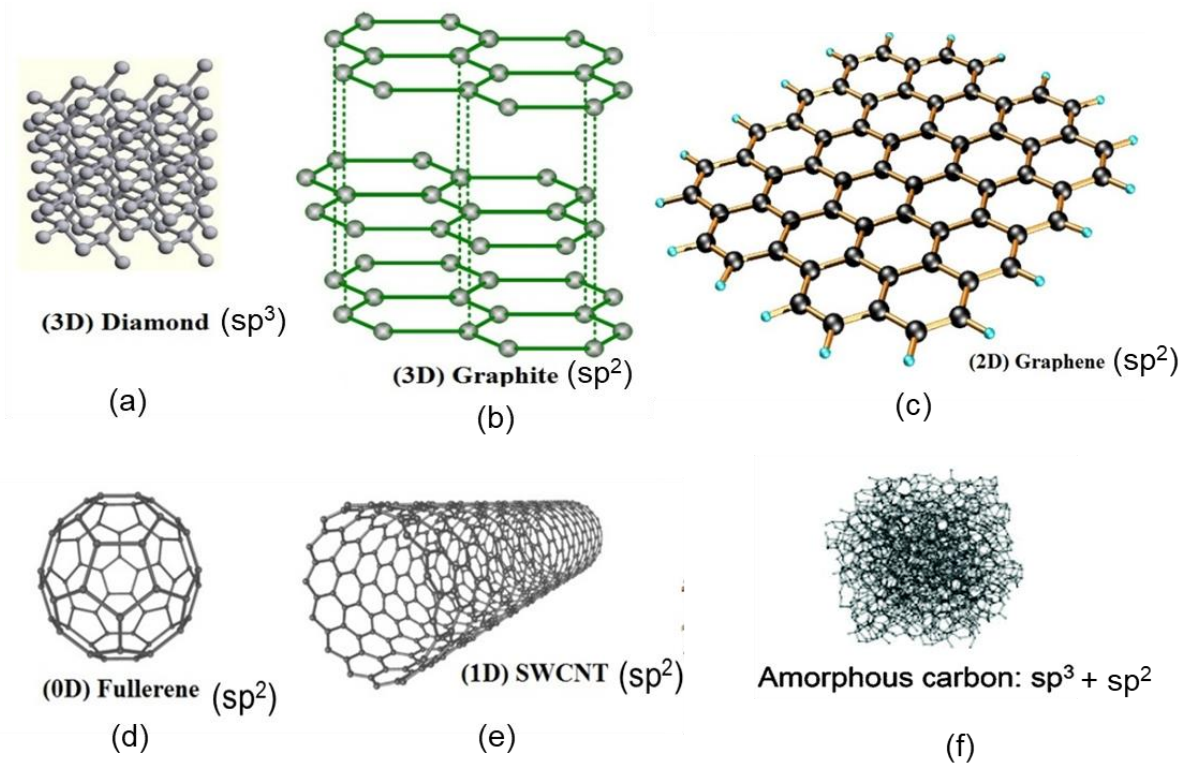

Figure 2.11. Allotropes of carbon: (a) diamond, (b) graphite, (c) graphene, (d) fullerene, (e) carbon nanotube, and amorphous carbon.

❖ *Graphene*

Graphene is an atomic-scale honeycomb lattice made of carbon atoms [Figure 2.11(c)], firstly achieved by Novoselov et al. [18] in 2004. It is undoubtedly emerging as one of the most promising nanomaterials, because of its unique combination of superb properties, include high strength and good conductivity of heat and electricity, resulting in an intense investigation of 2D materials. Graphene opens a wide domain of applications ranging from electronics to optics, sensors, and bio-devices.

❖ *Fullerene*

Fullerene structure [Figure 2.11(d)] was discovered by Kroto *et al.* [19] in 1985. First fullerene C_{60} was the first fullerene, composed of 60 carbon atoms arranged in 12 pentagons and 20 hexagons, in the shape of a "soccer ball". Afterward, various forms of fullerenes were observed such as C70, C76, C82, etc. Their unique molecular structure of fullerene results in extraordinary macroscopic properties, including high tensile strength, high electrical conductivity, high ductility, high heat conductivity, and relative chemical inactivity.

❖ *Carbon nanotube*

Carbon nanotubes (CNTs) were found by Sumio Iijima in 1991 [20]. CNTs have cylindrical carbon structures [Figure 2.11(e)]. They can be rolled up into a tube shape by one

atomic layer of graphene sheet as single-walled carbon nanotubes (SWCNTs) and multi-layers of graphene sheets as multi-walled carbon nanotubes (MWCNTs). They have a very high ratio surface area. Due to CNTs consisting of graphitic layers, the sp^2 bonding of graphite are more strength than sp^3 bonding in the other kind of carbon like diamonds. Also, CNTs can be formed as armchair, zigzag, and chiral tubes due to a unit vector of graphene crystal lattice.

❖ *Amorphous carbon*

Carbon can form an amorphous phase. Amorphous carbon (a-C) is obtained under controlled deposition by mixing of diamond (sp^3) and graphite (sp^2) structures and thus, it does not have any crystalline structure [Figure 2.11(f)]. a-C materials can also be stabilized by forming bonds with hydrogen (H). The structure and properties of a-C materials is mainly determined by composition ratios of sp^3-C, sp^2-C and H [21]. Amorphous carbon has attracted much attention, because of both scientific interest and promising industrial applications, owing to their excellent, wide-ranging physical and chemical characteristics.

2.5. Diamond-like carbon

2.5.1. Introduction

Studies of Diamond-like carbon (DLC) has been performed extensively since 1971, when Aisenberg and Chabot [22] first prepared such carbonaceous films by ion beam deposition that showed the properties of that resembled diamond as opposed to graphite. The transparency of the films indicated the absence of free electrons and the current-voltage measurement showed the high resistivity. It was found that these carbon films had many of the properties similar to diamond but the films were predominantly amorphous in nature and not a single crystal. Thus the name “diamond-like carbon” (DLC) material was introduced.

It is stated by the International Union of Pure and Applied Chemistry (IUPAC) that “Diamond-like carbon (DLC) films are hard, amorphous films with a significant fraction of sp^3-hybridized carbon atoms and which can contain a significant amount of hydrogen. Depending on the deposition conditions, these films can be fully amorphous or contain diamond crystallites. These materials are not called diamond unless a full three dimensional crystalline lattice of diamond is proven.”

However, DLC films have attracted increasing interest because of their many unique properties such as chemical inertness, thermal stability, optical transparency, high breakdown voltage, tunable band gap, low friction coefficient, high electrical resistivity and low dielectric constant, biocompatibility, and so on. These properties of DLC films make them ideal for a variety of microelectronic, technical and industrial applications, as summarized in Table 2.3.

Table 2.3. Summary of properties and applications of diamond-like carbon films [23]

Property	Type of use	Applications
Transparency in Vis and IR	Optical coatings	Antireflective and wear-resistant coatings for IR optics
Chemical inertness to acids	Chemically passivating coatings	Corrosion protection of magnetic media, biomedical
High hardness, low friction coefficient	Tribological, wear-resistant coatings	Magnetic hard drives, magnetic tapes, razor blades, bearings, gears
Nano-smooth	Very thin coatings	Magnetic media
Wide range of electrical resistivity	Insulating coatings	Insulating films
Low dielectric constant	Field emission	Field emission flat panel displays

2.5.2. Classifications of DLC

The types of DLC films depends on the relative concentration of the carbon atoms bonded by sp^2 and sp^3 hybridization as well as H distribution among these types of bonds. Figure 2.12 shows a ternary phase diagram of amorphous carbons depending on the sp^2, sp^3 and H concentrations, where the three corners correspond to diamond, graphite, and hydrocarbons, respectively. Depending on the sp^3 content and hydrogen content, DLC films can be classified into the following categories [24-25]:

❖ Tetrahedral amorphous carbon (ta-C)

ta-C is the DLC films consisting of the maximum sp^3 content (80-80%) and does not contain H. Its mechanical properties become diamond-like for very high sp^3-carbon contents. Thus, ta-C exhibits a very high hardness (80 GPa), which in many cases contributes to even better wear and friction performance compared to hydrogenated amorphous carbon.

❖ Hydrogenated amorphous carbon (a-C:H)

Hydrogenated amorphous carbon (a-C:H) films may contain up to 20-70% hydrogen and are quite different from the hydrogen free DLC films. Practically, the performance of the a-C:H films strongly depends on the ratio of sp^3 and sp^2 hybridizations and also on the hydrogen content. By varying the ratio of sp^3 and sp^2 bonds and H content, a wide range of films properties can be modified, which is one of the major goals of this thesis. However, hydrogenated amorphous carbon can also be classified into four types: —

(i) Polymer-like a-C:H (PLCH): This type of films has the highest hydrogen content (40–60%). The sp^3 content may be up to ~70%. Hydrogen prefers to bond in a sp^3 configuration.

These films are soft with low density and most of the sp^3 bonds are terminated by hydrogen. Its band gap above 2 eV and can reach up to 4 eV.

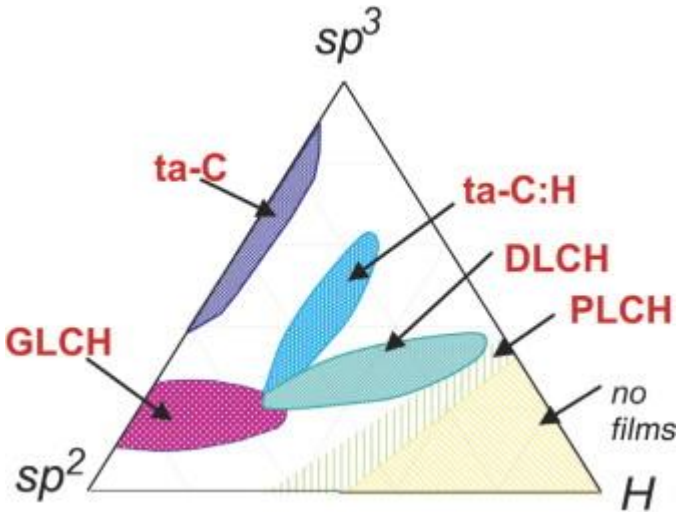

Figure 2.12. Ternary phase diagram of amorphous carbons. The three corners correspond to diamond, graphite, and hydrocarbons, respectively [25].

(ii) Diamond-like a-C:H (DLCH): a-C:H film with intermediate hydrogen contents between 20-40% and sp^3 content of 40-60%). They have higher C-C sp3 bond than that of PLCH. Thus, they have superior mechanical properties and their optical gap is between 1 eV and 2 eV.

(iii) Hydrogenated tetrahedral amorphous carbon (ta-C:H): This class of a-C:H is characterized with highest C-C sp^3 content up to 70% and hydrogen content about 25-30%. It has higher density (up to 2.4 g/cm^3), hardness (~50 GPa) and optical gap (2.0-2.4 eV).

(iv) Graphite-like a-C:H (GLCH): These types of amorphous carbon have low hydrogen content (less than 20%). They have high sp^2 content and sp^2 clustering. The band gap is less than 1eV. The conductivity of graphite-like amorphous carbon is very high close to that of graphite.

In addition, a few materials can be added to DLC films to improve their properties such as Si, N, metal atoms, and F. Accordingly, they are denoted by Si-C:H, a-C:H-N, Me-C:H, and a-C:H-F, respectively.

2.5.3. Synthesis of DLC films

The controllability of the growth parameters enhances the carbon microstructures as well as the properties of DLC films. Relatively lower cost of production and a broad variety of growth process may make this material attractive for numerous applications in industry.

2.5.3.1. *Growth mechanism*

To grow DLC films, it is essential to maximize the C-C sp^3 bonding, which is the liable of the mechanical properties of DLC films. The key process to enhance sp^3 bonding in DLC films is the ion bombardment process [26-27]. It is observed that the highest sp^3/sp^2 ratios are achieved by C^+ ions with ion energy around 100 eV.

However, special sputtering of sp^2 bonds during DLC film growth was considered as the main mechanism that increased sp^3 content by E.G. Spencer in 1976 [28]. Later, Lifshitz et al. [28] in 1990 investigated that DLC film growth was sub-surface. Then, the so-called *subplantation* model considers the advanced densification of DLC in a sub-surface layer. It is associated to the formation of metastable sp^3 sites owing to the penetration and relaxation of energetic ions as shown in Figure. 2.13. However, incoming neutrals and low-energy ions do not penetrate the surface and may stick onto the film surface, generating there a sp^2 rich outer layer. Moreover, the surface population is increased by sub-planted high-energy ions that overcome an energy barrier and, then, are able to relax to the more stable surface sp^2 states by an energy dissipation process [30].

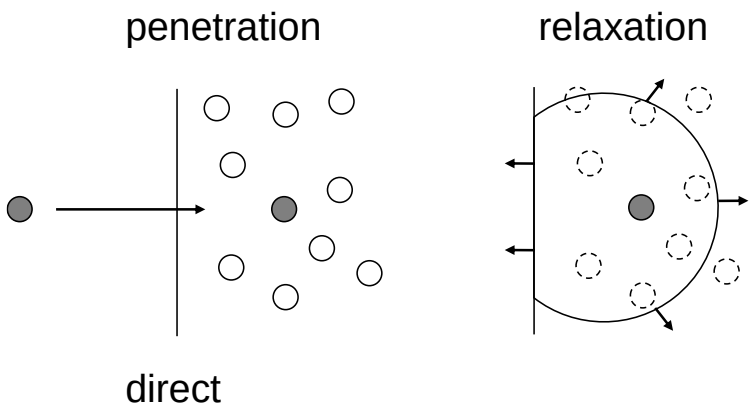

Figure 2.13. Schematic diagram of a subplantation process; direct penetration and relaxation mechanism of a densified region [31].

2.5.3.2. *Deposition methods of DLC*

The synthesis of a-C thin films is carried out by various deposition methods, as shown in Figure 2.14. Among these, some methods are suitable for laboratory studies, whereas some others are preferred in industrial applications

- *Ion beam deposition*

Ion beam deposition was the first method used for the synthesis of DLC by S. Aisenberg and R. Chabot in 1971 [22]. Carbon and hydrocarbon ions are generated by the sputtering of a graphite cathode. The generates ions are accelerated to the substrate by a bias voltage. Ion beam

sources can run well at higher ion energy ranges of 100-1000 eV. Moreover, mass selected ion beam (MSIB) techniques can provide a suitable selection of ion species and energy on the growing films, allowing precise control of deposition. However, due to relatively low deposition rate, this method is limited only for laboratory research. Besides, the ratio of energetic ions to neutral species is low, and thus, mechanical properties of DLC films by this method are not optimum [30-31].

❖ *Cathodic Arc*

Cathodic arc is an old vacuum deposition technique, where electric arc is employed to evaporate material from a cathode target. Due to high ion densities (~10^{12} A/m^2), the ionization of species becomes 100% of the total flux, and the maximized parameter is the electron current to the anode, which is called arc current. This method is really appropriated to obtain hard DLC films, with a significant sp^3 fraction. However, due to some difficulties, this method is limited in laboratories uses. Firstly, the films growing is not homogeneous and secondly, the production of micro-particles needs a filtering device. The second problem is solved by a filtered cathodic vacuum arc (FCVA) using a magnetic filter in S-bend or single bend configuration [30-31].

❖ *Pulse laser deposition*

Pulsed laser deposition (PLD) delivers energetic ions, as like cathodic arc process. So, it is probable to deposit DLC films with high *sp3* content by PLD, without the requirement of substrate biasing or great current discharges. The strong energy pulses (15-30 ns) of a laser beam are capable to evaporate a carbon target, which shows major advantages in case of graphite owing to reduce of droplets emission. Fluxes of neutrals, ions and particulates are emitted from the target through a strong plasma, which is known as plasma plume. The DLC films grown by PLD can be nanocrystalline diamond and ta-C [30-31].

❖ *Sputtering*

Sputtering is the most common industrial approach for synthesis of a-C films. Generally, Ar plasma is generated by a DC or RF power source. Then carbon radical species are produce by the bombardment of Ar ions on a graphite target, acting as the cathode of electrode. Commonly, magnetron sputtering (magnets attached below the target) is used for more sputter yield. Finally, a-C film would be grown on the surface of the substrate. Moreover, a-C:H films can be attained by using Ar and H_2 plasma. A dc bias power can also be employed to the substrate for the control of the ion energy. Usually, sputtering is also a popular method for industrial application to fabricate many different kinds of thin films by changing various target sources. However, the problem of relative low density of sp^3-C in the growth of DLC films exists in sputtering.

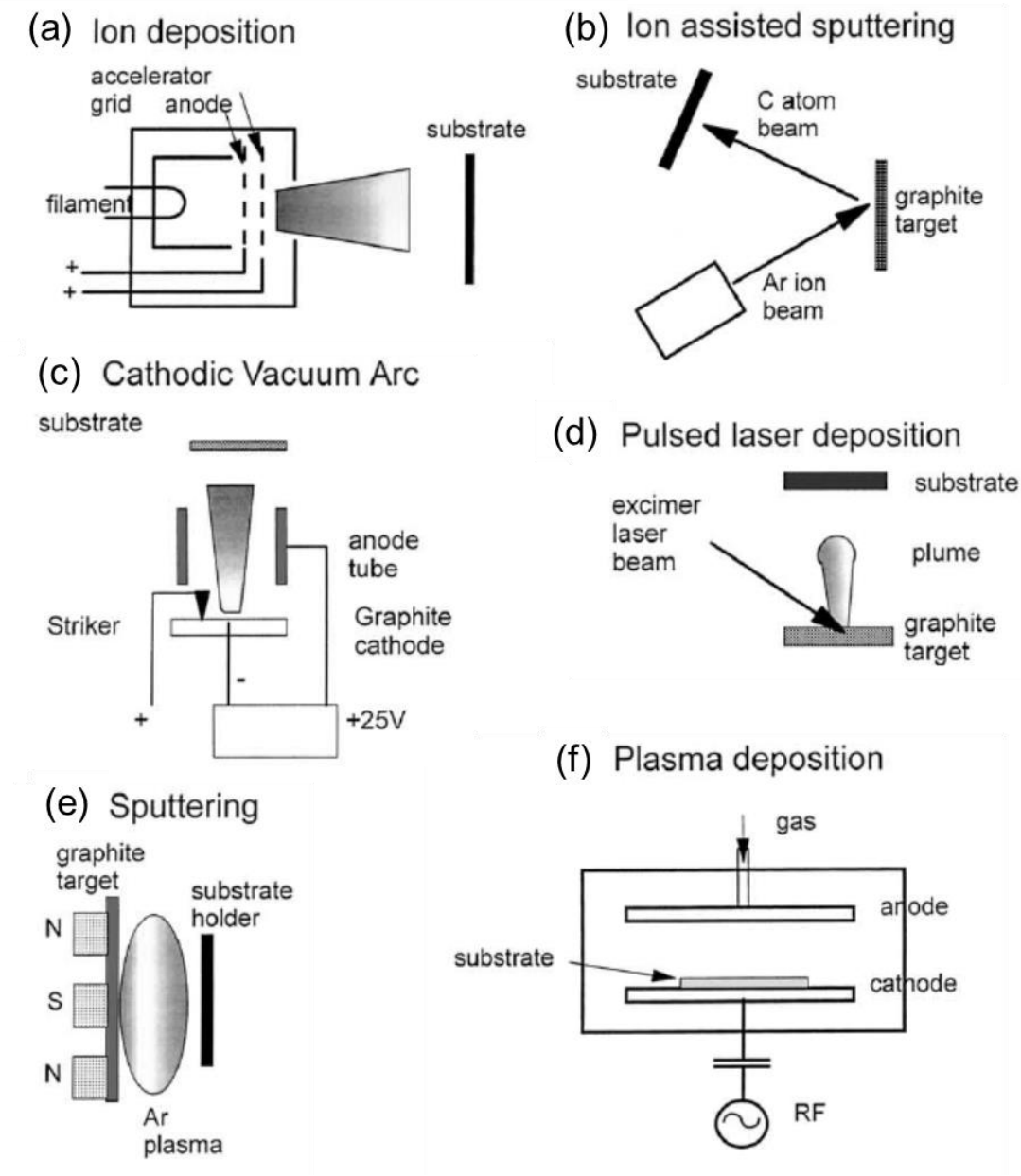

Figure 2.14. Schematics of various deposition systems for DLC [30].

❖ *Plasma-enhanced chemical vapor deposition*

Plasma-enhanced chemical vapor deposition (PECVD) is the most popular synthesis technique of DLC films from hydrocarbon gases for laboratory research. Generally, in PECVD, plasma is generated between two parallel electrodes, known as *capacitively coupled plasma* (CCP), where power is applied to the lower electrode (cathode), holding the substrate, and the upper one (anode) is kept grounded. For deposition of DLC films, the supplied power cannot DC, as DLC is electrically insulating. Thus, the PECVD processes of DLC films are driven by most common RF power.

Usually, the chamber wall of the reactor is grounded and the area of the grounded electrode becomes larger than that of the RF coupled one. When the RF power is applied, asymmetrical

discharge occurs, and both electrons and ions move and follow the change of electrical field. Electrons move faster than ions due to low mass that will cause an excess of ions accumulated near the electrodes, which is known as plasma sheath. Generally, plasma sheath acts as a diode, so that the RF voltage between electrodes can be considered as a DC self-bias voltage. This negative bias of substrate cathode accelerates the bombarding ions on the substrate to create sp^3 content. As the ion energy is vital for growth of DLC films, the collision of ions with other species should be avoided, to reduce an energy loss of ions. So, the mean free path of ions should be longer than the sheath thickness and relatively a lower pressure of precursor gas is preferable for the synthesis of DLC films by PECVD [30-31].

The advantage of PECVD are low temperature deposition, high deposition rate, large coverage, and uniform deposition area [30]. Basically, PECVD method is the chemical reaction in vapor phase of the constitutive elements in plasma to form material precursors. In a typical, PECVD process the substrate is exposed to one or more volatile precursors, which react and/or decompose on the substrate surface to grow films. Volatile by-products are often also produced, which are removed by gas flow through the reaction chamber. All these processes have a strong effect on the properties of the deposited films.

In PECVD, plasma is the key parameter and the growth process shows an important dependence of the reactor shape and of the technological parameters for the generation of plasma.

References

[1] Y.P. Raizer, *Gas Discharge Physics*, 1st ed., Springer-Verlag Berlin Heidelberg, 1991.

[2] M.J. Druyvesteyn and F.M. Penning. "The mechanism of electrical discharges in gases of low pressure". *Rev. Mod. Phys.*, 12(2) ,87– 176, (1940).

[3] M.A. Lieberman, A.J. Lichtenberg, *"Principles of Plasma Discharges and Materials Processing",* Wiley, New York, 1994.

[4] A. Schutze, J.Y. Jeong, S.E. Babayan, J. Park, G.S. Selwyn, R.F. Hicks, "The Atmospheric-Pressure Plasma Jet: A Review and Comparison to Other Plasma Sources", *IEEE Trans. Plasma Sci.* 26, 1685, (1998).

[5] J. Laimer, M. Fink, T. A. Beer, and H. Störi, "Plasma dynamics as a key to successful upscaling of pulsed plasma processes", *Surf. Coatings Technol.*, 174-175, 118 (2003).

[6] J. Choi, "Introduction of the magnetic pulse compressor (MPC) - Fundamental review and practical application," *J. Electr. Eng. Technol.* 5(3), 484–492, (2010).

[7] T. G. Engel, and W. C. Nunnally, "Design and operation of a sequentially-fired pulse forming network for non-linear loads", *IEEE Trans. Plasma Sci.* 33, 2060–2065, (2005).

[8] S. Zabihi, F. Zare, G. Ledwich, A. Ghosh, and H. Akiyama, “A new family of marx generators based on commutation circuits,” *IEEE Trans. Dielectr. Electr. Insul.* 18(4), 1181–1188, (2011).

[9] Y. Wu, K. Liu, J. Qiu, X. Liu, and H. Xiao, “Repetitive and high voltage marx generator using solid-state devices,” *IEEE Trans. Dielectr. Electr. Insul.* 14(4), 937–940, (2007).

[10] J. Rao, Z. Li, K. Xia, and S. Xin, “An all solid-state repetitive high-voltage rectangular pulse generator based on magnetic switch,” *IEEE Trans. Dielectr. Electr. Insul.* 22(4), 1976–1982, (2015).

[11] L. Pang, Q. Zhang, B. Ren, and K. He, “A compact repetitive high-voltage nanosecond pulse generator for the application of gas discharge,” *Rev. Sci. Instrum.* 82(4), 043504, (2011).

[12] T. Shao, W. Huang, W. Li, C. Zhang, Y. Zhou, P. Yan, and E. Schamiloglu, “A cascaded microsecond-pulse generator for discharge applications,” *IEEE Trans. Plasma Sci.* 42(6), 1721–1728, (2014).

[13] R. Chen, J. Yang, X. Cheng, and Z. Pan, “An all-solid-state microsecond-range quasi-square pulse generator based on fractional-turn ratio saturable pulse transformer and anti-resonance network,” *Rev. Sci. Instrum.* 88(3), 34701, (2017).

[14] T. Yokoo, K. Saiki, K. Hotta, and W. Jiang, “Repetitive Pulsed High-Voltage Generator Using Semiconductor Opening Switch for Atmospheric Discharge,” *IEEE Trans. Plasma Sci.* 36(5), 2638–2643, (2008).

[15] W. Jiang, K. Yatsui, K. Takayama, M. Akemoto, E. Nakamura, N. Shimizu, A. Tokuchi, S. Rukin, V. Tarasenko, and A. Panchenko, “Compact solid-state switched pulsed power and its applications,” *Proc. IEEE* 92(7), 1180–1195, (2004).

[16] https://en.wikipedia.org/wiki/Power_semiconductor_device

[17] https://www.utdallas.edu/~overzet/Puls_97/sld006.htm

[18] K. S. Novoselov, A. K. Geim, S. V. Morozov, D. Jiang, Y. Zhang, S. V. Dubonos, et al., “Electric field effect in atomically thin carbon films”, *Science* 306, 666–669, (2004).

[19] H. W. Kroto, J. R. Heath, S. C. O’Brien, R. F. Curl, R. E. Smalley, C60: “Buckminsterfullerene”, *Nature* 318, 162–163, (1985).

[20] S. Iijima, “Helical microtubules of graphitic carbon,” *Nature,* 354, 56–58, (1991).

[21] J. Robertson, “Amorphous carbon”, *Adv. Phys.*, 35(4), 317-374, (2006).

[22] S. Aisenberg and R. Chabot, “Ion-Beam Deposition of Thin Films of Diamondlike Carbon”, *J. Appl. Phys.* 42 (1971) 2953.

[23] A. Grill, “Diamond-like carbon: state of the art”, *Diamond Relat. Mater.*8, 428–434, (1999)

[24] C. Casiraghi, A.C. Ferrari, “Raman spectroscopy of hydrogenated amorphous carbons C. J. Robertson”, *Phys. Rev. B72,* 08540, (2005).

[25] C. Casiraghi, J. Robertson, and A. C. Ferrari, “Diamond-like carbon for data and beer storage”, *Mater. Today*, 10(1-2), 44-53, (2007).

[26] Y. Lifshitz et al., “Growth mechanisms of DLC films from C+ ions: experimental studies”, *Diamond Relat. Mater*., 4, 318-323, (1995).

[27] D. R. McKenzie “Tetrahedral bonding in amorphous carbon”, *Rep. Prog. Phys.* 59 1611, (1996).

[28] E. G. Spencer, P. H. Schmidt, D. C. Joy, and F. J. Sansalone, “Ion-beam-deposited polycrystalline diamondlike films”, *Appl. Phys. Lett.* 29, 118 (1976).

[29] Y. Lifshitz, S. R. Kasi, J. W. Rabalais, and W. Eckstein, “Subplantation model for film growth from hyperthermal species” *Phys. Rev. B* 41, 10468 (1990).

[30] C. Corbella, “Thin film structures of diamond-like carbon prepared by pulsed plasma techniques”, (*Doctoral dissertation,* chap. 2, pp.65, 2005). (Retrieved from—http://hdl.handle.net/10803/1772).

[31] Robertson, “Diamond-like carbon”, *J., Mater. Sci. Eng. R.* 37, 129-281, (2002).

Research Part-I: Pulsed plasma discharge for low-pressure synthesis of carbon thin films

Chapter 3

Pulsed DC plasma CVD system for the synthesis of DLC films

This chapter presents the development of pulsed DC plasma CVD system using a simple pulse power supply and customized CVD apparatus and the investigation of the growth of DLC films on silicon substrates from two different precursor gases with the variation of deposition temperature. The introduction, objectives, experimental methods and results are described. Finally, discussions and conclusions are drawn based on the experimental results.

3.1. Introduction

Diamond like carbon (DLC) is an amorphous carbon that contains a substantial amount of sp^3 bonded carbon. It has great academic and industrial interest due to its excellent properties, for example high degree of hardness, low coefficient of friction, high chemical stability, high optical index and high electrical resistivity. A variety of methods and different deposition conditions have been reported for the preparation of DLC films [1,2]. Among these techniques, Plasma Enhanced Chemical Vapour Deposition (PECVD) is one of the most widespread approaches for industrial applications of producing DLC using plasma technologies. In PECVD, the source gas molecules for thin film deposition can easily be stimulated, dissociated, and even ionized at a considerably low gas temperature [3-5]. Various types of power schemes, for example direct current (DC), radio frequency (RF), microwave and pulsed DC, have been developed for PECVD method. Among these, RF power is mostly used in PECVD particularly depositing DLC films of highly insulating properties, because the substrates were required to be powered with an alternating pulse [6]. The RF PECVD is advantageous to repeat reproducible deposition under an appropriate impedance matching between RF power source and electrode load with a matching circuit. For intentional control of CVD condition, however, the substrate bias voltage, one of important parameters for deposition, is not independent of other conditions but mostly determined by RF power density. Because the substrate bias influences ion energy falling on the growing film, it is expected to be controlled independently.

Pulsed DC plasma CVD is considered as an alternative to the RF PECVD and supposed to be a simple and cost effective deposition system that can be used to improve film properties as compared to widely used RF system [7]. In a pulsed DC PECVD system, pulsed DC power supply is a significant component for the reason that it may possible to change the gas phase chemistry, energy of ions bombardment on substrate, electron density, electron temperature to meet the requirements of highly selective deposition process by varying the pulse parameters [8,9]. However, most of the models of commercially available pulsed DC power supplies are expensive and custom-made which led to less flexibility to control pulse conditions. Consequently, a number of researchers reported pulsed DC power supplies with different approaches [10,11]. These works were reported to use magnetic pulse compression (MPC) technique to transfer charge and pulse transformers for high voltage isolation which lead to increase of cost as well as decrease the flexibility to vary pulse width. In addition, an asymmetrical bipolar pulsed DC power source has been reported for plasma CVD [12-15] where the voltage waveform consists of a fixed positive pulse amplitude followed by a variable negative pulse with a variation of duty cycle and frequency. However, we developed a simple unipolar configuration, variable pulse width and frequency, solid state switching based pulsed DC power supply for plasma CVD where the voltage waveform consists of a variable negative pulse followed by a ground voltage and a current control circuit is introduced to sustain the constant plasma discharge current within each pulse for a set value regardless of plasma characteristics impedance.

Usually, the deposition of DLC films are obtained from hydrocarbon source gases for example CH_4, C_2H_2 and C_6H_6 [16,17] by plasma CVD. The fabricated films come to be hydrogenated amorphous carbon (a-C:H) due to amalgamation of hydrogen (H) content from hydrocarbon source gases. It is recognized that microstructure of DLC films are considerably influenced with monovalent H content because it performs as terminating element of carbon-carbon bonds. It can restrict the formation of carbon-carbon sp^3 bonding that is preferred in DLC films [18, 19]. For reduction of hydrogen content in DLC films during deposition, one of the way to utilize hydrocarbon gases with lower H concentration. Considering these aspects, acetylene (C_2H_2) has been widely used. Moreover, carbon monoxide (CO) which is a hydrogen free gas can be an interesting candidate of carbon source for DLC films growth [20].

3.2. Objective

In this study, a prototype pulsed DC plasma CVD system was developed using a simple half-bridge switching circuit. Deposition of DLC films was performed from C_2H_2 and CO source gas with variation of substrate temperature. Because the substrate temperature during

deposition by the plasma CVD can dramatically change the DLC film properties [21], films were deposited both at room temperature and an increased temperature for comparison. The results were compared to our previous ones using a conventional RF CVD system [20].

3.3. Experimental procedures

3.3.1. Development of pulsed DC plasma CVD system

A prototype pulsed DC plasma CVD system was developed employing a minimum sized and conventional styled CVD apparatus, and a pulsed DC power supply to carry out the experiments. The photograph of the developed system is shown in Figure 3.1, however, for better understanding a simplified schematic view is presented in Figure 3.2.

❖ *CVD apparatus*

In this CVD apparatus, plasma chamber made of stainless steel has a small volume about 1.6 L which is much smaller than our previous RF plasma CVD chamber [20]. It is assumed that large volume of plasma is not effective for deposition but the interface between plasma and depositing surface performs most of chemical reaction. Because a larger volume of plasma will increase loss of material gas and electrical power, the chamber volume was intentionally reduced to the minimum size. The main vacuum chamber was a short cylindrical tube of 160 mm in inner diameter and 120 mm in height with 2.4 L in total volume. The actual volume for plasma operation was reduced to 1.6 L due to the volume of electrode.

The substrate holder (electrode) is round in shape with diameter of 118 mm. The upper part of the electrode is partially covered by a top cover that is grounded. The gap between grounded portion and the electrode is kept 2 mm to be confined the plasma only on the substrate. A circular deposition window of 90 mm in diameter is designed on the top of the electrode to enhance the deposition area as compare to our previously used RF CVD system with a deposition window of 30 mm in diameter.

An insulated heater with mosquito coil shape is embedded inside the electrode to facilitate the uniform temperature all over the electrode as presented in Figure 3.3. The core heating element of the heater is solid Nichrome wire. To protect the heating element from oxidation, the Nichrome wire is surrounded by a sheath material of stainless steel that is isolated from the heater wire by a compacted insulating but high thermal conducting layer. This strategy is advantageous in such a way that heating wire does not need to keep electrically isolated from the other parts of the heater assembly. The substrate temperature is monitored and controlled by a conventional thermocouple based temperature controller operated manually.

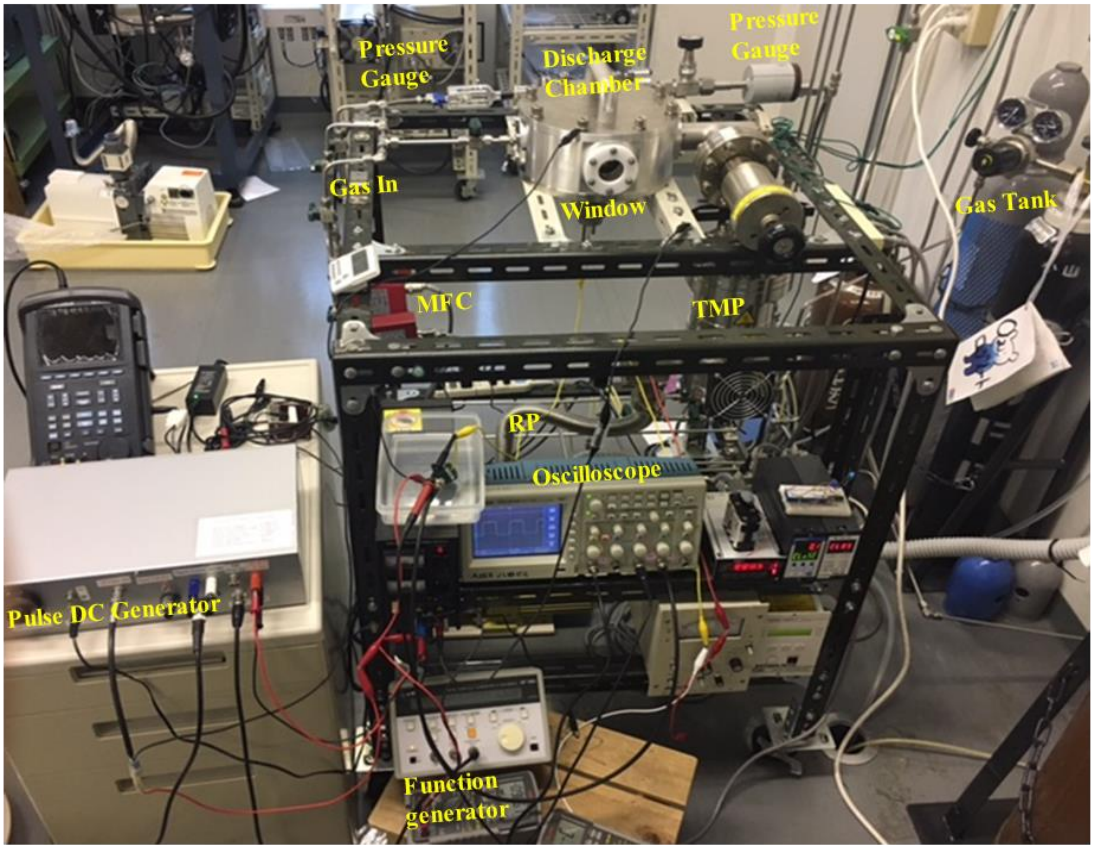

Figure 3.1. Picture of the developed pulsed DC plasma CVD system

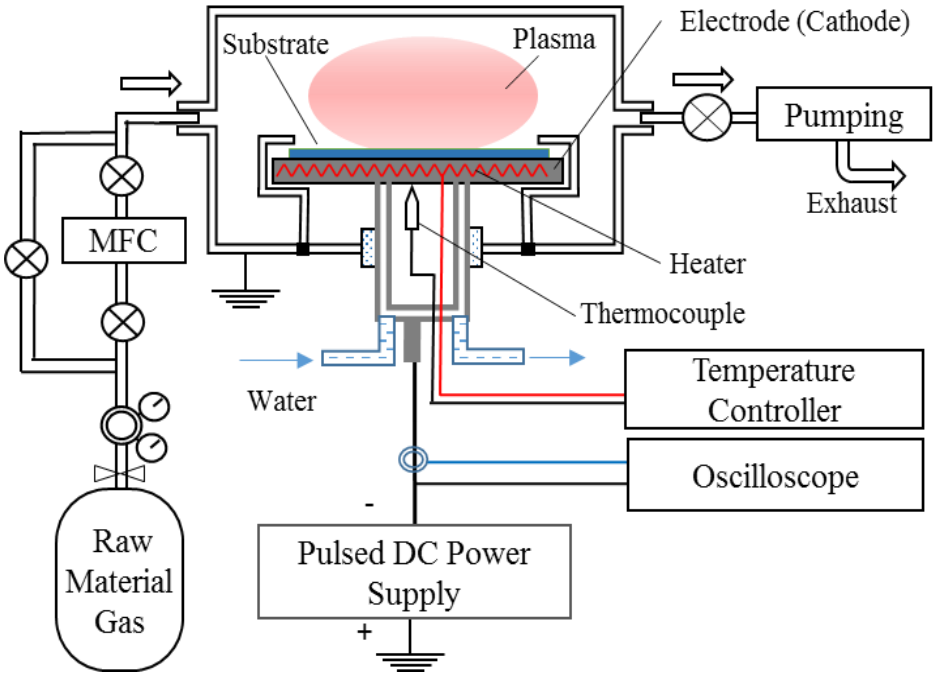

Figure 3.2. Schematic view of developed pulsed DC plasma CVD system.

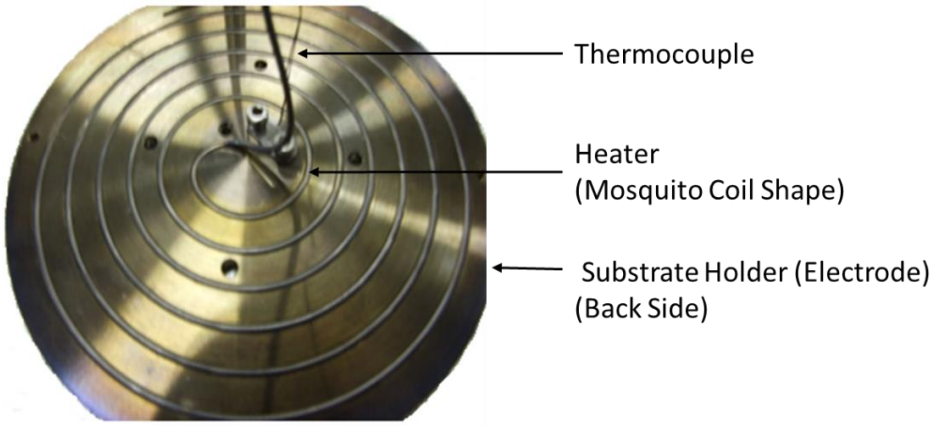

Figure 3.3. A view of substrate heater arrangement.

The gas flow arrangement is built and evacuation of the chamber is performed by an exhaust valve, a turbo molecular pump (TMP) and a rotary pump (RP). Water cooling is used for the safety of vacuum chamber during high temperature CVD operation. Lastly, the whole system structure was assembled in such a way as shown in Figure 3.2 to ensure electrically isolation among high voltage and low voltage sides.

❖ *Pulsed DC power supply (Pulsed DC Generator)*

A pulsed DC power supply was designed in a simple approach to carry out the pulse plasma discharges. The detail circuit layout and photo of the fabricated pulsed DC generator is shown in Figure 3.4 (a) and (b). In addition, Figure 3.5 shows the simplified schematic diagram of the pulsed DC power supply developed with considering the plasma discharge behavior for CVD. The diagram shows that the pulsed DC Power supply has three main blocks consisting of a high voltage DC power supply (HV DC PS), a solid-state switching unit (SSU) and a pulse generator (PG) enclosed by dotted lines in the diagram.

In this design, a high voltage regulated DC power supply (TMK 1.0-50, Takasago Ltd. Japan) is employed as the charger of the primary capacitor C0. This model of power supply can deliver variable voltage from 0-1 kV with a maximum output current of 50 mA. The foremost part SSU is employed for chopping the voltage stored in capacitor C0 to generate pulsed DC. The switching technique in SSU follows the half-bridge inverter topology [22]. SSU consists of a couple of Silicon-Carbide Metal-Oxide-Semiconductor Field Effect Transistors (SiC MOSFETs, SCT2450KE), named as M1 and M2, operated as high voltage switches. The MOSFETs are operated by gate driver circuits isolated by widely used photo-coupler TLP 351 (for simplification, detailed circuits are not shown).

As indicated in Figure 3.6, gate pulse of V_{G1} and V_{G2} are alternately applied to M1 and M2, respectively, from the pulse generator (PG) unit. When M1 is turned on, a negative voltage

from the power supply is applied to the electrode for a duration t_1. In turn, when M2 is turned on with a small delay time t_2 after turning off the M1, the electrode is grounded. After an interval for t_3, M1 is turned on with a small delay t_4 after M2 is turned off. The modulated output for the electrode is square wave negative pulsed DC voltage with wide variation of frequency and pulse width which are expected as useful parameters for control of film properties [23]. The pulse parameters are easily set by a high resolution function generator (DF1906, NF Corporation, Japan). In the used circuit, however, the maximum pulse frequency was limited below 40 kHz due to the response of the conventional photo-coupler.

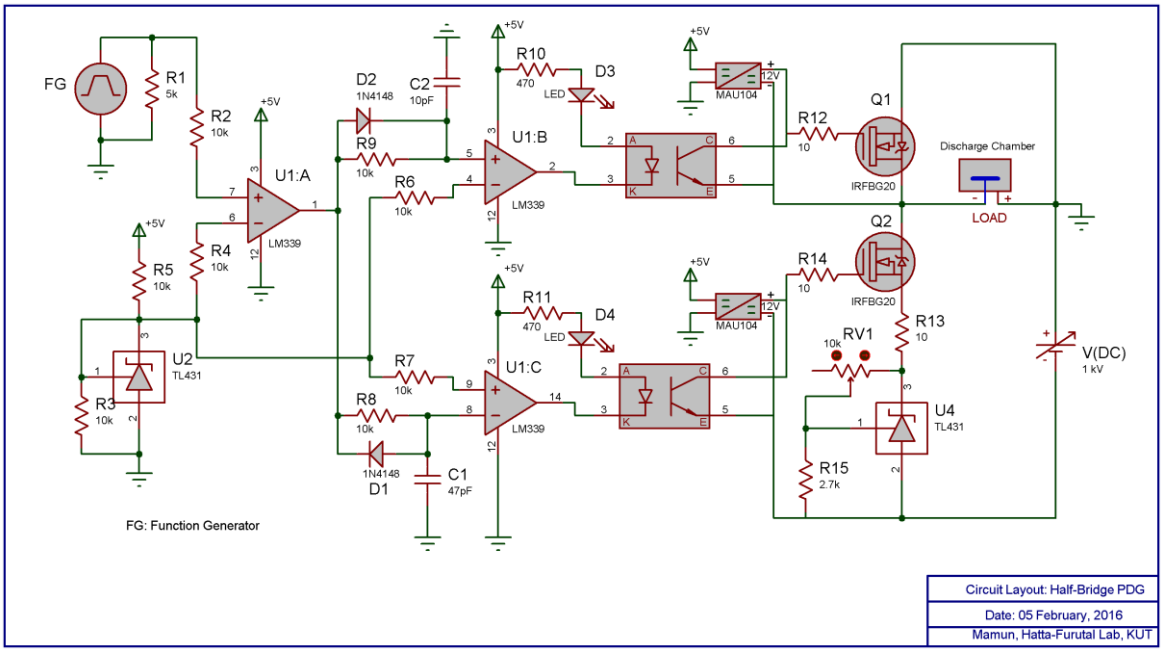

(a)

(b)

Figure 3.4. (a) Detail circuit diagram (b) image of the Half-Bridge Pulsed DC power supply.

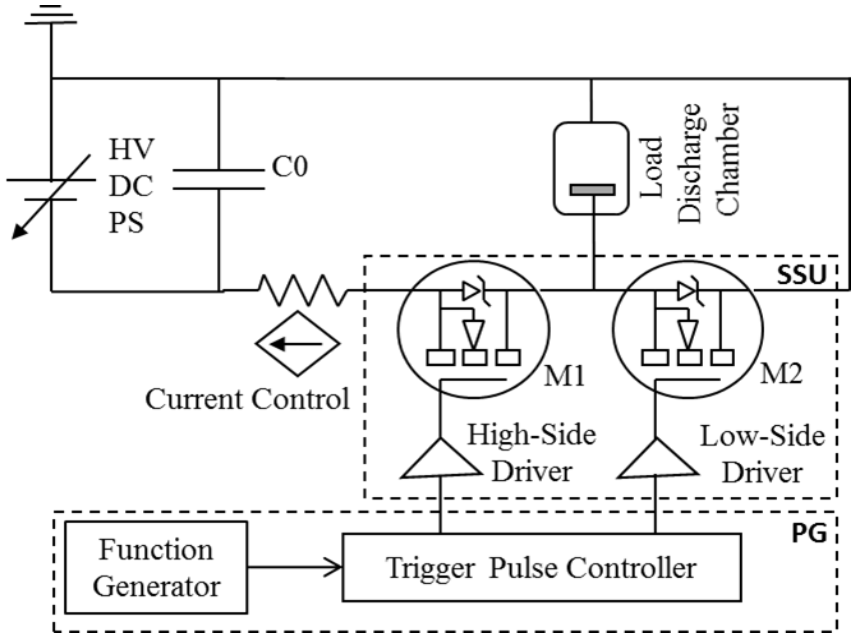

Figure 3.5. Schematic drawing for the pulsed DC power supply.

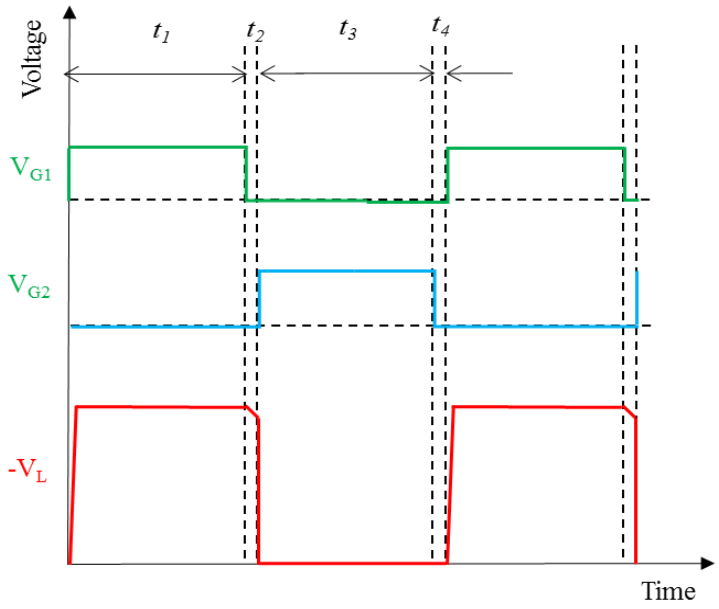

Figure 3.6. Timing sequence of the pulsed DC power supply.

It should be pointed out that one of the advantages of our developed pulsed DC power supply is control of plasma discharge current during discharge within a pulse. When a pulse from the DC power supply is applied to the electrode, which is slightly above the breakdown voltage for a typical discharge conditions, the plasma discharge occurs and discharge current starts to flow. In the case without constant current control, the power supply acts as a voltage source where the sustain voltage will drop due to internal resistance in the power source, so-

called output impedance, and finally match the plasma sustain voltage. Due to variation of plasma impedance, however, the discharge current cannot be controlled well.

In our developed pulsed DC power supply with the constant current circuit, when the discharge current reaches to a certain level, the power supply acts as current source; i.e., the current will tend to remain at the set value regardless of the variation of plasma impedance. The discharge current waveform becomes rectangular shape. Because the electron density of plasma which has been known as one of important plasma parameters for control of chemical reactions, mostly depend on the current density, the control of current level during pulse is important for reproducibility of CVD process. Under the current control mode, as the discharge voltage is completely assigned by the plasma impedance characteristics regardless of increment of input DC voltage, it is possible to apply higher input voltage for plasma ignition. Besides, to protect the power supply from surge current by unintentional arc discharge during operation [24], the current control circuit also performs to sense overcurrent and to limit the current.

3.3.2. Substrate preparation, films deposition and characterization techniques

Before CVD, for the assessment of the pulsed DC plasma system, plasma discharge was examined with wide range of pressure and variation of gas, pulse parameters. From the results of gas discharge, typical deposition conditions for DLC films are chosen as listed in Table 3.1. Due to difference in gas discharge property, C_2H_2 plasma was operated at a lower pressure 15 Pa while CO plasma was at 150 Pa. The operation pressure was intentionally chosen for keeping identical pulsed DC power supply operation. The deposition durations were 5 and 10 minutes for C_2H_2 and CO, respectively. The substrate was heated by the heater in the electrode up to 300^0C or was not intentionally heated. Without heating, the electrode temperature was kept at room temperature (25^0C). The pulse DC power supply was operated at negative high voltage of -800V, discharge current of 20 mA, frequency of 20 kHz and pulse width of 10μs. The actual working voltage of electrode was controlled by the MOSFET M1 to sustain the constant

Table 3.1. Films deposition conditions.

Sample	Gas	Pressure (Pa)	Deposition time (min)	Substrate Temperature (^{0}C)	Flow rate (sccm)	Electrode voltage (pulsed) (-V)	Discharge current (pulsed) (mA)	Frequency (kHz)	Pulse width (μs)
1	**C_2 H_2**	**15**	**5**	**25**	**100**	**800**	**20**	**20**	**10**
2	**CO**	**150**	**10**	**25**	**100**	**800**	**20**	**20**	**10**
3	**C_2 H_2**	**15**	**5**	**300**	**100**	**800**	**20**	**20**	**10**
4	**CO**	**150**	**10**	**300**	**100**	**800**	**20**	**20**	**10**

discharge current. The pulsed DC waveforms were monitored by a digital oscilloscope with a high voltage probe.

DLC films were prepared on Si substrates from C_2H_2 and CO, carbon-containing source gas. The electrode with substrate holder was designed for usage of a 4-inch wafer with an active deposition window of 90 mm in diameter (Figure 3.7 (a)). It is observed to deposit uniform film in whole the deposition window (Figure 3.7 (b)). For experiments, however, to reduce the consumption of Si wafer, a quarter part of the area was used for deposition. A mirror-polished n-type 4-inch Si wafer was cut into quarters as substrates. A cut of Si wafer was set on the electrode with a dummy substrate made of aluminium (Al) to cover the other 3 quarters part of the electrode (Figure 3.7 (c)). Before CVD, argon (Ar) plasma was operated for 1 minute at the same conditions as deposition to treat the substrate surface mostly for removal of inherent oxide layer as illustrated in Figure 3.8.

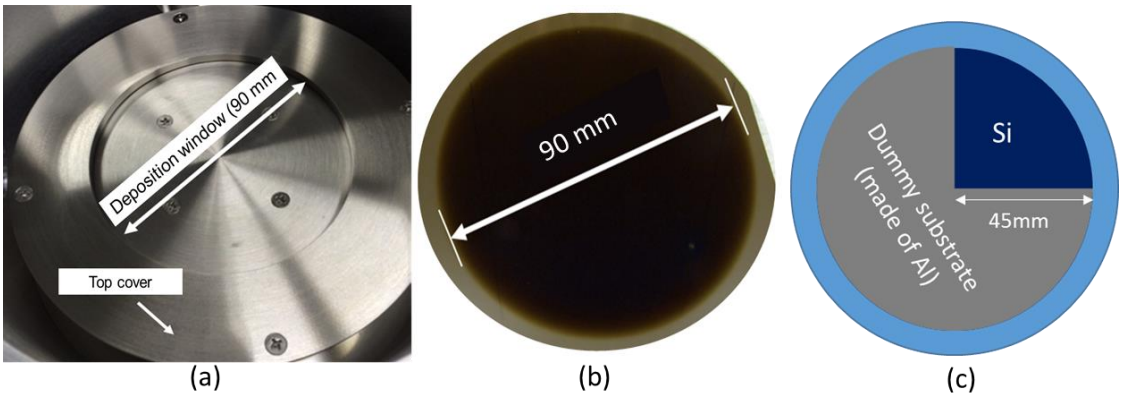

Figure 3.7. (a) Top view of electrode (b) Deposited film of entire deposition window (c) Arrangement of Si substrate and dummy substrate

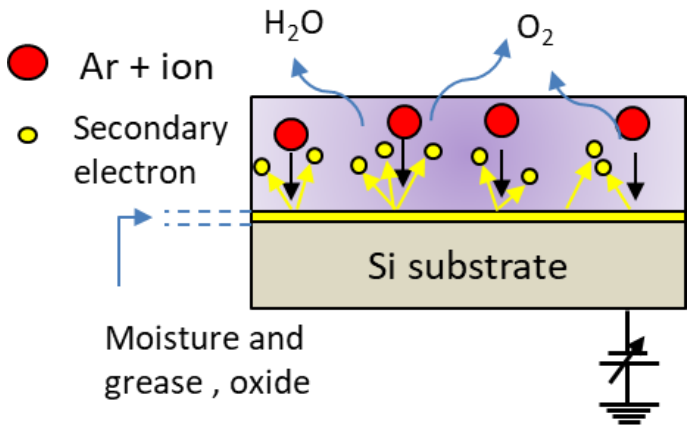

Figure 3.8. Illustration of Si substrate cleaning by Ar Plasma

The characterization of DLC films was carried out by Raman spectrometer (excitation wavelength 532.08 nm, Horiba Jobin Yvon HR-800) and FTIR spectrometer (Jasco FTIR 6100). The thickness of the films was observed using FE-SEM (JEOL JSM-74001) electron microscope.

3.4. Results and discussions

3.4.1 Gas discharge characteristics

Initially, gas discharge was examined at various working gas pressure of Ar by DC power supply to evaluate the discharge characteristics of the CVD apparatus as illustrated in Figure 3.9. It was observed that when a negative voltage over breakdown voltage was applied to electrode of chamber filled with gas, glow discharge occurred and discharge current started to flow [25-27]. Plasma discharge is caused by the impact ionization of electrons and neutral particles of gas molecules accelerated by an applied electric field.

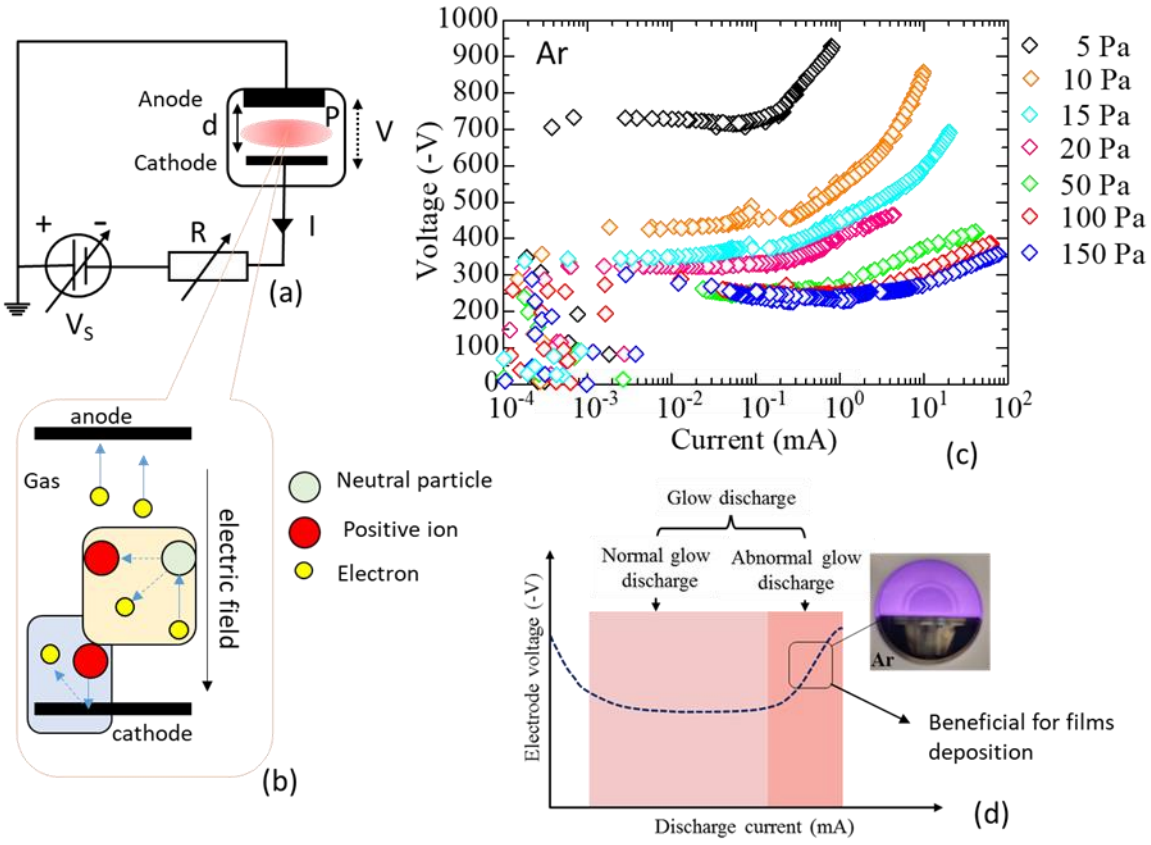

Figure 3.9. Gas discharge experiment (a) simplified schematic (b) discharge mechanism (c) discharge current and voltage waveforms at various working pressure of Ar gas (d) glow discharge characteristics.

There were 2 discharge modes appeared, so-called normal glow and abnormal glow, when the set current was varied. At lower discharge currents than a critical value, the normal glow discharge appeared where the discharge voltage was almost constant with variation of set current. When the discharge current was set at higher than the critical value, the discharge mode turned into abnormal glow where the discharge voltage gradually increased with increase of the set current. It is assumed that, the abnormal glow condition where the plasma covers entire surface of the electrode with increased electron density is superior for CVD operation.

Gas discharge was also examined by the developed pulsed DC plasma CVD system at several discharge conditions to optimize the abnormal glow discharge based on the results obtained from the DC gas discharge experiments. During the high voltage pulse is turned on, the MOSFET switch M1 performs to control the discharge current at the set value by decreasing the actual working voltage of electrode to the required value for the given conditions. Photographs of pulsed plasma discharges of Ar, C_2H_2 and CO gases at typical condition for each gas are presented in Figure 3.10. that confirms the generation of homogeneous abnormal glow plasma discharges.

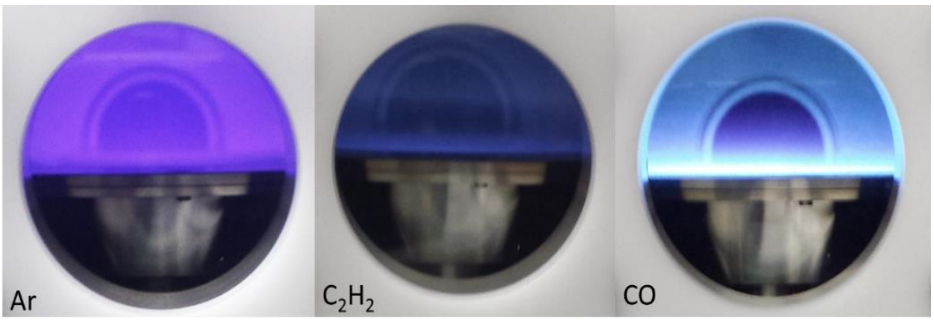

Figure 3.10. Photographs of typical pulsed plasma discharges of Ar, C_2H_2 and CO gas.

3.4.2. Deposited films properties

Figure 3.11 shows photographs for DLC films on Si wafer from C_2H_2 and CO source gas (sample 1 and 2). Sample 1 looks uniform in the deposited area surrounded by a ring shaped interference pattern due to thickness profile at the edge. This ring shaped interference appeared underneath the edge of deposition window in the top cover of electrode. In case of sample 2, a clear edge is observed with a uniform deposition area. The color of sample 1 as compared to Si wafer appeared brown while sample 2 appeared grey. Samples 3 and 4 showed almost the similar physical appearance like samples 1 and 2, respectively (not presented here).

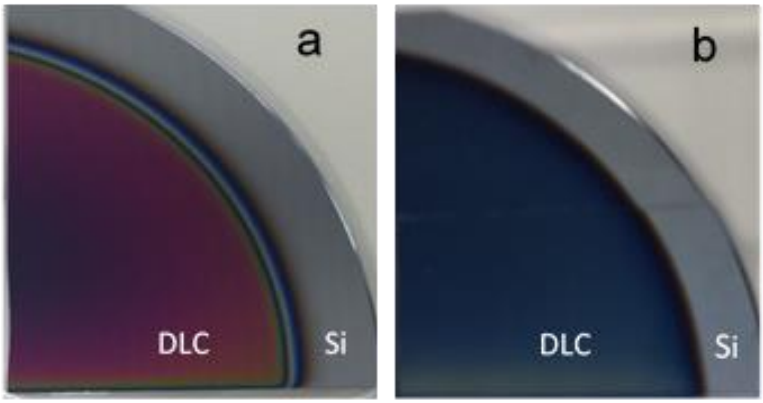

Figure 3.11. Photographs for deposited DLC films from C_2H_2 (a) and CO (b) at room temperature.

Figures 3.12 (a) and (b) show the Raman spectra of samples 1,3 and 2,4 which were deposited from C_2H_2 and CO respectively. Samples 1 and 2 were prepared at room temperature (25ºC) while samples 3 and 4 were at 300ºC. The Raman spectra comprise D peak and G peak regarding at about 1360 and 1590 cm^{-1}, respectively, as well known for typical DLC properties [28]. An example of precise analysis on Raman spectrum with separating two peaks for sample 1 is shown in Figure 3.13. This was subjected to peak separation by curve fitting using the two Gaussian functions. The separated spectra led to a D peak (1302 cm^{-1}) due to defects in six membered ring structure of carbon and a G peak (1520 cm^{-1}) due to the vibration in the regular six membered ring structure of carbon. The intensity ratio of D and G peaks, G peak position, and the full width at half maximum (FWHM) of the G peak evaluated by analysis demonstrate the dominating of nanocrystalline structure in amorphous carbon.

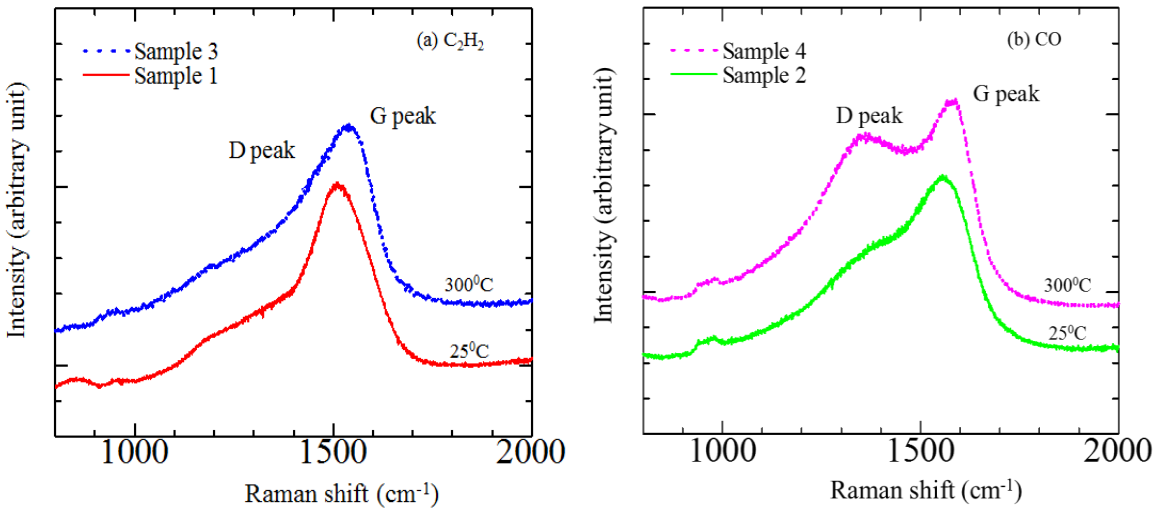

Figure 3.12. Raman spectra for DLC films deposited from (a) C_2H_2 (samples 1 and 3) and (b) CO (samples 2 and 4).

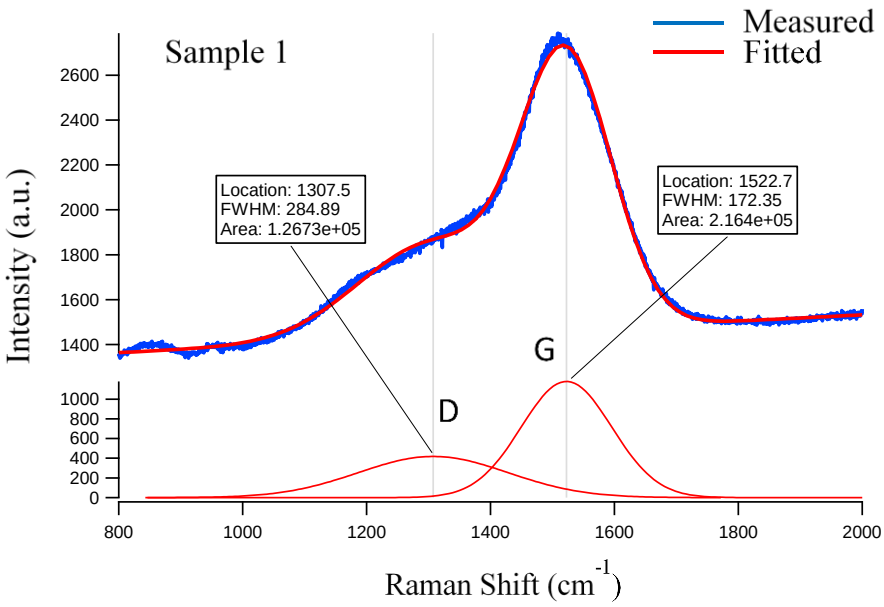

Figure 3.13. Peak analysis on the Raman spectrum for sample 1.

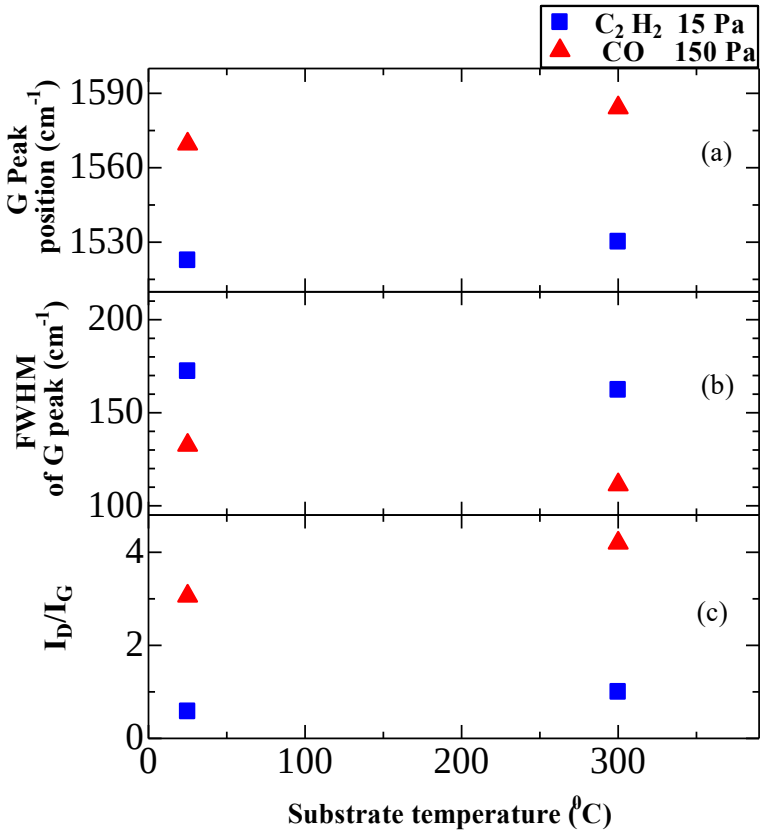

Figure 3.14. Plots of (a) G peak position, (b) FWHM of the G peak and (c) intensity ratio of the D and G peaks (I_D/I_G) as a function of substrate temperature.

The G peak position, FWHM of the G peak, and intensity ratio of the D and G peaks (I_D/I_G) of the deposited films are plotted in Figure 3.14. The distinctive features in the Raman spectra for the films from CO as compared to the films from C_2H_2 were increase of I_D/I_G ratio, decrease

of FWHM of the G peak, and shift of G peak position to the higher wavenumber. The manner of these changes in Raman spectra is usually related to enhanced growth in the number or size of sp^2 bonds of carbon atoms [28, 29]. The results proposed that the DLC films fabricated from CO gas possess progressive graphite-like structures than that fabricated from C_2H_2.

It is assumed that sp^3 bonding structures are stimulated by means of hydrogen atoms through terminating the dangling bonds. It can be expected a larger number of graphitized structure remains in the resulting films from CO rather than C_2H_2 due to low hydrogen content. It is also observed that the increase of electrode temperature introduced similar tendency to incorporate more graphite structure in the films deposited from both CO and C_2H_2 gas. It is supposed that increasing of substrate temperature enhance graphitization producing sp^2 bonds and hydrogen molecules from sp^3 bonds.

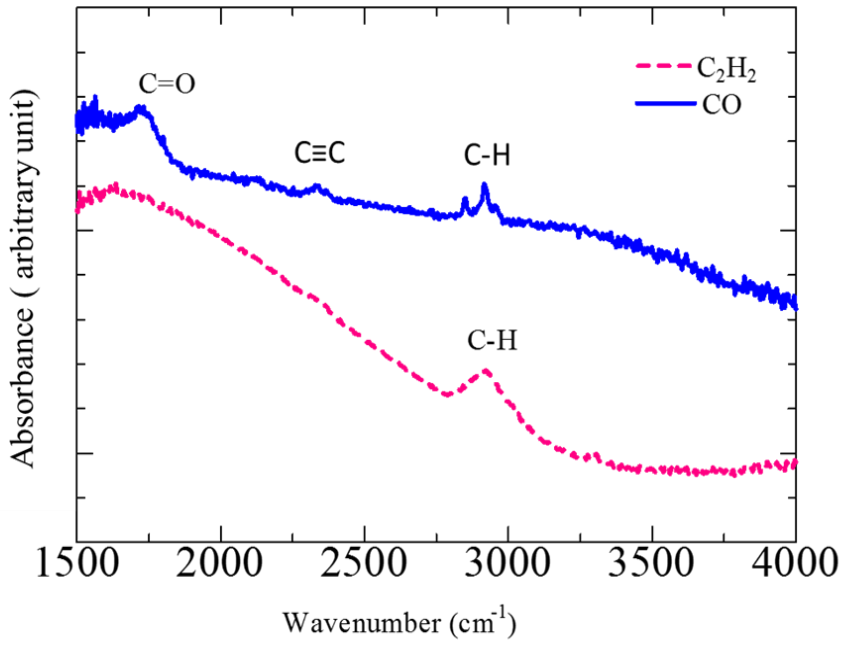

Figure 3.15. FTIR spectra for DLC films deposited from C_2H_2 (sample 1) and CO (sample 2) at ambient temperature (25^0 C).

The FTIR spectra for samples 1 and 2 in the range of 1500-4000 cm^{-1} are shown in Figure 3.15. The spectrum of the DLC from C_2H_2 shows only a broad peak appeared at around 2920 cm^{-1} conforming to C-H stretching mode. It should be pointed out that this peak was associated with the intense asymmetric stretching mode of C-H bonds in the form of asymmetric sp^3-CH and sp^3-CH_2, and enveloped by weaker shoulders of symmetric and asymmetric stretching mode of sp^3-CH_3 between 2850 and 3000 cm^{-1}. Substantial overlap of several of these groups effects in absorption that is objectively broad in this region usually observed in hydrogenated

amorphous carbon films [30]. It recommends that mostly hydrogenated DLC film is obtained from C_2H_2 and the H content is merged to the sp^3 carbon in the film.

The spectrum for the film deposited at room temperature from CO revealed characteristic peaks at 1716, 2333, 2850 and 2916 cm^{-1} attributed as C=O stretch bond, C≡C stretch bond and C-H stretching bonds, respectively [31]. It can be seen that C-H stretching bonds was fragmented into two sharp peaks where the peak around 2916 cm^{-1} with a small shoulder appeared as the conventional asymmetric stretching of C-H bonds. Besides, the peak around 2850 cm^{-1} can be distinguished as an additional type of C-H stretching mode and recognized as C-H stretch of an aldehyde, n(O=)CH [32]. It is believed that this featured C-H stretch was mostly induced by oxygen in the CO plasma during deposition.

It was found that even if the hydrogen free CO source gas was used, a small amount of hydrogen was contaminated. One of the possible reasons for hydrogen contamination in the films during CVD from CO gas is the base pressure of vacuum of the deposition chamber. As the identical CVD apparatus was used for both C_2H_2 and CO gases, there is a possibility of emission of hydrogen or hydrocarbon gases from the chamber wall and electrode in the CVD system and incorporate in the films grown from CO gas. During deposition of carbon films by sputtering method, hydrogen contamination from residual gas was also reported [33]. Furthermore, the base pressure was slightly increased during experiments due to the opening of evacuation valve for controlling to sustain pressure inside the chamber which may lead to contamination of gas. It is supposed that the contaminated gas was hydrogen or water vapor (H_2O). The incorporation of hydrogen from the gas phase into the carbon film terminates the carbon dangling bonds and breaks the carbon double bonds from sp^2 bonding to form hydrogenated sp^3 bonding.

The cross section images for samples 1 and 2 by FE-SEM observation are shown in Figure 3.16 (a) and (b), respectively. The thicknesses of DLC films prepared from C_2H_2 for 5 minutes and from CO for 10 minutes were 332 and 134 nm, and the deposition rates were 66.4 and 13.4 nm/min, respectively. The deposition rate from CO source gas was lower than that from C_2H_2 even though the operating pressure for CO gas pressure was 10 times higher than C_2H_2.It can be assumed that, from CO source gas, atomic oxygen is produced by reaction for depositing carbon film and the produced atomic oxygen will etch the deposited carbon in turn.

It is likely that the precursor gas and its pressure during deposition influence the deposition rate and various properties of DLC films. Although in this work two characteristic pressures 15 and 150 pa were used for the two precursor gases C_2H_2 and CO, respectively, to sustain the identical pulsed DC power supply operation, it can be discussed that the deposition rate increases with increasing of pressure of both gases. However, the increment of deposition rate

with pressure is much higher in C_2H_2 plasma rather than CO. This happens because of the variation of both carbon flux and ionization efficiency [34].

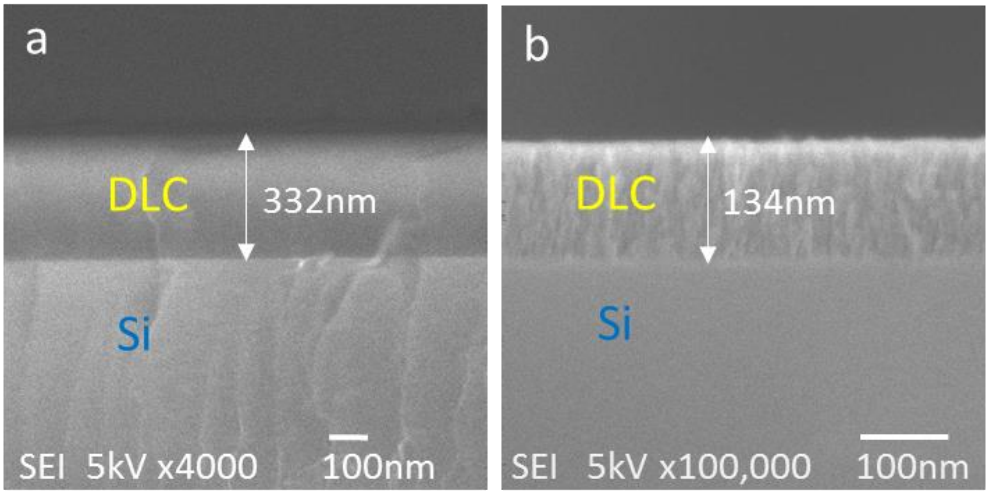

Figure 3.16. SEM cross section micrographs of the interface between Si substrate and DLC films, (a) sample 1 (deposited from C_2H_2) and (b) sample 2 (deposited from CO).

In case of carbon-monoxide, the film thickness slowly decreases from the middle to the outer at low pressure where it is uniform in deposition area for C_2H_2. In C_2H_2 plasma, the CVD process is almost dominated via hydrocarbon flux while in CO plasma, the CVD process is directed via the balance of deposition from the source gas and etching of carbon atoms by produced oxygen. At increased pressure, this balance become equilibrium and the thickness profile becomes almost uniform over the deposition area. In both cases of hydrocarbon and hydrogen free gas, the increasing of pressure introduces the increase of sp^2 hybridized bonds in carbon network that means the enhancement of graphitization in DLC films. Furthermore, it is also seen at higher pressure, due to fast deposition rate, the typical properties of DLC films have been varied such as the surface roughness increased, the hardness decreased and residual stress also increased [35,36,19].

The electrical conductivity of the films was simply tested by a conventional digital multimeter. It was found that the films deposited from C_2H_2 exhibited highly insulating nature whereas those from CO were objectively conductive. The conductivity suggests a considerable density of graphitic structures incorporated in the films from CO source gas.

The mechanical and tribological properties of DLC films are very important in their use as protective coatings. DLC films properties such as hardness and wear characteristics are

ultimately dependent on the microstructure of the films. Generally, for conventional DLC films, the hardness and wear resistance is directly correlated to the ratio of sp^3/sp^2 hybridized carbon bonding in the films where increasing of sp^3 (diamond-like) bonds leads to increase of the hardness and wear resistance, and increasing of sp^2 (graphitic- like) leads to decrease of the hardness and wear resistance. It is well-known that Raman spectra can offer the estimation about the sp^3 fraction. According to the model suggested by Ferrari and Robertson [2,28] the decreasing of I_D/I_G ratio and shifting of G peak position to lower wavenumber indicates increase of the sp^3 fraction in the films. The Raman results presented above suggest that the films prepared from the C_2H_2 have relatively higher concentration of sp^3 bonds rather than the films prepared from CO due to incorporation of a lot of graphitic-like (sp^2) structures. It can be projected that the films from C_2H_2 have high hardness, great wear resistance as similar to a conventional hydrogenated DLC film, while the films from CO have comparatively low hardness and less wear resistance but conductive. However, further investigations are necessary to improve the hardness and wear resistance of the films prepared from CO gas for the suitable application as a durable conductive coating, which will be considered as our future study.

3.4.3. Comparison of films properties

Here the DLC films prepared by the pulsed DC plasma CVD presented in this work is compared to the films deposited by our conventional RF CVD system previously reported [20]. It should be noted that the deposition conditions were not equal but has been optimized for each deposition system to operate stable and uniform discharges, and to obtain reproducible film properties. Because of difference in gas discharge performance, it is meaningless to compare at the exactly same conditions. The deposition rate, deposition area and power consumption are considered as crucial parameters for industrial application. For comparison, energy consumption for a unit deposition was evaluated by total input energy (in J) as the integrated power for a unit film thickness (in μm) in a unit area (in cm^2) as presented in Figure 3.17.

Additional parameters for operation of pulsed DC plasma CVD, such as frequency and pulse width, and also pulse waveform can be used while power is an only the tuning parameter for operation of the conventional RF CVD. Because of the small number of tuning parameter, the operation condition is fairly reproducible. For intentional modulation of deposition condition, however, the tuning parameter is limited and the film properties will not change dramatically.

The typical Raman spectra for DLC films from C_2H_2 and CO in our previous work [20] exhibits broad D peaks with increased peak intensity and shifting of G peaks position towards higher wavenumber. In this work (pulsed DC), we obtained lower intensity of D peaks as well

as shifting of G peaks position to the lower wavenumber in the typical Raman spectra for the films deposited from both gases as shown in Figure 3.18 (a). The results imply improvement of film properties by using the pulsed DC plasma CVD system.

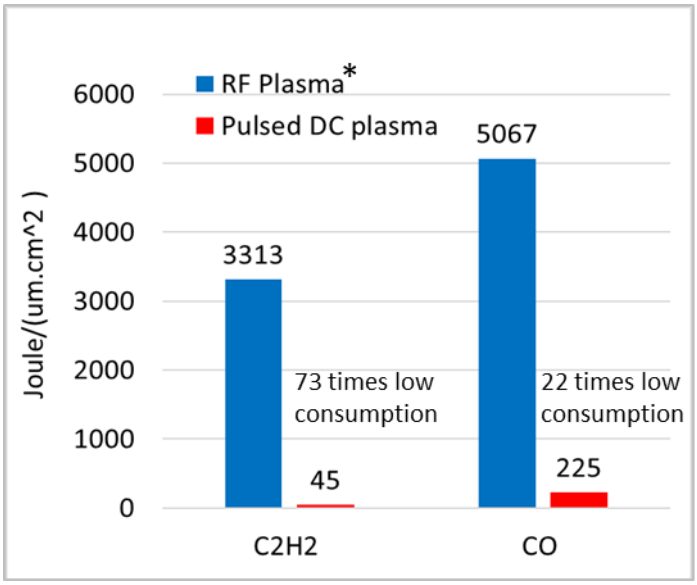

Figure 3.17. Comparison of energy consumption for a unit deposition of DLC film between our conventional RF plasma CVD system and developed pulsed DC plasma CVD.

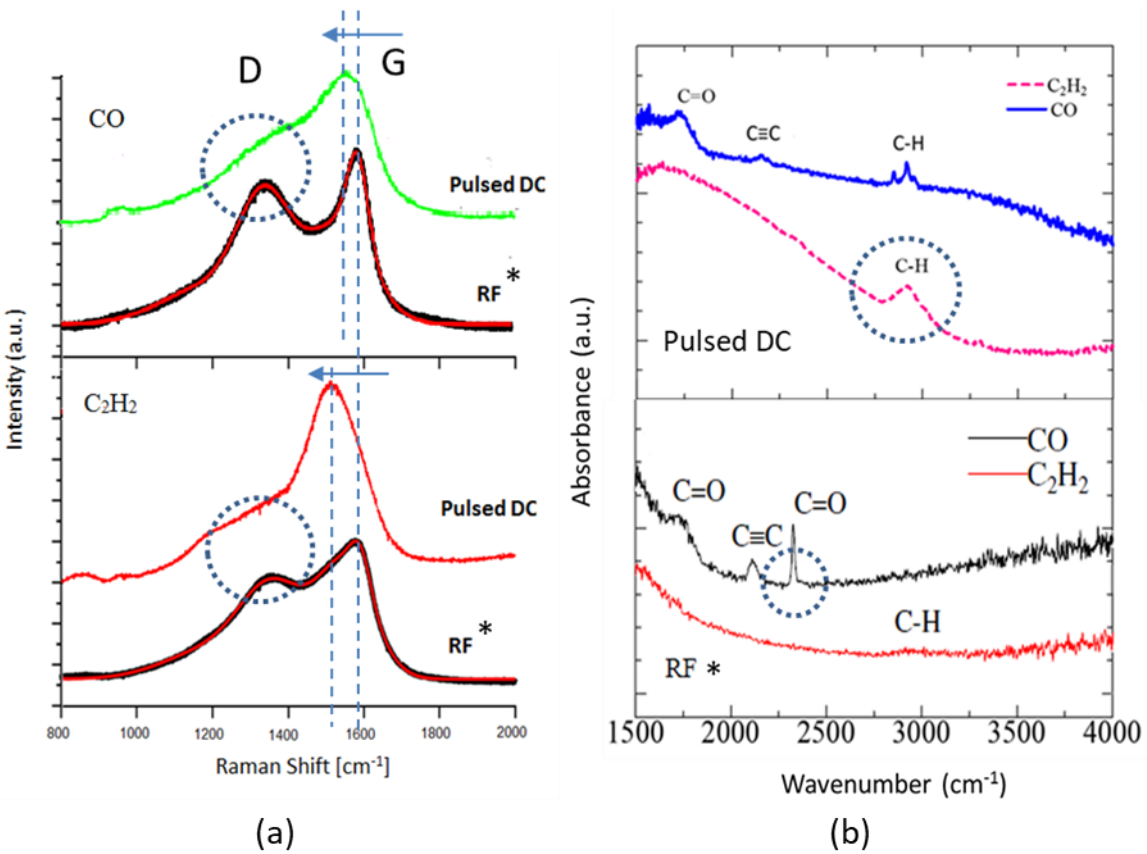

Figure 3.18. Evaluation of films properties prepared from RF and pulsed DC plasma CVD system (a) Raman Spectra (b) FT-IR spectra.

In Figure 3.18 (b), it was also noticed that the broad peak of C≡C bond and the sharp peak of CO_2 molecule appeared in the FT-IR spectrum for the film from CO by our conventional RF plasma [20]. In this work (pulsed DC), however, peak intensity of C≡C bond dramatically decreased and CO_2 molecule peak completely disappeared in the FT-IR spectrum for the film from CO. This result suggests that graphitic structure decrease and the contamination of CO_2 molecules into the film can be suppressed. It cannot be concluded that each result of film property is advantageous for application, it was demonstrated that the film property can be widely modified using the pulsed DC plasma CVD system.

3.5. Conclusion

In this study, a pulsed DC plasma discharge technique including simply configured pulse power supply and CVD apparatus was successfully developed. Deposition of DLC films were performed on Si wafers by employing the pulsed DC plasma CVD system from C_2H_2 and CO source gas. A large number of graphite-like structures, oxygen content, C=O bond, and C≡C bond were observed in the film deposited from CO gas. DLC films from CO also exhibited low deposition rate and appeared as a soft graphitic conducting DLC. Besides, DLC films from C_2H_2 showed higher deposition rate and looked as mostly conventional hydrogenated amorphous carbon with insulating properties. Raman analyses suggested an enhanced graphitization of the DLC films at an increased temperature. The obtained results reveal that the developed pulsed DC plasma CVD system is useful for the deposition DLC films with wide variation of deposition conditions for alternative of conventional RF CVD.

References

[1] A. Grill, “Diamond-like carbon: state of the art”, *Diamond Relat. Mater*. 8, 428 (1999).

[2] J. Robertson, “Diamond-like amorphous carbon”, *Mater. Sci. Eng. R* 37, 129 (2002).

[3] T. Lampe, S. Eisenberg, and E. Rodríguez Cabeo, “Plasma surface engineering in the automotive industry-trends and future prospectives”, *Surf. Coatings Technol.* 174-175, 1 (2003).

[4] J. R. Roth, *Industrial Plasma Engineering* (Institute of Physics, University of Reading, Berkshire, Vol. 2. 2001).

[5] Daniel Lundin, Jens Jensen and Henrik Pedersen, “Influence of pulse power amplitude on plasma properties and film deposition in high power pulsed plasma enhanced chemical vapor deposition”, *J. Vac. Sci. Technol. A* 32(3), 030602 (2014).

[6] C. Corbella, M. Vives, G. Oncins, C. Canal, J. L. Andújar, and E. Bertran, "Characterization of DLC films obtained at room temperature by pulsed-dc PECVD," *Diamond Relat. Mater.* 13 (4–8), 1494 (2004).

[7] R. A. Scholl, "Asymmetric bipolar pulsed power: a new power technology", *Surf. Coatings Technol.* 98, 823 (1998).

[8] S. Samukawa, T. Mieno, "Pulse-time modulated plasma discharge for highly selective, highly anisotropic and charge-free etching", *J. Plasma Sources Sci. Technol.* 5, 132 (1996).

[9] M. A. Lieberman, S. Ashida, "Global models of pulse-power-modulated high-density, low-pressure discharges", *J. Plasma Sources Sci. Technol.* 5, 145 (1996).

[10] J. Choi, "Introduction of the Magnetic Pulse Compressor (MPC) - Fundamental Review and Practical Application", *J. Elec. Engineering & Technol.* 5(3), 484 (2010).

[11] W. Jiang, "Compact Solid-State Switched Pulsed Power and Its Applications", *Proc. IEEE*. 92(7), 1180 (2004.

[12] V.J. Trava-Airoldi, L.F. Bonetti, G. Capot, J.A. Fernandes, E. Blando, R. Hübler, P.A. Radi, L.V. Santos, E.J. Corat, "DLC film properties obtained by a low cost and modified pulsed-DC discharge", *Thin Solid Films* 516, 272 (2007).

[13] V.J. Trava-Airoldi, L.F. Bonetti , G. Capote , L.V. Santos , E.J. Corat , "A comparison of DLC film properties obtained by r . f. PACVD, IBAD, and enhanced pulsed-DC PACVD", *Surf. Coatings Technol.* 202, 549 (2007).

[14] G. Capote, E. J. Corat, and V. J. Trava-airoldi, "Deposition of amorphous hydrogenated carbon films on steel surfaces through the enhanced asymmetrical modified bipolar pulsed-DC PECVD method," *Surf. Coatings Technol.* 260, 133 (2014).

[15] G. Capote, G.C. Mastrapa, V.J. Trava-Airoldi, "Influence of acetylene precursor diluted with argon on the microstructure and the mechanical and tribological properties of a-C:H films deposited via the modified pulsed-DC PECVD method", *Surf. Coatings Technol.*, 284, 145 (2015).

[16] M. Ban, T. Hasegawa, S. Fujii, and J. Fujioka, "Stress and structural properties of diamond-like carbon films deposited by electron beam excited plasma CVD", *Diamond Relat. Mater.* 12, 47 (2003).

[17] A. Grill and B. Meyerson, *Synthetic Diamond: Emerging CVD Science and Technology* (Wiley, New York, 1994, p. 91.)

[18] Z. F. Li, Z. Y. Yang, and R. F. Xiao, "Pulsed laser deposition of hydrogenated amorphous diamond-like carbon films from a polymer target", *J. Appl. Phys.* 80, 5398 (1996).

[19] R. S. R. P. Silva and G. A. J. Amaratunga, "The optical properties of band-gap-modulated diamond-like carbon thin films", *Diamond Relat. Mater.* 3, 817 (1994).

[20] Y. Yasuoka, T. Harigai, J.S. Oh, H. Furuta, A. Hatta, T. Suzuki, and H. Saitoh, "Diamond-like carbon films from CO source gas by RF plasma CVD method", *Jpn. J. of Appl. Phys.* 54, 01AD04 (2015).

[21] G.H. Xu, H. Liang, J. Woodford, J.A. Johnson and D. Yang, "Temperature dependence of tribological characteristics of DLC film*", J. Am. Ceram. Soc.* 88 (11), 3110 (2005).

[22] M.H. Rashid, *Power Electronics Handbook* (academic press. 2001 pp. 225–250).

[23] S. Fujimoto, N. Ohtake, and O. Takai, "Estimation of growth rate of Diamaon-like carbon films prepared by pulse plasma chemical vapor deposition", *J. of Solid Mechanics and Mater. Engineering.* 3(6), 910 (2009)

[24] W. Middleton, *Reference Data for Engineers: Radio, Electronics, Computers and Communications* (Newnes, 2002, pp.16-42.)

[25] H. Mase, "Plasma Production by D.C. Discharge, *Journal of Plasma and Fusion Research*", 69(3), 237 (1993).

[26] YP Raizer, *Gas Discharge Physics* (Springer Verlag. 1991).

[27] M. A. Lieberman, *Principles of plasma discharges and materials processing*, (John Wiley and Sons, 2005, 2nd ed. pp. 546).

[28] A. C. Ferrari and J. Robertson, "Interpretation of Raman spectra of disordered and amorphous carbon", *Phys. Rev. B 61*, 14095 (2000).

[29] S. Nakao, J. Choi, J. Kim, S. Miyagawa, Y. Miyagawa, and M. Ikeya, "Effects of positively and negatively pulsed voltages on the microstructure of DLC films prepared by bipolar-type plasma based ion implantation", *Diamond Relat. Mater.* 15, 884 (2006).

[30] J. Ristein, R. T. Stief, L. Ley, W. Beyer, J. Ristein, R. T. Stief, and L. Ley, "A comparative analysis of effusion by infrared spectroscopy and mass selected thermal," *J. of Appl. Phys.* 84, 3836, 1998.

[31] L. A. University of California, *IR Absorption Table*, Ucla. (2012).

[32] N. Roeges, *A Guide to the Complete Interpretation of Infrared Spectral of Organic Structures*, (Wiley, 1994, pp. 1-340).

[33] E. Mounier, F. Bertin, M. Adamik, Y. Pauleau, and P. B. Barna, "Effect of the substrate temperature on the physical characteristics of amorphous carbon films deposited by d.c. magnetron sputtering", *Diamond Relat. Mater.* 5, pp. 1509 (1996).

[34] P. Koidl, C. Wild, R. Locher and R. E. Sah, in R. E. Clausing, L. L. Horton, J. C. Angus and P. Koidl (eds.), "Diamond and Diamond-like Films and Coatings", *in NATO Adv. Stud. Inst. Ser., Ser. B.* 266, 243 (1991).

[35] L. Pantoja-Suárez, M. Morales, J.L. Andújar, J. Esteve, M. Segarra, E. Bertran, "Plackett-Burman experimental design for pulsed-DC plasma deposition of DLC coatings". *Cornell University Library – Condensed Matter*, 2015 [arXiv:1507.04267].

[36] J. Choi, S. Nakao, M. Ikeyama and T. Kato, "Effect of deposition pressure on the properties of DLC coatings deposited by bipolar-type PBII & D", *Surf. Interface Anal.* 40, 806, 2008.

Contributed paper: Md Abdullah Al Mamun, Hiroshi Furuta, Akimitsu Hatta, "Pulsed DC plasma CVD system for the deposition of DLC films", Materials Today Communications, ***14****, 40-46, (2017).*

Chapter 4

Novel pulsed DC generator for capacitively coupled plasma discharge

This chapter presents a novel pulsed DC generator (PDG) for capacitively coupled plasma discharge inside a vacuum chamber employing solid-state switches that can operate in pulsed DC mode with continuous power within a pulse, controllable pulse duration, and wide controllable frequency. Introduction, objectives, experimental methods, and results are described. The details of the fabrication and evaluation of the high-frequency PDG are reported. Finally, discussions and conclusions are drawn based on the experimental results.

4.1. Introduction

Pulsed power has been employed for decades in fields such as medical treatment, the food industry, water purification, and material processing [1-6]. For particular applications, several types of pulsed power schemes are used, and it has been found that the design and implementation of pulsed power generators are large. The application of pulsed power generators for low-temperature plasma discharge in the fields of chemical vapor deposition (CVD), surface modification, ion implantation, sputtering, diffusion, cleaning, and etching, has been investigated extensively in the literature [7-12]. It is found that, compared to ac-excited plasma, more controlled plasma can be generated using pulsed power. With the progressive increase of plasma research and applications, several pulsed power generator topologies using various techniques have been reported, including Marx generators (MGs) [13-14], magnetic pulse compressors (MPCs) [15-16], pulse forming networks (PFNs) [17], saturable pulse transformers (SPTs) [18], semiconductor opening switches (SOS) [19-20], and cascaded microsecond-pulse generators [21]. However, most of these designs are applied to high-impulse peak power (several tens of kilo-watts) with short duration (several hundreds of nanoseconds), fixed pulsed shape (impulse), and low repetition frequency (several hundreds of hertz). Typically, in these cases, gas/magnetic switching techniques are used to transfer charges, and pulse transformers are employed for high voltage isolation. These magnetic- and gas- based switches have basic advantages of providing a high blocking voltage and high current-carrying capabilities with relatively low transients, withstanding the action of the current pulse and achieving the desired energy. However, they also have undeniable disadvantages, including size, bulk, expense, inefficiency and limitations in either peak or average power output, short life span, and low operational frequency.

In general, the output power rating, output pulse shape, repetition frequency, lifetime, and compactness of a pulsed power generator depend on the performance of the switching devices. Therefore, the substitution of gas/magnetic-based switches by solid-state switches is considered to be an appropriate option for cost, loss, and volume reduction considerations. Recently developed solid-state technology demonstrates many favorable switches with high voltage ratings and switching frequency, making them suitable candidates for pulsed power generation. Insulated-gate bipolar transistors (IGBTs) (>1 kV, <20 kHz), metal–oxide–semiconductor field- effect transistors (MOSFETs) (<1 kV, <1 MHz), and silicon controlled rectifiers (SCRs) (>5 kV, <500 Hz) are examples of semiconductor switches [6] that can be utilized as reasonable replacements for existing switches. Power electronics converters offer attractive advantages for pulsed power applications; however, their compatibility with various load characteristics and demands is still a challenging issue. Nevertheless, the voltage ratings of these commercially available switches cannot currently satisfy many application requirements. Thus, several power electronics topologies with voltage boosting capabilities and their associated control methods are considered, and their performance properties are fully investigated, in order to present an optimum design for supplying plasma applications with maximum efficiency and flexibility.

Compared to high impulse power, plasma discharge by pulsed DC is more attractive due to the wide controllability of pulse parameters such as frequency, duty cycle, and output voltage level, which are supposed to directly influence the plasma deposition and diffusion processes [22]. Particularly, low duty cycle (short pulse-on period with respect to pulse-off period) is preferable to enhance the electron temperature in plasma, as supposed that the afterglow effect from the previous pulse reduces, electron collision decreases and attains high electron accelerating energy. The design of pulsed DC generators (PDGs) is significantly influenced by the topology of the plasma process. Typically, a system for plasma treatment consists of two electrodes (anode and cathode) placed a distance apart in a vacuum chamber filled with a gas mixture that acts as a capacitive load, i.e., the so-called capacitively coupled plasma (CCP). For capacitive loads, it is challenging to obtain rectangular pulses with fast rising and falling edges. There have been some attempts to produce rectangular pulses with very short rising (<200 ns) and falling times (<200 ns) [23-24]; however, they are limited by maximum operating frequency (20-50 kHz) and energy efficiency.

4.2. Objective

In this study, we present a new type of pulsed power generator employing solid-state switches that can operate in pulsed DC mode with continuous power within a pulse, controllable pulse duration, and controllable frequency (low to high). We attempted to design an easy,

consistent, and efficient circuit for the PDG to drive capacitively coupled plasma loads. The details of the fabrication of the high-frequency PDG are reported. By using the PDG, plasma discharge experiments are carried out inside a vacuum chamber with a wide range of discharge conditions for testing and verifying the performance of the PDG.

4.3. Design and construction of the pulsed DC generator

4.3.1. Design architecture

The design of our PDG is mainly focused on producing high voltage (HV) pulsed DC waveforms with fast rising and falling edges at high frequencies for plasma discharge between a pair of electrodes (anode and cathode) filled with low-pressure discharge gas. The electrodes in a chamber are configured similarly to a capacitor, that is, CCP, as depicted in Figure 4.1 (a). Even for the case of a single cathode configuration, the electrode performs as a capacitor with the grounded chamber wall surrounding the electrode. Typically, the rising and falling time of pulses depend on how fast the capacitive load is charged and discharged, respectively. Intense current is required to quickly charge the capacitor to the desired voltage, which ensures the fast-rising edge of the pulse. For the fast falling edge of the pulse, intense discharge current is required to release charge.

When plasma occurs between the electrodes, steady current is required to sustain a stable plasma discharge. For CCP, the plasma discharge current is much smaller than the charging current for the capacitance of electrodes. Due to the properties of plasma discharge at constant voltage (or rather negative resistivity) for the conventional glow discharge, the plasma discharge current should be intentionally limited by using a ballast resistance or a constant current circuit.

For quick termination of plasma discharge at the end of a pulse, in addition to the plasma discharge current being shut off, the remaining charge on the electrode should be quickly withdrawn. In a conventional pulse generator, the remaining charge on the electrodes is generally released to the ground, resulting in wasting energy at every pulse operation. The recovery of the remaining charge and energy from the electrode can improve the energy efficiency of the PDG.

We propose a new technique to generate pulsed HVDC for driving capacitive loads, particularly for CCP discharges. The simplified proposed topology and expected voltage and current waveforms of pulsed DC plasma discharges are shown in Figures 4.1 (b) and (c), respectively. Here, we introduce two well-known techniques: the inductor-capacitor (*LC*) resonant converter usually used in RF power transmission with impedance matching, widely used for RF plasma discharge; and stable DC current supply regulated with a ballast resistor,

generally used for DC plasma discharges. These two techniques are integrated and operated in fast switching mode. The *LC* resonant converter acts as a half resonant converter that delivers the intense current for rapid charging at the beginning of a pulse; thereafter, a regulated current is delivered from the DC power supply during the pulse on, and the *LC* resonant converter alternately discharges the capacitance of electrodes by recovering the remaining charge and energy to a storage capacitor at the end of the pulse.

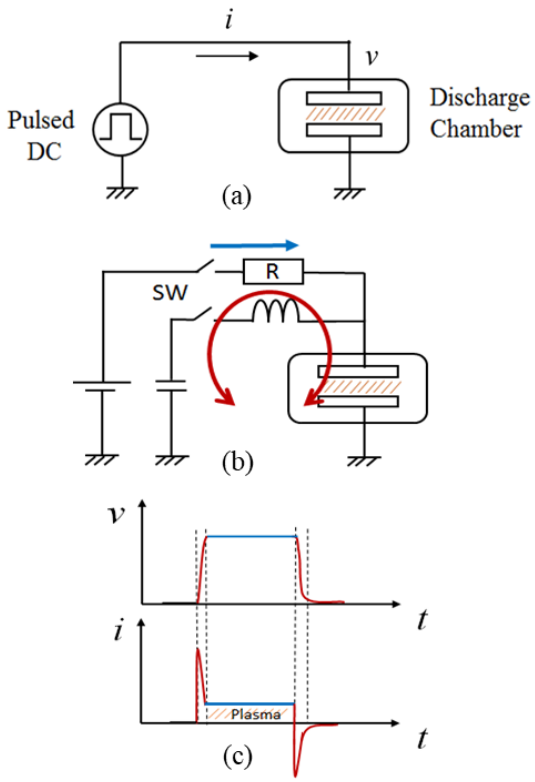

Figure 4.1. Pulsed dc plasma discharge scenario. (a) Basic scheme (b) Proposed topology (c) Expected voltage and current waveforms.

4.3.2. Topology of LC resonant converter

In our design, the most crucial part is the *LC* half resonant converter topology, since it can transfer energy with low switching loss and sub-microsecond level rising edge, essential for high-frequency operation, as discussed in a later section. In conventional pulse-width modulation (PWM) methods for power converters, the power flow is controlled by chopping at high frequency using power switches with sudden changes of voltages and currents. Due to the hard switching, substantial switching loss and noise occurs with PWM methods. By using resonant converters, where resonance occurs among capacitive and inductive elements in the circuit, the power flow is controlled as sinusoidal waves, introducing zero-current crossing. It has been known that switching at zero current, so-called soft switching or zero-current switching (ZCS), noticeably eliminates the switching losses in power switches [25]. Moreover,

the power interchange scheme between inductive and capacitive elements of resonant circuits is also advantageous for reducing current ripples and noises of high voltage power generators. For the above reasons, resonant converters have become more attractive in the field of power circuits for generation of high voltage and have been widely used in many applications [26]. In this work, for application to CCP discharge, where high peak current for charging is essential, *LC* resonant converters are considered to be the most suitable topology.

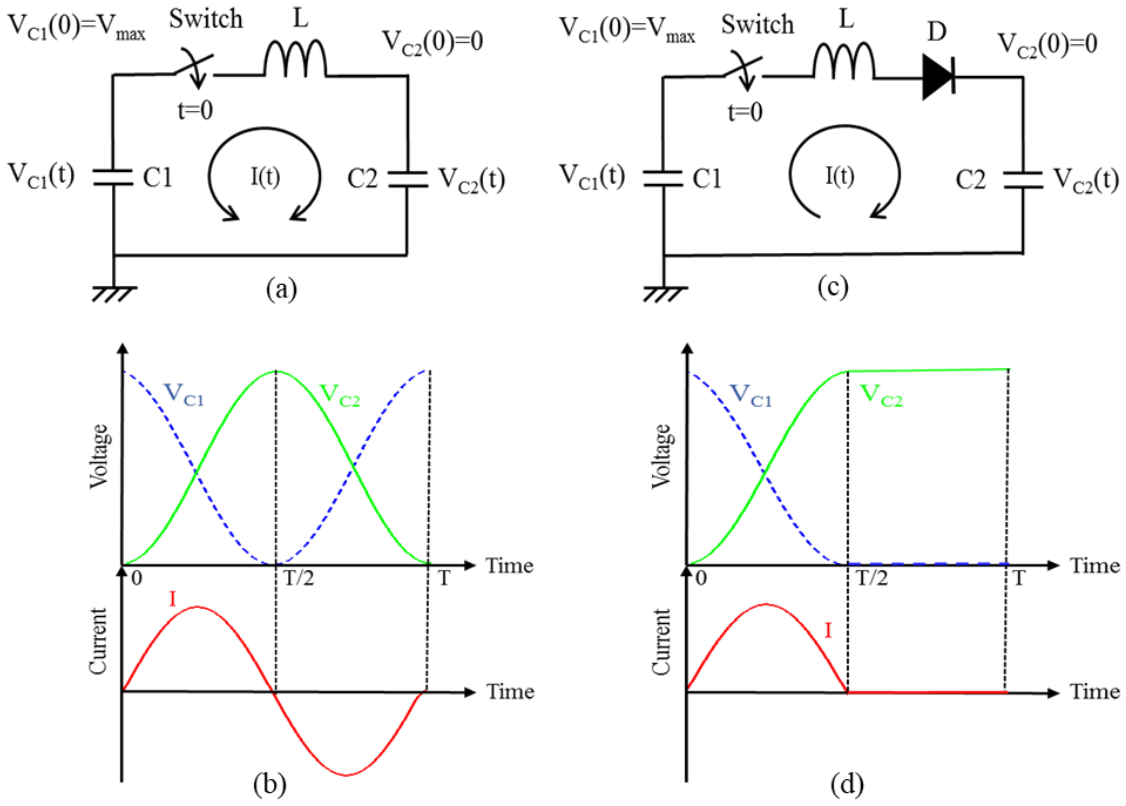

Figure 4.2 (a) Circuit diagram and (b) voltage and current waveforms of a typical *LC* resonant circuit, (c) circuit diagram and (d) voltage and current waveforms of a typical *LC* half-resonant converter.

Figure 4.2(a) shows the circuit diagram for a typical *LC* resonant circuit, and Figure 4.2(b) shows the voltage and current waveforms after the switch is closed. When the switch is closed at time t = 0, where the capacitor C1 is initially charged to voltage V_{max}, the initial charge in capacitor C1 is resonantly transferred to capacitor C2 through the inductor L. The oscillation between L and C generates the sinusoidal waves of voltage and current at a resonance frequency, expressed as equation (1):

$$f = \frac{1}{2\pi\sqrt{LC}} \tag{1}$$

where $C = C1C2 / (C1 + C2)$. When the capacitance C1 is the same as C2, the initial charge of C1 can be fully transferred to C2 in the first half cycle of resonance until t = T/2, where T is

the period of the full resonant cycle as an inverse function of frequency f. In the next half cycle, the charge and energy of C2 are fully recovered to C1.

The concept of half-resonant converter topology comes from this process, with a modification of blocking reverse current using a diode, as indicated in Figure 4.2(c). The diode performs as if the switch is automatically opened when the charge of C1 is fully transferred to C2, where the current crosses the zero point at t = T/2 while retaining the transferred charge in C2, as shown in Figure 4(d). By using another half-resonant circuit in the opposite direction (not indicated in Figure 4.2(c), the charge in C2 can be recovered to C1 in the same manner. For transferring and recovering all of the charge between C1 and C2, the capacitances should be same. If C2 is the capacitance of electrodes used in a plasma system, the storage capacitance C1 in the circuit should be tuned to the same value. The voltage rising and falling times can be reduced by decreasing the inductance L, whereas the waveforms in figures 4.2(b) and 4.2(d) are drawn deliberately as a slow sinusoidal wave. By using a sufficiently small inductance, the voltage waveform can be almost rectangular, for example, in microseconds.

4.3.3. Circuit layout and description

A diagram of the system architecture for our proposed PDG has been designed as shown in Figure 4.3. The PDG consists of an HVDC power supply as the primary energy source, a charging and energy storage unit, a pair of *LC* half resonant converters for energy transfer and recovery, an electrical grounding unit, a constant pulsed current controller, and a control system. A digital storage oscilloscope with a high voltage probe and a current probe is employed to monitor and store the current and voltage waveforms.

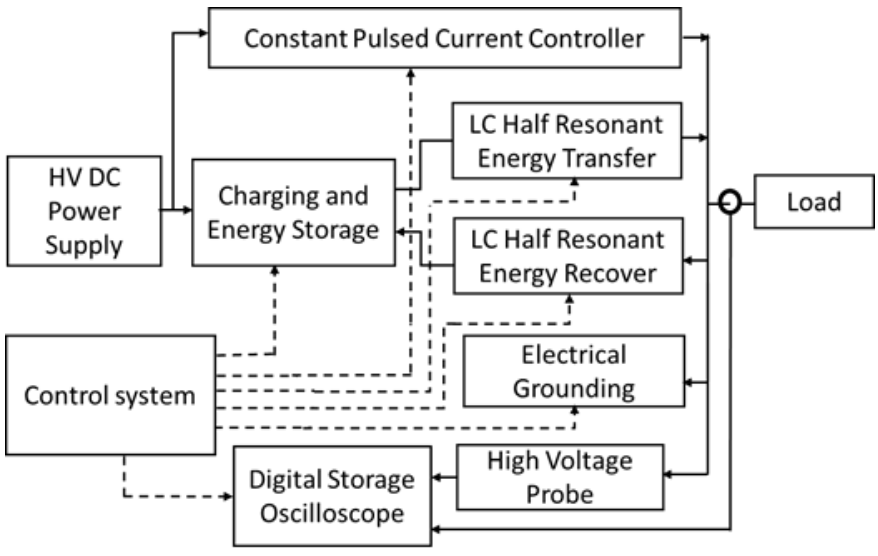

Figure 4.3. Structure diagram of the PDG.

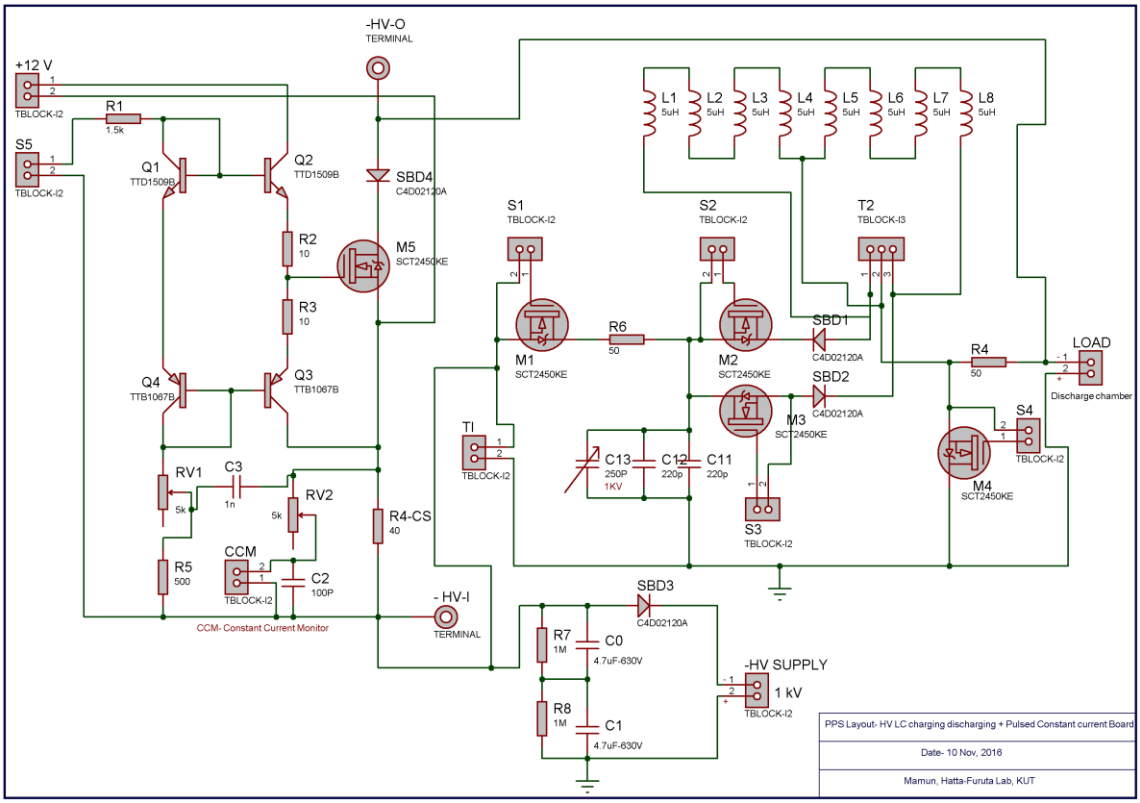

(a)

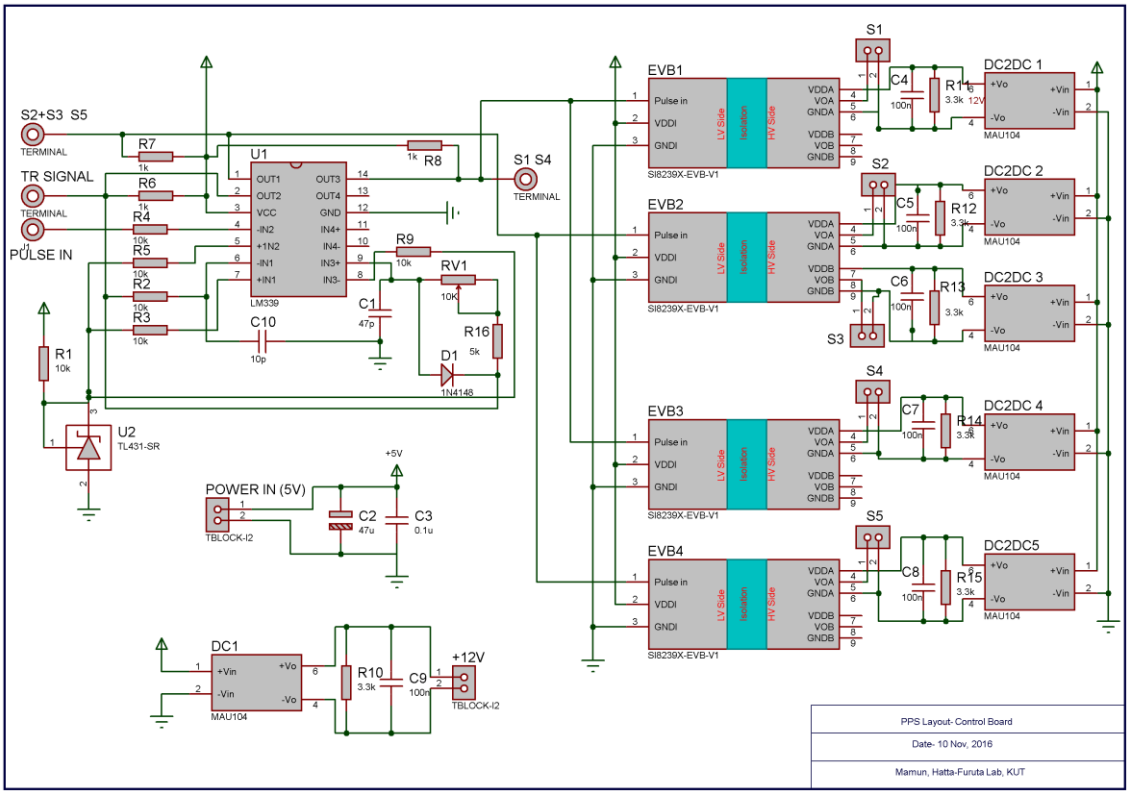

(b)

Figure 4.4. Detail circuit diagram of PDG (a) LC resonant charging-discharging circuit with pulsed constant current controller (b) gate pulse control system.

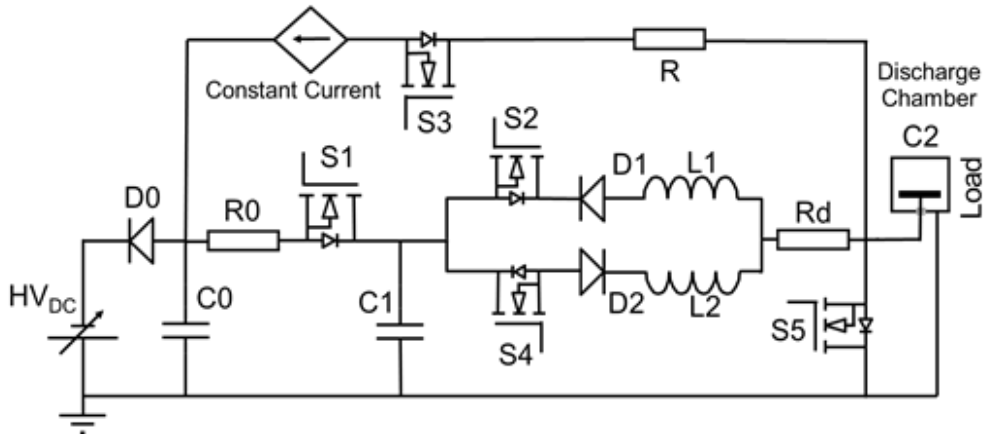

Figure 4.5. Simplified circuit layout of the pulsed dc generator (PDG).

The detail circuit diagram of the developed PDG is shown in Figure 4.4. However, for better understanding, the simplified circuit layout of the PDG is illustrated in Figure 4.5, where the control system is not shown (discussed in a later section). An HVDC power supply (TMK1.0-50, Takasago Ltd., Japan, 1 kV and 50 mA) is used for the negative HV source, with a sufficiently large capacitor C0 (a series connection of 2 capacitors, each rated at 4.7 uF, 630 V) for the current buffer. The diode D0 protects the back current to the power supply. For charging and energy storage, the capacitor C1 consists of four ceramic capacitors (1000 V, each 100 pF) and a variable capacitor (1000 V, 0–250 pF) connected in parallel is used. The variable capacitor is employed to balance the storage capacitance C1 with the load capacitance C2 (electrode in the discharge chamber) for efficient transfer and recovery of charge and energy. The actual load capacitance in the experiment is estimated as 450 pF. The resistor R0 (50 Ω) and switch S1 perform the primary charging of capacitor C1 from the power source.

One of the *LC* half-resonant converters, consisting of switch S2, diode D1, and inductor L1, performs charge transfer from the storage capacitor C1 to the load C2. The charge transfer is triggered by closing switch S2, and is automatically terminated by blocking the reverse current in diode D1. For the inductance L1, four ferrite core inductors (VHF inductor, B82111B, 10 A 5 μH 5 mΩ, EPCOS) are used in series. The rising time of voltage as a half cycle of resonance was expected to be approximately 300 ns from equation (1), with the parameters C1 = C2 = 450 pF and L1 = 20 μH.

In addition, the resistor Rd (50 Ω) is inserted to suppress oscillations at high frequencies, unexpectedly induced by stray capacitance and inductance existing in the circuit and components. When a resistor is introduced in a LC circuit, it is treated as a RLC circuit. In a RLC circuit, the resistor acts as an energy-dissipating element which tends to damp the oscillation of the LC circuit. Depending on the value of resistor, inductor and capacitor, the

circuit can be under-damped, critically damped or over-damped. In our design, the value of Rd is tuned for under-damped condition for the given C and L values to transfer and recover maximum charge. However, the stray capacitance and inductance values are assumed to be very small compared to C and L values and Rd can damp these high frequency ringing. Due to insertion of the series resistance, it is assumed that the actual rising time will be longer than the expected value.

A plasma discharge is ignited by the high voltage transferred to the electrode from C1. To sustain the plasma, a constant current is provided to the load from the pulsed current controller circuit through switch S3. During the plasma discharge, the current is controlled at a constant level given as an input signal voltage. The plasma discharge current is sensed by resistor R (50 Ω) and regulated by the MOSFET (switch S3). The gate voltage for S3 is controlled by a potentiometer for regulation of current through a feedback circuit from resistor R during pulse discharge on. The turn numbers of the potentiometer are calibrated with respect to the constant current value. By selecting the turn numbers of the potentiometer, the constant current value can be modified.

For termination of the plasma discharge, in addition to the constant current circuit being turned off by opening the switch S3, the remaining charge (voltage) of the electrode is quickly removed by two steps as follows. In the first step, the remaining charge is recovered to the storage capacitor C1, as much as possible, through the other *LC* half-resonant converter consisting of L2, D2, and S4. The inductance L2 is separately configured from L1 for further tuning of the circuit, whereas the inductance L2 = 20 μH (same as L1) is used in the experiment of prototype. Due to the inserted resistor Rd and some faulty performance of electrical components and wiring, the remaining charge on the electrode could not be recovered completely to the storage capacitor C1. In the second step, the electrode is completely grounded through switch S5, extinguishing the plasma due to the remaining charge, even after the charge recovery.

SiC MOSFETs (SCT2450KE, 1200 V 10 A, ROHM Co., Ltd.) are used for the switches because of their high speed, high reverse blocking voltage, low output capacitance, and low on state resistivity. For the reverse blocking diodes D1 and D2, silicon-carbide Schottky diodes (C4D02120A, 1200 V, 10 A, ROHM Co., Ltd.) are used.

4.3.4. Control system and operation modes

Figure 4.6 shows the block diagram of the control system of generating gate driving signals for the MOSFET switches (detail circuit diagram in Figure 4.4 (b)). It is expected that the PDG outputs nearly rectangular negative HV pulses with wide variations in amplitude (voltage and

current), frequency, and pulse duration, which are considered as effective parameters to govern the plasma properties.

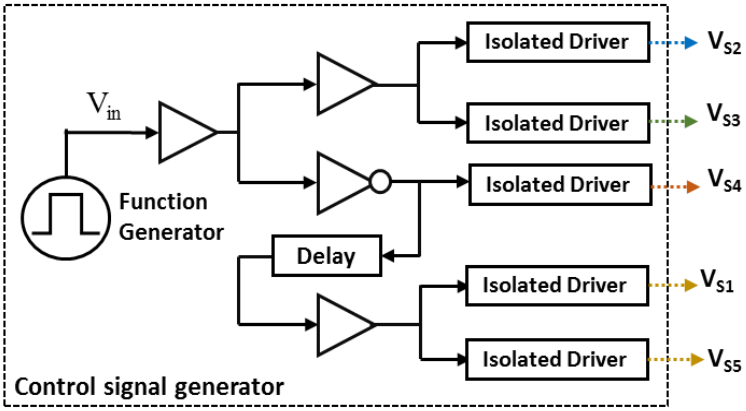

Figure 4.6. Block diagram of the control system with control signals.

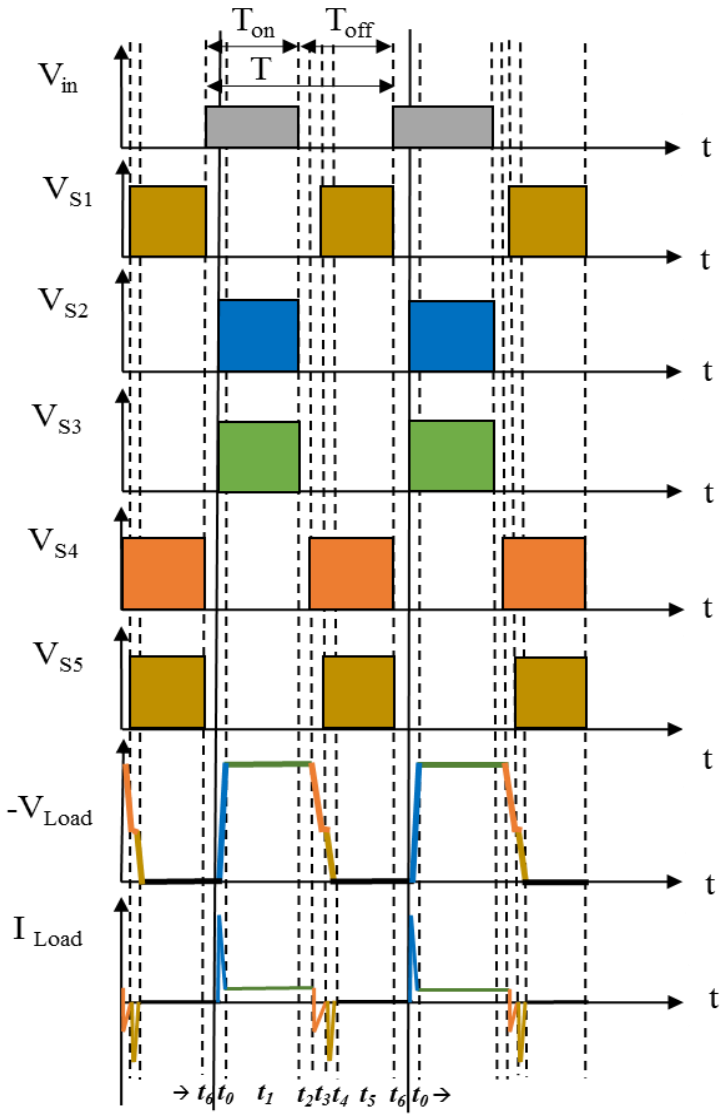

Figure 4.7. Timing sequence of the control signals.

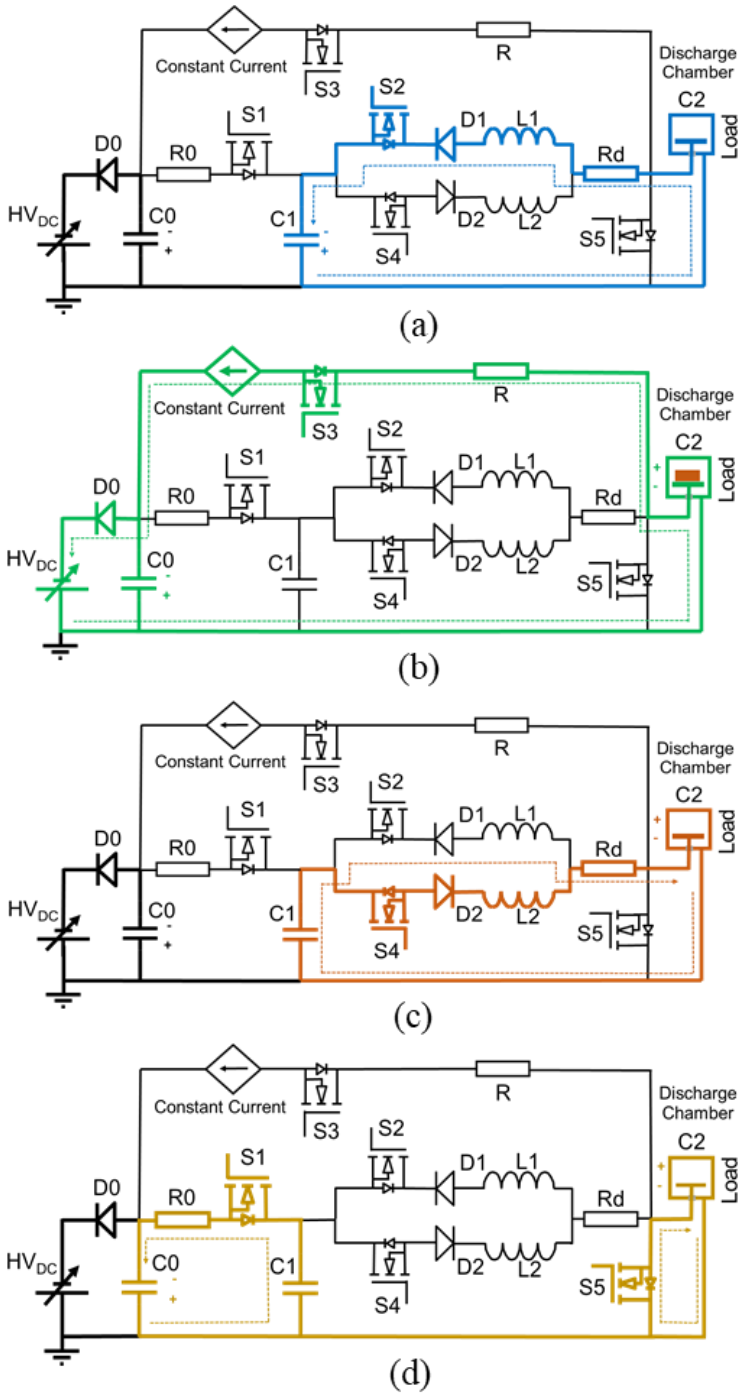

Figure 4.8. Operation modes of the PDG with the active circuit loop indicated as colored solid thick lines, and current as dotted lines. (a) Mode 1 (S2, S3, D1 on; S1, S4, S5, D2 off) (b) Mode 2 (S2, S3 on; S1, S4, S5, D1, D2 off) (c) Mode 3 (S4, D2 on; S1, S2, S3, S5, D1 off) (d) Mode 4 (S1, S5 on; S2, S3, S4, D1, D2 off).

In this design, the frequency and pulse duration is controlled by transistor-transistor logic TTL input signal Vin from a function generator (DF1906, NF Corporation). The MOSFET switches are driven through isolated gate driver modules (Si8239xISO-KIT, Silicon Laboratories Inc.) powered to the high side through an isolated DC-to-DC converter (MAU104, 5–12 V). The isolated gate driver has a programmable dead time for delayed turning on to avoid concurrent operation of MOSFET switches due to their switching delay. A dead time of 14.65 ns for the default value of the module is used.

Figure 4.7 shows the time sequence of driving signals. One switching cycle consists of four operation modes: mode 1 for turning on, mode 2 for the ON state, mode 3 for turning off, and mode 4 for the off state. For operation of MOSFET switches, the cycle is further divided into six time durations, from t_0 to t_6, as indicated in Figure 4.7.

In mode 1, for turning on, the output voltage rises through charge transfer from storage capacitor C1. The switches S2 and S3 are synchronized with the input signal Vin with a starting delay for t_6 due to the dead time setting. While the constant current circuit also supplies the regulated current through S3, most of the charge is rapidly transferred from C1 through S2, as indicated in Figure 4.8(a). The duration of mode 1, indicated as t_0 in Figure 4.7, is basically determined by a half- cycle of the *LC* resonance. The output voltage ($-V_{Load}$) goes up to a peak value nearly equal to the initial voltage of C1.

In the case of actual plasma discharge, when the peak voltage exceeds the plasma ignition voltage, the electrode voltage drops to the sustain voltage. Because the sustain voltage for plasma discharge is determined by discharge conditions and discharge current regardless of applied voltage, the working electrode voltage is controlled as a required value by the constant current circuit. An additional transition phase appears, in which the voltage decreases from the peak to the regulated level necessary for sustaining plasma discharge.

In mode 2, for the on state, the plasma discharge current is supplied through the constant current circuit. The constant current circuit controls the working voltage for regulation of plasma current at the set level. The current level is set by a DC signal voltage input. The duration of the on state is almost equal to the input pulse duration T_{on}. To be more precise, however, the steady ON state starts after t_6 for dead time and t_0 for turning on, and continues until a delay of t_2 after the end of the input pulse. The delay t_2 is the dead time for switch S4. After the constant current circuit is shut off by opening S3 at the end of the input pulse, the steady discharge is sustained for a while by the remaining charge on the electrode until it is intentionally removed by closing switch S4 in the next mode.

In mode 3, for turning off, switch S4 is closed to recover the remaining charge of electrode to the storage capacitor C1. The output voltage ($-V_{Load}$) is quickly diminished for termination of the plasma discharge. After an intentional delay t_3 for waiting charge recovery to C1, which is equal to the half-cycle of recovery of the *LC* resonant circuit, switch S5 is closed to forcibly ground the electrode. The intentional delay for t_3 is inserted in the control signal generator, as shown in Figure 4.6, to wait the time necessary for completion of recovery. Finally, the voltage quickly goes to zero in the short duration of t_4.

In mode 4, for the off state, the electrode is kept grounded for the duration t_5 until the start of the next input pulse. During the off state, switch S1 is closed to charge the storage capacitor C1 to the initial voltage, equal to the power source only for the deficiency of recovered charge.

4.4. Experimental setup

The plasma discharge by the PDG was tested with the experimental setup shown in Figure 4.9(a). The main unit of PDG performs switching of the HVDC according to the input pulse signal from the function generator and the input voltage for setting the current level. Figure 4.9(b) shows an equivalent circuit for the CCP discharge where C_G is the capacitance of electrodes (represented as C2 in the circuits in Figures 4.5 and 4.8). When a higher voltage pulse (HV_P) over the breakdown voltage is applied across the electrode, the plasma is produced by ionizing gas. The highly conductive plasma filling the gap is represented as the resistance R_P through the ignition switch S_B. The breakdown voltage and plasma resistance depend on the property and pressure of discharge gas, and the material and configuration of the electrodes. The working electrode was a stainless steel (SUS304) disk of 100 mm in diameter. The plasma discharge was operated between the working electrode and the inner wall of the vacuum chamber made of aluminum (Al), instead of the inserting counter electrode. The gap between the working electrode and the chamber wall was 50 mm. For the discharge gas, argon (Ar) was supplied through a mass flow controller at a 100 standard cubic centimeter per minute (SCCM) flow rate with continuous pumping-out. The gas pressure was controlled by the conductance of an evacuation valve. An absolute pressure transducer (MKS Baratron, type: 626, range: 1–133.33 Pa, accuracy: 0.5%) with a controller was installed to the vacuum chamber for measuring the working gas pressure.

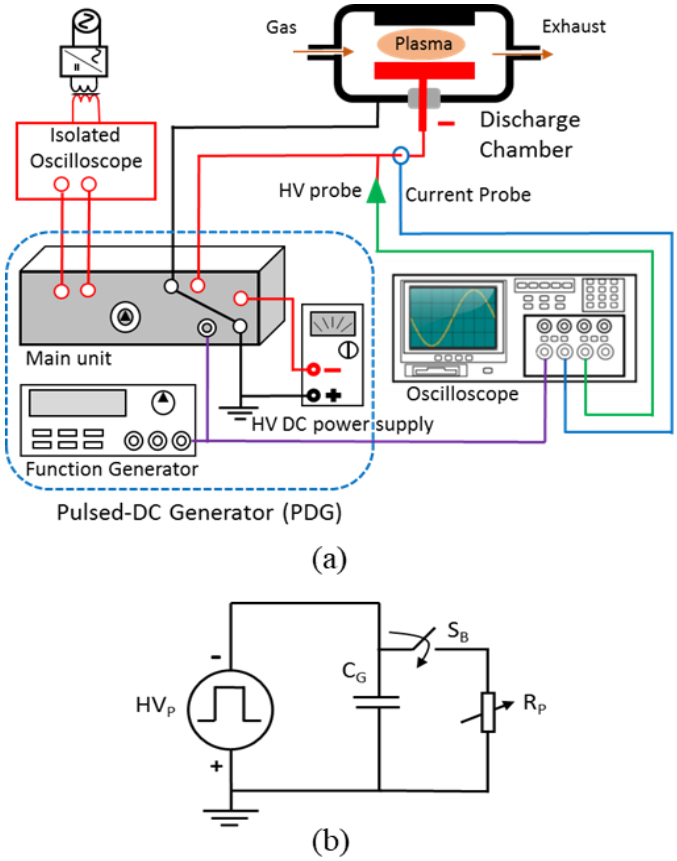

Figure 4.9. (a) Experimental setup and (b) equivalent circuit of the pulsed dc CCP system.

The performance of the PDG and the characteristics of plasma discharge were investigated by monitoring current and voltage waveforms using a digital storage oscilloscope (Tektronix 2014B, 100 MHz) with a high voltage probe and an isolated current probe. While the intense current pulses for charging and discharging capacitor C_G were more than 1 A at peak current, and were clearly observed by the current probe, it was difficult to observe the plasma discharge current below 100 mA. For monitoring the plasma discharge current, an electrically isolated oscilloscope (MDS202, Micronix) was used to measure the voltage drop across the current detection resistor R in the constant current circuit on the high voltage side.

Figure 4.10. Image of the fabricated Pulsed DC Generator (PDG)

Table 4.1. Specification of the developed PDG.

Element	Rating
Input voltage (DC)	0–1000 (-V)
Output voltage (pulse)	0–1000 (-V)
Output steady current during pulse	0–100 (mA)
Pulse frequency	0 (DC)–500 (kHz)
Pulse width (input)	1 (μs)–∞
Pulse rising time	<500 ns
Pulse falling time	<800 ns

4.5. Results and discussion

Figure 4.10 presents the photograph of the laboratory prototype level of the developed pulsed DC generator. The specification of PDG is shown in Table 4.1. The input and output voltages were limited by the HV power source used in the experiment while the absolute maximum rating of the used MOSFET was 1200 V. The output steady current during pulse is almost limited by the HV power source. The maximum pulse frequency was limited by the

pulse rising time and falling time. There is no constraint for duty ratio. The minimum pulse width of 1 μs is required for the input signal due to the pulse rising time and the dead time for MOSFET switch. The pulse rising time is longer than the expected value of 300 ns due to additional resistor Rd, internal resistance of inductors, source-drain capacitance of MOSFET, diode capacitance, and stray capacitance and inductance. The pulse falling time is further longer than the rising time mainly due to delay for completion of charge recovery.

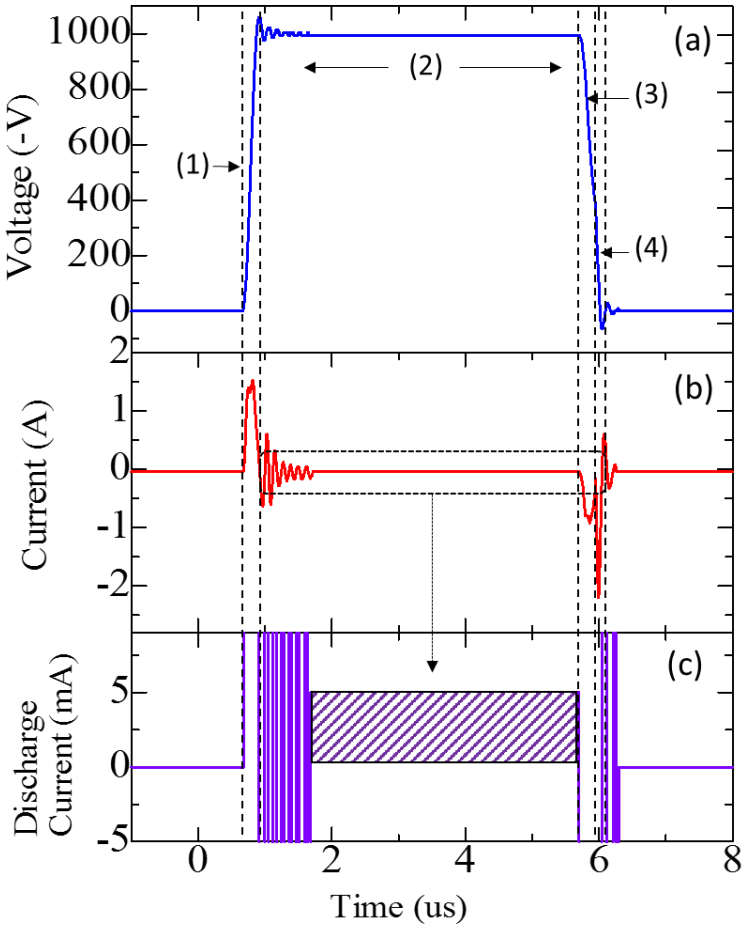

Figure 4.11. Discharge waveforms of (a) voltage, (b) total current, and (c) plasma discharge current for Ar plasma at 5 Pa, 100 kHz, 50% duty, and 5 mA set discharge current.

Figure 4.11 shows the typical current and voltage waveforms of Ar gas discharge at a pressure of 5 Pa, an input voltage (DC) of -1000 V, an input pulse frequency of 100 kHz, a duty ratio of 50%, and a pulse current of 5 mA. The waveform consists of four characteristic parts based on the operation modes defined in section 4.2.4. The first part, indicated as (1) in Figure 4.11, is mode 1 for duration t_0, where the electrode is quickly charged to the peak voltage with a large current pulse. The second part ((2) in Figure 4.11), is the steady current operation during

mode 2. After the ignition of plasma, a damping oscillation of voltage and current occurred with a decaying time of 600 ns.

After the oscillation, the current is well controlled at the set level of 5 mA, as shown in Figure 4.11(c), which is traced from a photograph on the isolated oscilloscope screen. The damping oscillation occurred possibly due to an excessive gain in the feedback circuit for constant current control. It can be eliminated by further tuning of the circuit parameters.

The third and fourth parts ((3) and (4) in Figure 4.11) are charge recovery to C1 during t_3 and forcible charge removal by grounding during t_4, respectively, both in mode 3 for turning off. In the current waveform, two negative peaks appeared for the two parts; the former peak is charge recovery approximately 1 A in height and 300 ns in width, and the latter is forcible grounding of approximately 2.5 A and below 100 ns. The observed waveforms of almost rectangular voltage pulse and stabilized current during a pulse are as expected in designing with an exception of damping oscillation.

The PDG is tested to operate discharge at the highest repeating rate of 500 kHz using the minimum input pulse width of 1 μs (50% in duty ratio) under the same conditions. As shown in Figure 9, the voltage waveform is a triangular wave consisting of only rising and falling edges. At the highest frequency, the steady discharge part was diminished. The plasma looked quite stable while the discharge current was not controlled through the constant current circuit, but was supplied as a part of transferred charge from C1. The operation of the PDG at the high frequency is similar to the conventional RF plasma sustained by the resonance between the electrode and the matching network.

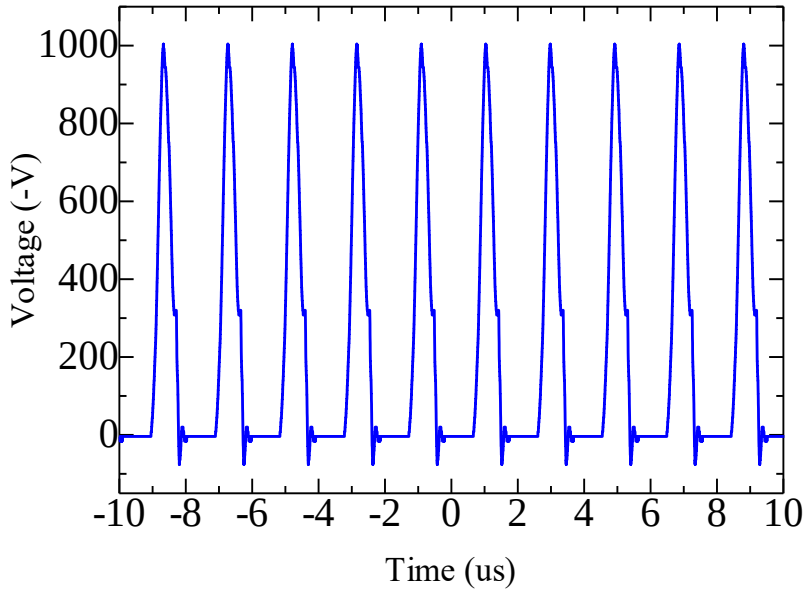

Figure 4.12. Discharge voltage waveform of Ar plasma (5 Pa) at 500 kHz, 50% duty cycle.

Figure 4.13 shows the voltage waveforms of Ar plasma discharges with different pulse widths at a pressure of 15 Pa, a pulse frequency of 20 kHz, an input voltage (DC) of -550 V, and a set discharge current of 20 mA. The input voltage was daringly decreased nearly to the plasma sustaining voltage of - 550 V. While the actual current was not levelled at the set value of 20 mA, the plasma was steadily sustained by the constant voltage during the pulse. At the beginning of the pulse, the voltage was boosted up to the peak of -625 V by intentionally increasing the capacitance C1 (described in section 2.3) more than C2. The output voltage can be enhanced by the *LC* resonance with unbalanced capacitance. After ignition of the plasma, the peak voltage quickly dropped to the input voltage in a sub-microsecond. When the pulse discharge operation follows the glow discharge scheme [27], a higher breakdown voltage than the sustain voltage is required for ignition of the plasma. The PDG effectively supplies the breakdown voltage for the short time, higher than the voltage source.

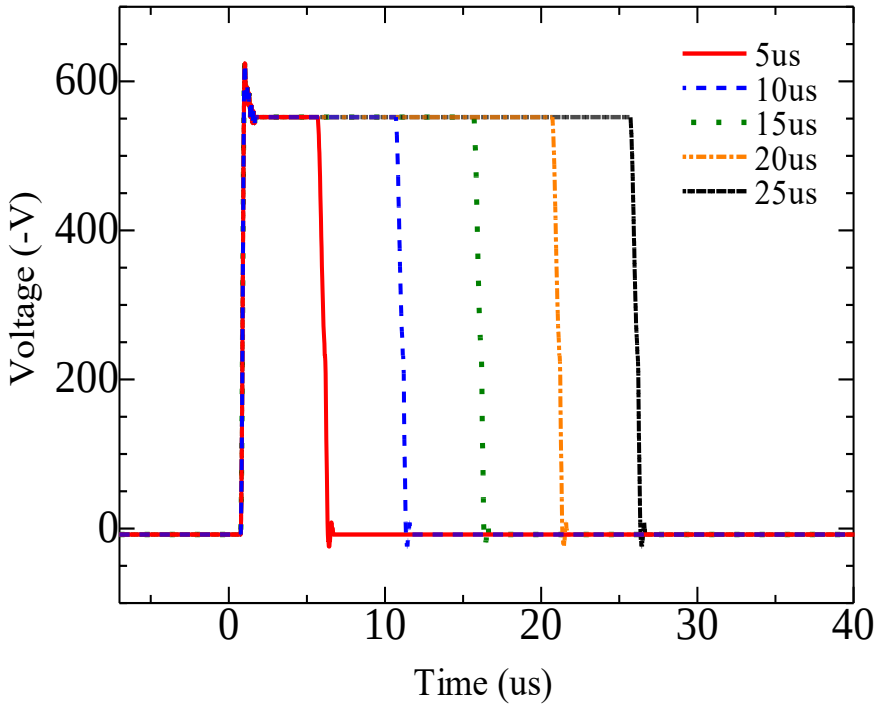

Figure 4.13. Discharge voltage waveforms of Ar plasma (15 Pa, 20 kHz, set discharge current 20 mA) with a variation of pulse width.

When the input voltage is nearly equal to the sustain voltage, the constant current circuit cannot regulate the current level at the set value due to insufficient voltage drop in the circuit. For precise control of current, the input voltage should be slightly higher than the sum of the sustain voltage for the plasma and the voltage drop necessary for current regulation, even if the breakdown voltage is supplied by the LC resonance. Compared to this PDG, in the conventional

operation of glow discharge, the voltage source should be higher than the breakdown voltage. After ignition of the plasma, a large portion of supplied voltage should be dropped in the ballast resistance or current control circuit, resulting in a large energy loss in the circuit. By using the *LC* resonance for charging the electrode, the energy loss for the voltage drop in the circuit can be reduced successfully.

The power conversion efficiency of the PDG was examined. In this work, the efficiency is defined as the ratio of the time average output power of pulsed DC to the DC input power from the HV source. To support the effectiveness of energy recovery, the efficiency was measured both with and without operating the energy recovery. As described in section 4.2.4, in the operating mode 3 (for turning off), switch S4 is turned on at first to recover energy. To cut the energy recovery operation, the driver circuit for S4 was intentionally disconnected. Without the operation of energy recovery, all of the charge and energy remaining on the electrode disappeared directly into the ground through switch S5 at the end of each pulse discharge.

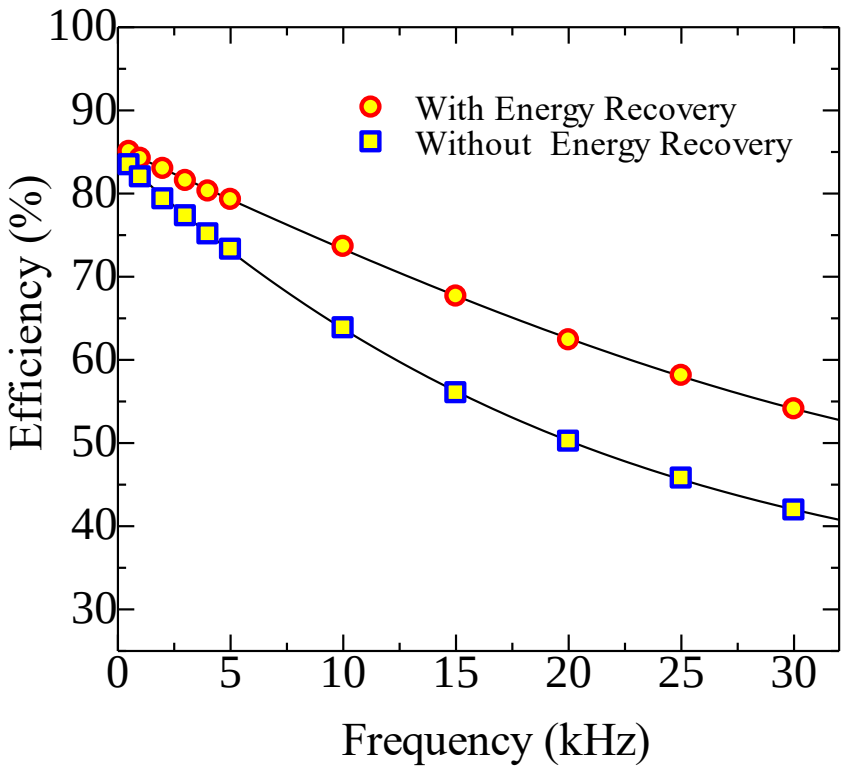

Figure 4.14. Efficiency of PDG with variation of pulse frequency with and without energy recovery operation for each pulse.

Figure 4.14 shows the conversion efficiency of the PDG with variation of pulse frequency, with and without energy recovery at Ar pressure of 15 Pa, DC input voltage of -625 V, discharge current of 20 mA, and 50% duty ratio. In this experiment, the storage capacitance C1 was tuned to be almost the same as the load capacitance C2 for the effective recovery of energy. At the

low frequency of 1 kHz, the efficiency was slightly improved from 83% to 85% by energy recovery. For the highest efficiency of 85%, the DC input power was 6.06 W for a pulsed output power of 5.15 W.

The efficiency decreased with an increase in the pulse frequency in both cases. Without energy recovery, the efficiency decreased more rapidly compared to the energy recovery. However, as observed in Figure 4.11, there was a significant amount of charge remaining on the electrode even after recovery, to be removed subsequently by grounding. The remaining charge in each pulse resulted in an increase of energy loss with an increase of frequency. From a comparison of inclinations, the energy loss was diminished by approximately half.

By extrapolating both lines, the efficiency approaches 86% at 0 kHz. The intercept value of efficiency is not induced by pulse switching, but due to the voltage drop for current regulation from the source voltage of -625 V to the actual sustain voltage. As mentioned previously, the energy loss due to the voltage drop can be reduced by decreasing the source voltage with unbalanced capacitance. By tuning the storage capacitance as unbalanced, however, the energy recovery ratio would deteriorate. Further optimization of the storage capacitance and a possible decrease of the source voltage will effectively improve the conversion efficiency of the PDG.

It was confirmed that the recovery of charge and energy from the load to the storage capacitor was effective for the improvement of power conversion efficiency. For further improvement, especially at higher frequencies, it is necessary to tune the circuit parameters of storage capacitance C1, inductances L1 and L2, resistance Rd, and so on, for effective recovery of the energy with a diminution of the remaining charge. The tuning of circuit parameters for the PDG is similar to impedance matching for the RF transmission line.

It is confirmed by the experimental results that the designed PDG was available for operation of CCP discharge. However, the repeatability, reproducibility and life time of the generator are also considered as significant parameters along with electrical characteristics to validate a newly developed PDG. The repeatability of the PDG was characterized by the variations observed in different measurements for an experiment operated under the same conditions in a short period of time. The reproducibility was also tested by the ability to replicate independently a previously performed experiment results under same conditions. These observations recommend satisfactory repeatability and reproducibility of the PDG. All-solid-sate approach by using semiconductor switches (MOSFETs) with a stable control method is employed to develop the proposed PDG. Hence, the adopted PDG is compact, and has long maintenance-free lifetime and high reliability.

Lastly, the performance of the developed novel (improved) PDG (presented above) can be evaluated compared to our previously developed simple half-bridge PDG (Chap. 3,

Sec.3.2.1.2). However, most important parameters are considered to assess the pulse rising edge and efficiency of energy conversion with pulse repeating rate. Figure 4.15 shows the pulse rising edges for a CCP load by the improved PDG and the half-bridge PDG. The pulse rise time of the improved PDG is 300 ns, which is 10 times faster than the half-bridge PDG at a voltage of -550 V for Ar plasma (15 Pa).

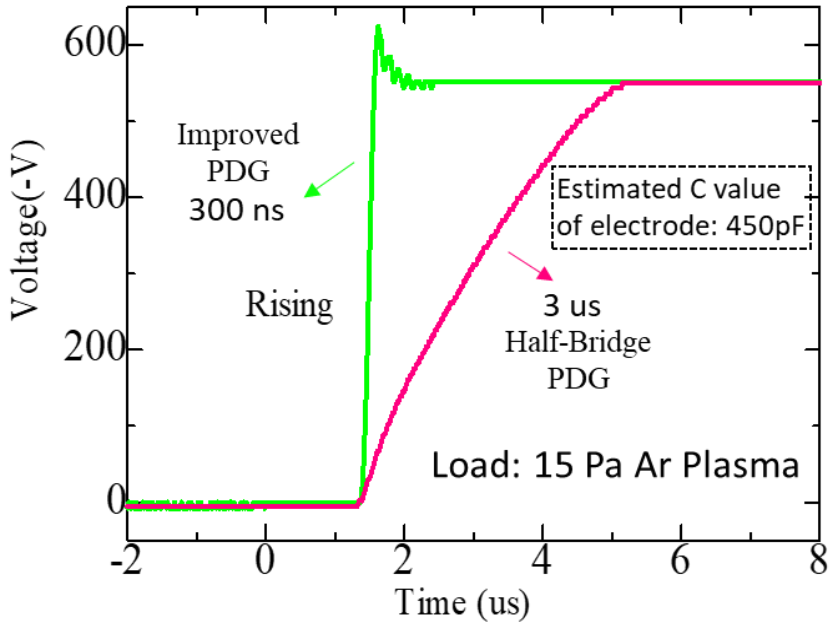

Figure 4.15. Pulse rising edge for a CCP load by the improved PDG and the half-bridge PDG.

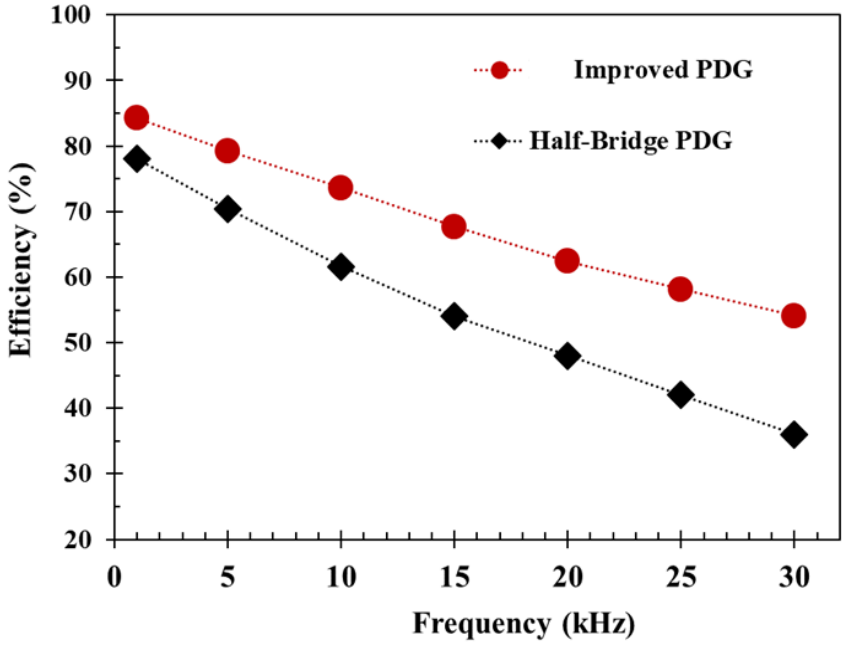

Figure 4.16. Efficiency of improved PDG and half-bridge PDG with variation of pulse frequency.

Figure 4.16 shows the conversion efficiency of the improved PDG and half-bridge PDG with variation of pulse frequency, at Ar pressure of 15 Pa, DC input voltage of -625 V, discharge current of 20 mA, and 50% duty ratio. The efficiency is calculated as the ratio of the time average output power of pulsed DC to the DC input power from the HV source. The efficiency decreased with an increase in the pulse frequency in both cases. However, it was observed that the efficiency decreased more rapidly in half-bridge PDG compared to improved PDG. The energy conversion efficiency by the improved PDG is approximately 15% higher than half-bridge PDG at a pulse operation of 30 kHz.

4.6. Conclusion

In this study, a new model for a pulsed DC generator (PDG) was designed and constructed using an *LC* half-resonant converter and a constant current controller with high-frequency solid-state switching to deliver high-voltage pulses for capacitive coupled plasma discharge in a vacuum chamber. Pulsed DC plasma discharge was operated using the prototype PDG for the monitoring of voltage and current waveforms, and evaluation of power conversion efficiency. In the order of microseconds, the voltage waveform was nearly rectangular and the current level was stable at the set value during the pulse on state. The generator can deliver maximum negative pulses of 1000 V with rise time less than 500 ns and fall time less than 800 ns, respectively. The controllable pulse duration is 1μs – ∞, and operating frequency range is 0 (DC) – 500 kHz. By recovering charge and energy from the capacitive load to the storage capacitor in the PDG, conversion efficiency from the HVDC input to the pulsed DC output at a repetition rate of 30 kHz was considerably improved approximately 12.2%, as expected from the design. The PDG can produce stable and uniform plasma suitable for material processing in a wide range of discharge conditions. It is our belief that this study will stimulate the further investigations on the development of high-frequency energy-efficient pulsed-DC generators for plasma discharge processes.

References

[1] E. L. Neau, "Environmental and industrial applications of pulsed power systems," *IEEE Trans. Plasma Sci.* 22, 2–10, (1994).

[2] H. Akiyama, T. Sakugawa, T. Namihira, K. Takaki, Y. Minamitani and N. Shimomura, "Industrial Applications of Pulsed Power Technology," *IEEE Trans. Dielectr. Electr. Insul.* 14(5), 1051-1064, (2007).

[3] H. Akiyama, S. Sakai, T. Sakugawa, and T. Namihira, “Invited Paper - Environmental Applications of Repetitive Pulsed Power,” *IEEE Trans. Dielectr. Electr. Insul.* 14(4), 825–833, (2007).

[4] X. Lan, M. Long, X. Zi-Jie, X. Qin, Z. De-Qing, and Y. Zi-Kang, “A novel generator for high-voltage bipolar square pulses with applications in sterilization of microorganism,” *IEEE Trans. Dielectr. Electr. Insul.* 22(4), 1887–1895, (2015).

[5] Y. Sun, S. Xiao, J. A. White, J. F. Kolb, M. Stacey, and K. H. Schoenbach, “Compact, nanosecond, high repetition rate, pulse generator for bioelectric studies,” *IEEE Trans. Dielectr. Electr. Insul.* 14(4), 863–870, (2007).

[6] W. Jiang, K. Yatsui, K. Takayama, M. Akemoto, E. Nakamura, N. Shimizu, A. Tokuchi, S. Rukin, V. Tarasenko, and A. Panchenko, “Compact solid-state switched pulsed power and its applications,” *Proc. IEEE* 92(7), 1180–1195, (2004).

[7] T. Opali, B. Ulejczyk, and K. Schmidt-szałowski, “Applications of Pulsed Discharge to Thin-Film Deposition,” *IEEE Trans. Plasma Sci.* 37(6), 934–940, (2009).

[8] S. Samukawa, and T. Mieno, “Pulse-time modulated plasma discharge for highly selective, highly anisotropic and charge-free etching,” *J. Plasma Sources Sci. Technol.* 5, 132-138, (1996).

[9] M. A. Lieberman, and S. Ashida, “Global models of pulse-power-modulated high-density, low-pressure discharges,” *J. Plasma Sources Sci. Technol.* 5(2), 145-158, (1996).

[10] A. Fridman, A. Chirokov, and A. Gutsol, “Non-thermal atmospheric pressure discharges”, *J. Phys. D: Appl. Phys.* 38(2), R1– R24, (2005).

[11] J. Pelletier, and A. Anders, “Plasma-based ion implantation and deposition: a review of physics, technology, and applications”, *IEEE Trans. Plasma Sci.* 33(6), 1944-1959, (2005).

[12] K. Takaki, H. Ogiso, S. Nakano, and K. Yukimura, “A New Approach to High-Power Pulsed Glow Plasma Generation: Shunting Glow Plasma,” *IEEE Trans. Plasma Sci.* 40(7), 1801–1808, (2012).

[13] S. Zabihi, F. Zare, G. Ledwich, A. Ghosh, and H. Akiyama, “A new family of marx generators based on commutation circuits,” *IEEE Trans. Dielectr. Electr. Insul.* 18(4), 1181–1188, (2011).

[14] Y. Wu, K. Liu, J. Qiu, X. Liu, and H. Xiao, “Repetitive and high voltage marx generator using solid-state devices,” *IEEE Trans. Dielectr. Electr. Insul.* 14(4), 937–940, (2007).

[15] J. Rao, Z. Li, K. Xia, and S. Xin, “An all solid-state repetitive high-voltage rectangular pulse generator based on magnetic switch,” *IEEE Trans. Dielectr. Electr. Insul.* 22(4), 1976–1982, (2015).

[16] J. Choi, “Introduction of the magnetic pulse compressor (MPC) - Fundamental review and practical application,” *J. Electr. Eng. Technol.* 5(3), 484–492, (2010).

[17] T. G. Engel, and W. C. Nunnally, “Design and operation of a sequentially-fired pulse forming network for non-linear loads”, *IEEE Trans. Plasma Sci.* 33, 2060–2065, (2005).

[18] R. Chen, J. Yang, X. Cheng, and Z. Pan, "An all-solid-state microsecond-range quasi-square pulse generator based on fractional-turn ratio saturable pulse transformer and anti-resonance network," *Rev. Sci. Instrum.* 88(3), 34701, (2017).

[19] T. Yokoo, K. Saiki, K. Hotta, and W. Jiang, "Repetitive Pulsed High-Voltage Generator Using Semiconductor Opening Switch for Atmospheric Discharge," *IEEE Trans. Plasma Sci.* 36(5), 2638–2643, (2008).

[20] L. Pang, Q. Zhang, B. Ren, and K. He, "A compact repetitive high-voltage nanosecond pulse generator for the application of gas discharge," *Rev. Sci. Instrum.* 82(4), 043504, (2011).

[21] T. Shao, W. Huang, W. Li, C. Zhang, Y. Zhou, P. Yan, and E. Schamiloglu, "A cascaded microsecond-pulse generator for discharge applications," *IEEE Trans. Plasma Sci.* 42(6), 1721–1728, (2014).

[22] J. Laimer, M. Fink, T. A. Beer, and H. Stori, "Plasma dynamics as a key to successful upscaling of pulsed plasma processes," *Surf. Coatings Technol.* 174-175, 118–123, (2003).

[23] L. Li, K. Liu, and J. Qiu, "Repetitive high voltage rectangular waveform pulse adder for pulsed discharge of capacitive load," *IEEE Trans. Dielectr. Electr. Insul.* 20(4), 1218–1223, (2013).

[24] S. K. Sharma and A. Shyam, "Design and testing of 45 kV, 50 kHz pulse power supply for dielectric barrier discharges", *Rev. Sci. instrum.* 87,105115, (2016).

[25] H. Choi, "Design Consideration of Half-Bridge LLC Resonant Converter," *J. Power Electron.* 7(1), 13–20, (2007).

[26] C. Bhuvaneswari and R. S. R. Babu, "A Review on LLC Resonant Converter", *in International Conference on Computation of Power, Energy Information and Communication* (ICCPEIC, 2016), pp. 620–623.

[27] Y. P. Raizer, *Gas Discharge Physics* (Springer-Verlag, Berlin Heidelberg, 1991) p.1-3.

---

*Contributed paper: Md Abdullah Al Mamun, Hiroshi Furuta, Akimitsu Hatta, "Novel high-frequency energy-efficient pulsed-dc generator for capacitively coupled plasma discharge", Review of Scientific Instruments, **89**, 033506, (2018).*

Chapter 5

Deposition and characterization of a-C:H films using a high-repetition microsecond-pulsed DC capacitive-couple plasma CVD system

This chapter presents the investigation of the growth of hydrogenated amorphous carbon (a-C:H) films on silicon substrates with the variation of pulse repetition rate using a developed high-frequency pulsed DC capacitive-couple plasma CVD system. The introduction, objectives, and experimental methods are described. The study of the influence of the pulse repetition rate on the plasma characteristics is performed. Furthermore, the deposition rate and films properties are presented as a function of pulse operating frequency. Finally, discussions and conclusions are drawn based on the experimental results.

5.1. Introduction

Diamond-like carbon (DLC) is an amorphous carbon (a-C), whereas hydrogenated amorphous carbon (a-C:H) films consist of a combination of sp^2 and sp^3 carbon bonds. DLC films are the focus of great interest because of their several industrial applications due to their magnificent properties such as high hardness, low frictional coefficient, high insulation properties, chemical inactiveness, and optical transparency [1–4]. The DLC films exhibit various properties because of their different microstructures depending on the synthesis approach and the process parameters used. There are various deposition methods employed to produce DLC films, such as sputtering, [5–7], filtered-arc deposition [8], pulsed laser ablation [9] and plasma-enhanced chemical vapor deposition (PECVD) [10–11] employed to produce DLC films. Among these method, PECVD is widely used to prepare a-C:H films from hydrocarbon discharges owing to its advantages of considerably low deposition temperature, higher throughput, and uniform deposition area. [12–13]. PECVD involves chemical processes that occur in the vapor phase on the substrate surface to form films. Basically, two types of plasma species, radicals (chemically active neutral species) and ions that diffuse from the plasma, drift toward the substrate surface to form films. The plasma species and ionic energies as well as densities are widely affected by the discharge process [14].

PECVD is usually carried out using various power systems such as microwave (2.4 GHz), radio frequency (RF13.56 MHz), pulsed DC (adjustable frequency range Hz to kHz), and DC (0 Hz) systems. Among these, definitely, plasma discharge by pulsed DC introduces considerable advance in material synthesis owing to the stability and controllability of plasma

properties [15] and it is advantageous for the deposition of insulating thin films, for example, a-C:H films, because the substrates are required to be powered with an alternating current [16]. The pulse parameters, specifically frequency and pulse width, directly affect the plasma deposition and diffusion processes used, which are supposed to the key factors for the enhancement of film properties. A pulse with high voltage, short rise time, and high repetitive rate can produce a strong electric field that accelerates electrons to a high-energy state and increases electron-excitation temperature, which is interesting for amorphous carbon thin-film processing. Thus, the plasma discharge characteristics are significantly affected by the design of pulsed DC power supply (PDPS) as well as the arrangement of electrodes inside the chamber. When two electrodes (anode and cathode) separated by a certain distance and set similarly to parallel plates in a vacuum chamber filled with a process gas, they function as a capacitive load, the so-called capacitive-coupled plasma (CCP). For capacitive loads, to achieve high-frequency pulses with very short rise and fall times is challenging because strong current is necessary for fast charging and discharging to them [17]. Moreover, the efficiency of the power supply is seriously degraded as pulse frequency increases owing to switching loss. Therefore, it is attractive to design an energy-efficient high-frequency (several hundreds of kHz) pulsed DC power supply for CCP that can drive a wide range of pulsed plasma discharge operations with various pulse parameters, such as frequency, duty cycle, and amplitude.

Hence, understanding the processes occurring in CCP during high-frequency pulsed DC is required. One of the techniques to realize a glow discharge is based on the electrical behavior of CCP. For example, CCP can be observed from its current-voltage (I-V) characteristics when it runs under steady condition, which is crucial for the homogeneous discharge as well as efficient excitation and ionization [18]. Furthermore, optical emission spectroscopy (OES) is considered as the popular tool used for the examining glow discharge parameters [19]. The optical emissions from plasma discharge occur via numerous excited particles, and it has been reported that electron-excitation temperature in plasma can be estimated from the relative intensities of spectral lines [20]. In particular, it is expected that the electron-excitation temperature and the species generated in plasma may be affected by the high-frequency operation of pulsed power, which are considered as important parameters in film growth applications.

However, several studies [15, 21–23] have been carried out for the preparation of a-C:H films by conventional pulsed plasma CVDs, in which the pulse frequencies and widths were 20-40 kHz and 10-30 μs, respectively. In contrast, very few works [24–25] have been reported for the deposition of a-C:H films using high-frequency pulsed DC plasma discharge, in which the maximum operating pulse frequency was limited to 250 kHz. In addition, the impact of

plasma-generated hydrocarbon species on the formation of films was not discussed. It is expected that pulsed discharge carried out further than this being more interesting for films deposited at higher frequencies may increase the ionization efficiency leading to a higher plasma density and greater contribution of plasma-generated hydrocarbon species. Therefore, the study of high-frequency pulsed DC plasma glow discharge by OES for CVD of a-C:H films has attracted much attention.

5.2 Objective

In this study, a new method of the deposition of a-C:H films using a high-frequency pulsed DC plasma CVD system inside a vacuum chamber is presented. The high-frequency pulsed glow discharge characteristics analyzed by OES and their effects on the growth process and structural properties of the deposited films at various pulse frequencies were investigated.

5.3. Experimental and methods

Figure 5.1. shows a schematic diagram of the high-frequency microsecond-pulsed DC capacitive-couple plasma CVD system developed by means of a novel pulsed-DC generator (described in chap. 4) and a customized vacuum discharge chamber apparatus (described in chap. 3). High-repetitive capacitive-couple plasma discharge was operated between the working electrode and the inner wall of the vacuum chamber made of Al instead of inserting a counter electrode. The gap between the working electrode and the chamber wall was 50 mm. Negative pulse voltage was applied to the electrode, and the chamber wall was kept electrically grounded. The main component of the system is a pulsed DC power supply (PDPS), which provides the power required to ignite and sustain the plasma discharge inside the chamber. As the plasma discharge characteristics are notably affected by the design of the power supply [26–28], it is vital to understand the operation of the developed prototype PDPS (not presented here for simplicity, described in chap. 4, section 4.3.4).

For the experiments, firstly the discharge chamber was evacuated using a turbomolecular pump (TMP) and a rotary pump (RP) below a base pressure of $8x10^{-3}$ Pa. The gas fed into the chamber was controlled by mass flow controllers (MFCs), and the working pressure was maintained by controlling the evacuation valve (EV). For the assessment, gas discharge experiments were carried out under various discharge conditions. a-C:H films were deposited on mirror polished, n-type Si (100) wafers placed at the top of the electrode from C_2H_2 hydrocarbon gas at room temperature. In this proposed system, the electrode with the substrate holder was considered for the use of a 4-inch wafer with an active circular deposition window

of 90 mm diameter. It was confirmed that the film was deposited in the entire deposition window; however, in this study, only a quarter of the circular deposition window was used to decrease the consumption of Si wafers.

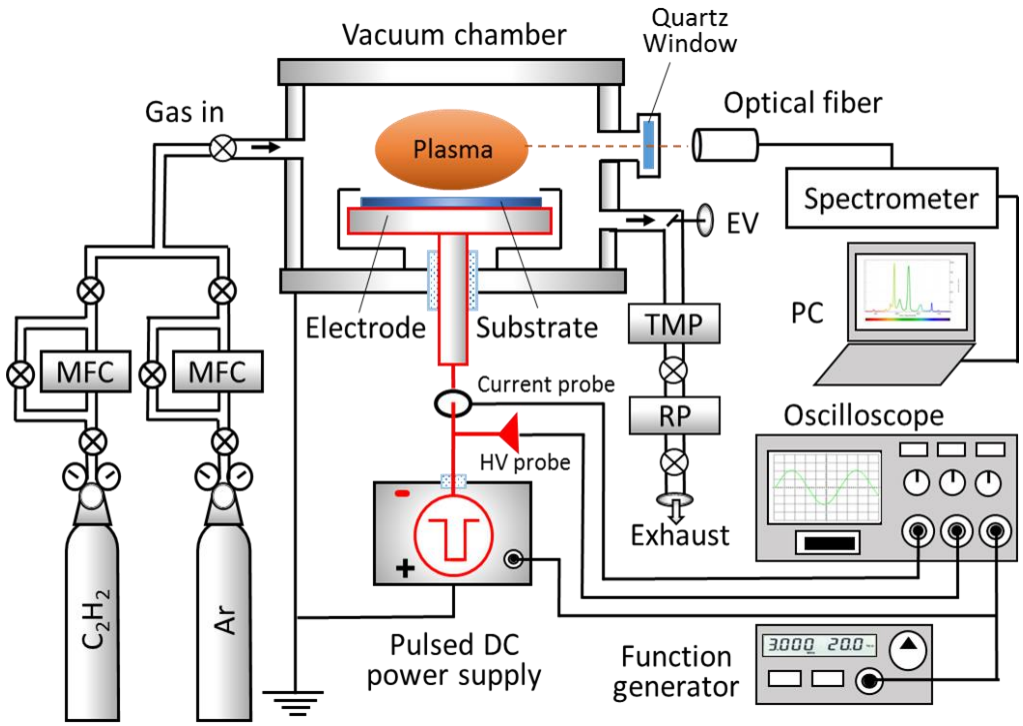

Figure 5.1. Schematic view of experimental setup of the pulsed DC plasma glow discharge system.

Table 5.1. Plasma CVD conditions for deposition of a-C:H films.

Gas	Pressure (Pa)	Deposition time (min)	Flow rate (sccm)	Electrode voltage (pulsed) (V)	Constant current set (mA)	Pulsed width (μs)	Frequency (kHz)
C_2H_2	15	10	100	-800	10	10	50
						5	100
						2.5	200
						1.67	300
						1.25	400

The deposition conditions are shown in Table 5.1. by keeping other conditions unchanged, plasma CVD was carried out at various pulse frequencies at a constant duty cycle of 50%. In this approach, a higher repetition rate contributes to generating minute negative pulses for plasma discharge. Before each film deposition, argon (Ar) plasma was operated for one minute

under the same conditions as those for deposition. It is considered as a preprocessing treatment of the Si substrate for the elimination of the native oxide layer from the substrate surface.

Plasma discharge characteristics were examined by current-voltage waveform analysis and OES. The current-voltage waveforms were measured and stored in a digital storage oscilloscope (Tektronix 2014B, 100 MHz) for further investigation using an isolated-current probe and a high-voltage probe. For OES measurements, the plasma emission light through a quartz view port was introduced into a bare optical fiber (Ocean Optics P1000-1-SR) connected to a multichannel spectrometer (Ocean Optics USB4000; measurement range, 178-888 nm; optical resolution, 1.46 nm) interfaced with a PC. The optical data acquisition conditions were set as follows: accumulation time, 100 ms; average number of scans, 50; and number of boxcar segments, 10. The sensitivity of the spectrometer and optical fiber was calibrated as absolute spectral irradiance using a deep-UV deuterium and tungsten halogen light source (Ocean Optics DH-2000-DUV). The thickness of the deposited films was evaluated using a benchtop stylus profilometer (KLA-Tencor Alpha-Step IQ). The film properties were characterized using a Raman spectrometer (Horiba Jobin Yvon HR-800; laser excitation wavelength, 532.08 nm), a Fourier transform infrared (FT-IR) spectrometer with an evacuation system (JASCO FT-IR-6100), and a resistivity meter (Loresta EP MCP-T360, 4-pin probe; measurement range, 10^{-2} – 10^{6} Ω).

5.4. Results and discussion

5.4.1. Discharge Characteristics

From the gas discharge experiments, it was confirmed that the developed PDPS can deliver nearly rectangular negative pulses of up to1 kV with short rise time (<500 ns) and fall time (<800 ns) even for the CCP load. The maximum operating pulse frequency was 500 kHz with a minimum pulse width of 1 μs. Figure 5.2(a) shows typical current-voltage waveforms of a single pulse obtained from the C_2H_2 gas discharge at a pressure of 15 Pa, an input voltage (DC) of -800 V, an input pulse frequency of 100 kHz, a duty ratio of 50%, and a steady pulse current of 10 mA. The waveforms have four characteristic timing modes of operation. For the duration t_1, the electrode is quickly charged to a peak voltage (V_p) with a large peak current (1.28 A) pulse for the ignition of discharge. After ignition of plasma, damping oscillation of voltage and current appears and peak voltage gradually decreases to reach a stable discharge voltage (V_d), at which the discharge current is well controlled at the set level of 10 mA, and uniform plasma discharges were observed, as shown on the inset in Figure 5.2(a). This is the steady discharge duration of t_2, which varies according to the set pulse frequency and duty cycle. During t_3,

charges from the electrode are recovered to the energy storage capacitor with a peak current (0.8 A), and during t_4 charges are forcibly eliminated from the electrode by grounding with another peak current (1.7 A) within 100 ns. The voltage waveforms of almost rectangular and stabilized current confirmed the wide pulse frequency range of operation. For the deposition of a-C:H films, however, we intentionally chose five distinct pulse frequencies to investigate the high frequency dependence on the film properties.

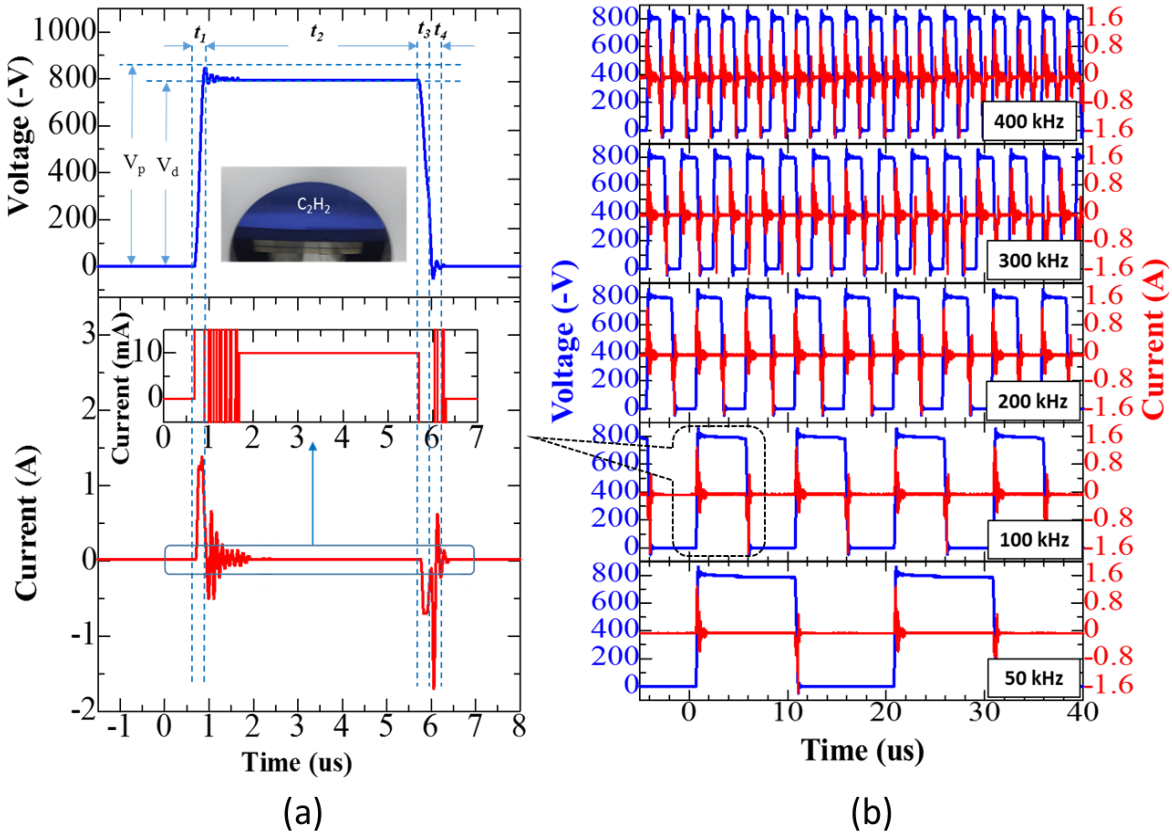

Figure 5.2. Discharge current-voltage waveforms of the deposited films (a) a typical individual pulse at 100 kHz (b) pulses of different frequency vertically placed within a time frame of 45μs.

Figure 3(b) shows the discharge current-voltage waveforms during the deposition of films at different pulse frequencies which are vertically demonstrated within a fixed time frame of 45 μs. It is observed that the number of pulses increases and the pulse width decreases with increasing frequency. At a higher frequency, the steady-discharge part was almost diminished and the discharge was mostly sustained by the transferred charge from the energy storage capacitor. The high-frequency-operated pulse discharge has large impact on the initiation of plasma generation rather than the steady state. Hence, the operation of pulsed discharge at a higher frequency may increase the ionization efficiency, and it seems that the conventional RF plasma sustained through resonance between the electrode and the matching network.

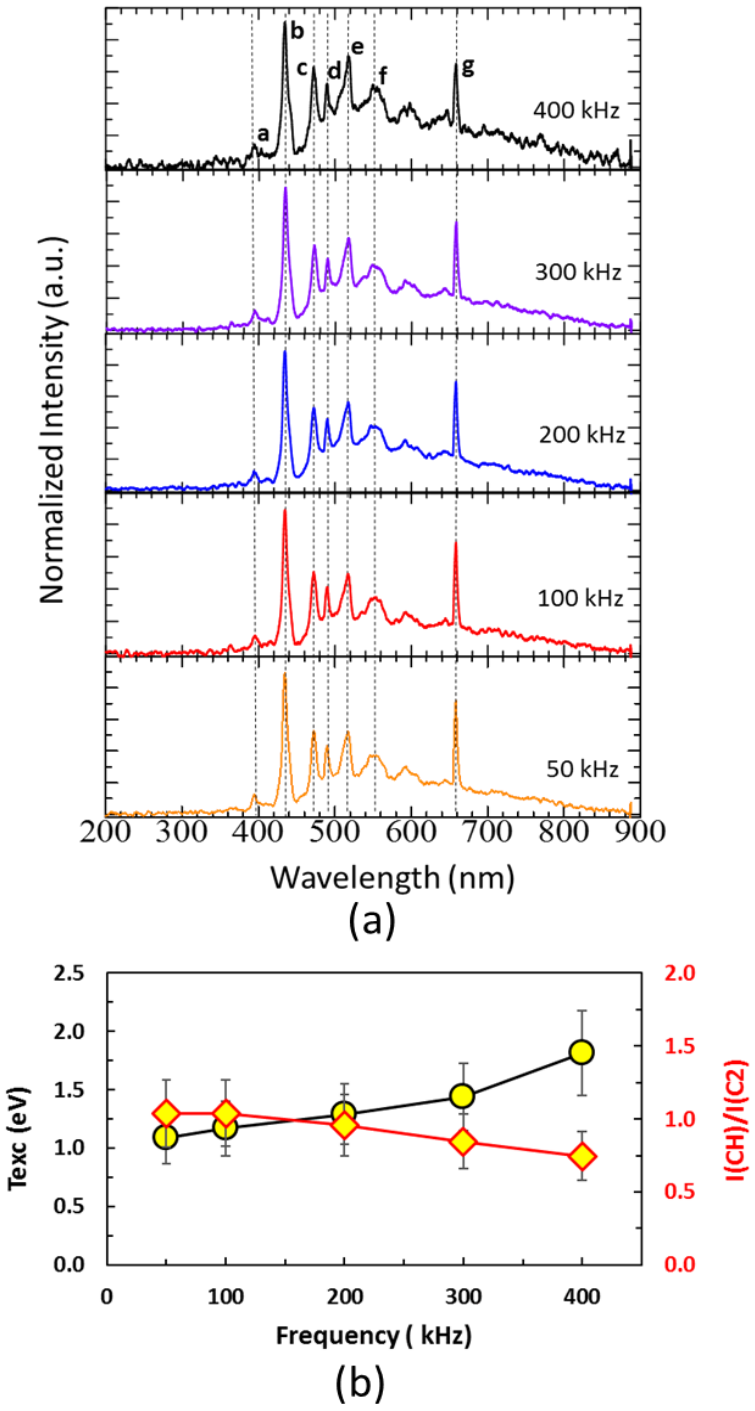

Figure 5.3. (a) Optical emission spectra of the C_2H_2 in pulsed DC plasma CVD at different pulse frequency. Each spectrum was normalized using the CH emission intensity. (b) Electron excitation energy and intensity ratio of CH/C_2 in C_2H_2 plasma with a variation of pulse operating frequency.

The study of hydrocarbon plasma discharge by OES has gained prominent attention for identifying the active species that play leading roles in the growth of films [29]. The optical emission spectra of C_2H_2 plasma operated at different pulse frequencies in the broad range of 200-900 nm during the deposition of films are shown in Figure 5.3(a). Prominent emission lines of CH, C_2, H_α, and H_β are clearly identified in the spectra [30], where each spectrum was

normalized by the CH peak intensity at 431 nm. These observed species are presented in Table 5.2. The relative time average intensities of these peaks were evaluated by fitting each peak to the Lorentzian distribution after deducting the continuum emission as the background. It is a well known method for determining of the electron-excitation temperature (T_{exc}) using the intensities of H_α and H_β lines emitted from the plasma. The T_{exc} in the plasma has been evaluated in electron-volt (eV) using the technique described in the literature [31]. Figure 5.3(b) shows the T_{exc} and the intensity ratio of the CH peak (431 nm) to the Swan band of the C_2 peak (516 nm), [I(CH)/I(C_2)] of C_2H_2 plasma operated at different pulse frequencies. The figure shows that the electron excitation energy gradually increases while I(CH)/I(C_2) decreases with the increase in pulse frequency and becomes more prominent at frequencies higher than 200 kHz. It is suggested that C_2H_2 becomes more dissociative at higher pulse frequencies. This effect has great impact on the growth of hydrogenated a-C films, and the film properties in our current experiments are in agreement with those obtained in some previous works [32–34].

Table 5.2. Main species of OES spectra in C_2H_2 plasma.

Peak	Position (nm)	Species	Transition
a, b	390, 431.1	CH	$B^2\Pi^- \rightarrow X^2\Pi$, $A^2\Delta \rightarrow X^2\Pi$
c, e, f	473.7, 516.5, 563.5	C_2 (Swan Band)	$A^3\Pi \rightarrow X^3\Pi$
d, g	486.1, 656.3	H_β , H_α (Balmer series)	n= 4→2, 3→2

5.4.2. Characterization of a-C:H films

Figure 5.4(a) shows the deposition rate of the a-C:H films as a function of pulse frequency. It was found that the deposition rate of the films increases slightly with pulse frequency up to 200 kHz, and with the further increase in pulse frequency until 400 kHz, the deposition rate tends to decrease. The maximum deposition rate was attained 60 nm/min at 200 kHz with a pulse duration of 2.5 μs and a low gas pressure of 15 Pa. Nevertheless, the formation of dangling bonds in the film determines the growth rate, i.e., the surface having more dangling bonds shows a higher growth rate [35]. Two complementary impacts of the H species in hydrocarbon plasma on the growth of a-C:H films have been reported, namely, the formation of dangling bonds by ions bombardment, which increases the deposition rate, and the etching of weak neighboring dangling bonds, which reduces the growth rate. However, an almost uniform deposition area of the deposited films was observed from the radial profile of film thickness, as shown in Figure 5.4(b). This result also correlates to the uniformity of the plasma discharge, as mentioned in earlier section.

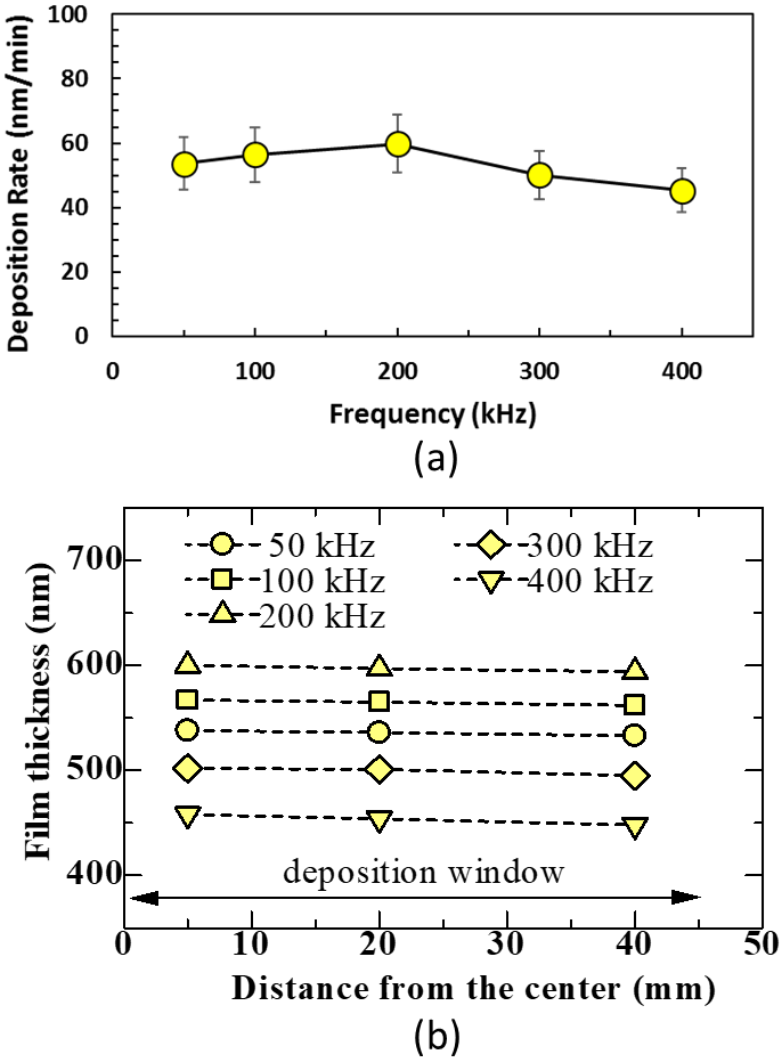

Figure 5.4. (a) Deposition rate of the films as a function of pulse frequency and (b) radial profiles of thickness of the deposited films.

Raman spectroscopic measurements were carried out to examine the microstructural properties of the films. The visible Raman spectra of films synthesized at various pulse frequencies are shown in Figure 5.5. These spectra show a broad peak that overlapped with a dominant peak positioned at ~1520 cm^{-1} and a shoulder peak at ~1400 cm^{-1} assigned as the so-called G (graphitic) and D (disordered) peaks, respectively. These peaks of the Raman spectra suggest typical characteristics of a-C:H films. The G peak appears because of the stretching vibration mode of sp^2 sites either in chains or aromatic rings, whereas the D peak appears owing to the breathing mode of sp^2 sites in aromatic rings [1-3].

Besides, an inclined background overlaid on each Raman spectrum was observed, which was attributed to the photoluminescence (PL) background. The hydrogen (H) content in the a-C:H films markedly affects the slope of the PL background and it can be estimated according to the formula stated in the literature [36], where the laser excitation wavelength is 514.5 nm. It

is supposed that the trend in the slope of the PL background with the increase in the hydrogen content in the films is not changed by a small shifting of the laser excitation wavelength to 532.08 nm employed in this work, but the accuracy of the estimated H content may slightly diverge.

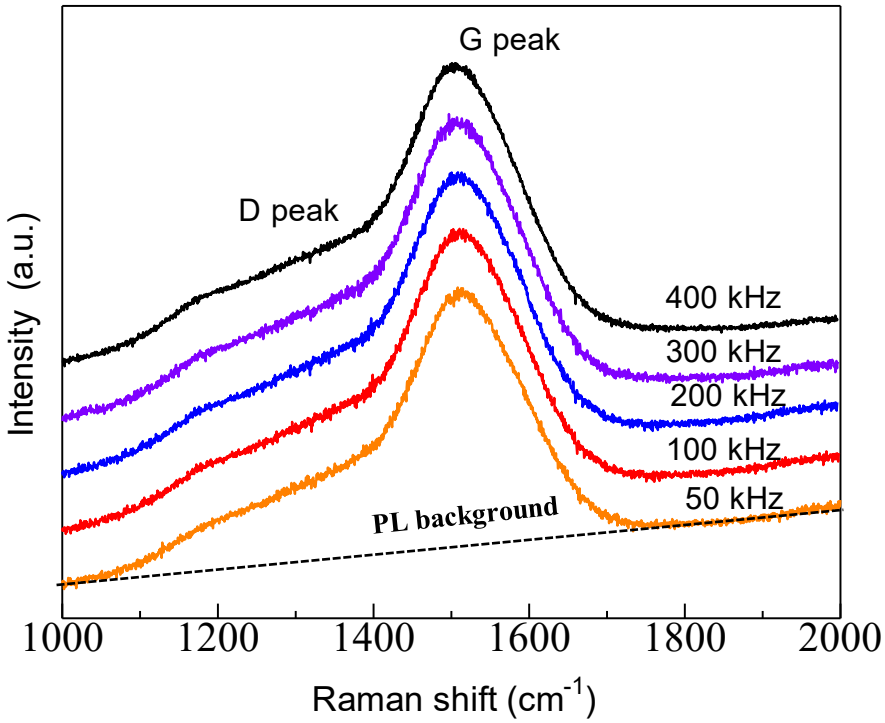

Figure 5.5. Raman spectra of the a-C:H films prepared at different pulse frequency where the spectra are set vertically for clarity.

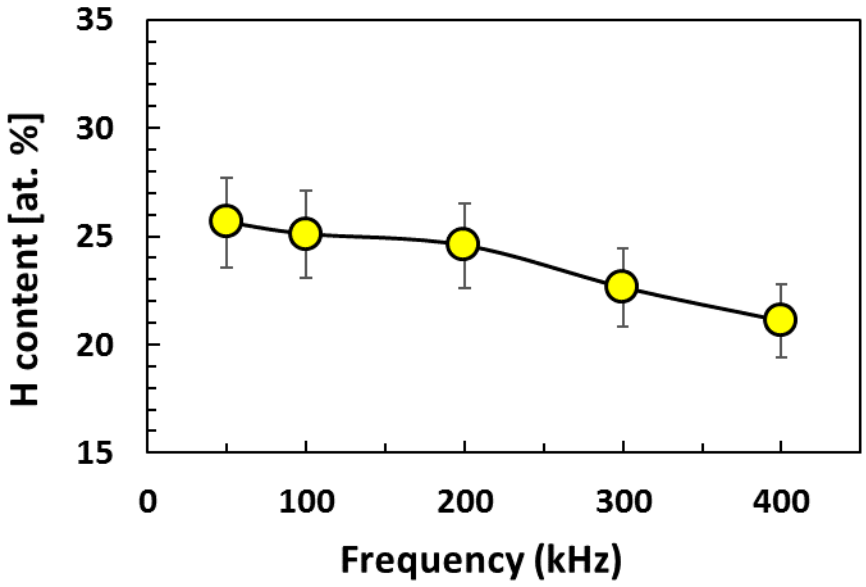

Figure 5.6. Hydrogen content of the a-C:H films evaluated using the Raman spectra as a function of the pulse frequency.

However, using this technique, the hydrogen content of the deposited films at various pulse frequencies was evaluated, as shown in Figure 5.6. It is found that the hydrogen content decreases from 25 to 21 (at. %), when the pulse frequency increases from 50 to 400 kHz, where the decrease rate is larger at higher pulse frequencies, specifically after 200 kHz. A probable explanation is that, when the plasma discharge is operated at higher frequencies, ion impinge on the substrate is enhanced as expected owing to the contribution of ions extracted from the afterglow of the previous pulse to the next pulse, which may contribute to the preferential H release from the a-C:H films [37]. Such a decrease in hydrogen content in high-frequency operation of pulsed glow discharge plasma is observed in the DLC films prepared from methane gas [25].

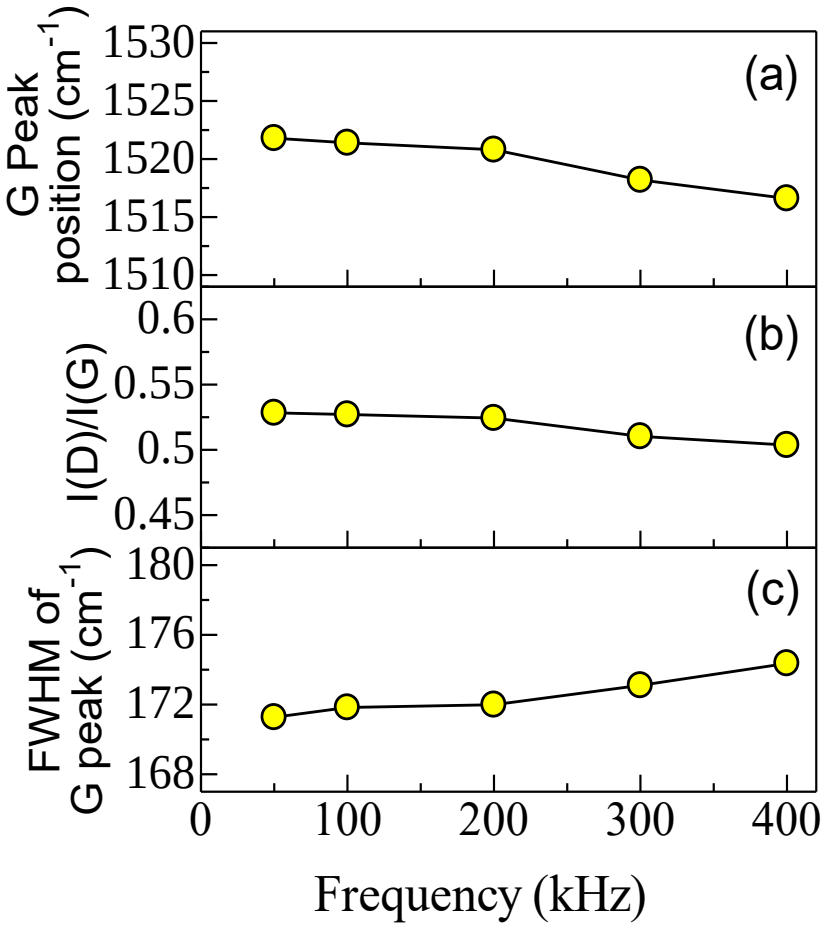

Figure 5.7. Raman spectral parameters (a) G peak position (b) I(D)/I(G), and (c) FWHM of G peak all as function of pulse frequency.

For the investigation of the microstructure of the deposited a-C:H films, Raman spectra were fitted by two Gaussian distributions for the D and G peaks after deducting the PL background. The G peak position, the full width at half maximum (FWHM) of the G peak, and the intensity ratio of the D peak to the G peak (I(D)/I(G)) were evaluated. Figures 5.8(a)-5.8(c)

show the correlation of these Raman spectral parameters with the variation of pulse frequency. The "three-stage" model, [1,38] recommended by Robertson's group, is commonly used for the examination of Raman spectra; the evaluation of the microstructural properties of the films in this work is basically based on this model. In general, for a conventional a-C:H film, the shifting of the G peak position to the lower wave number, the decrease in I(D)/I(G), and the increase in the FWHM of the G peak correspond to the growth of a diamond-like structure in the films. The film characteristics in the case of increasing pulse frequency are as follows: the G peak position comparatively has a lower wave number and marginally decreases with increasing pulse frequency from 1521.8 to 1516.6 cm^{-1}; I(G)/I(D) is comparatively low and slowly decreases from 0.53 to 0.50; and the FWHM of the G peak is comparatively high and rises from 171.27 to 174.36 cm^{-1}. In particular, our deposited films show good agreement with the tendency found in stage 2 of the three-stage model. These results of Raman spectral analysis reveal that the sp^3 content (amorphization) of the films slightly increases as the pulse frequency increases. It is supposed that the slight growth of C-C bonds may be enhanced by the formation of dangling bonds from the broken C-H bonds cause by more ions impinge at a higher pulse frequency.

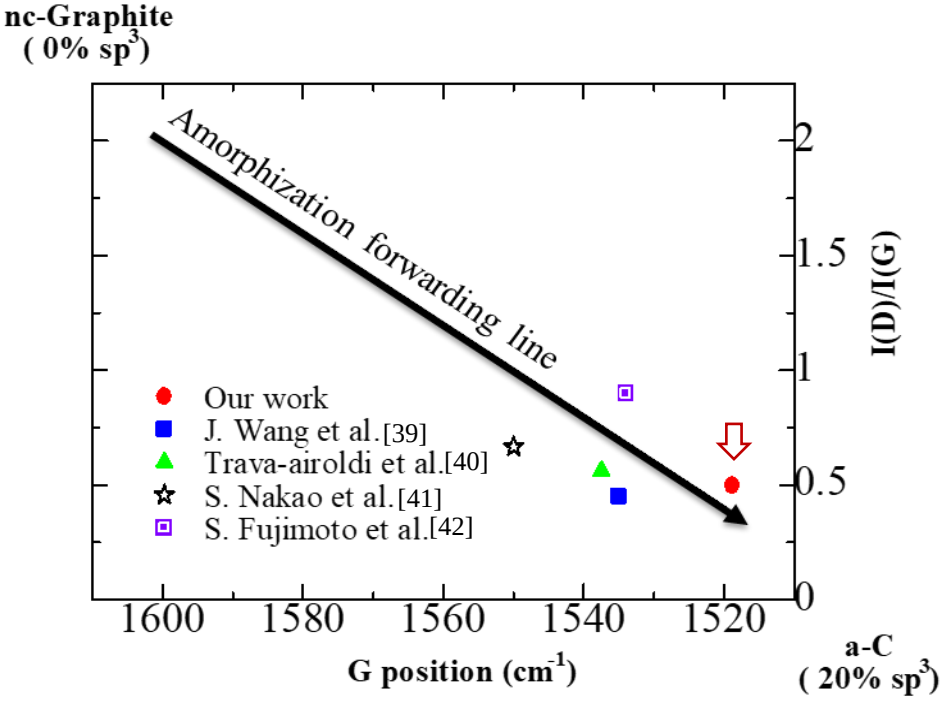

Figure 5.8. Amorphization evaluation diagram of the film prepared at the highest pulse frequency (400 kHz) compared to some previous works based on Robertson's three stage model.

Furthermore, the amorphization of the film prepared at the highest pulse frequency (400 kHz) is compared to some previous works [39-42] based on Robertson's three stage model, as

shown in Figure 5.8. Amorphization forwarding line shows enhanced sp^3 content in the film prepared by our developed high-frequency pulsed-dc plasma CVD system, in contrast of previously performed some pulsed plasma CVD works of hydrogenated amorphous carbon films.

Generally, the microstructure of a-C:H films significantly influences the mechanical and tribological properties such as hardness and wear resistance which are interrelated to the fraction of the sp^3/sp^2 hybridization of carbon atoms in the films. The increase in the number of sp^3 (diamond-like) bonds enhances the hardness and wear resistance of the films, while the increase in the number of sp^2 (graphitic-like) bonds degrades these properties. The Raman spectroscopic analysis results presented above suggests that the films prepared at a higher pulse repetition rate have relatively higher concentrations of sp^3 bonds. It can be clearly expected that the hardness and wear resistance of the a-C:H films are improved, as the operating pulse repetition rate of microsecond-pulsed DC plasma CVD increases.

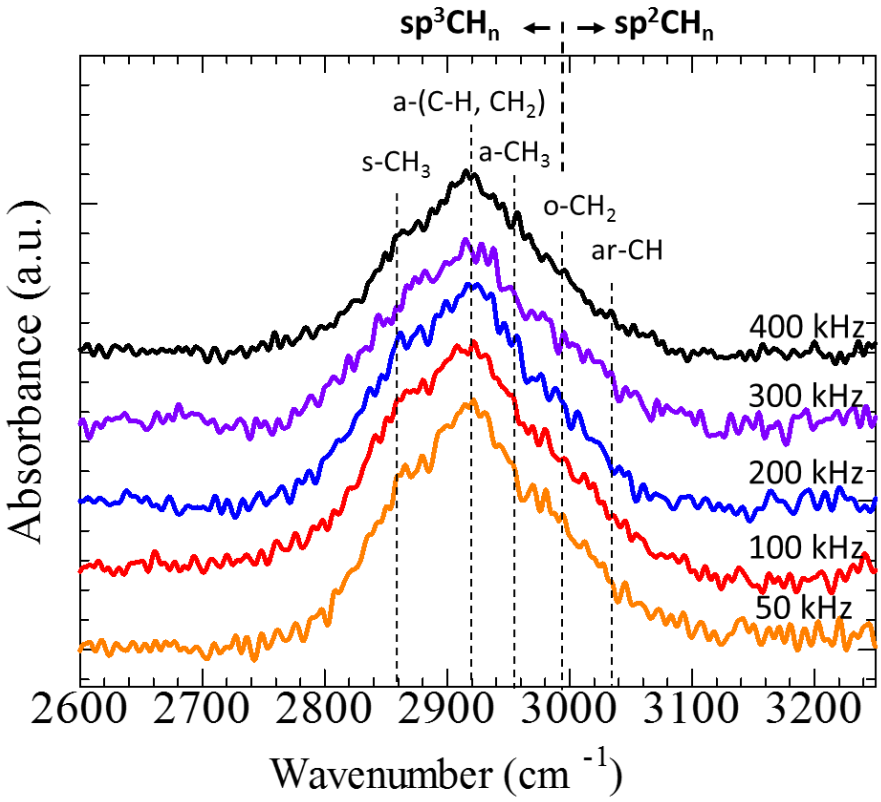

Figure 5.9. FT-IR spectra of the a-C:H films deposited by varying pulse frequency from 50 to 400 kHz.

Hydrogen plays a significant role in the physical properties of hydrogenated a-C films and it can be used to sense the assembly of bonded carbon atoms because of the confined vibration mode of the C-H bonds. FT-IR spectroscopy is broadly employed to explore the C-H bonding in a-C:H films [1,43]. Figure 5.9 shows the FT-IR absorption spectra of the prepared films at

various pulse frequencies, in which all spectral intensities are normalized by the film thickness. Each spectrum shows both the sp^3CH_n and sp^2CH_n stretching mode peaks within 2860-2955 cm^{-1} and 2995-3080 cm^{-1}, respectively, which are generally observed in a-C:H films [44]. It is identified that the C-H absorption peaks are centered at 2920 cm^{-1}, which appeared to be due to the asymmetric stretching mode of the hydrogen bonds in the form of sp^3CH and sp^3CH_2, associated with the overlapped shoulder peaks at 2860, 2955, 2995, and 3035 cm^{-1}, which are attributed to the symmetric sp^3CH_3 mode, asymmetric sp^3CH_3 stretching mode, symmetric olefinic sp^2CH_2, and aromatic sp^2CH, respectively [43]. However, the intensities of the sp^3C-H stretching mode peaks are apparently higher than the sp^2C-H peaks, which suggests that the hydrogen atoms in the films mostly formed sp^3 hybridized bonds to the carbon atoms.

It is also noted that the intensity of the C-H absorption peaks of the films gradually decreases with increasing pulse frequency. As the intensity of the C-H absorption peak is the sign of the bonded hydrogen content in the films, it is assumed that the bonded hydrogen content in the films decreases with increasing pulse frequency owing to the large number of ions impinging on the surface of the substrate, resulting in the breakage of the weak C-H bonds. Moreover, this reduction in the content of hydrogen forming bonds inside the films with increasing pulse frequency is also confirmed by Raman spectrometry analysis.

The electrical resistivity of all the a-C:H films was examined by the four-point probe measurement technique. The resistivity results of all the films showed highly insulating properties (unable to measure, over loaded, above 10^6 Ω/□), which are consistent with the results obtained from microstructural analysis that the films contained less graphitic structure with sp^2 hybridization. These types of films have high potential applications in passive electrical devices as protective coatings.

It can be generally considered that the growth mechanism of hydrogenated a-C films by the plasma CVD method is mainly based on the ionic impact and chemical absorption on the substrate. It is recognized that C_2H_2 gas molecules are decomposed by plasma, resulting in the production of neutral and ionic radicals of hydrocarbon along with atomic or ionic hydrogen. Generally, hydrocarbon ions (positive) are accelerated in the substrate (negative) and form dangling bonds, with which the neutral hydrocarbon radicals are absorbed and enhance the growth of a-C:H films, whereas the growth or etching of the surface of the films also occur with hydrogen ions (atoms). It can be suggested that growth mechanism of the hydrogenated a-C films is the balance between the deposition and removal of hydrocarbon radicals, which is mostly governed by the ions impinging on the surface of the substrate. Finally, the hydrogen content remaining in the films depends on the competition between the subtraction and incorporation of hydrogen. In this study, it is found that the subtraction of hydrogen is

stimulated at high pulse frequencies as the number of ions impinging on the substrate increases owing to the hydrocarbon dissociation enhanced by the increased electron excited energy, resulting in the slight decrease in hydrogen content as well as the modification of the film properties. An expected model can be demonstrated as shown in Figure 5.10.

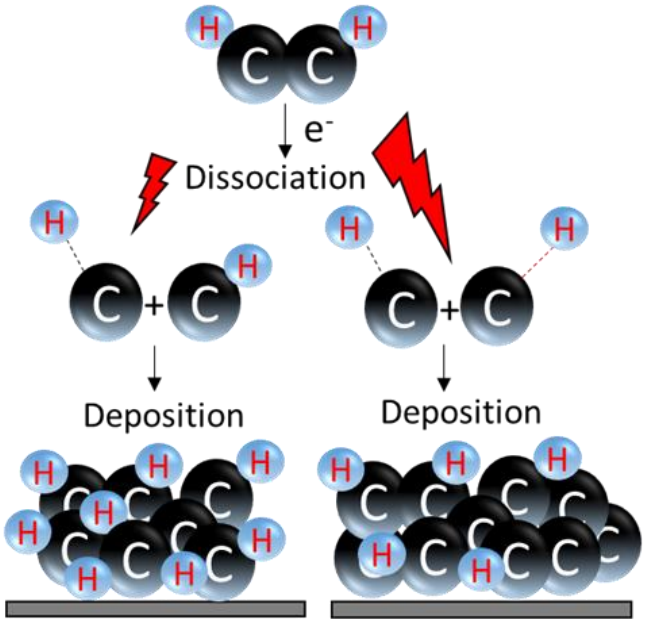

Figure 5.10. An expected model of C_2H_2 electron impact dissociation and film growth at lower and higher electron excited energy.

However, the impact of H species on the formation of a-C:H films is relatively complex. Therefore, the complex process from gas phase to the surface and their relationship with the plasma parameters, the ion energy distribution and quantitative correlations to the resulting films should be studied in future works.

The interesting features of this novel pulse discharge system are that it can operate using capacitive-coupled plasma (CCP) in a wide range of high frequencies up to 400 kHz with stable current and broad variation of pulse modulating parameters. The major advantage is the possibility to modify the electron excitation energy in the glow discharge by tuning the pulse parameters. In pulsed plasma, the electron excitation energy is boosted by starting each pulse to reach a higher electron temperature as the driving frequency becomes high. This results in the production of more chemically active plasma and introduction of more exciting species to take part in the deposition process. Moreover, in highly repetitive pulsed plasma, the impact of afterglow is also dominant. It can be assumed that at a low frequency the afterglow of the previous pulse discharge vanishes as the next pulse approaches. In high-frequency operation, the afterglow discharge generated from the preceding pulse discharge exists and contributes as a pre-ionization effect on the subsequent pulse discharge. As a result, the plasma discharge

driven at a high frequency contributes more ions to the growth of films. However, the control of electron density in plasma, which is basically governed by current density is also crucial for controlling the reproducibility of the CVD system. In the current control mode, this pulse discharge system can keep the set discharge current stable regardless of the plasma characteristics impedance, which is very effective for the deposition of insulating films to confirm the uniform deposition area. Furthermore, the modulation of pulse parameters such as the variations in pulse duty and voltage amplitude and the energy recovery technique also make this developed system more versatile than the conventional pulsed discharge system. It seems that the plasma discharge characteristics and the deposition of films and their properties can be widely modified using the high-frequency pulsed DC plasma discharge system, which can open new possibilities in etching, ion implanting, and sputtering applications in material processing.

5.5. Conclusion

A new model of high frequency pulsed DC plasma CVD system has been developed for the deposition of a-C:H films from C_2H_2 gas. This technique is employed by a developed pulsed DC power supply (PDPS) which can produce highly repetitive microsecond pulsed plasma glow discharge at considerably low pressure inside a customized vacuum chamber. The deposition of a-C:H films was carried out on Si substrates with a variation of pulse frequency up to 400 kHz at 50% duty cycle by keeping gas pressure of 15 Pa and negative pulse magnitude of 800 V. The impacts of increasing of pulse frequency on the plasma discharge characteristics, generated hydrocarbon species, deposition rate and structural properties of films were examined. The results show that the dissociation of C_2H_2 became higher with the increasing of pulse repetition rate as the electron excited energy increases. The growth rate slowly increases with pulse frequency until 200 kHz and after that a gradual reduction is observed. The hydrogen atoms in the films are mostly formed sp^3 hybridized bonds to the carbon atoms and it decreases with the increasing of pulse frequency. All the prepared films demonstrate highly insulating properties while the amorphization (sp^3 content) increases with the increase of pulse operating frequency. The results suggest that the proposed pulsed DC plasma CVD system driven by tiny high voltage pulses (few microseconds) with high repetition rate (several hundreds of kilohertz up to 400 kHz) can be considered as advantageous for the preparation of a-C:H films.

References

[1] J. Robertson, “Diamond-like amorphous carbon”, *Mater. Sci. Eng. R* 37, 129 (2002).

[2] A. Grill, “Diamond-like carbon: state of the art”, *Diamond Relat. Mater.* 8, 428 (1999).

[3] J. Robertson, "Plasma Deposition of Diamond-Like Carbon" *Jpn. J. Appl. Phys.* 50, 01AF01 (2011).

[4] Y. Lifshitz, "Diamond-like carbon — present status", *Diamond Relat. Mater.* 8, 1659 (1999).

[5] S. Aisenberg, R. Chabot, "Ion-beam deposition of thin films of diamond like carbon", *J. Appl. Phys.* 42, 2953 (1971).

[6] S. Kumar, K. S. A. Butcher, and T. L. Tansley, "X-ray photoelectron spectroscopy characterization of radio frequency reactively sputtered carbon nitride thin films", *J. Vac. Sci. Technol. A* 14, 2687 (1996).

[7] A. Czyzniewski, "Preparation and characterization of a-C and a-C:H coatings deposited by pulsed magnetron sputtering", *Surf. Coatings Technol.* 203, 1027 (2009).

[8] K.W. Weng, S. Han, and Y. Chen, "Characteristics of diamond-like carbon film deposited by filter arc deposition", *J. Mater. Process. Technol.,* 203, 117 (2008).

[9] A. Kumar, U. Ekanayake, and J.S. Kapat, "Characterization of pulsed laser-deposited diamond-like carbon films", *Surf. Coatings Technol.* 102, 113 (1998).

[10] L. Kaczmarek, D. Kottfer, M. Marton, M. Ferdinandy, P. Trebu, and I. Aluminum, "A Study of structural and wear properties of PACVD deposited a-C:H thin", *Phys. Status Solidi A* 212(10), 2271 (2015).

[11] M. Pandey, D. Bhatacharyya, D.S. Patil, K. Ramachandran, and N. Venkatramani, "Diamond-like carbon coatings: AFM and ellipsometric studies," *Surf. Coatings Technol.* 182, 24 (2004).

[12] Th. Lampe, S. Eisenberg, and E. Rodríguez Cabeo, "Plasma surface engineering in the automotive industry-trends and future prospectives", *Surf. Coatings Technol.,* 174-175, 1-7, (2003).

[13] M. A. Lieberman, *Principles of plasma discharges and materials processing* (John Wiley and sons, New Jersey, 2005).

[14] N. Mutsukura, S. Inoue, Y. Machi, N. Mutsukura, S. Inoue, and Y. Machi, "Deposition mechanism of hydrogenated hard-carbon films in a CH_4 rf discharge plasma", *J. Appl. Phys.* 72(1), 43 (1992).

[15] J. Laimer, M. Fink, T. A. Beer, and H. Störi, "Plasma dynamics as a key to successful upscaling of pulsed plasma processes", *Surf. Coatings Technol.,* 174-175, 118 (2003).

[16] C. Corbella, M. Vives, G. Oncins, C. Canal, J. L. Andújar, and E. Bertran, "Characterization of DLC films obtained at room temperature by pulsed-dc PECVD", *Diamond Relat. Mater.* 13, 1494, (2004).

[17] L. Li, K. Liu, and J. Qiu, "Repetitive high voltage rectangular waveform pulse adder for pulsed discharge of capacitive load", *IEEE Trans. Dielectr. Electr. Insul.* 20, 1218 (2013).

[18] N. S. Kopeika, J. Rosenbaum, and R. Kastner, "Abnormal glow discharge detection of visible radiation", *Appl. Opt.* 15, 1610 (1976).

[19] R. Payling and T. Nelis, *Glow Discharge Optical Emission Spectroscopy: A Practical Guide* (The Royal Society of Chemistry, UK, 2003).

[20] A. Qayyum, “Characterization of Argon Plasma by Use of Optical Emission Spectroscopy and Langmuir Probe Measurements”, *Int. J. Mod. Phys. B* 17, 2749 (2003).

[21] T. Michler, M. Grischke, I. Traus, K. Bewilogua, H. Dimigen, “DLC Films deposited by bipolar pulsed DC PACVD”, *Diamond Relat. Mater.* 7, 459 (1998).

[22] G. Guo, G. Tang, Y. Wang, X. Ma, M. Sun, L. Wang, K. Yukimura, “Structure and hardness of a-C:H films prepared by middle frequency plasma chemical vapor deposition”, *Appl. Surf. Sci.* 257, 4738 (2011).

[23] G. Capote, E. J. Corat, and V. J. Trava-airoldi, “Deposition of amorphous hydrogenated carbon films on steel surfaces through the enhanced asymmetrical modified bipolar pulsed-DC PECVD method”, *Surf. Coatings Technol.* 260, 133 (2014).

[24] L. Pantoja-Suárez, M. Morales, J.L. Andújar, J. Esteve, M. Segarra, and E. Bertran, “Plackett-Burman experimental design for pulsed-DC plasma deposition of DLC coatings” *Cornell University Library-Condensed Matter,* (2015) [arXiv:1507.04267].

[25] Y. Kikuchi, M. Ogura, T. Maegawa, A. Otsubo, Y. Nishimura, M. Nagata, and M. Yatsuzuka, “Diamond-like carbon film preparation using a high- repetition nanosecond pulsed glow discharge plasma at gas pressure of 1 kPa generated by a SiC-MOSFET inverter power supply”, *Jpn. J. Appl. Phys.* 56, 100306 (2017).

[26] K. Takaki, H. Ogiso, S. Nakano, and K. Yukimura, “ A New Approach to High-Power Pulsed Glow Plasma Generation: Shunting Glow Plasma”, *IEEE Trans. Plasma Sci*., 40, 1801 (2012).

[27] H. T. Truong, M. Hayashi, Y. Uesugi, Y. Tanaka, T. Ishijima, “Novel design of high voltage pulse source for efficient dielectric barrier discharge generation by using silicon diodes for alternating current”, *Rev. Sci. Instrum.* 88(6), 065105 (2017).

[28] Y. Kikuchi, M. Ogura, A. Otsubo, Y. Nishimura, M. Nagata, M. Yatsuzuka, “Characteristics of Sub-Atmospheric Pressure Glow Discharge Plasmas for Preparation of a-C:H Films “, *Vacuum*, 136, 196 (2017).

[29] J. Zhou, and E. R. Fisher, “Surface Reactivity and Energetics of CH Radicals during Plasma Deposition of Hydrogenated Diamondlike Carbon Films,” *J. Phys. Chem. B*, 110(43), 21911 (2006).

[30] R. W. B. Pearse and A. G. Gaydon, *The Identification of Molecular Spectra* (Chapman & Hall, London, 1950)

[31] J. Cui, Z. Xu, J. Zahang, Q. Nie, G. Xu, and L. Ren, “Online diagnosis of electron excitation temperature in CH_4+H_2 discharge plasma at atmospheric pressure by optical emission spectra”, *Sci. China Ser. G-phys. Mech. Astron.* 51, 1892 (2008).

[32] C. Hopf, K. G. Y. Letourneur, W. Jacob, T. Schwarz-Selinger, and A. von Keudell, “Surface loss probabilities of hydrocarbon radicals on amorphous hydrogenated carbon film surfaces”, *Appl. Phys. Lett.* 74, 3800 (1999).

[33] M. C. M. van de Sanden, M. F. A. M. van Hest, A. de Graaf, A. H. M. Smets, K. G.Y. Letourneur, M. G. H. Boogaarts, and D. C. Schram, “Plasma chemistry of an expanding Ar/C_2H_2 plasma used for fast deposition of a-C:H”, *Diamond Relat. Mater.* 8, 677 (1999).

[34] J. Benedikt, K. Focke, A. Yanguas-Gil, and A. von Keudell, Appl., "Atmospheric pressure microplasma jet as a depositing tool", *Phys. Lett.* 89, 251504 (2006).

[35] A. von Keudell, and W. Jacob, "Surface relaxation during plasma-enhanced chemical vapor deposition of hydrocarbon films, investigated by in situ ellipsometry", *J. of Appl. Phys.* 81, 1531 (1997).

[36] C. Casiraghi, F. Piazza, A. C. Ferrari, D. Grambole, and J. Robertson, "Bonding in hydrogenated diamond-like carbon by Raman spectroscopy", *Diamond Relat. Mater.* 14, 1098 (2005).

[37] S. Prawer, R. Kalish, M. Add, and V. Richter, "Effects of heavy ion irradiation on amorphous hydrogenated (diamondlike) carbon films", *J. Appl. Phys.* 61, 4492 (1987).

[38] C. Casiraghi, A.C. Ferrari, and J. Robertson, "Raman spectroscopy of hydrogenated amorphous carbons", *Physical Review B* 72, 085401 (2005).

[39] J. Wang, Z. Cao, F. Pan, F. Wang, A. Liang, and J. Zhang, "Tuning of the microstructure, mechanical and tribological properties of a-C:H films by bias voltage of high frequency unipolar pulse", *Appl. Surf. Sci.* 356, 695 (2015).

[40] V. J. Trava-Airoldi, L. F. Bonetti, G. Capot, J. A. Fernandes, E. Blando, R. Hübler, P.A. Radi, L. V. Santos, E. J. Corat, "DLC film properties obtained by a low cost and modified pulsed-DC discharge", *Thin Solid Films* 516, 272 (2007).

[41] S. Nakao, J. Choi, J. Kim, S. Miyagawa, Y. Miyagawa, and M. Ikeya, "Effects of positively and negatively pulsed voltages on the microstructure of DLC films prepared by bipolar-type plasma based ion implantation", *Diamond Relat. Mater.* 15, 884 (2006).

[42] S. Fujimoto, H. Akasaka, T. Suzuki, N. Ohtake, and O. Takai, "Structure and Mechanical Properties of Diamond-Like Carbon Films Prepared from C_2H_2 and H_2 Mixtures by Pulse Plasma Chemical Vapor Deposition", *Jpn. J. Appl. Phys.* 49, 075501 (2010).

[43] J. Ristein, R. T. Stief, L. Ley and W. Beyer, "A comparative analysis of a-C:H by infrared spectroscopy and mass selected thermal effusion", *J. Appl. Phys*. 84, 3836 (1998).

[44] C. Thomsen and S. Reich, "Double Resonant Raman Scattering in Graphite", Phys. Rev. Lett. 85, 5214 (2000).

Contributed paper: Md Abdullah Al Mamun, Hiroshi Furuta, Akimitsu Hatta, "Preparation of a-C:H films using a microsecond pulsed DC capacitive-coupled plasma CVD system operated at high frequency up to 400 kHz", Japanese Journal of Applied Physics, ***57****, 06JF02, (2018).*

Chapter 6

Investigation of pulsed plasma characteristics and deposition of carbon thin films with a variation of discharge conditions

This chapter provides the investigation of pulsed plasma characteristics with the variation of discharge conditions using optical emission spectroscopy (OES). A trial deposition of carbon thin films is also examined by the developed novel pulsed discharge system, following the results obtained from the optimization process. Introduction, objectives, and used methods are described. The deposited films properties are characterized. Finally, conclusions are drawn based on the experimental results.

6.1. Introduction

Plasma chemical vapour deposition (CVD) is widely used in the field of material processing for coatings, material surface treatment, and thin-film deposition owing to its advantages of considerably low deposition temperature, high yield, and large area of uniform deposition [1]–[11]. In plasma CVD, chemical processes occur in the vapor phase where basically two types of plasma species—radicals (chemically active neutral species) and ions that diffuse from the plasma—drift toward the surface of the substrate surface and grow films. As plasma is the dominant factor in plasma CVD, the growth processes by plasma species demonstrate a significant dependence on the design of the discharge system architecture.

Nowadays, the pulsed-DC discharge has significant potential in plasma CVD systems for the synthesis of thin films and is considered a popular method. Compared to the commonly used DC and RF discharges, the pulsed-DC discharge has the advantages of suppressing the development of arc discharges, higher energy efficiency, and less electromagnetic interference. Furthermore, the pulsed-DC discharge introduces more stability in plasma production and maintains broad controllability of plasma properties [12]–[14].

In addition, the pulsed-DC discharge is advantageous for the synthesis of insulating thin films, for example, diamond-like carbon (DLC) films [15] where substrates to be powered by alternating pulses are needed [16]. Generally, a pulsed-DC discharge for plasma CVD is carried inside a chamber filled with a gas mixture by a pulsed-DC generator. In this case, pulse parameters such as the pulse shape, amplitude, repetition rate, and duty cycle directly influence the plasma properties that are key factors in the growth of the film and the modification of its properties. However, the control of these parameters across a wide range during a pulsed-DC discharge is limited because it mostly depends on the design of the pulsed-DC generator and the arrangement of electrodes inside the discharge chamber.

Capacitively coupled plasma (CCP) is one of the most important configurations for plasma processes owing to its simple, relatively inexpensive structure and good plasma uniformity [17]–[19]. In CCP, a gas discharge is performed between two electrodes (anode and cathode) at a short distance from each other, configured as parallel plates and placed in a reactor chamber. The gas pressure in the reactor can be low or near to atmospheric depending on the particular purpose of the application. The CCP is usually driven by the RF generator at a high frequency (typically 13.56 MHz) in a sinusoidal wave through a matching network. For CCP operation, however, it is challenging to attain nearly rectangular high-voltage pulses with fast rising and falling edges, high repetition rates, and varying pulse widths. This is because CCP performs as a capacitive load and short, intense current is required to quickly charge and discharge the load [20].

Numerous studies [13], [21]–[27] have reported on the pulsed-DC discharge in CCP; however, the flexibility of the control of pulse operation conditions can be further enhanced. It is projected that the pulsed-DC discharge in CCP with a wide variation of pulse operation can make the system more versatile and more interesting for film deposition. Thus, development of the wide controllability of a pulsed-DC discharge operation and its impact on the plasma and film properties has gained extensive attention.

6.2. Objective

In this study, a new pulsed-DC discharge system for capacitively coupled plasma CVD using a developed pulsed-DC generator and a vacuum discharge chamber is demonstrated. Gas discharge experiments are carried out to investigate the plasma discharge characteristics. A wide variation of pulse parameters and plasma conditions were studied by optical emission spectroscopy (OES). Furthermore, a trial deposition of DLC and ultrathin pyrolytic carbon (PyC) films was also discussed.

6.3. Experimental setup

Figure 6.1. shows the setup of pulsed-DC discharge system developed by means of a novel pulsed-DC generator [27] (described in chap. 4) and a customized vacuum discharge chamber apparatus [15] (described in chap. 3). The pulsed-DC generator is a vital part of this system as it plays an important role for the generation of plasma. The design of the system mainly focused on the generation of plasma by high-voltage negative pulses with fast rising and falling edges and controllable pulse widths using half-resonant converter topology [28].

Argon (Ar) gas discharge was used to evaluate the pulsed plasma characteristics with the variation of discharge conditions. For the experiments, the chamber was always evacuated

under a base pressure of $8x10^{-3}$ Pa for the removal of inherent contaminated gas from the chamber. The gas out system of the chamber consisted of a turbo molecular pump (TMP) as the main evacuator, and a rotary pump for backup of TMP.

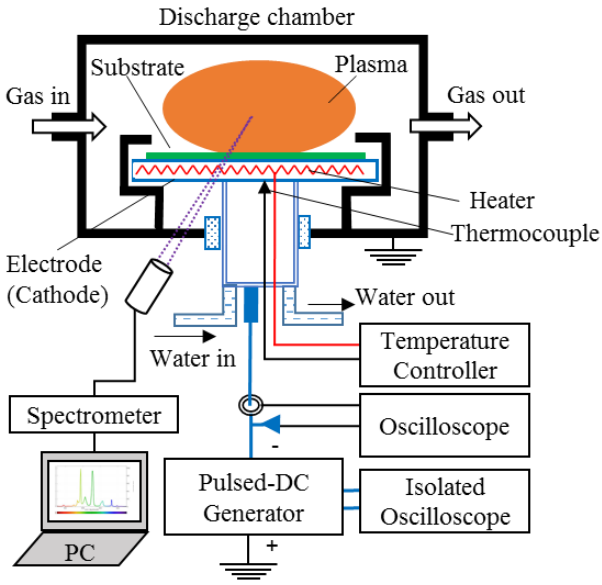

Figure 6.1. Schematic diagram of the experimental setup for pulsed-DC discharge.

The electrode voltage was observed using a high-voltage probe (Tektronix, 12000 V, 100:1). A current probe was used to measure all currents during discharge operations. The current-voltage waveforms were monitored and stored by a digital storage oscilloscope (Tektronix, 2014B). However, the magnitude of the steady discharge current was very low compared to the other currents and it was challenging to extract it from the main current waveforms. An isolated oscilloscope (Micornix) was introduced on the high-voltage side to monitor the steady discharge current separately. However, it was difficult to store these current waveforms in a computer using the isolated oscilloscope as it was configured to be electrically isolated from the ground. Hence, a digital camera was used to take photographs of these current waveforms from the monitor of the isolated oscilloscope. After that, these photographs were digitized to extract the functional numerical data for plotting the graphs. Photos of the glow plasma were also captured.

To observe the optical emission spectra, a multichannel spectrometer (Ocean Optics USB4000, measuring range 178–888 nm, optical resolution 1.46 nm) with a bare optical fiber (Ocean Optics P1000-1-SR) was set up in front of a quartz window of the discharge chamber. The intensity of the optical spectra was monitored and recorded by a personal computer (PC). During data acquisition, the accruing time was set to 20 ms, and the average scan was 50 times. All acquired spectra under the studied experimental conditions were fitted by IGOR Pro software to evaluate the spectral line intensity for further analysis.

6.4. Gas discharge characteristics

Gas discharge experiments were carried out using the developed system with a variation of discharge conditions. From the gas discharge experiments, it was established that our newly designed pulsed-DC generator can deliver nearly rectangular negative pulses up to 1000 V with fast rising (<500 ns) and falling (<800 ns) even in CCP with a broad variation of pulse parameters. The maximum pulse repetition rate attained was 500 kHz. The pulse duty (on and off time) can be varied conveniently, and a minimum pulse width of 1 μs was obtained. The steady discharge current can be controlled independently within a pulse regardless of the discharge conditions. The energy recovery technique also showed an improvement in efficiency from DC to pulsed-DC during high-frequency operation.

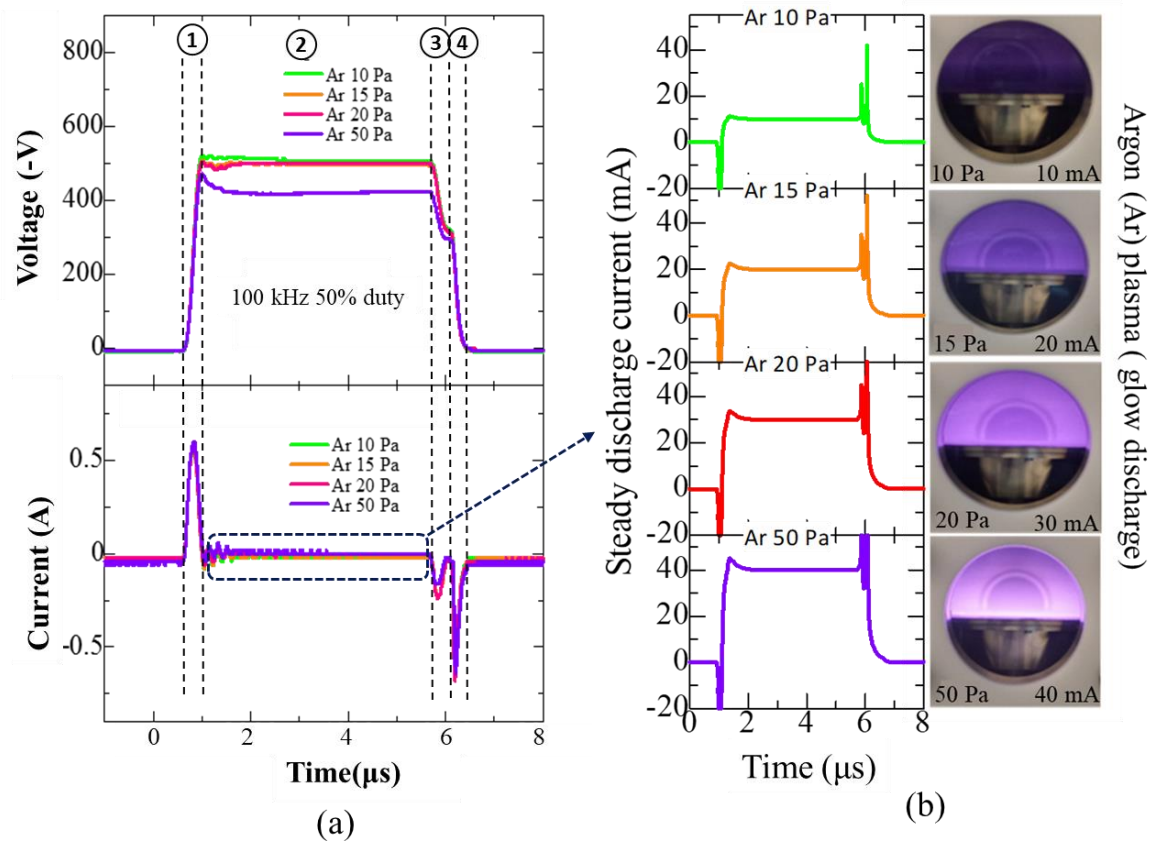

Figure 6.2. Pulsed-DC discharge with a variation of working argon (Ar) gas pressure and steady discharge current. (a) typical current-voltage waveforms (b) photographs of steady discharge current waveforms and glow plasma.

Figures 6.2(a) and (b) show the typical current-voltage waveforms and the steady discharge current waveforms (traced from the photographs on the isolated oscilloscope screen) with photographs of glow plasma during pulsed-DC glow discharge using argon (Ar) gas, respectively. The pressure was varied from 10 to 50 Pa by keeping a constant gas flow rate of 100 sccm, while the discharge current was varied in the range of 10 to 40 mA at a fixed applied

input DC voltage of -500 V. The maximum discharge current limit was set to 40 mA. The pulse repetition rate was 100 kHz with a 50% duty cycle.

The pulsed operation is divided into four stages, as follows. In stage 1, the electrode is quickly charged to a peak voltage that is almost equal to the input voltage through intense current (peak of ~0.625 A). The current is sinusoidal because of energy transferred through LC resonance. This stage is recognized as the ignition of discharge. After ignition of discharge, a glow discharge plasma appears in stage 2. In this stage, an almost-steady discharge current with uniform plasma all over the electrode was observed [Figure 6.2(b)]. The time duration of this stage was nearly 5 μs depending on the pulse frequency and duty cycle conditions. This can be conveniently controlled by changing the pulse frequency and duty cycle ratio.

In stage 3, charge from the electrode is recovered to the energy storage capacitor by a reverse recovery current (peak of ~0.25 A) through LC resonance. The energy recovery is crucial to diminishing the switching loss at higher frequency. A forcible elimination of the residual charge from the electrode by introducing a ground current (peak of ~0.70 A) is performed in stage 4 at the end of a pulse. The experimental current-voltage waveforms show good agreement with our design.

The electrode voltage and discharge current waveforms appeared almost rectangular in shape in the operation of a pulsed-DC discharge with a variation of working gas pressure. It was observed that the discharge current as well as the glow intensity of the plasma increased as the argon gas pressure rose. However, in comparison with the voltage waveforms, a lower electrode voltage was seen at a gas pressure of 50 Pa. This is because the discharge current is limited by the set value of the constant-current control circuit. In this mode, the generator operates as a constant-current source instead of a voltage source. Thus, the electrode voltage drops slightly lower than the supply voltage to sustain the constant discharge current regardless of the plasma impedance.

From the current-voltage (I-V) characteristics, it was confirmed that the plasma ran under steady conditions. This is crucial for a homogeneous discharge as well as efficient excitation and ionization [29]. This pulsed plasma operation can be considered as very beneficial for the uniform deposition of thin films.

6.5. Optical Emission Spectral Analysis of Plasma

Optical emission spectroscopy (OES) is a popular method for examining glow discharge plasma [30]. Optical emission lines are emitted from the excited particles of plasma. The electron excited temperature (T_{exc}), known as a critical parameter of plasma, can be evaluated in time-averaged mode from the relative intensities of the emitted spectral lines [31]. In

particular, the electron excited temperatures and generated species in plasma are considered to be significant factors in film growth applications. It is expected that these plasma parameters can be mutually tuned by the pulse parameters (power, repetition rate, and duty cycle) and precursor gas parameters (pressure and flow rate). Hence, the examination of T_{exc} in pulsed-DC glow discharge plasma with a variation of discharge conditions has garnered extensive attention.

Figure 6.3(a) shows a typical emission spectrum of Ar plasma obtained by a pulsed-DC discharge under specific discharge conditions. Mostly intense lines were observed in the region between 690 and 850 nm. These lines were emitted from excited argon atomics Ar(I) by 4 p → 4 s transitions. Among these lines, two characteristic lines [clearly shown in Figure 6.3(b)] at 750.39 nm [$3p^5(^2P^o_{1/2})4p–3p^5(^2P^o_{1/2})4s$] and 811.53 nm [$3p^5(^2P^o_{3/2})4p–3p^5(^2P^o_{3/2})4s$] were selected for the evaluation of T_{exc} at all studied discharge conditions. The double-line method [32] was used to determine the T_{exc} of plasma in Kelvin (K) by the following equation:

$$T_{exc} = -\frac{E_1-E_2}{k}\left[ln\left(\frac{A_1 g_1 I_2 \lambda_2}{A_2 g_2 I_1 \lambda_1}\right)\right]^{-1} \quad \ldots\ldots\ldots\ldots\ldots\ldots\ldots\ldots (6.1)$$

where *A, g, I, λ,* and *E* are the transition probability, weighting factor, intensity, wavelength, and excitation energy of the first and second spectral lines. *k* is the Boltzmann constant.

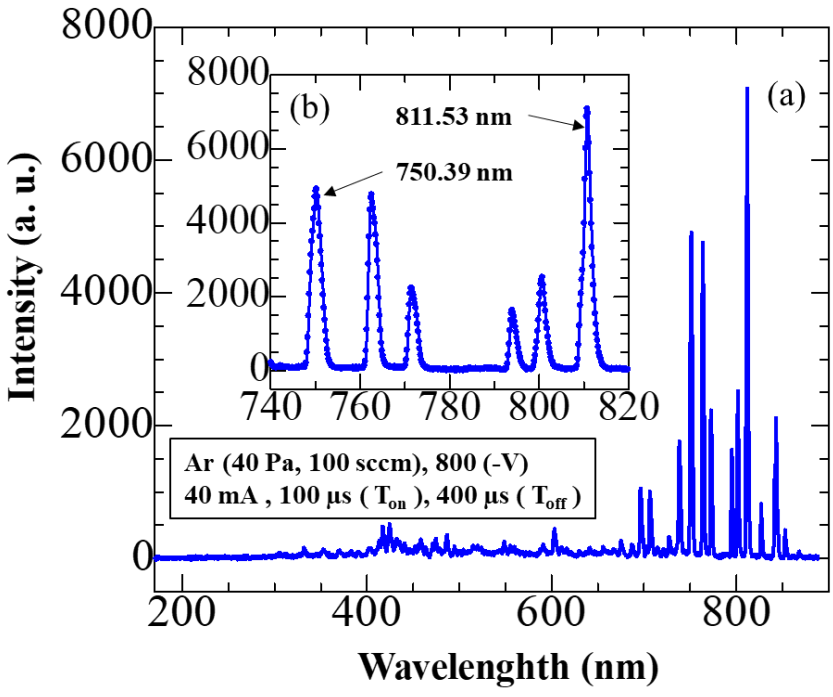

Figure 6.3. (a) Typical OES spectrum of Ar plasma obtained by pulsed-DC glow discharge at gas pressure: 40 Pa, flow rate: 100 sccm, input DC voltage: -800 V, set discharge current: 40 mA, pulse on (T_{on}): 100 µs, pulse off (T_{off}): 400 µs. (b) Expanded view of the Ar(I) 750.39 nm and 811.53 nm emission lines of spectrum in (a) employed for the evaluation of T_{exc} in this study.

The first and second spectral lines were assigned to 750.39 nm and 811.53 nm, respectively. The line intensities were obtained from the time-averaged optical emission spectra. Other values were taken from the tables of the National Institute of Standards and Technology (NIST) [33]. In a pulsed plasma, actual T_{exc} is dynamically changed with pulses. The evaluation of T_{exc} by time-averaged spectra will not show the real plasma parameter, but is an indication to demonstrate the effects of pulsed modulation. While this method is simple and easy, but may include errors of about 20% during measurements.

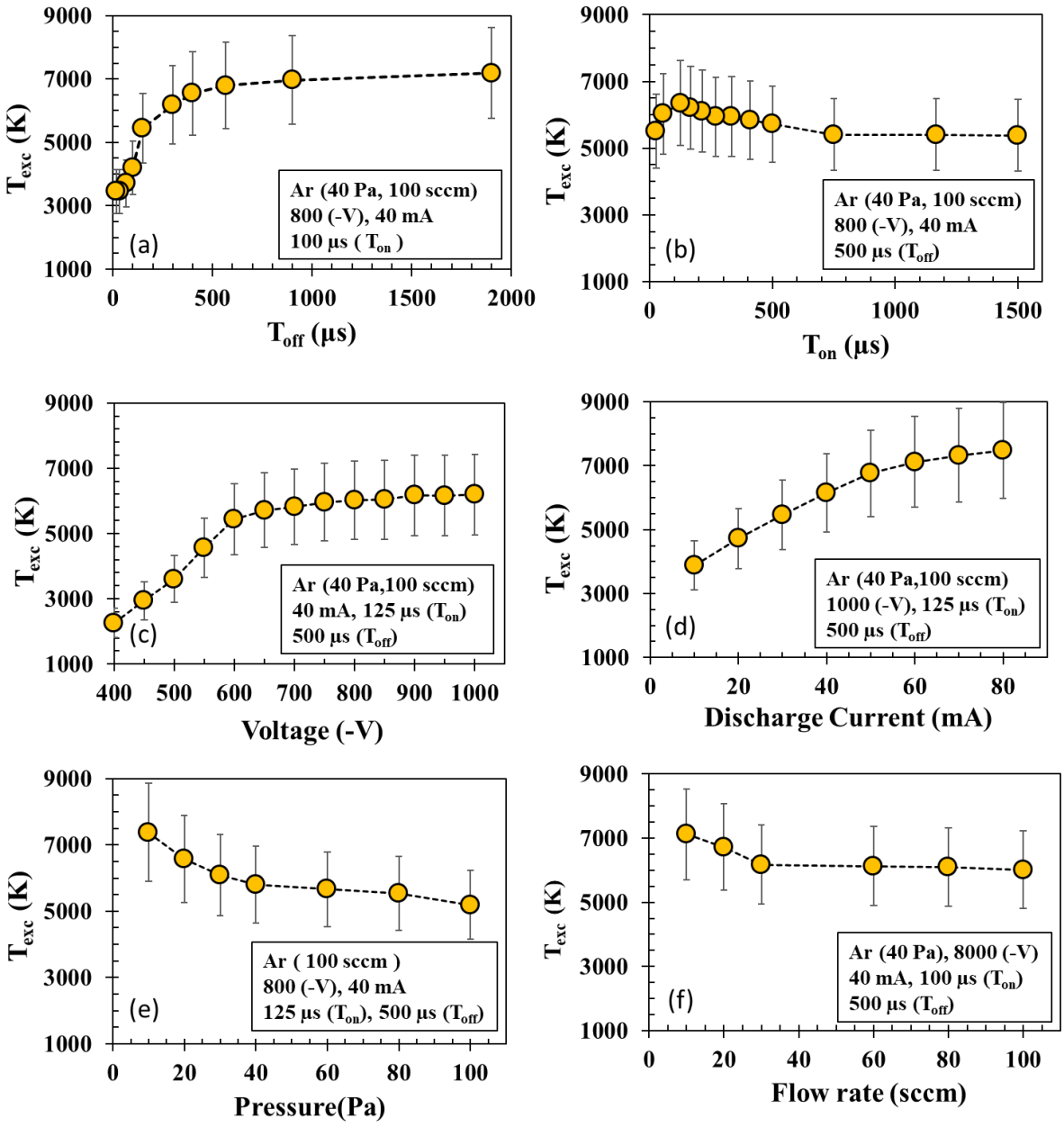

Figure 6.4. Evaluation of electron excitation temperature, T_{exc} with a variation of discharge conditions such as (a) pulse off time (T_{off}) (b) pulse on time (T_{on}) (c) applied negative voltage (d) controlled discharge current (e) precursor gas pressure and (f) gas flow rate.

Figure 6.4. demonstrates $T_{exc,}$ evaluated by the double-line method using time-averaged spectra with variations of discharge conditions. The variation of the pulse-off time (T_{off}) showed a significant influence on the T_{exc} values in Figure 6.4(a), while other parameters (pressure: 40 Pa, flow rate: 100 sccm, applied voltage: -800 V, set discharge current: 40 mA, and pulse on-time T_{on}: 100 μs) were unchanged. T_{exc} gradually increased with an increase in T_{off} to a certain value (approximately 500 μs). After that, it became almost stable (~7000 K) even though further increment of T_{off}. It is supposed that the complete diminishing of the afterglow effect contributed to the previous pulse takes at around 500 μs, where the number of electron collisions decreased and attained a high accelerating energy to excite the gas molecules further.

By contrast, T_{exc} was slightly influenced by T_{on} when T_{off} was set to 500 μs. The other parameters remained the same, as shown in Figure 6.4(b). The maximum T_{exc} (~6500 K) was observed when T_{on} was 125 μs. After that, T_{exc} marginally decreased and reached a stable value of ~5400 K with an increase in T_{on}. These results suggest that a low duty cycle of pulsed DC is preferable for enhancing the electron excitation energy in plasma. This was also reported for pulsed-DC magnetron Ar discharges [34].

Figure 6.4(c) shows a considerable effect on T_{exc} with a variation of applied voltage while other discharge parameters were fixed at pressure: 40 Pa, flow rate: 100 sccm, set discharge current: 40 mA, T_{on}: 125 μs, and T_{off}: 500 μs. T_{exc} increases progressively with an increase in applied voltage, and saturates to a value of ~6000 K when the applied voltage is in the range of -650 to -1000 V. It can be explained that in this range, the applied voltage is limited by the constant-current control circuit, and the plasma discharge is operated by a constant-current source instead of a voltage source at the sustained voltage, which stabilizes the electron excitation energy. In addition, T_{exc} also increases with an increase in the set discharge current at an applied voltage of -1000 V, and other parameters were kept identical to previous values, as shown in Figure 6.4(d). The increase in the discharge current at a fixed applied voltage increases the pulsed power that enhances the electron accelerating energy. A similar tendency was observed in the RF plasma discharge when the RF power increased [35].

Figure 6.4(e) demonstrates the dependency of T_{exc} with a variation of the working gas pressure at a constant flow rate of 100 sccm, applied voltage of -800 V, set discharge current of 40 mA, pulse-on time (T_{on}) of 125 μs, and a pulse-off time (T_{off}) of 500 μs. At low pressure (10 Pa), T_{exc} is high and gradually decreases to 40 Pa. After that, T_{exc} becomes nearly stable until 100 Pa. It is supposed that the electron density increases as the gas pressure increases to 40 Pa, which leads to more electron collisions and decreases the electron energy [36]. After 40 Pa, the electron density is limited by the constant current, which sustains the T_{exc} value at an almost stable value even though the working pressure increases further.

Figure 6.4(f) shows the dependency of T_{exc} with a variation of the working gas flow rate at a constant gas pressure of 40 Pa, applied voltage of -800 V, set discharge current of 40 mA, pulse-on time (T_{on}) of 125 μs, and a pulse-off time (T_{off}) of 500 μs. At low flow rate (10 sccm), T_{exc} is high and sharply decreases to 30 sccm. After that, T_{exc} becomes almost stable until 100 sccm. It is supposed that less electron collisions with gas molecules occur when the flow rate is very flow and increases the electron energy, however it becomes stable at higher flow rate.

From a spectroscopic analysis of the plasma, it is realized that electron excitation energy is mostly influenced by the precursor gas pressure and the pulse-DC parameters (power and duty cycle). It is expected that a low gas pressure and rationally high voltage with low pulse duty will be beneficial for the deposition of thin films.

6.6. Carbon Film Deposition

6.6.1. DLC films

As a preliminary test, DLC films were deposited on silicon (Si) wafers from acetylene (C_2H_2) gas at room temperature using the developed pulsed-DC plasma CVD system. The deposition conditions are presented in Table I. Typical deposition conditions were selected based on the results of gas discharge experiments. Three samples of DLC films were examined with a variation in gas pressure, electrode voltage, and discharge current, while the other conditions were kept unchanged. The deposition time was varied to maintain nearly the same thickness.

Table 6.1. Deposition Conditions of DLC Films

Parameters	Sample1 (S1)	Sample2 (S2)	Sample3 (S3)
Pressure (Pa)	15	20	30
Electrode Voltage (-V)	800	1000	1000
Discharge current (mA)	10	15	40
Deposition time (min)	10	05	03
Pulse on time, T_{on} (μs)	125	125	125
Pulse off time, T_{off} (μs)	500	500	500
Flow rate (sccm)	60	60	60
Deposition Temperature (^{0}C)	25	25	25

Before CVD, a silicon wafer with a 4-in diameter was cut into quarters. A piece of Si wafer was placed on the electrode as a substrate, while the other part of the electrode was covered by

a dummy cover made of Al. The discharge chamber was pumped out below a base pressure. The Si substrates were cleaned by Ar plasma to remove the native oxide layer. The thickness of the deposited films was measured by a benchtop stylus profilometer (KLA-Tencor Alpha-Step IQ). The film properties were characterized using a Raman spectrometer (Horiba Jobin Yvon HR-800, laser excitation wavelength 532.08 nm) and a resistivity meter (Loresta EP MCP-T360, four-pin probe, measurement range: 10^{-2}–10^{6} Ω).

The thickness of all deposited films—sample1 (S1), sample2 (S2), and sample3 (S3)—was almost identical at around 300 nm, and the deposition rates were evaluated as approximately 30, 60, and 100 nm/min, respectively. The results reveal that an increase in the deposition rate is mostly influenced by the working gas pressure, whereas the electrode voltage and discharge current also influence the deposition rate.

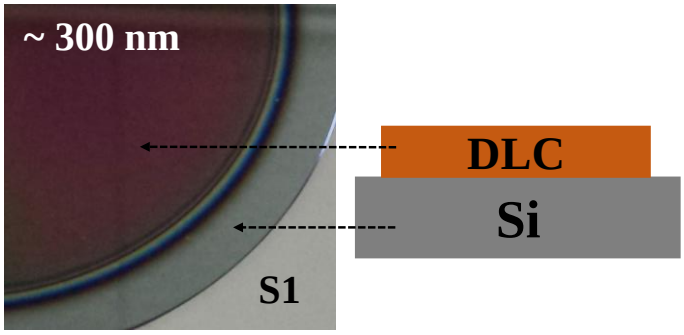

(a)

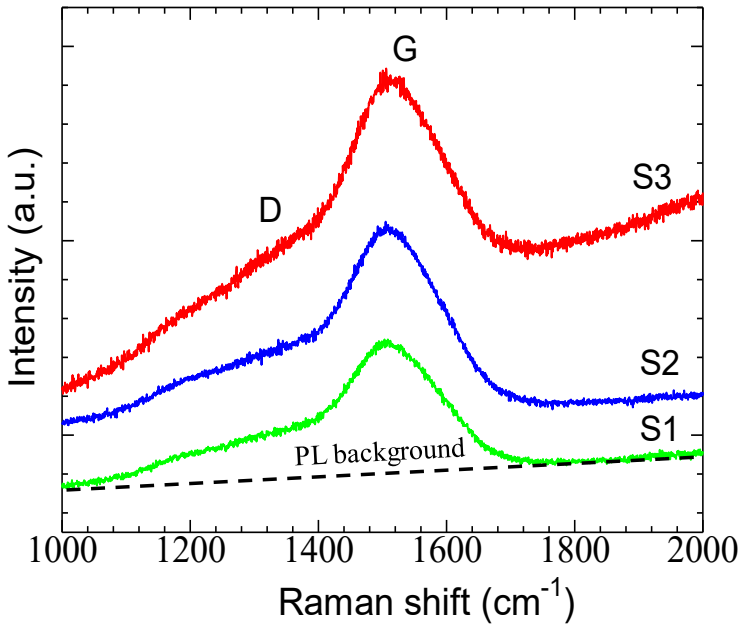

(b)

Figure 6.5. Deposited DLC films: (a) physical appearance of a typical DLC film (S1) and (b) Raman spectra.

Figure 6.5(a) shows the physical appearance of the deposited film for S1, where the sample color appeared brown as compared to the Si wafer. An almost uniform deposited area with a clean and smooth surface was observed to be surrounded by a ring-shaped interference pattern owing to the thickness profile at the edge. This ring-shaped interference appeared underneath the edge of the deposition window in the top cover of the electrode. Nevertheless, S2 and S3 showed nearly the same appearance of S1 (not shown here). Figure 6.5(b) presents the Raman spectra of samples S1, S2, and S3, in which two overlapping bands known as the D-peak and G-peak were observed. This confirms that the films consist of DLC [37].

In addition, an inclined background overlaid on each Raman spectrum was noticed. This is considered a photoluminescence (PL) background. A higher slope of the PL background was seen in S3 than in S1 or S3. As the hydrogen (H) content in the DLC films significantly influences the slope of the PL background [38], it can be expected that more H content was incorporated in S3 as it was deposited at higher hydrocarbon gas pressure. It is also well known that H content plays a substantial role in the microstructure of DLC films.

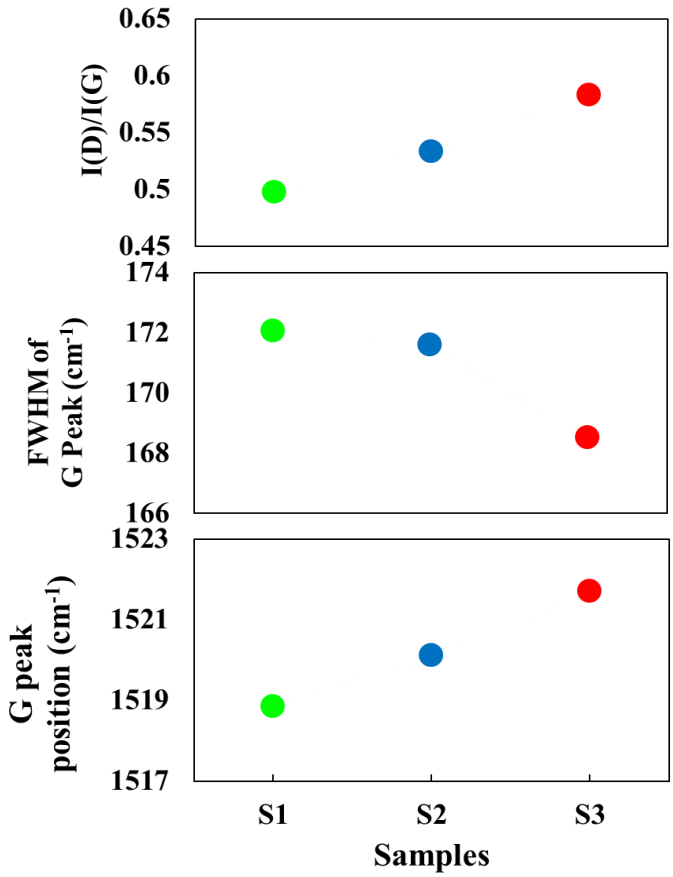

Figure 6.6. Intensity ratio of D peaks to G peaks [I(D)/I(G)], FWHM of G peaks, and G peak positions for different samples.

To examine the microstructure of the DLC films, each Raman spectrum was fitted by two Gaussian lines to separate the D and G peaks after subtracting the PL background. Afterward,

the intensity ratio of the D-peak to the G-peak [I(D)/I(G)], the full width at half maximum (FWHM) of the G-peak, and the G-peak position were assessed for samples S1, S2, and S3, as shown in Figure 6.6. This showed a shift of the G-peak position to a higher wave number, a decrease in the FWHM of the G-peak, and an increase in the I(D)/I(G) ratio for samples S1, S2, and S3, respectively. An evaluation of the film properties was performed by a well-known three-stage model suggested by Robertson [37], [38].

Generally, for a conventional DLC film, the shifting of the G-peak position to lower value, an increase in the FWHM of the G-peak, and a decrease in the I(D)/I(G) ratio result in a more diamond-like structure in the films. This suggests that sample S1 contains more sp^3 content than S2 or S3. A probable explanation is that when the pulsed-DC plasma discharge is operated at a low gas pressure with a sufficient pulse-off time, a higher electron excitation temperature is obtained [Figure 6.4(e)]. In addition, the ion impingement to the substrate is supposed to be improved, which may contribute to enhancing the sp^3 content (amorphization) of the DLC films. However, all deposited DLC films showed good agreement with the tendency found in stage 2 of the three-stage model.

The electrical resistivity of these three DLC films had been examined. It showed that all the films were highly insulating (unable to measure, over loaded, above 10^6 Ω/□), which was consistent with the Raman microstructural analysis that the films contain less graphitic structure with sp^2 hybridization. All these results suggest that pulsed-DC discharge for plasma CVD system is suitable for the synthesis of hard insulating carbon thin films like DLC.

6.6.2. Ultrathin PyC films

At present, the synthesis of ultrathin PyC films has garnered significant interest for the use of transparent electrodes owing to their good transparency and electrical conductivity. In addition, they are an alternative to commonly used indium tin oxide (ITO) [39]– [41]. However, the control of the thickness of PyC films is difficult when using a conventional CVD system.

A trial deposition of ultrathin PyC films was performed on glass substrates, followed by a nano-thickness metal catalyst, from C_2H_2 gas using the developed pulsed-DC plasma CVD system. A nano-thickness metal catalyst bilayer made of copper (Cu) and nickel (Ni) was grown on a glass substrate (26 mm × 25 mm) by direct-current magnetron sputtering. The sputtering was carried out using metal targets of Cu and Ni with a diameter of 2 in for Ar plasma at a pressure of 0.8 Pa, flow rate of 28 sccm, discharge current of 20 mA, and discharge voltage of 270 to 300 V. The thickness of the metal films was controlled by adjusting the sputtering time, and a value was chosen that could transmit light as well as show conductivity. In this experiment, for all samples, a Ni metal catalyst of 5 nm was first grown on the glass substrate, and then a

layer of 5 nm of Cu was deposited to form a bilayer metal catalyst of 10 nm. The as-deposited samples were inserted into the CVD chamber for the deposition of thin PyC films.

For all samples, a pulsed-DC plasma discharge was carried out from C_2H_2 gas at a pressure of 20 Pa, gas flow rate of 60 sccm, applied voltage of -800 V, steady discharge current of 20 mA, pulse-on time (T_{on}) of 125 µs, and pulse-off time (T_{off}) of 500 µs. The deposition temperature was increased from 300 to 500 ºC, while the deposition time was decreased from 5 to 2 s. The experiments focused mainly on the impact of the deposition temperature and the short time of deposition for the growth of films.

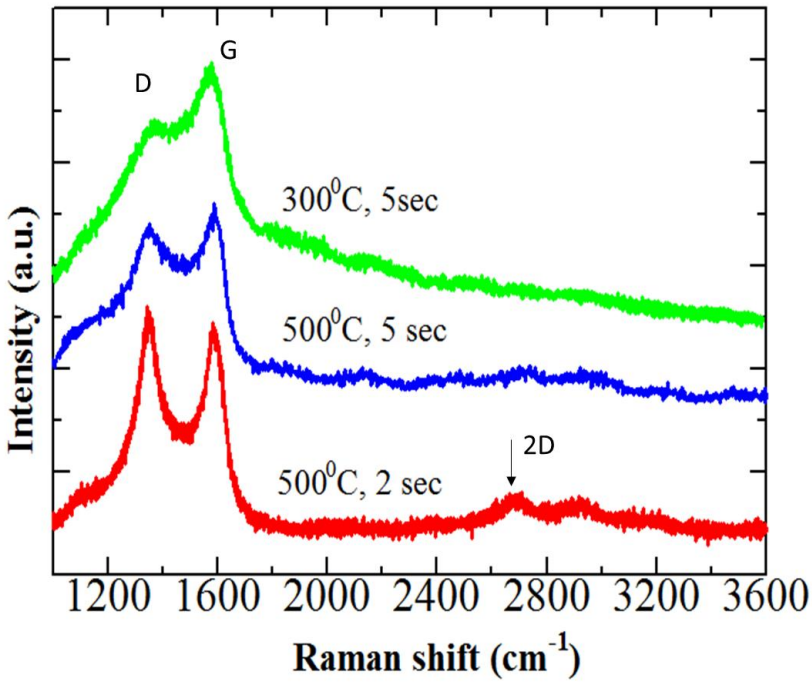

(a)

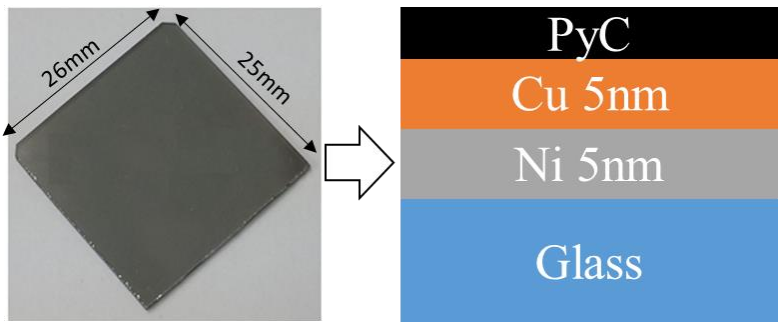

(b)

Figure 6.7. Deposited thin carbon films. (a) Raman spectra (b) physical appearance and structure of a typical ultrathin PyC film (500 ^{0}C, 2 s).

The deposited films were characterized by Raman spectroscopy in the range of 1000–3600 cm^{-1}. Figure 6.7(a) shows the Raman spectra of the deposited trial samples, where each

spectrum consists of characteristic D (~1340 cm^{-1}) and G (~1580 cm^{-1}) peaks. However, the sample prepared at 500 ºC with a short deposition duration of 2 s exhibited more separated D and G peaks with an additional weak peak at ~ 2690 cm^{-1}. This weak peak is known as 2D peak, an indication of the growth of PyC films [42].

As the deposition time was too low compared to that of conventional CVD, a very thin film (below 5 nm, estimated from the CVD deposition rate) was supposed to grow with a uniform thickness. The physical appearance and structure are shown in Figure 6.7(b). The sheet resistance of this ultrathin PyC film including the metal bilayer was measured with a four-point probe resistivity meter (Loresta EP MCP-T360). This value was ~170 Ω/□ after averaging the values from five different positions. This confirms that the prepared metal catalyzed ultrathin PyC film is objectively conductive.

In addition, the optical transmittance measured with respect to a bare glass substrate by a UV–VIS spectrometer (Hitachi U-3900) was approximately 60% in the visible range. These results reveal that the advantage of tuning a very short duration of deposition by our developed plasma CVD offers more controllability to govern the source of carbon atoms for depositing conducting ultrathin carbon films such as PyC. However, further investigations are required to optimize the discharge parameters for the fine growth of thin carbon films.

6.7. Conclusion

A new model of a pulsed-DC discharge system is presented that employs a developed pulsed-DC generator and a vacuum discharge chamber. The pulsed-DC generator can deliver negative-high-voltage, nearly rectangular pulses with fast rising and falling edges at a high repetition rate even in CCP.

Ar gas discharge experiments were examined by varying the discharge conditions, thus exhibiting significant flexibility to control the plasma discharge characteristics. The optical emission spectra of the Ar glow plasma were observed, and the electron excitation temperature (T_{exc}) was evaluated. It was confirmed that the electron excitation energy can be tuned by varying the precursor gas pressure and pulse parameters such as voltage, current, and duty cycle.

Diamond-like carbon (DLC) films were deposited on silicon (Si) substrates from acetylene (C_2H_2) with a variation of gas pressure, applied voltage, and discharge current. The Raman spectra confirmed the DLC properties of the deposited carbon films. All DLC films demonstrated highly insulating properties, and the amorphization increased with a decrease in gas pressure, voltage, and discharge current. In addition, ultrathin pyrolytic carbon (PyC) films were produced on glass substrates using nano-thickness metal catalysts from C_2H_2. The ultrathin PyC films exhibited conductive and semitransparent properties.

It can be suggested that our developed pulsed-DC discharge system for plasma CVD is beneficial for the synthesis of insulating hard as well as soft-conducting carbon thin films with a broad variation of discharge conditions. However, the impact of pulsed plasma on CVD is relatively complex, and further investigation is required on the complex process of the gas phase to the surface and their relationship with the plasma parameters, ion energy distribution, and quantitative correlations to the resulting film.

References

[1] M. A. Lieberman and A. J. Lichtenberg, *Principles of plasma discharges and materials processing*, Hoboken, New Jersey: Wiley, 2005, pp. 621-630.

[2] T. Lampe, S. Eisenberg, and E. R. Cabeo, "Plasma surface engineering in the automotive industry-trends and future prospectives," *Surf. Coatings Technol.* 174-175, 1-7, (2003).

[3] D. R. Cote, S. V. Nguyen, A. K. Stamper, D. S. Armbrust, D. Tobben, R. A. Conti, and G. Y. Lee, "Plasma-assisted chemical vapor deposition of dielectric thin films for ULSI semiconductor circuits," *IBM J. Res. Dev.*, 43(1.2), pp. 5-38, (1999).

[4] M. Belyansky, M. Chace, O. Gluschenkov, J. Kempisty, N. Klymko, A. Madan, A. Mallikarjunan, S. Molis, P. Ronsheim, Y. Wang, D. Yang, and Y. Li, "Methods of producing plasma enhanced chemical vapor deposition silicon nitride thin films with high compressive and tensile stress," *J. Vac. Sci. Technol. A*, 26 (3), 517-521, (2008).

[5] K. C. Park, J. H. Moon, J. Jang, M. H. Oh, K. C. Park, J. H. Moon, and J. Jang, "Deposition of hydrogen - free diamond - like carbon film by plasma enhanced chemical vapor deposition," *Appl. Phys. Lett.,* 68, 3594-3595, (1996).

[6] Z. Bo, Y. Yang, J. Chen, K. Yu, J. Yan and K. Cen, "Plasma-enhanced chemical vapor deposition synthesis of vertically oriented graphene nanosheets," *Nanoscale,* 3, 5180-5204, (2013).

[7] T. Harigai, H. Koji, H. Furuta, and A. Hatta, "Formation of Nanofibers on the Surface of Diamond-Like Carbon Films by RF Oxygen Plasma Etching," *Jpn. J. Appl. Phys*., 50, 08JF12 , (2011).

[8] Y. Yasuoka, T. Harigai, J. Oh, H. Furuta, and A. Hatta, "Diamond-like carbon films from CO source gas by RF plasma CVD method," *Jpn. J. Appl. Phys*., 54, 01AD04, (2014).

[9] Gil Capote, Vladimir J. Trava-Airoldi, and Luis F. Bonetti, "Plasma Treatments for Metallic Surface Modification to Obtain Highly Adherent Diamond-Like Carbon Coatings," *IEEE Trans. Plasma Sci.*, 42, 1742-1746, (2014).

[10] D. Lundin and H. Pedersen, "High power pulsed plasma enhanced chemical vapor deposition: a brief overview of general concepts and early results," *Phys. Procedia.*, 46, 3-11, (2013).

[11] N. Mutsukura, S. Inoue, Y. Machi, N. Mutsukura, S. Inoue, and Y. Machi, “Deposition mechanism of hydrogenated hard-carbon films in a CH4 rf discharge plasma,” *J. Appl. Phys.*, 72(1), 43–53, (1992).

[12] R. A. Scholl, “Asymmetric bipolar pulsed power: a new power technology,” *Surf. Coatings Technol*. 98, 823-827, (1998).

[13] M. Zlatanović and I. Popović, “Gas discharge static characteristics in pulse regime,” *Contemporary Materials,* I-2, 138–143, (2010).

[14] J. Laimer, M. Fink, T. A. Beer, H. Störi, “Plasma Dynamics as a Key to Successful Upscaling of Pulsed Plasma Processes,” *Surf. Coatings Technol*., 174−175, 118-123, (2003).

[15] M. A. A. Mamun, H. Furuta, and A. Hatta, “Pulsed DC plasma CVD system for the deposition of DLC films,” *Mater. Today Commun.*, 14, 40–46, (2018).

[16] C. Corbella, M. Vives, G. Oncins, C. Canalc, J. L. Andujara, E. Bertrana, “Characterization of DLC films obtained at room temperature by pulsed-dc PECVD,” *Diamond Relat. Mater.* 13, 1494-1499, (2004).

[17] M. A. Lieberman and A. J. Lichtenberg, *Principles of plasma discharges and materials processing,* New Jersey: Wiley, 2005, pp. 387-460.

[18] P. Chabert and N. Braithwaite, *Physics of radio-frequency plasmas,* New York: Cambridge University Press, 2011, pp.131-174.

[19] X. Zhu, W. Chen, S. Zhang, Z. Guo, D. Hu, and Y. Pu “Electron density and ion energy dependence on driving frequency in capacitively coupled argon plasmas,” *J. Phys. D: Appl. Phys.* 40, 7019–7023, (2007).

[20] L. Li, K. Liu, and J. Qiu, “Repetitive high voltage rectangular waveform pulse adder for pulsed discharge of capacitive load,” *IEEE Trans. Dielectr. Electr. Insul.,* 20, 1218–1223, (2013).

[21] C. Corbella, M. Rubio-roy, E. Bertran, and J. L. Andújar, “Plasma parameters of pulsed-dc discharges in methane used to deposit diamondlike carbon films,” *J. Appl. Phys.,* 103, 033302, (2009).

[22] V. J. Trava-airoldi, L. F. Bonetti, G. Capote, J. A. Fernandes, E. Blando, and R. Hübler, “DLC film properties obtained by a low cost and modified pulsed-DC discharge,” *Thin solid films*. 516, 272–276, (2007).

[23] A. N. Obraztsov, A. A. Zolotukhin, A. O. Ustinov, A. P. Volkov, Y. Svirko, and K. Jefimovs, “DC discharge plasma studies for nanostructured carbon CVD,” *Diam. Relat. Mater.*, 12, 917–920, (2003).

[24] M. Noda, H. Yukawa, M. Matsushima, H. Uchida, and M. Umeno, “Porous carbon film electrodes prepared by pulsed discharge plasma CVD,” *Diam. Relat. Mater.*, 18, 426–428, (2009).

[25] V. V. Ivanov, K. S. Klopovsky, D. V. Lopaev, Y. A. Mankelevich, A. T. Rakhimov, and T. V. Rakhimova, “Structure and dynamics of a pulsed dc discharge in pure oxygen,” *IEEE Trans. Plasma Sci.,* 31, 528–541, (2003).

[26] J. García-Céspedes, M. Rubio-Roy, M. C. Polo, E. Pascual, J. L. Andújar, and E. Bertran, "Carbon nanotubes grown by asymmetric bipolar pulsed-DC PECVD," *Diam. Relat. Mater.*, 16, 1131–1135, (2007).

[27] M. A. A. Mamun, H. Furuta, and A. Hatta, "Novel high-frequency energy-efficient pulsed-dc generator for capacitively coupled plasma discharge," *Rev. Sci. Instrum.*, 89, 033506, (2018).

[28] S. Zabihi, F. Zare, G. Ledwich, and A. Ghosh, "A bidirectional two-leg resonant converter for high voltage pulsed power applications," in *Proc. IET Eur. Pulsed Power Conf.*, Sep. 21–25, 2009, pp. 1–4.

[29] N. S. Kopeika, J. Rosenbaum, and R. Kastner, "Abnormal glow discharge detection of visible radiation," *Appl. Opt.*, 15, 1610-1615, (1976).

[30] A. Kolpaková, P. Kudrna, and M. Tichý, "Study of Plasma System by OES (Optical Emission Spectroscopy)," in *Proc. (contributed papers) WDS Conf.*, 2011, vol. part II, pp. 180–185.

[31] A. Qayyum, "Characterization of Argon Plasma by Use of Optical Emission Spectroscopy and Langmuir Probe Measurements," *Int. J. Mod. Phys. B*, 17, 2749–2759, (2003).

[32] R. K. Marcus and J. A. C. Breaker, *"Glow discharge plasmas in analytical spectroscopy,"* West Sussex, England: Wiley, 2003.

[33] *Handbook of Basic Atomic Spectroscopic Data*, National Institute of Standards and Technology (NIST). [online]. Available: http://physics.nist.gov/PhysRefData/Handbook/Tables/argontable3.htm.

[34] S. H. Seo, J. H. In, H. Y. Chang, and J. G. Han, "Effect of duty cycle on plasma parameters in the pulsed dc magnetron argon discharge," *Appl. Phys. Lett.*, 86, 262103, (2005).

[35] F. J. Gordillo-Vázquez, M. Camero, and C. Gómez-Aleixandre, "Spectroscopic Measurements of the Electron Temperature in Low Pressure Radiofrequency $Ar/H_2/C_2H_2$ and $Ar/H_2/CH_4$ Plasmas Used for the Synthesis of Nanocarbon Structures," *Plasma Sources Sci. Technol.*, 15, 42–51, (2006).

[36] X. M. Zhu and Y. K. Pu, "Using OES to determine electron temperature and density in low-pressure nitrogen and argon plasmas," *Plasma Sources Sci. Technol.*, 17, 024002(1-6), (2008).

[37] A. C. Ferrari and J. Robertson, "Interpretation of Raman spectra of disordered and amorphous carbon," *Phys. Rev. B*, 61, 14095–14107, (2000).

[38] J. Robertson, "Diamond-like amorphous carbon," *Mater. Sci. Eng. R.*, 37, 129–281, (2002).

[39] N. McEvoy, N. Peltekis, S. Kumar, E. Rezvani, H. Nolan, G. P. Keeley, W. J. Blau, and G. S. Duesberg, "Synthesis and analysis of thin conducting pyrolytic carbon films," *Carbon*, 50, 1216–1226, (2012).

[40] C. T. Hsiao, S. Y. Lu, and T. Y. Tsai, “Pyrolytic carbon from an aromatic precursor and its application as a counter electrode in dye-sensitized solar cells,” *Chem. - A Eur. J.*, 17, 1358–1364, (2011).

[41] T. Kaplas and P. Kuzhir, “Ultra-Thin Pyrocarbon Films as a Versatile Coating Material,” *Nanoscale Res. Lett.*, 12, 121(1-6), (2017).

[42] T. Kaplas and Y. Svirko, “Direct deposition of semitransparent conducting pyrolytic carbon films,” *J. Nanophotonics*, 6, 61703, (2012).

Contributed paper: Md Abdullah Al Mamun, Hiroshi Furuta, Akimitsu Hatta, “Pulsed-DC Discharge for Plasma CVD of Carbon Thin Films”, IEEE Transactions on Plasma Science, ***46****, (2018) (Early access: DOI:10.1109/TPS.2018.2853717).*

Research Part-II: Pulsed plasma discharge for atmospheric-pressure plasma jet

Chapter 7

An impulse generator for atmospheric-pressure plasma jet (APPJ)

This chapter presents the development of a high-voltage high-frequency impulse generator for atmospheric-pressure plasma jet (APPJ) using dual resonance pulse transformer (DRPT). The principle, design and construction of DRPT are demonstrated. Introduction, objectives, operations and results are described accordingly. A conclusion is drawn based on the experimental results.

7.1. Introduction

Low pressure plasmas are widely used in surface treatment and material processing applications, since the plasma can be delivered in large area with uniformity on the surface of substrates [1-2]. However, the operation of plasma at low pressure includes vacuum systems, which are expensive and need precautions. Recently, the development of plasmas on the micro-sale at atmospheric pressure [3], especially generated by dielectric barrier discharge (DBD), has attained much interest to provide economical processing solutions by omitting the vacuum systems. Atmospheric pressure plasma jet (APPJ) [4] is a such kind of plasma device that can be run under atmospheric-pressure at various gases and is technically simple, low-cost, environment-friendly and usefulness of small size in treating localized regions. APPJ has wide application fields including material deposition [5], etching [6], surface modification [7-8], sterilization [9], and biomedical treatment [10]. The APPJ source can produce a stable, homogeneous, and uniform plasma discharge at atmospheric pressure and very low temperature.

In an APPJ system, however, the power supply is considered to one of the significant components, as it plays a key role on the discharge characteristics of the APPJ [11-14]. Various power supplies are used based on required voltage and applications [15]. Generally, direct current (DC), alternating current (AC), radio frequency (RF), and microwave generators are employed to operate APPJs. In recent times, pulsed generators are becoming more attractive owing to control the generation of non-thermal plasmas and their chemical and physical properties. In comparison with these generators, pulsed generators can deliver high instantaneous power with respect to low average power, offer fast rise time and high repetition

rate which are advantageous to control the production of high electron density and more active plasma species [16-19].

It is noted that the generation of APPJ by flowing gas in a dielectric tube wrapped with tube-shaped electrodes needs of short pulses (several microseconds) with a high voltage (several kV) and a low repetition rate (several kHz). Therefore, to meet the growing demand of APPJ applications, various types of high-voltage pulsed generators [20] have been developed with different techniques and parameters, such as Marx generator, magnetic pulse compression based generator, inductor-capacitor resonant converter based generator and magnetic pulse transformer (PT) based generator. Typically, magnetic PT based generators are convenient in these applications where generating high voltage impulses of order kilovolt to megavolt [21]. However, there are some weakness of magnetic PT based architecture, such as low efficiency, a limited repetition rate of operation, core saturation, and high electromagnetic interfaces. Considering these, it is feasible to design a magnetic PT in a dual resonance mode, namely dual resonance pulse transformer (DRPT), beyond a conventional approach. In general, conventional DRPTs are employed to generate very high voltage (up to MV) pulses for charging the capacitive loads, for example, pulse forming transmission lines (PFLs) using an air core (no magnetic core) and gas-filled/spark gap based switches [22-26]. Air core transformers, however, have lower coupling coefficient than that the magnetic core transformers. This constraint makes the air core transformers less energy efficient and bulky in size. Besides, gas-filled/spark gap switches have low lifetime, longer pulse rise time, and poor operating frequency range. Recently, power semiconductor switches overcome most of these difficulties of conventional switches [27]. Hence, the development of a compact high voltage, high repetition, and energy efficient pulse generator based on DRPT technique employing a magnetic core and solid-state switches, is of a great interest.

7.2. Objective

At first, a theoretical investigation of dual resonance pulse transformer (DRPT) principles is presented. Then, the design concept and implementation of a compact microsecond DRPT based impulse-generator (IG) for APPJ using a magnetic core and semiconductor switches are described. The generation of atmospheric-pressure plasma plume is performed by DPPT-IG.

7.3. Dual resonance pulse transformer (DRPT) principles

Pulse transformer circuits are usually employed for charging capacitive loads to a high voltage through set-up operation of transformer. Figures 7.1 (a) and (b) show a diagram of pulse transformer for charging a capacitor and its equivalent circuit, respectively. In the circuit

diagram, C1 and C2 are the primary and secondary capacitors, and L1, L2 and M are the primary secondary and mutual inductances of the pulse transformer (PT), respectively. The primary capacitor C1 is initially charged. When the switch S1 is closed, the charge is transferred to C2 from C1 via PT.

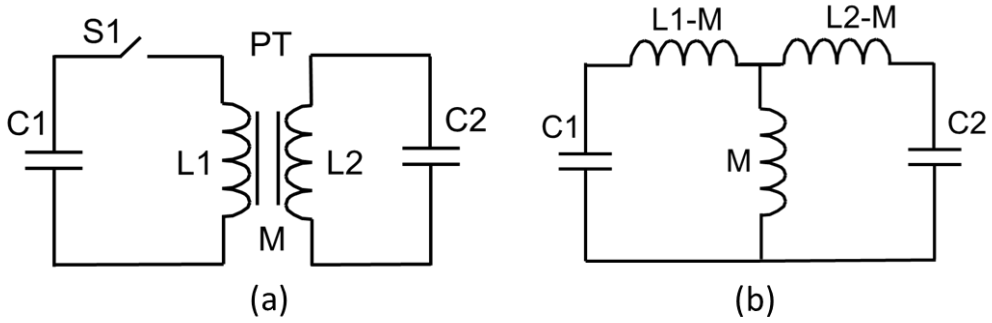

Figure 7.1. Pulse transformer coupled capacitor charger (a) circuit diagram and (b) its equivalent circuit.

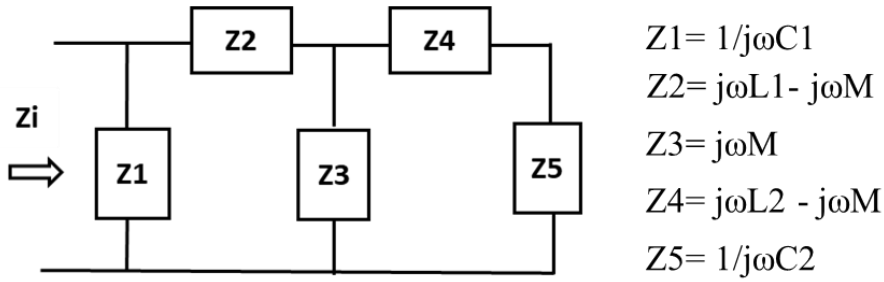

Figure 7.2. Equivalent input impedance model.

Generally, in a pulse transformer, charge and current in the primary circuit may still exit even the capacitor in the secondary circuit is at maximum voltage and zero current. This indicates that transferable energy in the primary capacitor still remains to be transferred in the secondary capacitor [28]. Hence, the use of a conventional pulse transformer to charge one capacitor from another is often inefficient. To derive the condition at which such kind of energy transfer inefficiency eliminates, is crucial.

It is supposed that if the circuit is tuned to resonance, energy is efficiently transferred from C1 to C2. To analyze the resonance conditions, the input impedance model is designed from the equivalent circuit [Figure 7.1. (b)] and presented in Figure 7.2. The equivalent input impedance, Zi is defined as,

$$\mathrm{Zi} = [\{(\mathrm{Z4} + \mathrm{Z5}) \parallel \mathrm{Z3}\} + \mathrm{Z2}] \parallel \mathrm{Z1}$$

$$= \frac{(Z1Z2Z3 + Z1Z2Z4 + Z1Z2Z5 + Z1Z3Z4 + Z1Z3Z5)}{(Z1Z3 + Z1Z4 + Z1Z5 + Z2Z3 + Z2Z4 + Z2Z5 + Z3Z4 + Z3Z5)}$$

$$= \frac{-\mathrm{j}\omega\{\omega^2(\mathrm{L1L2C2} - \mathrm{M^2C2}) - \mathrm{L1}\}}{\omega^4(\mathrm{L1L2C1C2} - \mathrm{M^2C1C2}) - \omega^2(\mathrm{L1C1} + \mathrm{L2C2}) + 1}$$

Where, ω is the angular frequency and $\omega = 2\pi f$

At resonance, $Zi \rightarrow \infty$ that implies,

$$\Rightarrow \omega^4(\mathrm{L1L2C1C2} - \mathrm{M^2C1C2}) - \omega^2(\mathrm{L1C1} + \mathrm{L2C2}) + 1 = 0$$

$$\Rightarrow (1 - \mathrm{k^2})\omega^4 - (\omega_1{}^2 + \omega_2{}^2)\omega^2 + \omega_1{}^2\omega_2{}^2 = 0$$

This is the characteristic equation of the system

where,

$$\omega_1{}^2 = \frac{1}{L1C1}, \quad \omega_2{}^2 = \frac{1}{L2C2}, \quad k^2 = \frac{\mathrm{M}^2}{\mathrm{L1L2}}$$

ω_1 is the angular resonant frequency of primary circuit when secondary is opened,

ω_2 is the angular resonant frequency of secondary circuit when primary is opened, and

k is the coupling coefficient of PT.

The characteristics equation suggests that the resonant frequency of the system is significantly influenced by the k value of transformer. If the open-circuit resonant frequencies of the two circuits are coincide and equal to $\omega_1 = \omega_2 = \omega_0$, for the theoretically possible limiting values of k , which are 0 (for no-coupled transformer) and 1 (for tight-coupled transformer), a single frequency appears in each case attributed as $\omega = \omega_0$ and $\omega = \frac{\omega_0}{\sqrt{2}}$, respectively. However, beats cannot occur in these cases, even at any ordinary values of k. Hence, it is very essential to determine the first condition of k value at which the maximum energy transfer occurs between primary and secondary circuit by neglecting dissipation of energy.

The roots of the characteristic equation can be defined as,

$$\omega_{\pm}^2 = \frac{(\omega_1{}^2 + \omega_2{}^2)}{2(1 - \mathrm{k^2})} \pm \frac{\sqrt{(\omega_1{}^2 + \omega_2{}^2)^2 - 4(1 - \mathrm{k^2})\omega_1{}^2\omega_2{}^2}}{2(1 - \mathrm{k^2})}$$

Obviously it is found that two natural modes of resonant frequencies defined as $\omega_+ \; and \; \omega_-$ and two negative modes of these frequencies are exist in the transformer-coupled capacitor charger circuit . Thus, the negative frequency modes have the same amplitude of voltage as to the positive frequency modes. A general voltage equation can be derived for both capacitors,

$V = V^+ cos\omega_+ t + V^- cos\omega_- t$, where $V^+ = V^- = \frac{V}{2}$

For primary capacitor with a subscript 1, the voltage equation becomes

$V_1 = V_1{}^+ cos\omega_+ t + V_1{}^- cos\omega_- t$

Since initially at t=0, $V_2 = 0$, implies $V_2{}^+ = -V_2{}^-$

For secondary capacitor with a subscript 2, the voltage equation becomes

$V_2 = V_2{}^+ cos\omega_+ t - V_2{}^- cos\omega_- t$

It indicates that the secondary voltage is a superposition of two weakly damped sinusoidal waves of equal magnitude and opposite initial phase. The secondary voltage has the largest possible subsequent maximum, when these sinusoids achieve maxima simultaneously. This happens when ω_+ becomes twice of ω_-. It is known as dual resonance condition where closed circuit resonances have a frequency ratio of 2:1 and the frequency of open circuit resonances must be equal. The theoretical voltage waveforms are shown in Figure 7.3. The two normal modes of resonance are in identical amplitude to the primary and secondary oscillation, but with corresponding initial phases. Then, the primary and secondary capacitors play exchanged roles after a period T. There is an amplitude reversal of -0.56 in both primary and secondary capacitors.

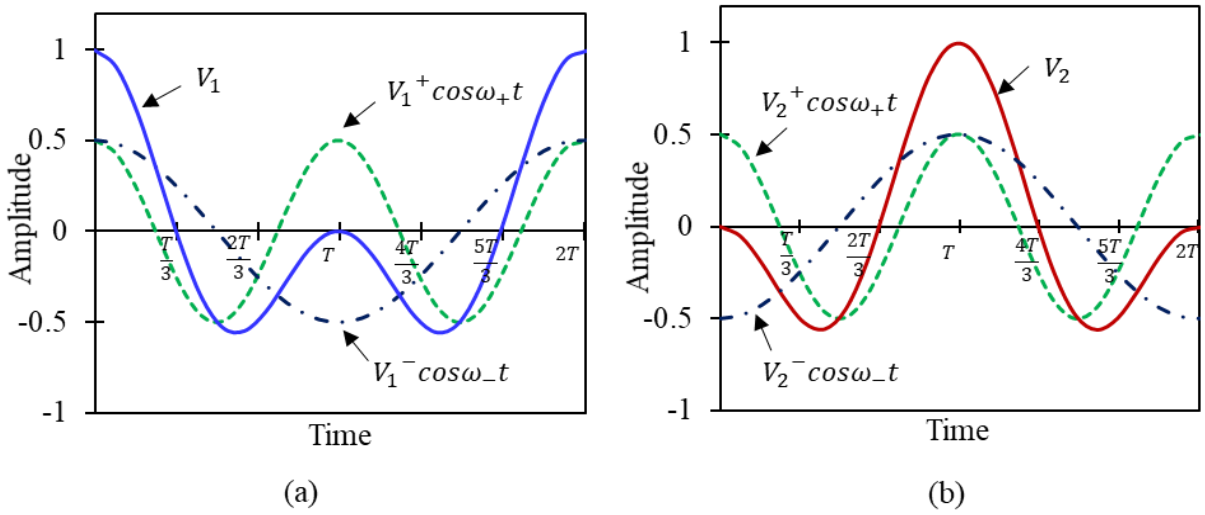

Figure 7.3. Theoretical voltage waveforms at dual resonance condition (a) primary capacitor (b) secondary capacitor.

Now the value k for dual resonance can be determined by considering $\omega_1 = \omega_2 = \omega_0$. The characteristic equation of the roots becomes

$$\Rightarrow \omega_{\pm}^2 = \frac{\omega_0{}^2(1 \pm k)}{(1 - k^2)}$$

The ratio of the roots is obviously

$$\Rightarrow \frac{\omega_+^2}{\omega_-^2} = \frac{(1 + k)}{(1 - k)}$$

The dual resonance condition is $\omega_+ = 2\omega_-$ and it implies

$$\Rightarrow \frac{(1 + k)}{(1 - k)} = 4$$

$$\Rightarrow k = \frac{3}{5} = 0.6$$

This exclusive value of k is practical for construction in a pulse transformer discussed later.

In a DRPT the high voltage is formed by resonance, however, the output voltage is not proportional to the turns ratio, as in an ordinary transformer. It can be evaluated nearly from conservation of energy. Initially, all of the energy in the primary circuit stored in the primary capacitor C1 can be defined as $W1 = \frac{1}{2}C1{V_1}^2$ and this energy is transferred to the secondary circuit through dual resonance principle after a period T. Then all the energy stored in secondary capacitor can be expressed as $W2 = \frac{1}{2}C2{V_2}^2$. In ideal case, assuming no energy losses implies $W2 = W1$. As a result, the ratio of the secondary to primary voltage amplitudes is simply, $\frac{V_2}{V_1} = \sqrt{\frac{C1}{C2}} = \sqrt{\frac{L1}{L2}}$, The last part is derived from the dual resonance condition, L1C1=L2C2. If the capacitance of the secondary circuit is very small compared to the primary capacitor and the inductance of secondary coil is very large compared to the primary coil, the primary voltage is stepped up to a high value in secondary.

7.4. Design and construction of the DRPT impulse-generator (IG)

7.4.1. Design consideration

In general, alternative current (AC) HV power sources of sinusoidal wave at lower frequency than a several 10s of kHz are widely used for the operation of APPJ, because it is easy to boost the voltage by using a transformer. In most cases, the APPJ is operated at a fixed frequency and a fixed voltage. For research and development of APPJ technology, however, it is important to examine the effects of operation frequency and waveforms on the plasma properties and processed results. For operation of DBD, the voltage increasing rate, decreasing rate, pulse width and pulse interval are crucial parameters [29]. For control of APPJ process induced in gas jet, the operation frequency is also an important parameter. In the case of conventional sinusoidal wave ACHV, with the variation of operation frequency and peak voltage, the voltage increasing rate, decreasing rate, pulse width and pulse intervals automatically varies. Because of the sinusoidal property, it is impossible to control the important discharge parameters intentionally. For advancing research on APPJ, it is necessary to develop a novel pulse power source which enables independent control of frequency, voltage, and waveforms.

Accordingly, an intermittent pulse operation of DRPT is proposed. In this model, the pulse width and rise time are determined by the dual resonance principle which is almost fixed whereas pulse repetition rate is controlled by the switching based on the intermittent period. The shape of voltage waveforms with the variation of frequency in the both conventional HV AC and our proposed DRPT-IG is demonstrated in Figure 7.4. It is expected that the control of

frequency in our proposed method is more efficient as the occurrence of the similar pulses just varies with the pulse repetition rate. It offers high frequency operation of pulsed plasma discharge without interfering the pulse shape that is supposed to crucial for the investigation of high frequency operation of APPJ.

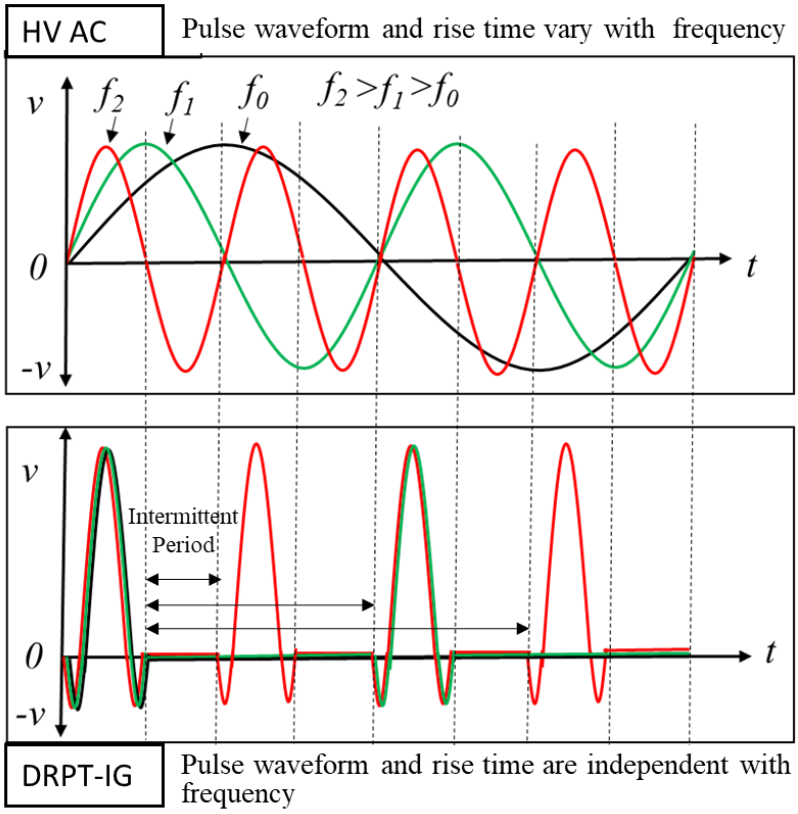

Figure 7.4. Design considerations for DRPT-IG.

7.4.2. Design layout and circuit diagram

Figure 7.5. shows the architectural block diagram of the proposed DRPT impulse generator. The generator consists of the following parts: a high-voltage (HV) DC power supply, a primary energy storage, an intermediate energy storage, solid-state switches, a trigger pulse control system, a function generator, a dual resonance pulse transformer, and the load. Pulse control system receives an input signal from a function generator and generates the corresponding trigger pulses for the switches. Initially, the energy supplied from the HV DC power supply is stored in the primary energy storage, which is transferred to the intermediate energy storage through a solid-state switch. After that, the energy of the intermediate energy storage is transferred to the load and is recovered from the load to the intermediate energy storage via a solid-state switch and a dual resonance pulse transformer. Consequently, a desired high voltage impulse is generated on the load.

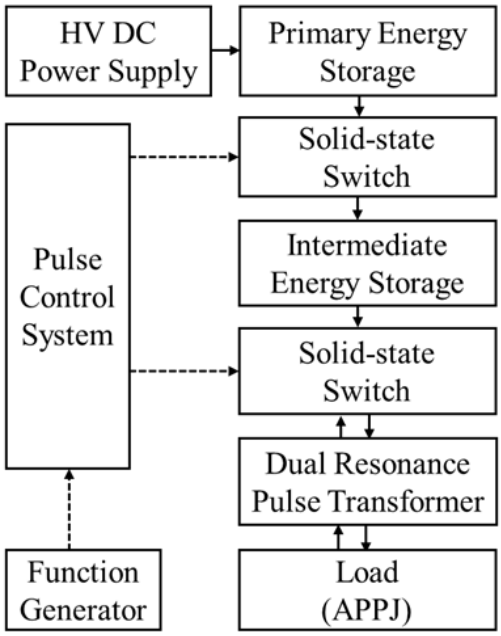

Figure 7.5. Architectural block diagram of DRPT impulse generator.

Figures 7.6(a) and 7.6(b) show the detail and simplified circuit diagram of the DRPT based high-voltage impulse generator, respectively. A high voltage regulated DC power supply (PA500-0.1A, Kenwood) is connected to the capacitor C0 via a diode D0 (C4D02120A, 1200 V, 10 A) which protects C0 from discharging back to the power supply. The DC power supply can deliver the variable voltage from 0-500 V with the variation of current from 0-100 mA. The capacitor CO acts as a primary energy storage which consists of two metallized polyester film type capacitors (each rated at 4.7 uF, 630 V) connected in series. Resistor R0 (50 Ω) and switch S1 mutually performs the charging of capacitor C1 that acts as an intermediate energy storage. Capacitor C1 consist of two ceramic capacitors (each rated at 3.3 nF, 1000V) along with a variable capacitor (3.3 nF, 1000V) connected in a parallel configuration to reduce the total series resistance of the capacitor C1. Moreover, a variable capacitor is employed to effectively tune the performance of DRPT.

Employing dual resonance pulse transformer topology, the scheme of energy transferring to and recovering from load has been designed. The pulse shape depends on the design of the DRPT is discussed in detail in the section 7.3. The energy from the capacitor C1 is transferred to the load C2 (APPJ) through mutually switch S2 and DRPT. The energy recovery from the load C2 to the intermediate energy storage C1 is executed through switch S2 and DRPT in the reverse way. The built-in diode of switch S2 allows to flow reverse current during dual resonance operation. The circuit components were optimized in the design for the efficient energy exchange between C1 and C2.

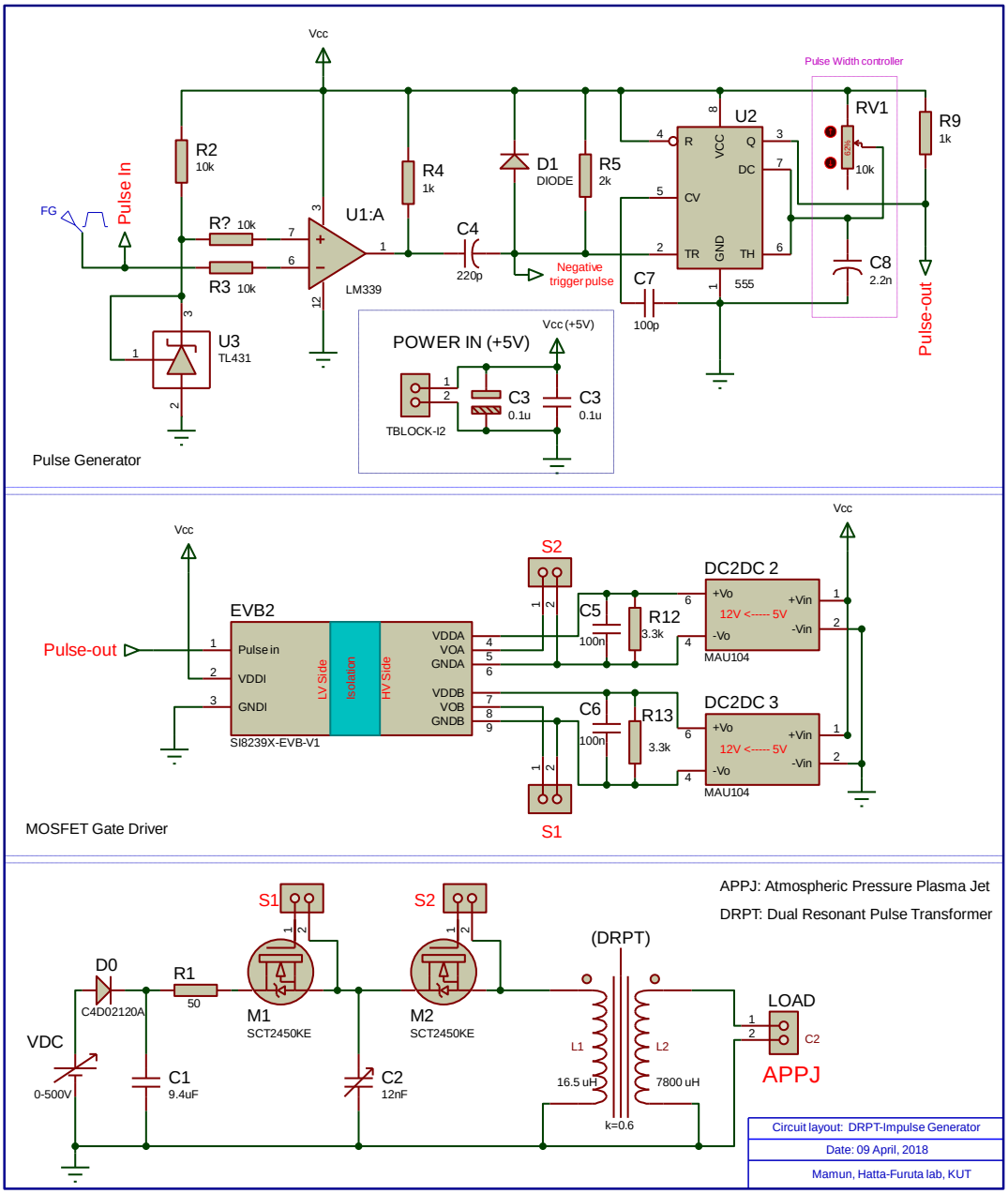

(a)

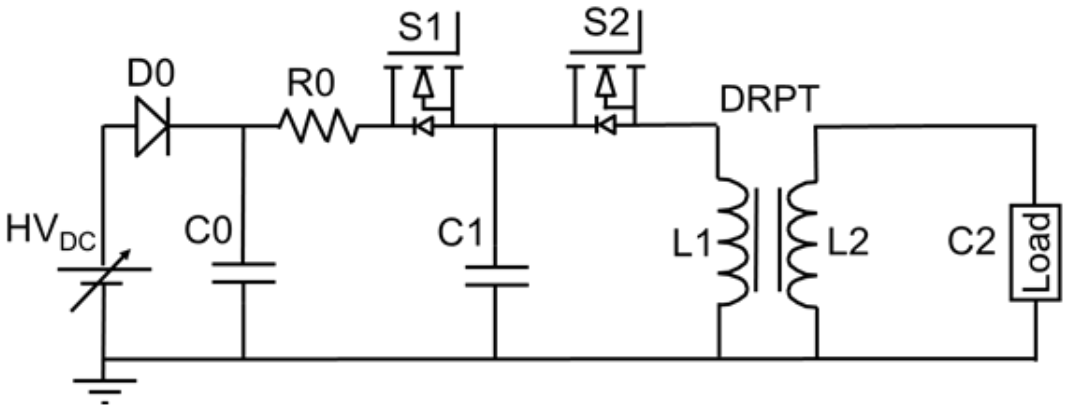

(b)

Figure 7.6. Circuit layout of the proposed impulse generator (a) detail (b) simplified.

In this design, silicon-carbide metal-oxide-semiconductor-field-effect-transistors (SiC MOSFETs, SCT2450E, 1200 V, 10 A) are used for all the switches. These MOSFETs have interesting features such as high speed, high reverse blocking voltage, low output capacitance and low on state resistivity which are considered as the crucial parameters for high performance switching operation. Moreover, the low voltage and high voltage parts of the circuit are kept completely in electrical isolation.

7.4.3. Construction of the DRPT

The design of the DRPT plays an important role on the formation of the output impulse characteristics of the generator. The core material, shape, and winding arrangement influence the electromagnetic processes in it. Figure 7.7(a) shows the model of the pulse transformer that consists of a pair of EC type Mn-Zn Ferrite core (PC40 EC120-Z, TDK) employed in a face to face arrangement where core 1 and core 2 act as a primary side and secondary side, respectively. The primary winding consists of 7 turns of insulated multicore copper wire (AWG 18) whereas the secondary windings consists of 115 turns of insulated multicore coper wire (AWG 30). An air gap distance is inserted between two cores to control the coupling coefficient of the transformer.

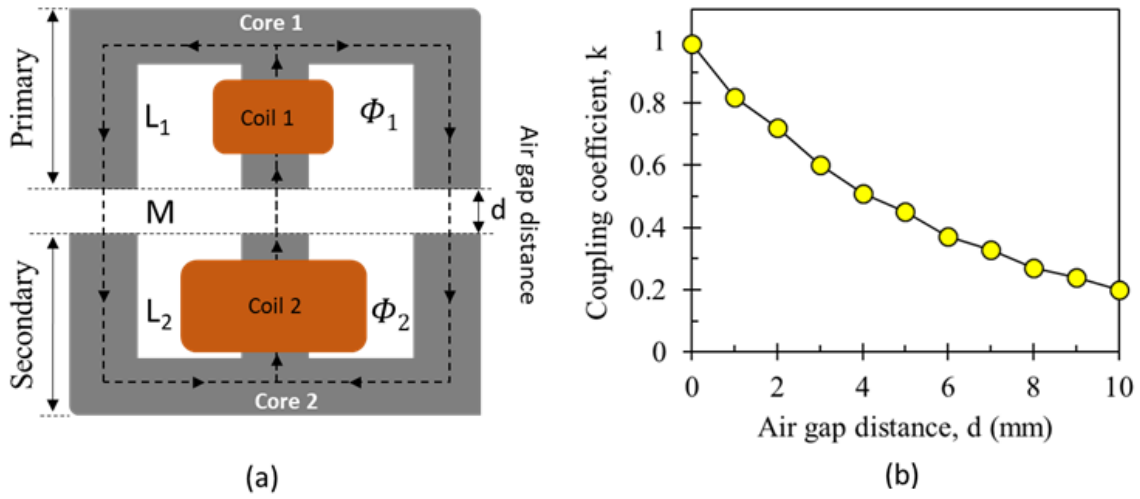

Figure 7.7. (a) Design model of the DRPT (b) Dependence of the coupling coefficient with the variation of air gap distance.

As shown in the Figure 7.7(b), the coupling coefficient shows a close relation to the air gap distance. As the air gap distance increases the rapid attenuation of the inductance parameters, the coupling coefficient reduces greatly. The coupling coefficient of pulse transformer is crucial for dual resonance principle and it should be 0.6. Thus, the tuning of the coupling coefficient by this approach is more convenient to design efficiently the DRPT. In this design, the air gap

distance is kept 3 mm for the coupling coefficient of 0.61. The primary (L_1), secondary (L_2), and mutual (M) inductances are 16.5 µH, 7800 µH, and 219 µH, respectively. The expected voltage gain of the DRPT is about 22.5. Furthermore, insulation between the transformer core and windings are taken into account in the design of DRPT.

7.4.4. Control Module and operation modes

Figure 7.8 shows the pulse control system for generating trigger signals of the corresponding switches. It is expected that the output of the generator is high voltage impulse with wide variation of amplitude and repetition rate which are supposed to be effective parameters for the plasma discharge properties. For this, a high resolution function generator (DF1906, NF Corporation) is employed to produce a transistor-transistor-logic (TTL) trigger signal so that pulse parameters can be set more conveniently. This TTL signal, V_{in} is fed to an inverting buffer for generating negative trigger pulses of the monostable multivibrator. A resistor-capacitor (RC) timing network is used to control the width of the output pulse of the monostable multivibrator. The output pulse of the multivibrator and its inverted pulse are fed to a couple of isolated gate driver modules (Si8239xISO-KIT, Silicon Laboratories) powered by isolated DC-DC converters (MAU104, 5 V-12 V), to generate the driving signals of the MOSFET switches. The driving signals V_{S1} and V_{S2} are allocated for the MOSFET switches S1 and S2, respectively. The gate driver introduces built-in dead time (14.65 ns) to avoid the concurrent operation of MOSFET switches.

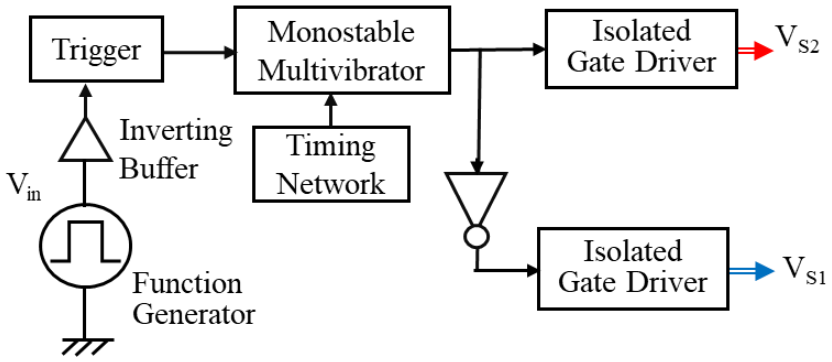

Figure 7.8. Schematic diagram of pulse control system.

Figure 7.9. presents the time sequence of driving signals of the impulse generator through which the pulse control system takes charge of operation modes of the generator to yield output impulses of voltage. One switching cycle is divided into six-time durations, as t_0 to t_5 and consists of three operation modes: mode1 for the energy transfer to the load, mode 2 for the energy recover from the load, and mode 3 for the off-state.

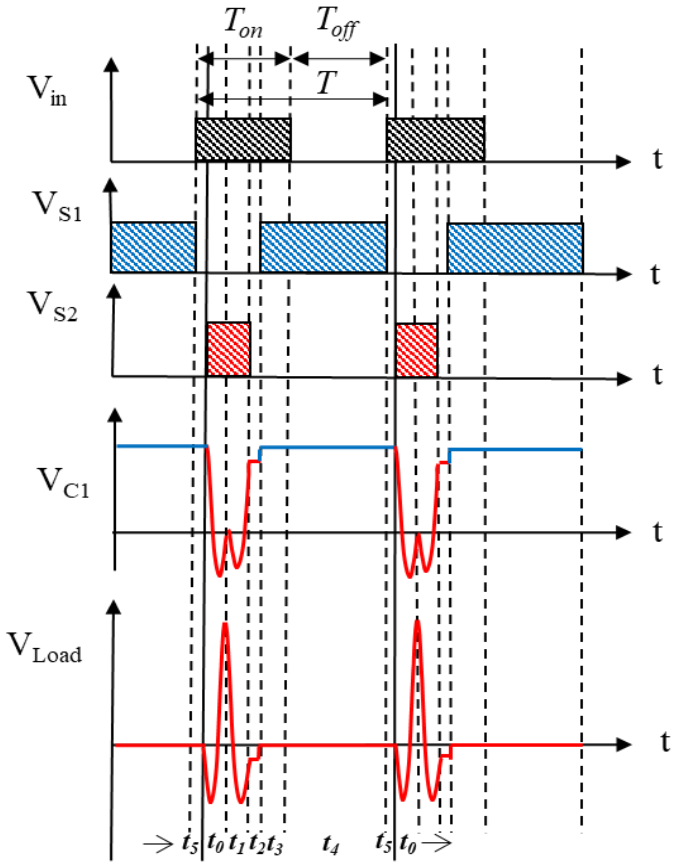

Figure 7.9. Timing diagram of control signals and expected voltage waveforms across the C1 and load.

In mode 1, for the energy transfer to the load, the control signal V_{S2} is applied to turn on S2 which allows to transfer the stored energy from C1 to the primary side of the pulse transformer. After that, the induced energy in the primary side transfers to the secondary side and to the load by means of dual resonance principle (stated in section 7.2.) as indicated in Figure 7.10(a). The output voltage (V_{Load}) rises rapidly to a peak value at a time t_0, equal to the period of a full-cycle of dual resonance circuit.

In mode 2, for the energy recover from the load, the load voltage (V_{Load}) starts to fall rapidly after the peak value that energizes the secondary windings of the DRPT. The energy is recovered from the secondary side to the primary side of DRPT by means of dual resonance principle and stored in C1 in a reverse way of mode 1, as indicated in Figure 7.10(b). As a result, the voltage of C1 (V_{C1}) rises to the near of the initial voltage of C1 at a time t_1, equal to the period of a full-cycle of dual resonance circuit.

In mode 3, for the off state, the switch S2 is turned off and kept open until the start of the next input pulse. The off-state time t_3 *and* t_4 are mutually defined as intermittent period, which can be changed to control the operating frequency of impulse. During the off state, switch S1 is turned on to charge the intermediate energy storage capacitor C1 to the initial voltage, equal to the DC power supply only for the deficiency of recovered charge, as indicated in Figure

7.10(c). The switches S1 and S2 are synchronized with the input signal Vin with delay times t_5 and t_2 due to the dead time setting.

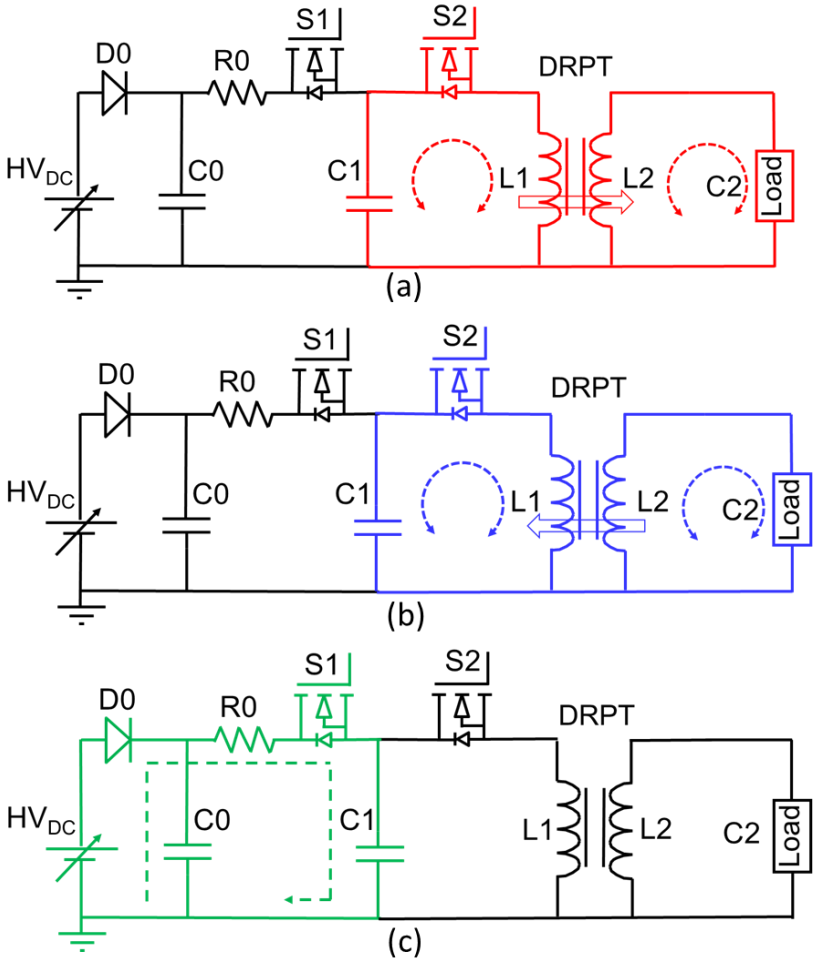

Figure 7.10. Operation modes of the DRPT impulse generators: (a) mode 1, for the energy transfer to the load (b) mode 2, for the energy recover from the load (c) mode 3, for the off-state. Solid colored lines are the indication of active circuit loops in each mode.

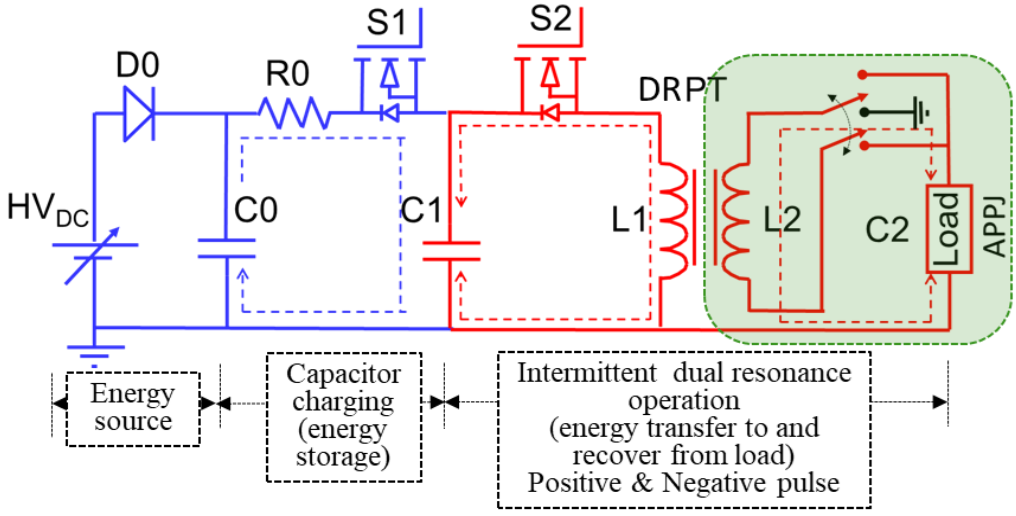

Figure 7.11. Arrangement of secondary circuit to produce both positive and negative impulse

In general, the above circuit configuration [Figure 7.10.] is intentionally preferred for better understanding of the operation of the generator for producing conventional positive impulse. However, this generator can also generate negative impulse. The secondary circuit of the generator can be arranged in such a way that it can produce both positive and negative impulse by keeping the identical operation of primary side as shown in Figure 7.11. A double-line slider switch is used to change the polarity of the output impulse, which is supposed to be advantageous for the investigation of positive and negative discharge characteristics in AAPJ.

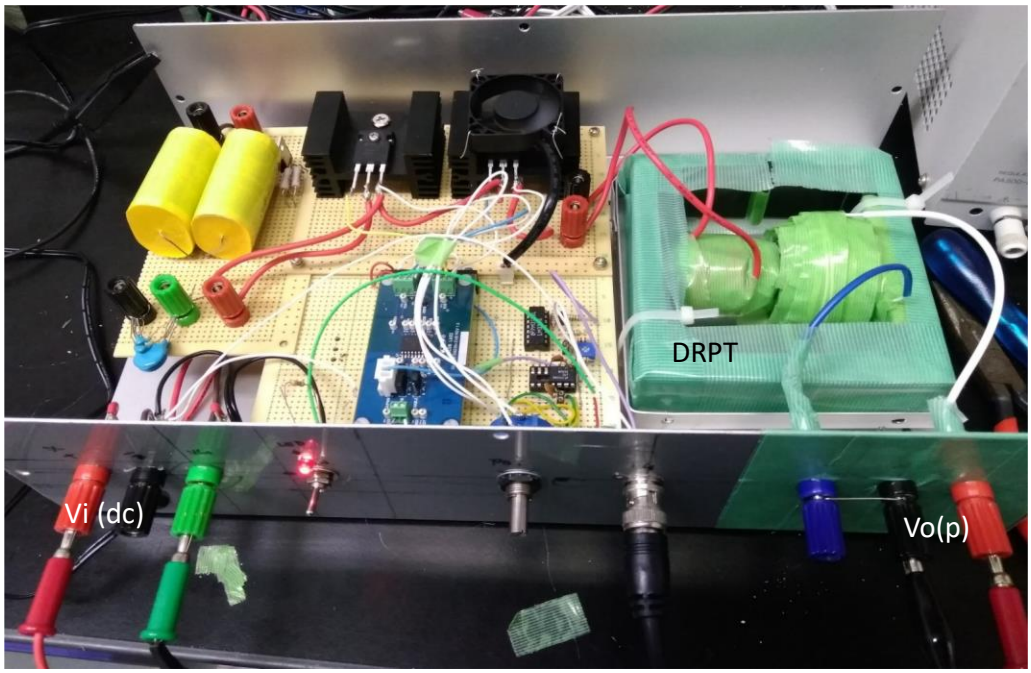

(a)

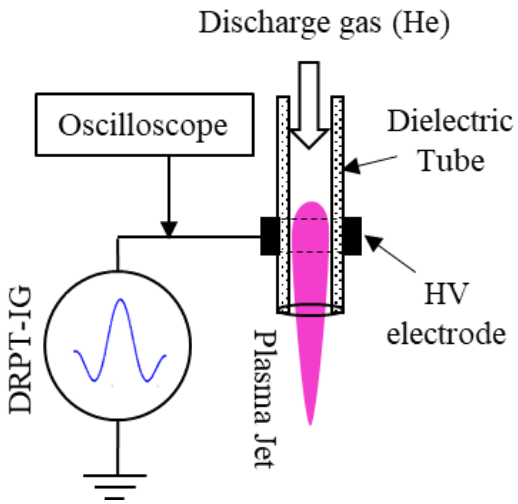

(b)

Figure 7.12. (a) Photo of the developed DRPT-IG (b) schematic of test setup for APPJ using DRPT-IG.

7.5. Test of impulse generator

The testing of the fabricated laboratory prototype dual resonance pulse transformer based impulse generator (DRPT-IG) is carried out using a APPJ load. Figure 7.12(a) shows a photo of the developed laboratory level prototype DRPT impulse generator (DRPT-IG) and Figure 7.12(b) shows a schematic diagram of test setup for APPJ by DRPT-IG, respectively. APPJ is configured as a dielectric barrier discharge (DBD) load (equivalent to load C2 indicated in the design circuit, Figure 7.6), made of a glass tube. The inner and outer diameters, thickness and length of the glass tube are 4 mm and 3.2 mm, 0.8 mm and 120 mm, respectively. Helium (He) gas is used as discharge gas and its flow rate is of 0.5 standard liters per minute (slm) controlled by a mass flow controller. APPJ is arranged in a single electrode configuration [30], where only HV voltage electrode is used and ground electrode is eliminated. The HV electrode is 15 mm wide, made of copper tape wrapped outside on the glass tube and placed at a distance of 5 mm from the tube end.

The impulse generator is turned on and the high-voltage pulses are generated across the APPJ load. During APPJ operation, the current and voltage waveforms were investigated using a digital storage oscilloscope (Tektronix 2014B, 100 MHz) with a high voltage probe (1000:1). DRPT-IG can deliver high-voltage impulse peak voltage up to 11 kV from a low voltage DC of 500 V, which ensures the voltage gain of almost 22.5. It has a convenient operation of frequency and can be changed widely from 0.5 kHz to 100 kHz. The pulse width is approximately 4 μs with a pulse rise and fall time about 2 μs. The specification of the developed DRPT-IG is given in Table 7.1.

Table 7.1. Specification of the developed DRPT-IG.

Element	Rating
Input voltage (DC)	0–500 (V)
Output voltage (impulse) (Peak to Peak) *(Positive or Negative)*	0–11 (kV)
Voltage step-up factor	~22.5
Pulse frequency	0.5–100 (kHz)
Pulse width	~4 (μs)
Pulse rising time	~ 2 μs
Pulse falling time	~ 2 μs

Figure 7.13 (a) and 7.13 (b) show the typical voltage waveforms and photo during APPJ operation, respectively. The discharge was performed using He gas with a flow rate of 0.5 L/min, an input voltage (DC) of 450 V, and an output voltage of 10 kV with an input pulse frequency of 10 kHz. The waveforms consist of three characteristic parts based on the operation

modes defined in section 7.4.4. The first part, indicated as (I) in Figure 7.13, is mode 1 for duration of ~2 μs, where the energy is transferred to the load from the intermediate storage capacitor through DRPT principle, quickly the load peak voltage goes to a peak voltage over than the breakdown voltage and plasma ignites. The second part, indicated as (II) in Figure 7.13, is mode 2 for the duration of ~2 μs, where the energy is recovered from load to intermediate storage capacitor via DRPT and the load peak voltage quickly falls. However, as the electrical components are on ideal, total amount of energy can be recovered. A small amount of energy still remains in the secondary circuit after recovery that forms very weak damping oscillation. The third part, indicated (III) as in Figure 7.13, is mode 3 which is called off- state (intermittent period) of the pulse for the period of occurring next pulse, where the load is kept turned off and the intermediate capacitor is charge to a voltage equal of input DC voltage. The observed waveforms almost following the dual resonance pulse operation as expected in our design.

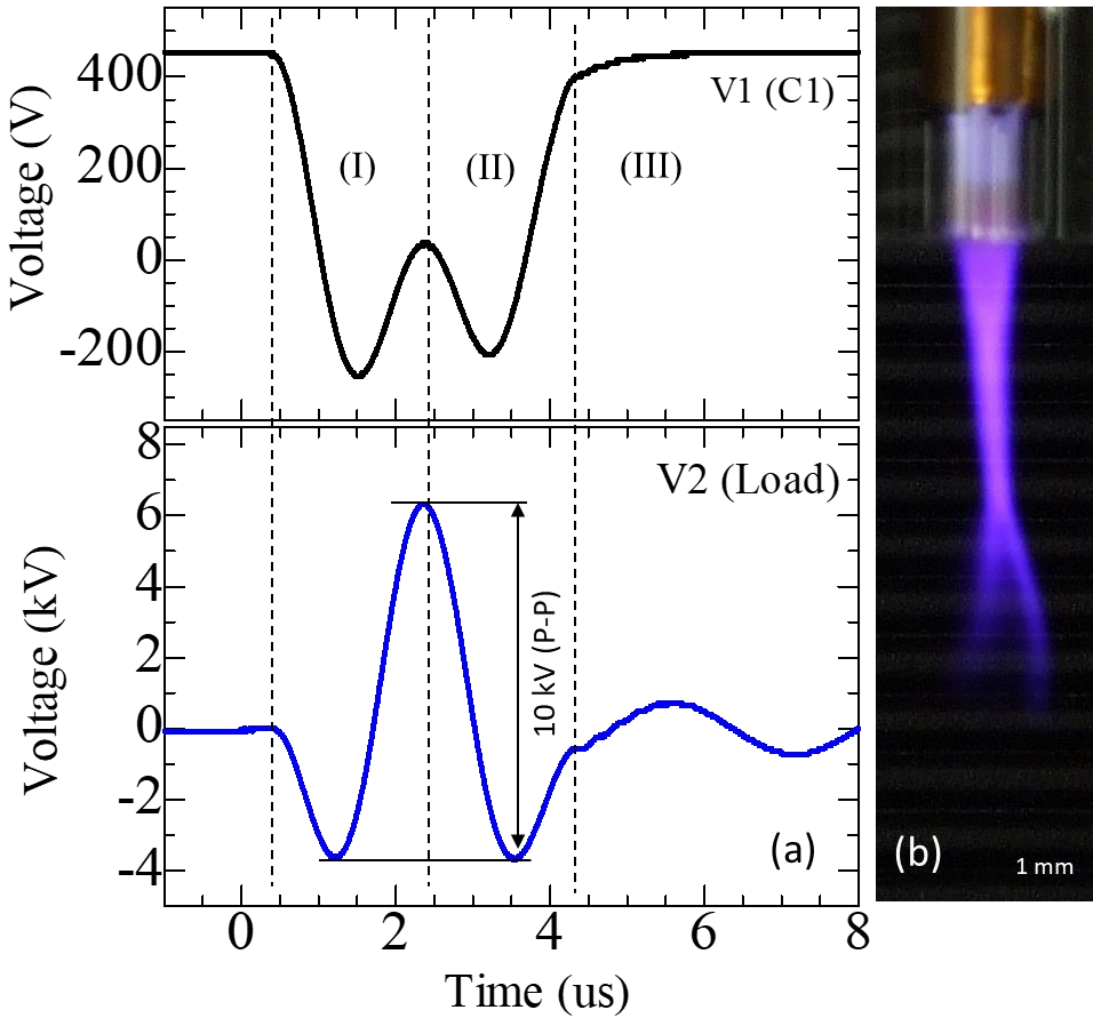

Figure 7.13. APPJ operation (a) typical voltage waveforms and (b) photograph of plasma plume.

The experimental results show that the developed prototype DRPT-IG is suitable for operation of APPJ. In addition, all-solid-state approach by using semiconductor switches (MOSFETs) with a stable control method of DRPT is employed to develop the proposed generator. Hence, the DPRT-IG is compact and its long maintenance-free lifetime with high reliability is expected. However, the further investigation of APPJ discharge characteristics using DRPT-IG at various discharge conditions will be required, discussed in chapter 8.

7.6. Conclusion

In this study, a high-voltage impulse generator (IG) was designed and constructed using a step-up dual resonance pulse transformer (DRPT) and solid-state switches to drive atmospheric-pressure plasma jets. Dual resonance operation conditions were studied and achieved by optimizing the pulse transformer parameters. The developed generator is compact and has convenient control for voltage and frequency selection. It can deliver high-voltage impulses (peak to peak) of 0–11 kV with the pulse repetition rates of 0.5-100 kHz. The impulse rise-time and fall-time are almost 2 μs, and the pulse width is approximately 4 μs. The performance of DRPT-IG was evaluated and tested by generating a stable room-temperature atmospheric pressure plasma plume using He gas flow in a plasma jet device with single electrode configuration. It is expected that this study will stimulate the further investigations on the development of pulsed generators for atmospheric-plasma discharge processes.

References

[1] M. Strobel, C. S. Lyons, and K. L. Mittal, *"Plasma surface modification of polymers: relevance to adhesion",* (VSP BV, The Netherlands, 1994), chapter 1.

[2] M. A. Lieberman and A. J. Lichtenberg, *"Principles of Plasma Discharges and Materials Processing",* (Wiley, New York, 1994), Chapter 1.

[3] K. Tachibana, "Current status of microplasma research", *IEEJ Trans. Electr. Electron. Eng.* 1, 145, (2006).

[4] H. Koinuma, Ohkubo, T. Hashimoto, K. Inomata, T. Shiraishi, A. Miyanaga, and S. Hayashi, "Development and application of a microbeam plasma generator", *Appl. Phys. Lett.* 60, 816, (1991).

[5] Y. Ito, K. Urabe, N. Takano, and K. Tachibana, "High speed deposition of SiO2 films with plasma jet based on capillary dielectric barrier discharge at atmospheric pressure", *Appl. Phys. Express* 1, 067009, (2008).

[6] J. Y. Jeong, S. E. Babayan, V. J. Tu, J. Park, I. Henins, R. F. Hicks, and G. S. Selwyn, "Etching materials with an atmospheric-pressure plasma jet", *Plasma Sources Sci. Technol.* 7, 282, (1998).

[7] T. Shao, W. Yang, C. Zhang, Z. Niu, P. Yan, and E. Schamiloglu, “Enhanced surface flashover strength in vacuum of polymethylmethacrylate by surface modification using atmospheric- pressure dielectric barrier discharge”, *Appl. Phys. Lett.* 105, 071607, (2014).

[8] E. J. Szili, A. S. Al-Baraineh, P. M. Bryant, R. D. Short, J. W. Bradley, and D. A. Steele, “Controlling the spatial distribution of polymer surface treatment using atmospheric-pressure microplasma jets”, *Plasma Process. Polym.* 8, 38, (2011).

[9] K. Lee, K-H. Paek, W-T. Ju, and Y. Lee, “Sterilization of bacteria, yeast, and bacterial endospores by atmospheric-pressure cold plasma using helium and oxygen”, *J. Microbiol.* 44, 269, (2006).

[10] X. Zhang, D. Liu, R. Zhou, Y. Song, Y. Sun, Q. Zhang, J. Niu, H. Fan, and S. Yang, “Atmospheric cold plasma jet for plant disease treatment”, *Appl. Phys. Lett.* 104, 043702, (2014).

[11] X. Lu, M. Laroussi, and V. Puech, “On atmospheric-pressure non- equilibrium plasma jets and plasma bullets”, *Plasma Sources Sci. Technol.* 21, 034005, (2012).

[12] M. Shibata, N. Nakano, and T. Makabe, “Effect of O_2 ($a^1\Delta_g$) on plasma structures in oxygen radio frequency discharges,” *J. Appl. Phys.* 80, 6142, (1996).

[13] J. S. Oh, Y. Aranda-Gonzalvo, and J. W. Bradley, “Time-resolved mass spectroscopic studies of an atmospheric-pressure helium microplasma jet,” *J. Phys. D. Appl. Phys.* 44, 365202, (2011).

[14] W. Jiang, J. Tang, Y. Wang, W. Zhao, and Y. Duan, “Characterization of argon direct-current glow discharge with a longitudinal electric field applied at ambient air,” *Sci. Rep.* 4, 6223, (2014).

[15] A. Schutze, J. Y. Jeong, S. E. Babayan, Jaeyoung Park, G. S. Selwyn and R. F. Hicks, “The atmospheric-pressure plasma jet: a review and comparison to other plasma sources”, *IEEE Trans. Plasma Sci.* 26, 1685, (1998).

[16] T. Shao, W. Yang, C. Zhang, Z. Fang, Y. Zhou, and E. Schamiloglu, “Temporal evolution of atmosphere pressure plasma jets driven by microsecond pulses with positive and negative polarities”, *EPL (Euro-physics letters)* 107, 65004, (2014).

[17] C. Zhang, T. Shao, P. Yan, and Y. Zhou, “Nanosecond-pulse gliding discharges between point-to-point electrodes in open air”, *Plasma Sources Sci. Technol.* 23, 035004, (2014).

[18] J. L. Walsh, D. X. Liu, F. Iza, M. Z. Rong, and M. G. Kong, “Contrasting characteristics of sub-microsecond pulsed atmospheric air and atmospheric pressure helium–oxygen glow discharges”, *J. Phys. D: Appl. Phys.* 43, 032001, (2010).

[19] S. Hofmann, A. Sobota, and P. Bruggeman, “Transitions between and control of guided and branching streamers in dc nanosecond pulsed excited plasma jets”, *IEEE Trans. Plasma Sci.*, 42, 2888, (2012).

[20] J. Mankowski and M. Kristiansen, “A review of short pulse generator technology,” *IEEE Trans. Plasma Sci.* 28, 102, (2000).

[21] Z. Zhang and X. Tan, “Review of High Power Pulse Transformer Design,” Phys. Procedia 32, 566 (2012).

[22] J. P. O'Loughlin, J. D. Sidler, and G. J. Rohwein, “Air core pulse transformer design”, *Proceedings of the 18th IEEE Power Modulator Symposium* 1988, Hilton Head, South Carolina, USA.

[23] G. J. Rohwein, “Design of Pulse Transformers for PFL Charging”, *Proceedings of the 2nd IEEE International Pulsed Power Conference* 1979, Lubbock, Texas, USA.

[24] G. J. Rohwein, “A Three MV Transformer for PFL Pulse Charging”, *IEEE Trans. Nucl. Sci.* NS26, 4211, (1979).

[25] Z. Shotts, F. Rose, S. Merryman, and R. Kirby, “Design Methodology for Dual Resonance Pulse Transformers”, *Proceedings of the IEEE Pulsed Power Conference* 2005, Monterey, California USA.

[26] S. Lim, “Fabrication and Operation Testing of a Dual Resonance Pulse Transformer for PFL Pulse Charging,” *J. Korean Phys. Soc.* 59, 3679, (2011).

[27] W. Jiang, K. Yatsui, K. Takayama, M. Akemoto, E. Nakamura, N. Shimizu, A. Tokuchi, S. Rukin, V. Tarasenko, and A. Panchenko, “Compact solid-state switched pulsed power and its applications,” *Proc. IEEE* 92(7), 1180–1195, (2004).

[28] D. Finkelstein, P. Goldberg, and J. Shuchatowitz, “High voltage impulse system,” *Rev. Sci. Instrum.* 37, 159, (1966).

[29] U. Kogelschatz, B. Eliasson, and W. Egli, “Dielectric-barrier discharges. Principle and applications,” *J. Phys. IV*, 07(C4), C4-47–C4-66, (1997).

[30] X. Lu, Z. Jiang, Q. Xiong, Z. Tang, and Y. Pan, “A single electrode room temperature plasma jet device for biomedical applications,” *Appl. Phys. Lett.* 92(15), 151504, (2008)

Chapter 8

Investigation of pulsed plasma discharge characteristics for APPJ

This chapter presents the investigation of pulsed plasma discharge characteristics for APPJ by the developed impulse generator based on DRPT. The brief introduction, experimental methods and results are described. The effects of pulse amplitude, repetition rate and electrode configurations on the plasma plume length and characteristics of APPJ are discussed by means of electrical and optical properties. Furthermore, the dependency of pulse operating frequency and polarity on plasma jet characteristics and RONS production in PAW are also presented.

8.1. Introduction

Generally, in atmospheric-pressure plasmas, gas is excited by means of a high voltage pulses (several kV) under atmospheric pressure. Atmospheric pressure plasmas overcome the disadvantages of vacuum operation. It is useful in a verity of materials processes at ambient and plays a vital role in biomedical applications [1]. Specifically, for biomedical applications, non-equilibrium cold plasmas are crucial [2]. However, it is difficult to sustain non-equilibrium cold and uniform plasma discharge because of high pressure and occurrence of electrical arcs. Dielectric barrier discharge (DBD) is widely used method for generating non-equilibrium cold atmospheric plasmas [3]. In general, DBD is the electrical discharge between two electrodes, where at least one electrode is insulated by a dielectric barrier to eliminate the occurrence of arcing. DBD devices can be made in many configurations, typically planar, using parallel plates separated by a dielectric or cylindrical, using coaxial plates with a dielectric tube between them.

Atmospheric-pressure plasma jet (APPJ) [4-8] is a common arrangement for cylindrical configuration of DBD. Normally, it is filled with either a rare gas or rare gas mixture at atmospheric pressure and the tube walls acting as the dielectric barrier. Due to the atmospheric pressure level, such processes require high energy levels to sustain. Common dielectric materials include glass, quartz, ceramics and polymers. The gap distance between electrodes varies considerably, from few millimeters to several centimeters. Therefore, the discharge characteristics in a APPJ usually varies with the power supply parameters, for example voltage, current, operating frequency and pulse width, construction of jet set-up, for example diameter of tube, dielectric materials and electrode configuration, and discharge gas materials for example types of gas, flow rate. By optimizing these factors, it can be facilitated the APPJ to enhance the plasma plume and jet length, generate a large amount of chemically reactive species at atmospheric pressure.

8.2. Objective

The aim of this study is to investigate of the effects of pulse amplitude, polarity, repetition rate, electrode configurations, and gas flow rates on the plasma plume length and characteristics of APPJ. Furthermore, APPJ generated species and their profile along with the plume length, production of reactive oxygen and nitrogen species (RONS) in plasma-activated water (PAW) are also presented.

8.3. Experimental setup

Figure 8.1. shows the schematic of the experimental setup of the developed atmospheric-pressure plasma jet device with APPJ load model. A dual resonance pulse transformer based impulse generator (DRPT-IG) is developed to drive APPJ (described in details at chapter 7). The body of the plasma jet is made of a glass tube. The inner and outer diameters, thickness and length of the glass tube are 4 mm and 3.2 mm, 0.8 mm, and 120 mm, respectively. Helium (He) gas was introduced to the glass tube and its flow rates are 0.5 and 1 slm, controlled by a mass flow controller.

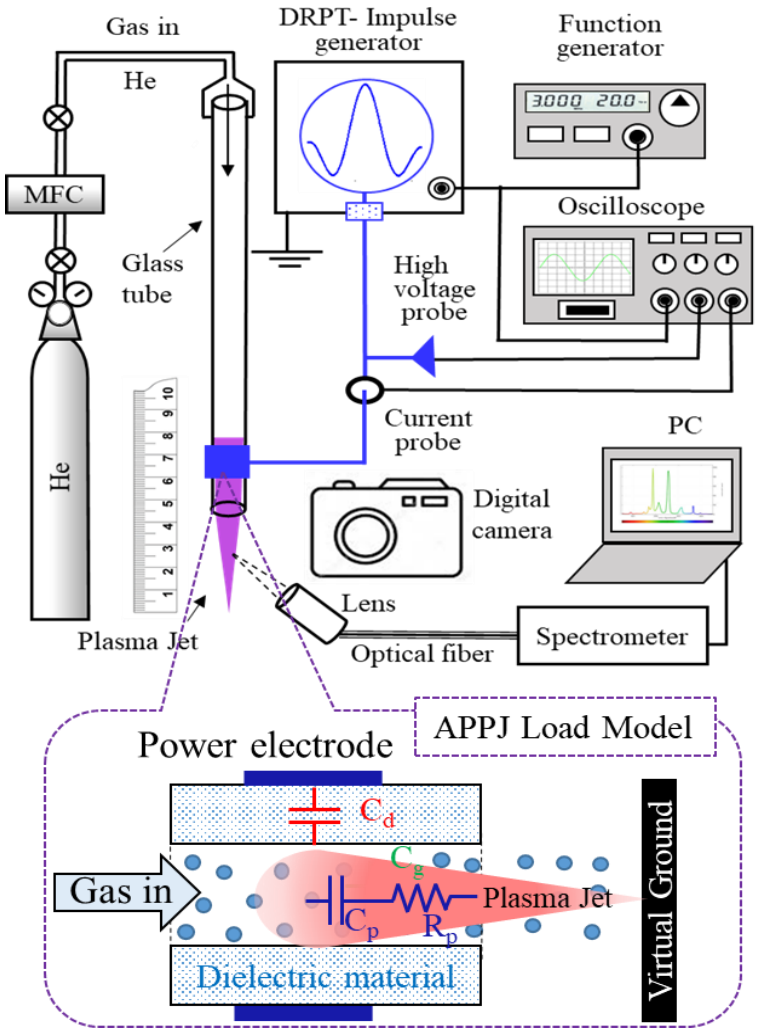

Figure 8.1. Experimental setup of atmospheric-pressure pulsed plasma jet device with APPJ load model.

APPJ is arranged in a single electrode configuration [9], where only HV voltage electrode is used and ground electrode is virtual. Two different HV electrode configurations are employed shown in Figure 8.2. The first configuration of electrode is made of a copper foil of 15 mm in wide wrapped outside the glass tube indicated as “strip-electrode” whereas the second configuration is made of a tin plating copper wire of 0.5 mm in diameter wrapped outside the glass tube indicated as “wire-electrode”. The distance between the electrode and the tube end for both electrodes is 5 mm.

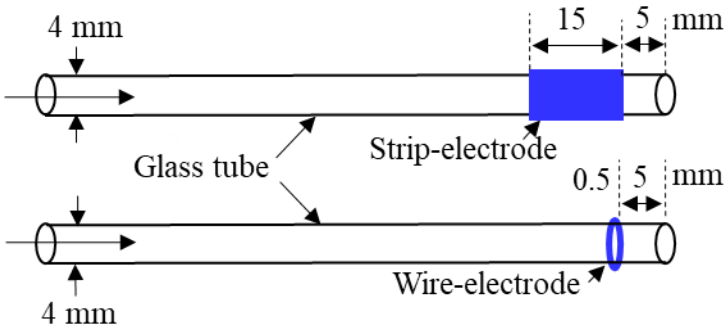

Figure 8.2. Two different HV single electrode configurations of plasma jet.

The impulse generator is turned on and the high-voltage pulses are generated across the APPJ load. During APPJ operation, the current and voltage waveforms were investigated using a digital storage oscilloscope (Tektronix 2014B, 100 MHz) with a high voltage probe (1000:1) and an isolated current probe. The plasma discharge photos are captured by a Fujifilm (FinePix S6000fd) digital camera. A multichannel spectrometer (Ocean Optics USB2000, measuring range 200–850 nm, optical resolution 1.5 nm) and an optical fiber (Ocean Optics P400-1-SR) with focusing lens are used to observe the optical emission spectra of plasma jet. The optical emission spectra are measured along plasma jet plume and recorded by a personal computer (PC).

8.4. Experimental results and discussions

8.4.1. Discharge characteristics

Figure 8.3 shows the equivalent circuit diagram of the APPJ device (presented in Figure 8.1.), which is arranged as a single dielectric electrode configuration. Since there is no physical ground electrode, it is assumed that a virtual remote ground plane completes the discharge circuit and plasma jet ignites. In the equivalent load model of APPJ, C_d is the dielectric capacitance of the glass tube and C_g is the air gap capacitance between the dielectric and the remote virtual ground. When a higher voltage pulse (V_P) over the breakdown voltage is applied across the electrode, the plasma discharge is produced by ionizing gas. The breakdown switch

S_b becomes closed and a conductive plasma channel appears represented by a series combination of R_p and C_p, which are the capacitive and resistive modeling response of plasma. In the circuit, I_t, I_d, and I_p are is the total current, displacement current and plasma conduction current, respectively.

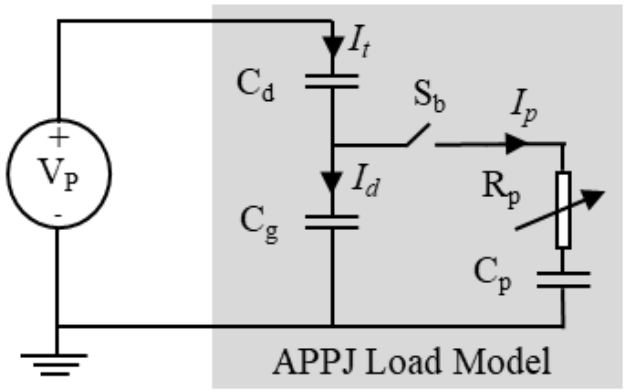

Figure 8.3. Equivalent circuit diagram of the APPJ device.

Without electrical breakdown, the equivalent capacitance C of the circuit and the total current become simply displacement current I_d, can be expressed, respectively,

$$C = \frac{C_d C_g}{C_d + C_g}$$

and

$$I_d = C \frac{dV_p}{dt}$$

When breakdown occurs, the total current I_t becomes,

$$I_t = I_d + I_p$$

Then

$$I_p = I_t - I_d$$

$$I_p = I_t - C \frac{dV_p}{dt}$$

Therefore, the plasma conduction current can be calculated easily by subtracting the displacement current from the total current. Displacement current is usually measured when there is no gas flow and no plasma discharge [10]. It is observed from the circuit analysis that the DBD characteristics of APPJ mostly depend on the variation of applied voltage and the equivalent capacitance of the circuit. However, these two key parameters are influenced by the power supply configuration, jet setup, electrode configuration, type of discharge gas and its flow rate.

Figure 8.4 shows typical waveforms of applied voltage V_p, total current I_t, displacement current I_d and plasma conduction current I_p at a peak applied voltage of 10 kV with operating frequency of 10 kHz for the strip-electrode type APPJ. Discharge is performed by flowing He

gas at a flow rate of 0.5 standard liters per minute (slm). It is observed that the phase different between V_p and I_d is about 90^0, which reveals the capacitive load model of APPJ (Figure 8.3). However, the amplitude of I_p is very much smaller than that of I_t, as I_d consumes a large portion of the I_t to accumulate charge of the dielectric surface. Almost in each half period of applied impulse, a lots of filament-like discharges appear on the plasma conduction current waveform, as same as a typical DBD at atmospheric-pressure [11-12].

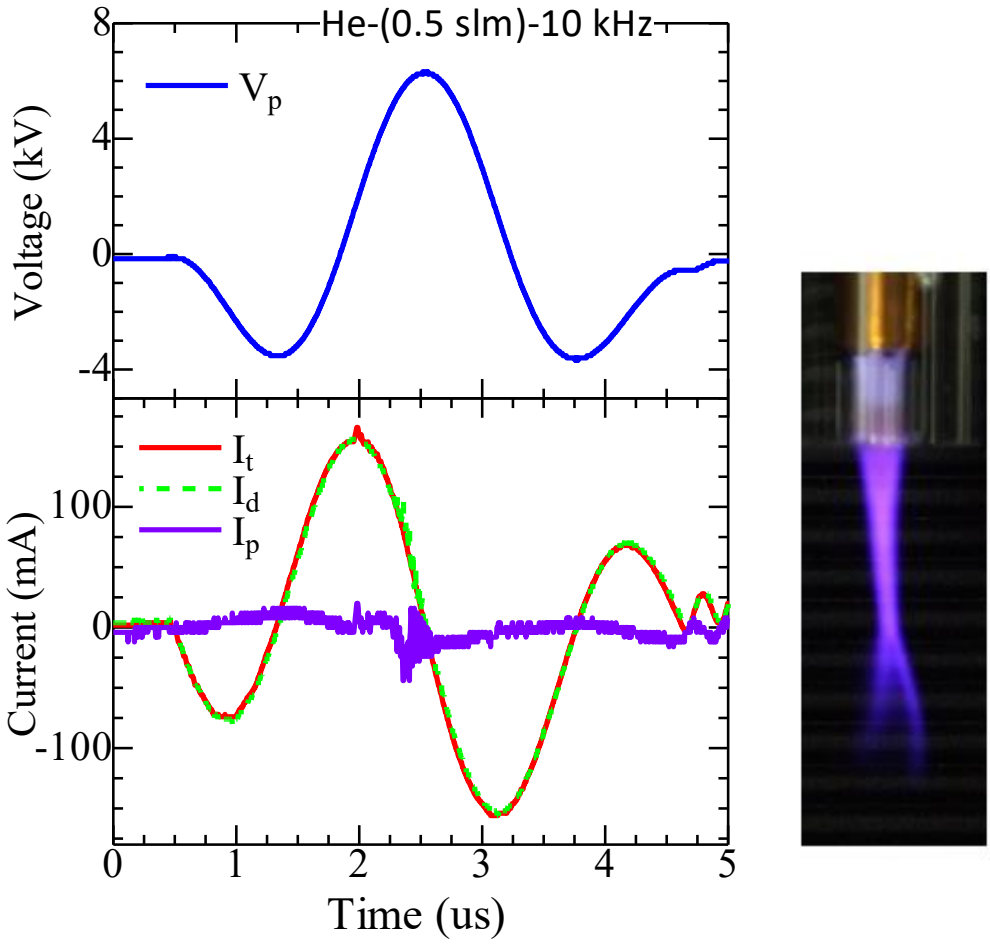

Figure 8.4. Typical waveforms of applied voltage V_p, total current I_t, displacement current I_d and plasma conduction current I_p and discharge image of the strip-electrode type APPJ.

The effect of applied impulse voltage on the discharge characteristics of the strip-electrode type APPJ was investigated as shown in Figure 8.5. The applied voltage is varied from 5.5 to 10 kV (peak to peak) where other experimental conditions are kept fixed. The other conditions are as He gas flow of 0.5 slm, pulse frequency of 10 kHz, and camera exposure time of 1 s. It can be seen that the pulse width is identical of about 4 μs, whereas only the amplitude increases at different applied voltages. Besides, the amplitude of the total current also increases with the applied voltage, however, there is no obvious difference except the position of discharge peak occurrence [Figure 8.5 (a)]. The plasma jet images show that the plasma plume length gradually

increases with the applied voltage, as increase of applied voltage introduces more consumption of DC power [Figure 8.5 (b) and (c)].

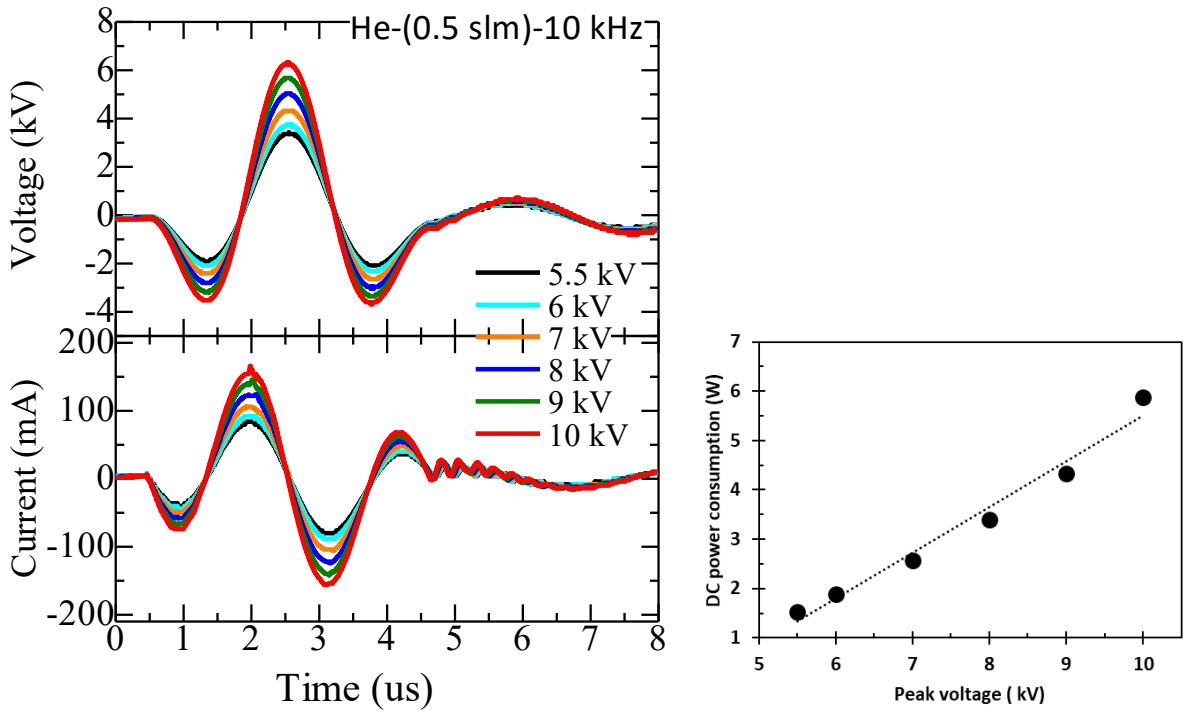

(a) (b)

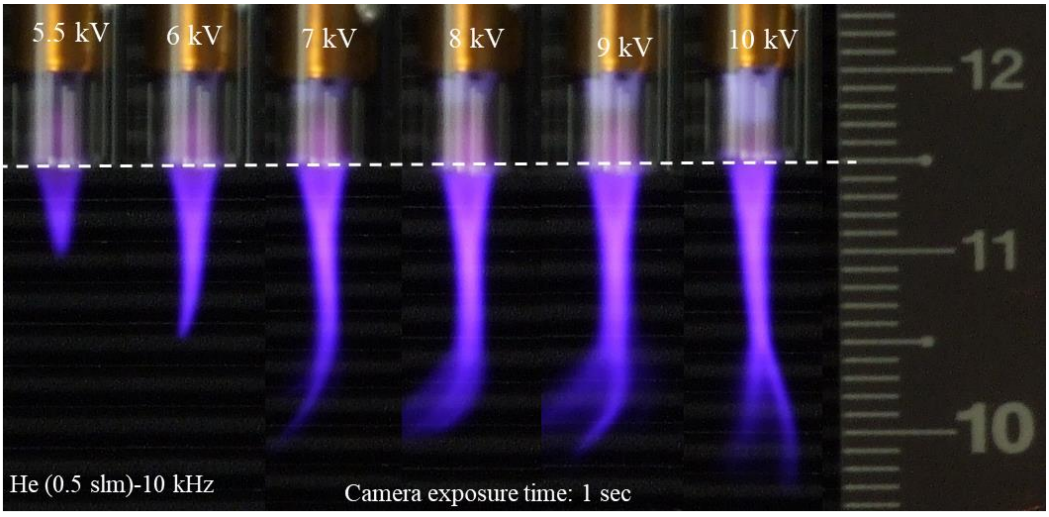

(c)

Figure 8.5. Dependency of the peak applied voltage on the characteristics of the strip-electrode type APPJ (a) Voltage and total current waveforms, (b) DC power consumption and (c) plasma jet photos.

The effect of impulse frequency on the discharge characteristics of the strip-electrode type APPJ was investigated as shown in Figure 8.6. The operating frequency is varied from 10 to 100 kHz where other experimental conditions are kept fixed. The other conditions are as He gas flow of 0.5 slm, applied voltage of 7 kV (peak to peak), and camera exposure time of 1 s. It can be seen that the output voltages are almost identical with a fixed pulse width of about 4

μs at different operating pulse frequencies, which indicates the developed impulse generator can produce stable output voltages and they are not altered by the pulse repetition rate [Figure 8.6(a)]. Besides, the amplitude of the total current increases slightly with the frequency, as increase of frequency introduces more consumption of DC power [Figure 8.6(b)]. As the camera exposure time is 1 s for all the jet images, the brightness of the plasma slightly increases with the pulse frequency [Figure 8.6(c)]. However, the plasma plume length decreases slightly with the increase of pulse frequency.

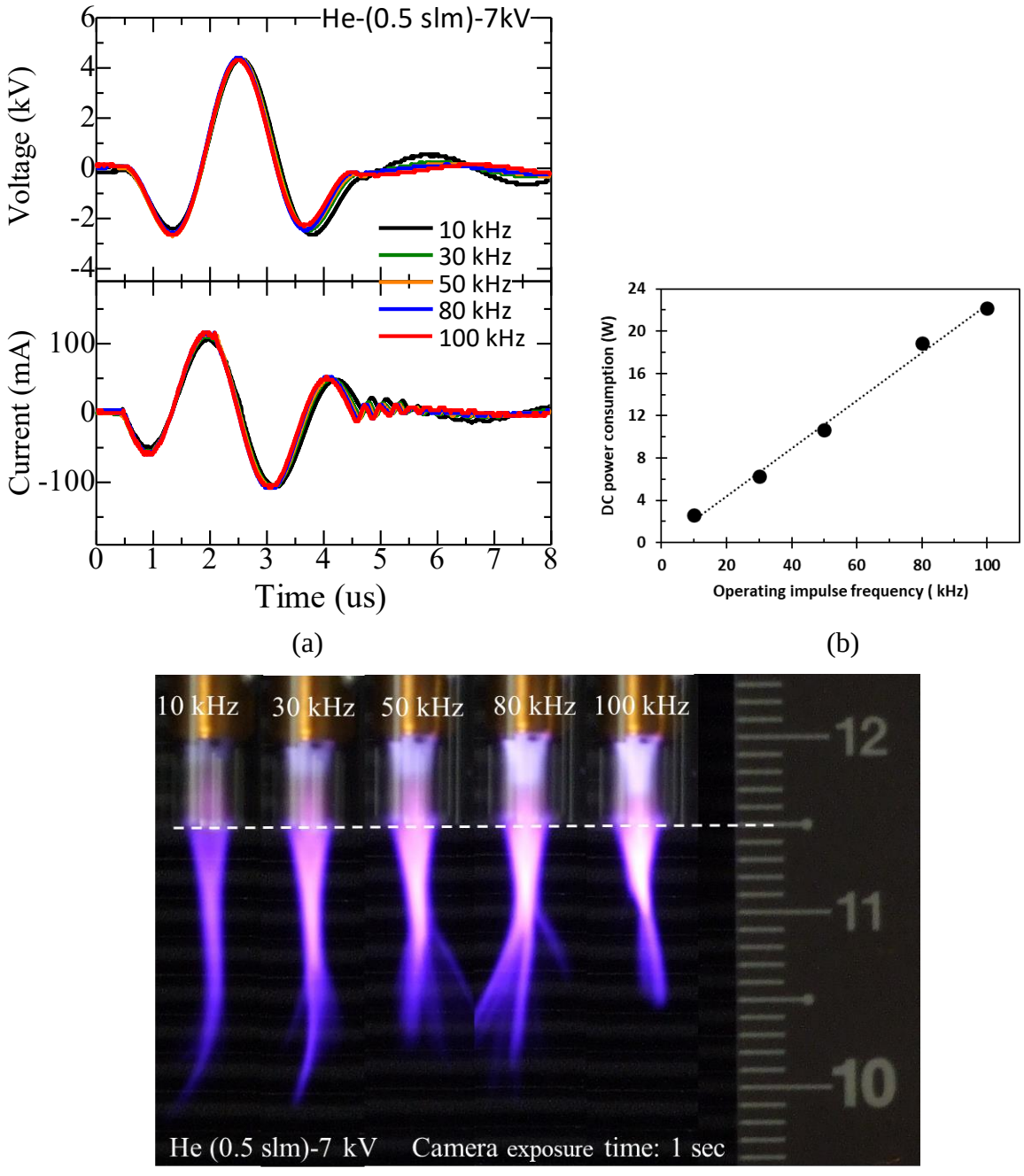

(a) (b)

(c)

Figure 8.6. Dependency of the impulse frequency on the characteristics of the strip-electrode type APPJ (a) Voltage and total current waveforms, (b) DC power consumption and (c) plasma jet photos.

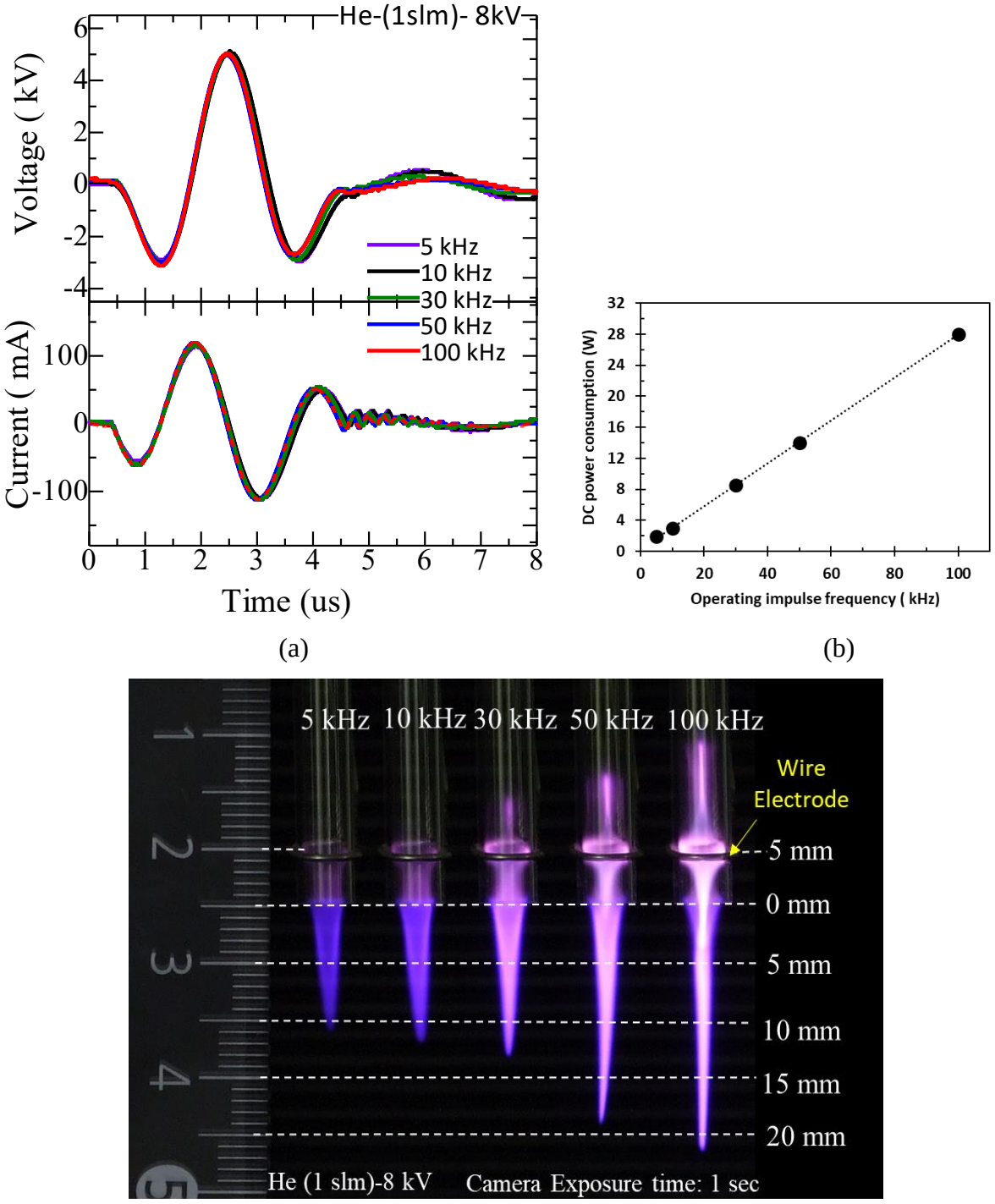

Figure 8.7. Dependency of the impulse frequency on the characteristics of the wire-electrode type APPJ (a) Voltage and total current waveforms, (b) DC power consumption and (c) plasma jet photos.

It is supposed that at increased frequencies the power is mostly consumed by the electrode capacitance rather than the jet discharge, which makes strong discharge confined on the electrode area and offers less contribution on the forming of plasma plume length. Moreover, strong turbulence on the plasma plume is observed. It is probable that due to strong interaction

between the air and He plasma, the turbulence occurs. So, to reduce these effects, two ways can be proposed. One is to increase the He gas flow rate and another one is to reduce the electrode area for decreasing electrode capacitance. Accordingly, a wire-electrode type APPJ with increased gas flow rate is introduced.

The effect of impulse frequency on the discharge characteristics of the wire-electrode type APPJ was investigated as shown in Figure 8.7. The operating frequency is varied from 5 to 100 kHz, where other experimental conditions are kept fixed. The other conditions are as He gas flow of 1 slm, applied voltage of 8 kV (peak to peak), and camera exposure time of 1 s. It can be seen that the total current and output voltages are almost steady with the frequency [Figure 8.7(a)], which indicates stable atmospheric-pressure plasma discharge. The turbulence along with the plasma jet reduces and plasma plume length increases with the increase of operating frequency. It is expected that the increase of frequency introduces more power to the plasma, and accordingly enhances the plasma plume length [Figure 8.7(b) and (c)].

8.4.2. Spectral characteristics

The optical emission spectral analysis is a popular tool to examine the plasma generated species and discharge parameters [13-15]. The optical emission spectroscopy (OES) measurement was performed along with the axial length (l) of the plasma plume at fixed three different points of 0 mm, 5 mm, and 10 mm, respectively [indicated in Figure 8.7(c)]. Figure 8.8. shows the optical emission spectral profile in the range of 250 to 850 nm at a voltage of 8 kV (peak-to-peak) with the variation of pulse operating frequency from 5 to 100 kHz and He gas flow rate of 1 slm for the wire-electrode type APPJ. The data acquisition time for the spectrometer is optimized to set as 4 s for 5 kHz, 2 s for 10 kHz, and 1 s for 30 to 100 kHz. It clearly shows that the active species such as NO, N_2, N_2^+, He, O and OH exits in the plasma plume. Moreover, their spectral intensities increase with the increase of pulse frequency and become mostly dominant at 100 kHz. The plasma plume profile at 100 kHz shows that the region, close to the nozzle at 0 mm has strong intensities of OH, N_2^+, He and O species. An atomic H-Balmer-α line is also observed. However, moving away from the nozzle along the plasma plume length at 5 mm, an immediate change in emission spectra is observed. The intensities of NO/N_2 species are increased, whereas OH, He and O species are reduced. Moving along with the plasma plume length at 10 mm, the intensities of all these species overall are reduced considerably except NO/N_2 species.

This results reveal that high frequency operation of plasma jet is preferable for generation of more reactive species as well as plasma plume profile analysis is suitable to know the concentration of different species along with the jet radial axis. It is expected that the developed wire-electrode type APPJ can be used for surface modification, sterilization, and biomedical

applications. However, in this work one of the biomedical applications is focused by the developed APPJ system that will be discussed in the later section.

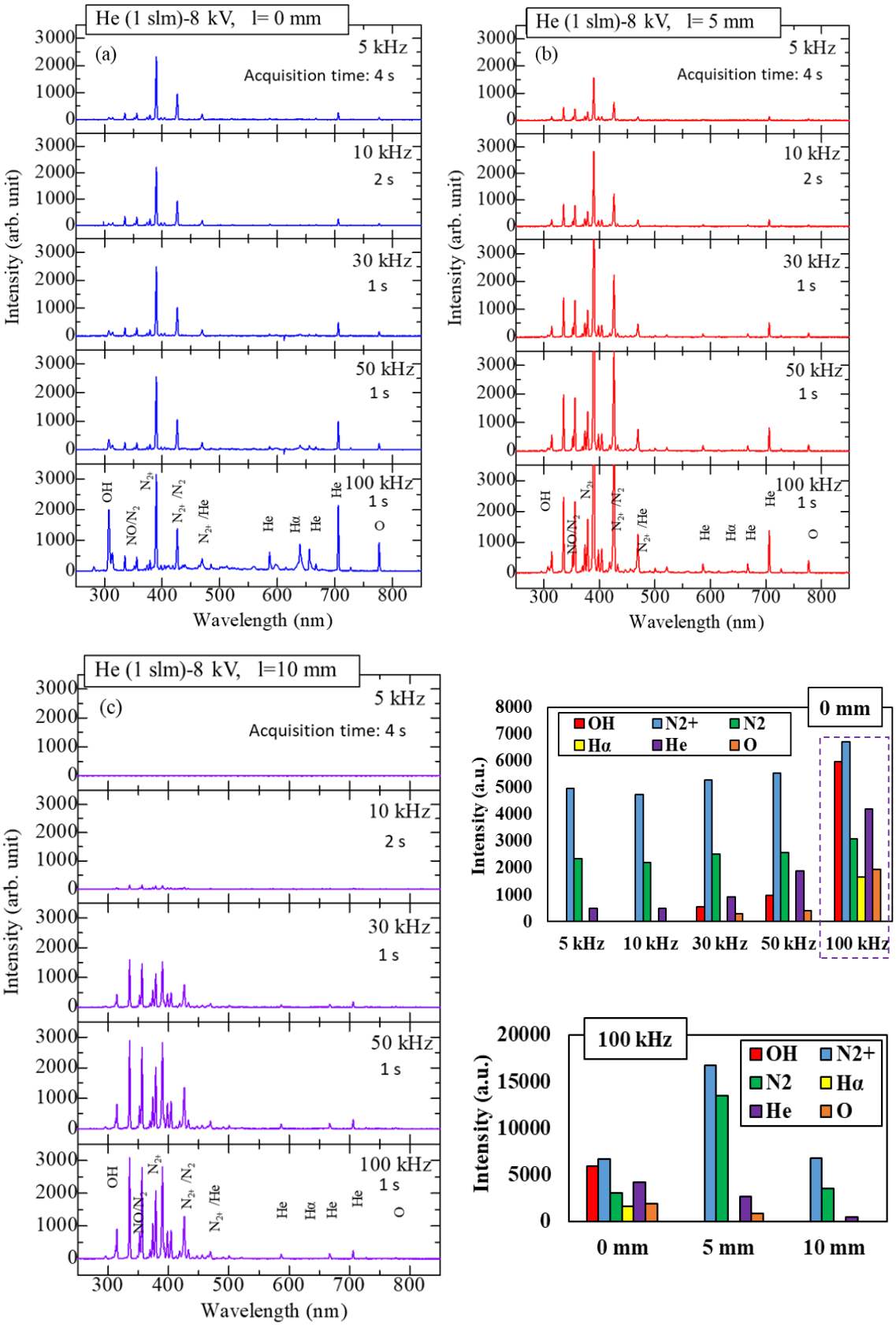

Figure 8.8. Optical emission spectral analysis of wire-electrode type APPJ.

8.4.3. Production of RONS in plasma-activated water (PAW)

Plasma-activated water (PAW) has been explored to be applied in medical applications [16]. PAW is also known as “water of death” owing to it has huge potential in killing bacteria [17, 18] and for cancer therapy [19-21]. In this procedure, water is simply treated by atmospheric-pressure plasma jet (APPJ). Hence, APPJ is supposed as a fourth cancer treatment method regarding the conventional methods such as surgery, anti-cancer drug and radiation therapy. In general, APPJ generated reactive oxygen and nitrogen species (RONS) are dominant for antibacterial activities [22] and effective for selective killing of cancer cells [20] illustrated in Figure 8.9.

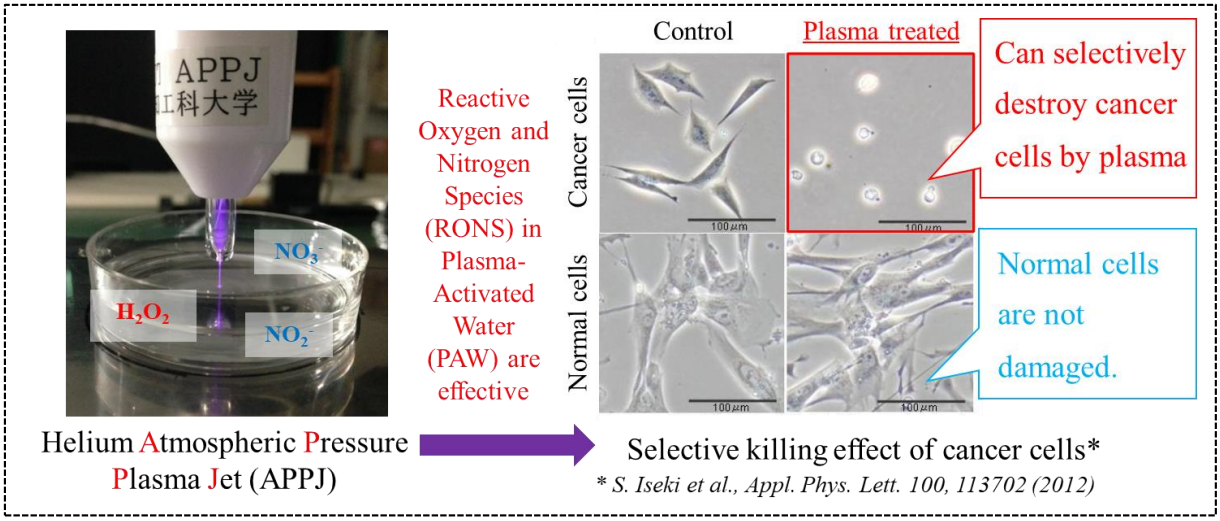

Figure 8.9. Selective killing effect of cancer cells by RONS in PAW.

At first, RONS produced by plasma–air interactions in the gas phase and afterward dissolve into the water. The major RONS in PAW that are deliberated for its antimicrobial acts are hydrogen peroxide (H_2O_2), nitrite (NO_2^-), and nitrate (NO_3^-) [23]. Basically, RONS are able to destroy the cancer cells by augmented oxidative stress [23] or DNA demolition [24]. Therefore, it is significant to control the production of RONS in PAW for achieving preferred effects in particular biological or medical applications.

Here, the concentrations of longer-lived RONS (H_2O_2, NO_2^-, and NO_3^-) and molecular oxygen (O2) in PAW have been investigated by the developed APPJ system. It is mostly focused on how pulse operating frequency influences these concentrations.

Figure 8.10 (a) shows the experiment setup of PAW employing the developed ring wire-electrode type APPJ and the dual resonance pulse transformer based impulse generator (DRPT-IG). He gas was fed into the tube with a constant gas flow rate of 1 slm via a mass flow controller. A high-voltage positive impulse of 8 kV (peak to peak) with pulse frequencies of 5-100 kHz was applied to the metallic wire-electrode. Quartz cuvettes (Hellma analytics) filled with deionized water (DIW) were employed under the APPJ for the treatment to produce PAW.

The treatment distance and time were kept fixed to 10 mm and 5 min, respectively. Figure 8.10 (b) shows the photographs of plasma treatment of DIW with a variation of frequency from 5 to 100 kHz. It is observed that the plasma jet intensity is enhanced with the increase of frequency that may contribute more production of RONS in PAW.

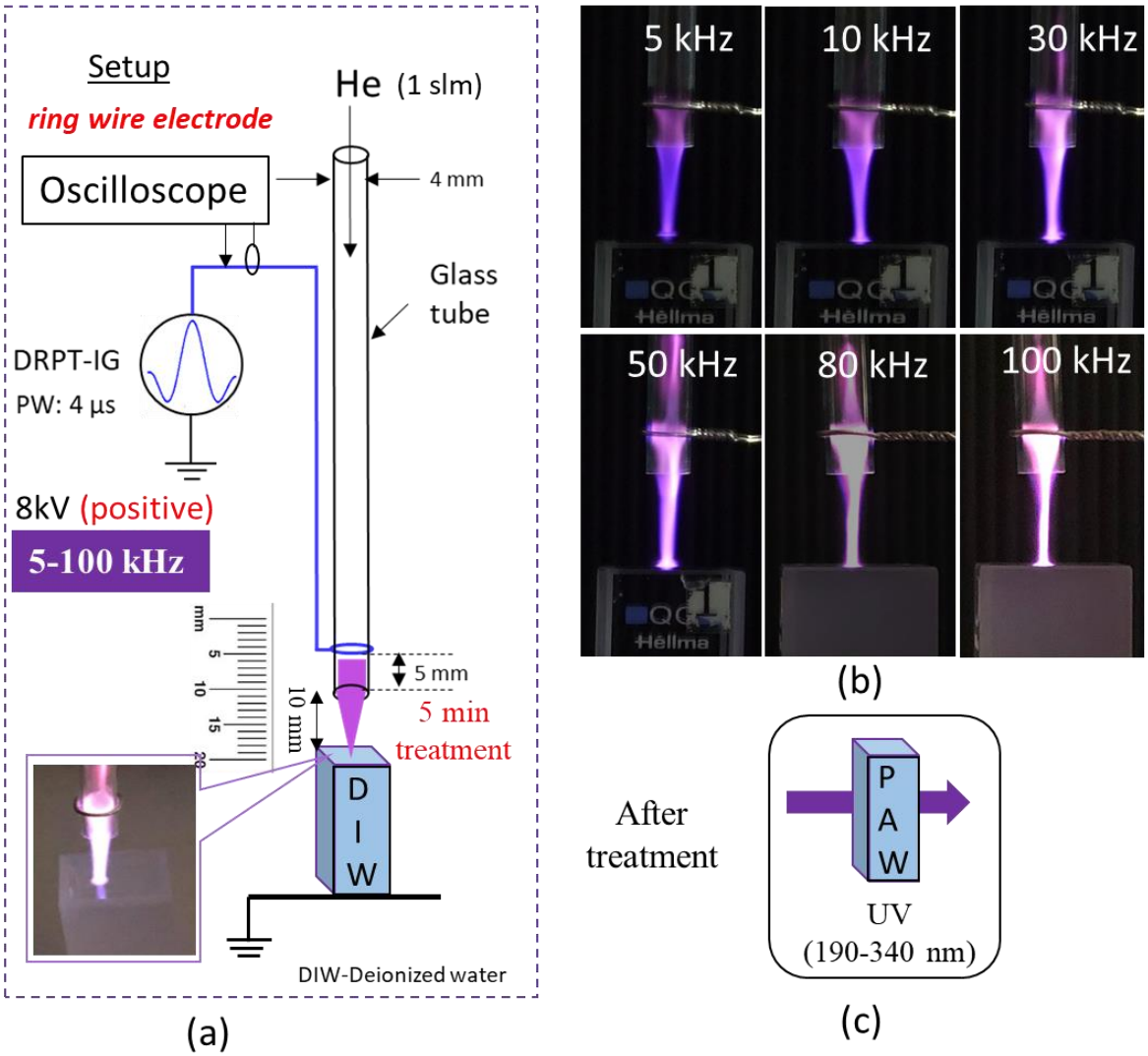

Figure 8.10. (a) Experimental setup of PAW, (b) photographs of plasma treatment of DIW at various frequencies, and (c) measurement of transmittance by UV absorption spectroscopy.

It is noticed that UV-visible spectroscopy is comparatively simple and effective method for the measurement of RON concentration in PAW [25]. A UV-visible spectrometer (Hitachi U-3900) was used for the measurement in the range of 190 nm to 340 nm [Figure 8.10(c)] with a spectral resolution of 0.2 nm and a scan speed of 120 nm/min. At first, empty quartz cuvettes were placed in both reference and sample chambers for baseline correction. Then the transmittances of DIW and PAW were measured in the sample chamber by keeping empty cuvette as reference. The UV absorbance spectrum was evaluated from the transmittance spectra of DIW and PAW as indicated in Figure 8.11.

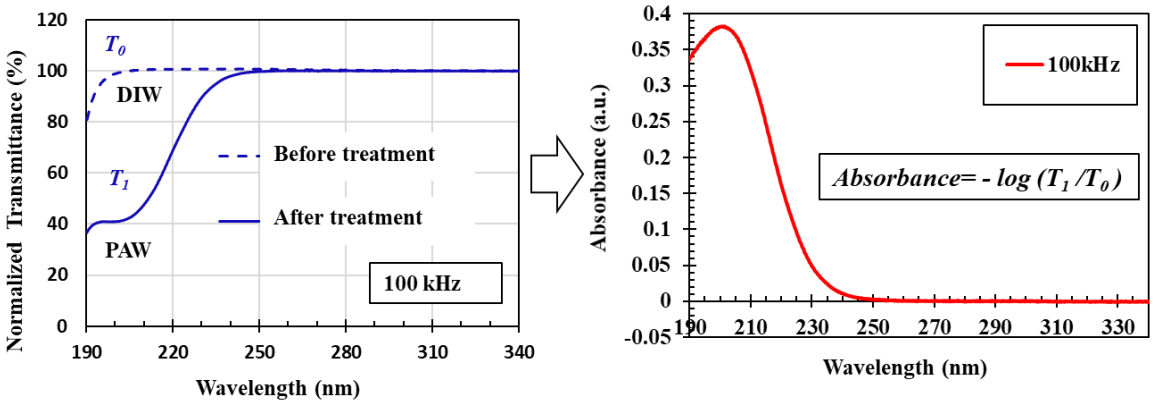

Figure 8.11. Method to evaluate the UV absorption spectrum of PAW

Figure 8.12 shows typical spectra of PAW prepared with the variation of pulse frequency from 5 to 100 kHz. As expected, the enhanced intensity of the absorption spectra was observed with the increasing of pulse operating frequency. Moreover, the absorption profiles were appeared to similar but not identical. This indicates that not only the concentration of RONS and O_2 have been changed with operating frequency but also the composition of RONS in PAW. Therefore, it necessary to quantify the concentrations of different RONS and O_2 in PAW. This was performed by a curve fitting routine of UV absorption spectrum as suggested by J.-S. Oh et al. [25]. The curve fitting of a typical UV absorption spectrum of 100 kHz is shown in Figure 8.13. It shows a linear relationship between UV absorption peak intensity and different RONS concentrations such as H_2O_2, NO_2^-, and NO_3^- as well as dissolved O_2 in PAW.

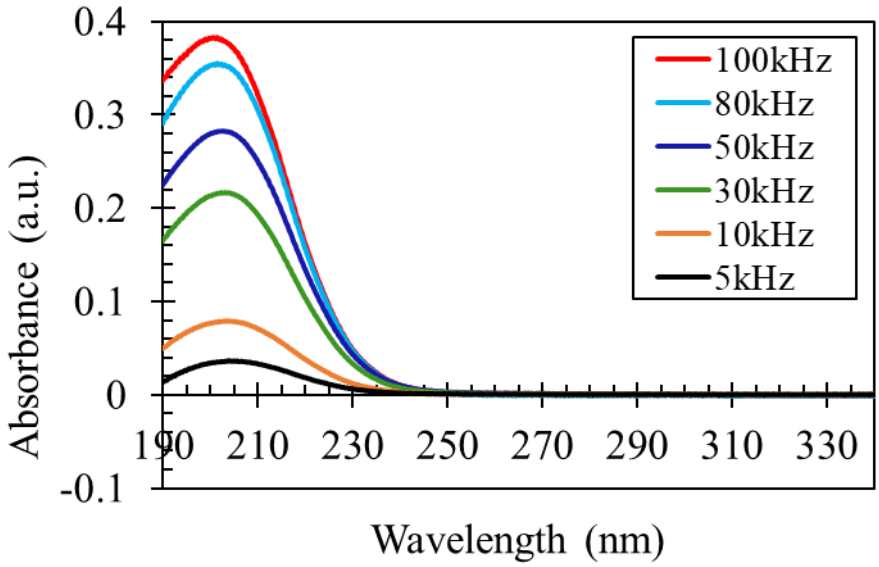

Figure 8.12. UV absorption spectra of PAW with the variation of pulse operating frequency.

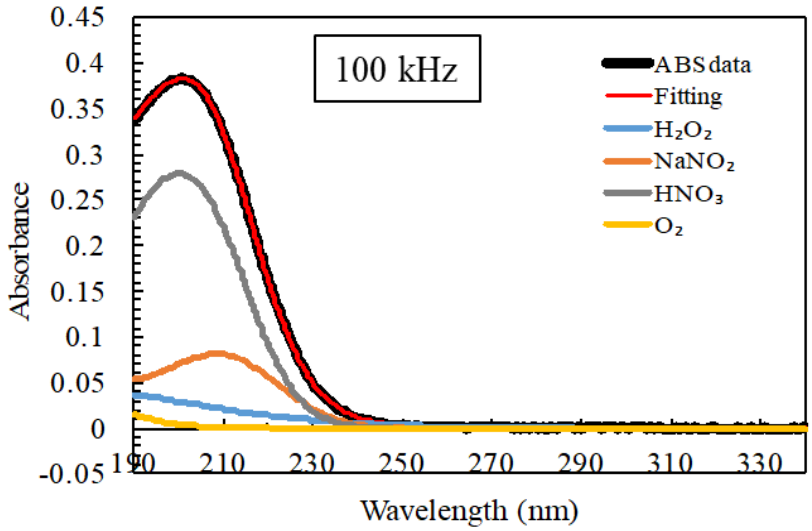

Figure 8.13. Fitting of a typical UV absorption spectrum.

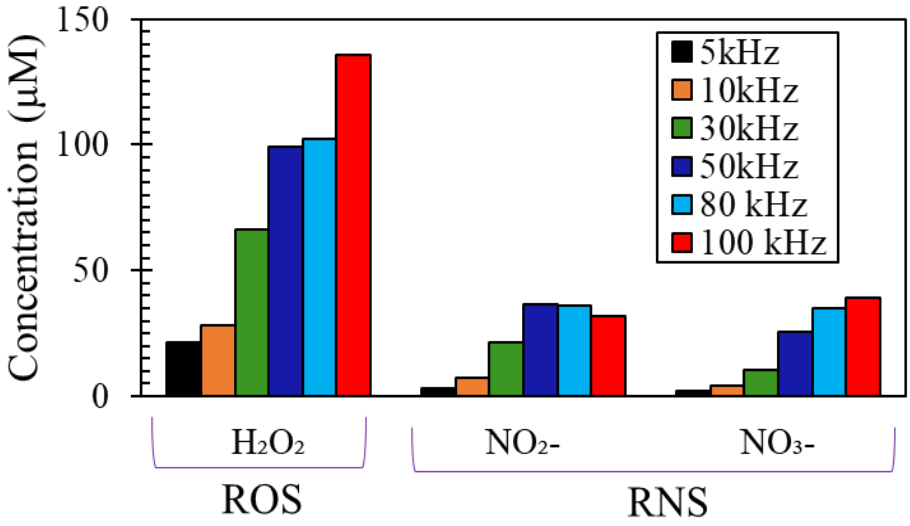

Figure 8.14. Evaluated absolute concentration of the RONS in PAW with the variation of pulse operating frequency. H_2O_2 is denoted as reactive oxygen species (ROS), whereas NO_2- and NO_3- are together denoted as reactive nitrogen species (RNS).

The absolute concentration of the plasma-generated RONS (H_2O_2, NO_2^-, and NO_3^-) and O_2 in PAW was evaluated employing the outcomes from curve-fitting procedure. Figure 8.14 presents the evaluated absolute concentration of the RONS in PAW as a function of pulse operating frequency. It revealed that the concentration of RONS increased linearly with increasing of frequency. The concentration of ROS (H_2O_2) was always higher than the concentration of RNS (NO_2^- and NO_3^-). However, a decrease concentration of NO_2^- was noticed after 50 kHz. It can be defined that the concentration of H_2O_2 becomes high at higher frequencies, which can facilitate the generation of more NO_3- via the consumption of NO_2- according to the following equation [26].

$$NO_2^- + H_2O_2 + H^+ \rightarrow NO_3^- + H_2O + H^+$$

Moreover, the dissolved O_2 concentration in PAW was found increasing as a function of pulse operating frequency shown in Figure 8.15. It is expected that higher concentrations of RONS at increased frequencies increase the generation of O_2 by-products from the chemical reactions of RONS during the treatment of DIW. However, the negative concentration indicates that generally O_2 concentration in PAW becomes lower than the initial concentration of O_2 in DIW due to the effect of He gas purge. Higher concentrations of dissolved O_2 in PAW are supposed to be advantageous for normal living cells during cancer treatment.

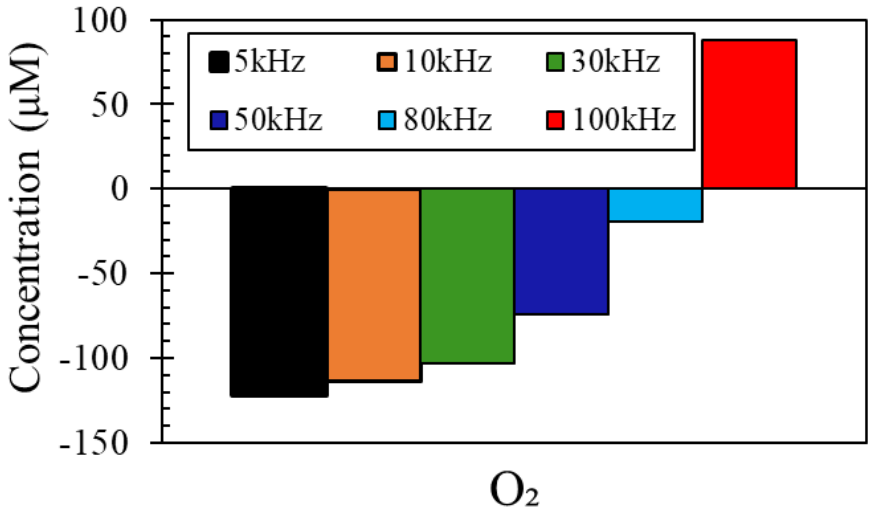

Figure 8.15. Evaluated concentration of dissolved O_2 in PAW with the variation of frequency.

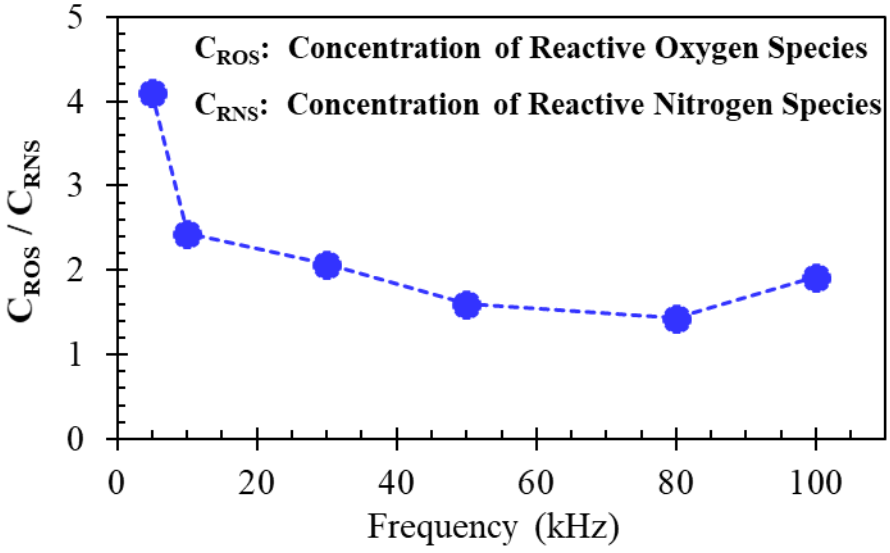

Figure 8.16. The concentration ratio of ROS and RNS with the variation of frequency.

Figure 8.16. shows the concentration ratio of ROS and RNS in PAW as a function of pulse operating frequency. The result reveals that the variation of pulse operating frequency during treatment influences not only the RONS (H_2O_2, NO_3-, and NO_2-) concentrations but also the concentration ratio of these ROS and RNS. Therefore, the concentration of RONS and its ratio

in PAW can be controlled by simply varying the pulse operating frequency of APPJ during treatment of DIW.

For further analysis of RONS production processes in PAW, it is important to know the about the plasma-liquid interactions. A probable model of bulk plasma interaction with bulk liquid (water) can be demonstrated in Figure 8.17 based on the reasonable assumptions that are known from the literatures [27-28]. It is sure that the plasma–liquid chemistry is a complex process, mostly at the plasma–liquid interface where many highly reactive RONS are generated including the hydroxyl radical (OH), hydro-nitro-oxide radicals (HNO_2, HNO_3), super-hydro-oxide radicals (H, O), ozone (O_3), and so on. Actually, when the plasma comes in contact with the liquid surface (water), it will enhance the generation of RONS, including aqueous OH and H_2O_2. Then these RONS are dissolved into the bulk liquid through diffusion and solvation processes. Moreover, recombination of OH radicals can also lead to further formation of H_2O_2. The initial liquid chemistry generated by plasma treatment may strongly affect the longer-term chemistry and antimicrobial property of PAW.

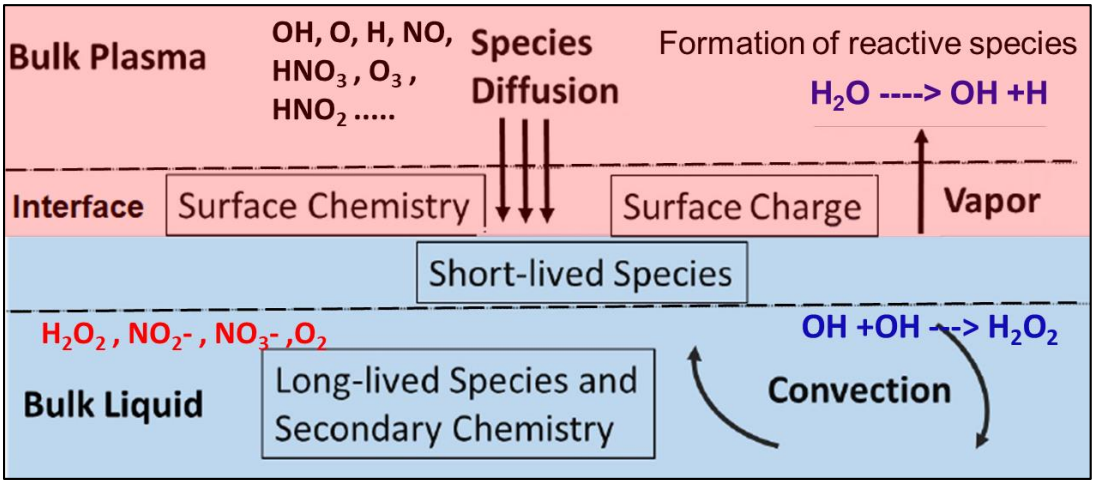

Figure 8.17. A probable model of bulk plasma interaction with bulk liquid (water).

It can be noted that water vapor from the surface of the bulk liquid plays a great role in formation of reactive species. When the water vapor interacts with the plasma, hydrolysis reactions are occurred by the reaction of water molecules with some other molecules or ions existed into the plasma as demonstrated in the model.

The Schlieren images in Figure 8.17 shows that the rate of water evaporation is higher at higher frequency (50 kHz) compared to lower frequency (5 kHz), creating a more humid environment. Therefore, it can be stated that as the pulse operating frequency increases, the interaction of plasma with water enhances, which may lead to produce higher concentration of RONS in PAW.

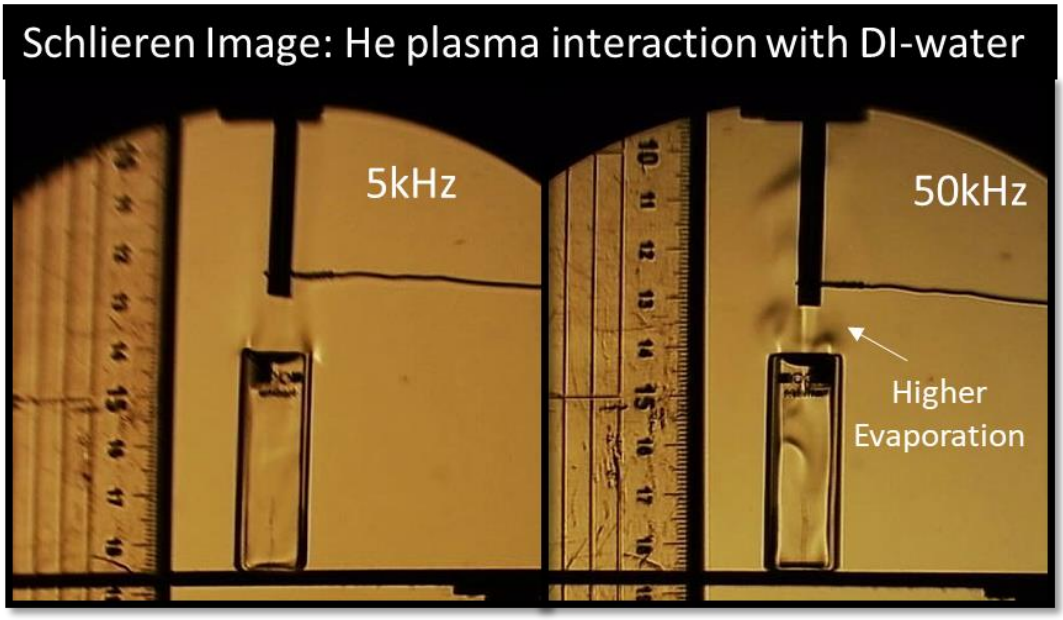

Figure 8.18. Schlieren image of He plasma jet interaction with DIW.

8.4.4. Typical observations - *APPJ operated by positive and negative pulses*

Owing to observe the pulse polarity-induced effects on plasma discharge characteristics, emission spectra, and RONS production in PAW, the developed APPJ system was driven by positive and negative pulses. The experimental conditions were as follows- pulse voltage: 8 kV (peak-peak) with positive and negative polarity, frequency: 50 kHz, gas: He, flow rate: 1 slm, treatment distance: 10 mm, and time: 5 min. Some typical observations are presented here.

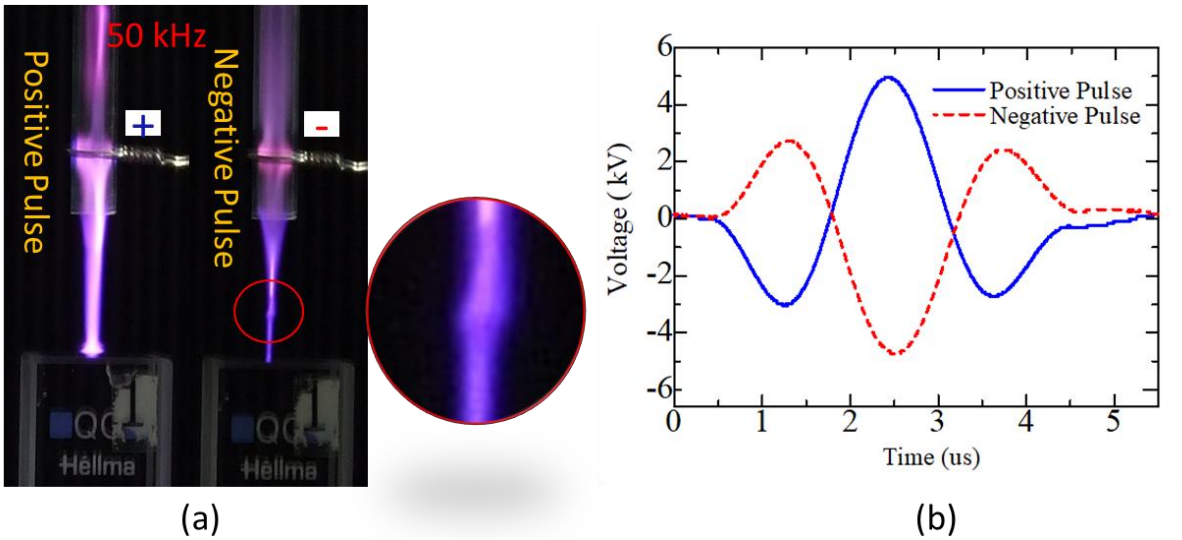

Figure 8.19. (a) Photographs of plasma jet-water medium interaction and (b) voltage waveforms under positive and negative pulse.

Figure 8.19(a) and (b) shows the images of plasma jet-water medium interaction and voltage waveforms of positive and negative pulse, respectively. It can be clearly seen that the plasma jet driven by negative pulse exhibits substantially different characteristics compared to

positive pulse operation. The width of plasma jet and propagation length at negative polarity are smaller than those at positive polarity. Moreover, positive pulse operated plasma jet shows the cylindrical shape and intense appearance, whereas negative pulse operated plasma jet displays conical and less intense. A circle-like plasma distribution is also observed in case negative pulse driven APPJ. At this point, however, there is no direct evidence of occurring these behaviors but can be made reasonable assumptions on the basis of literature.

Accordingly, the behaviors of APPJ driven by positive and negative pulses were studied as reported in some previous works [29-32], though electrode and tube configurations and temporal forms of applied voltage in these works were quite different. Based on the assessment of these previous works as well as current results from this work, a probable model of APPJ discharge characteristics by positive and negative pulse can be demonstrated according to the Figure 8.20 (a) and (b), respectively.

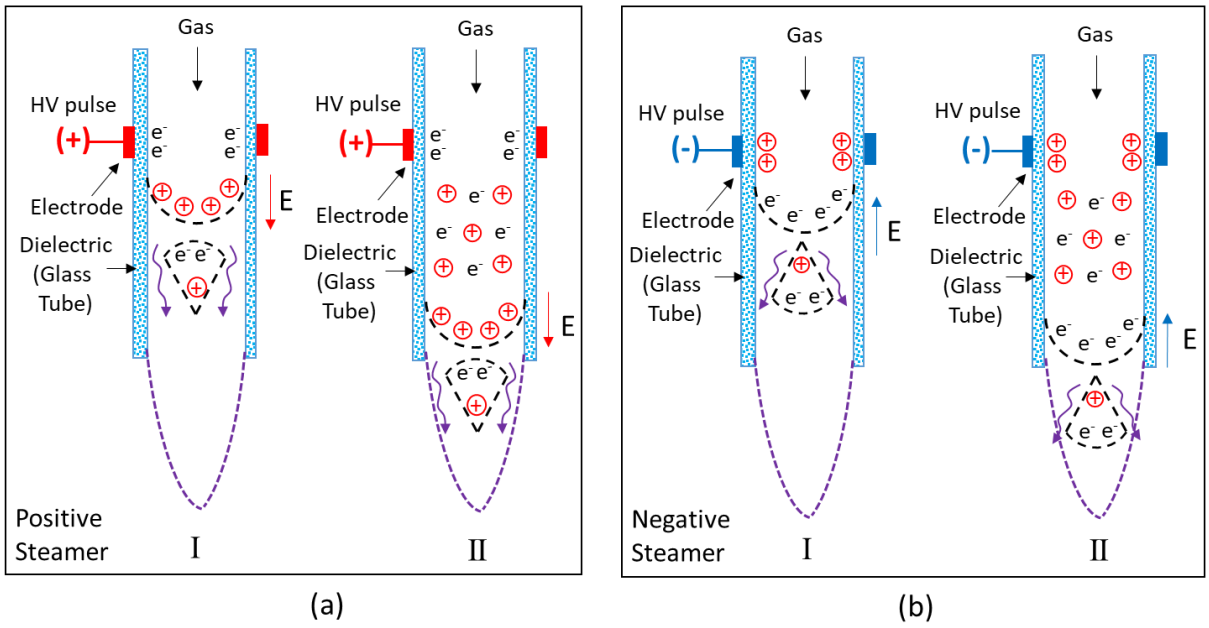

Figure 8.20. Probable model of APPJ discharge characteristics by (a) positive pulse and (b) negative pulse. I and II denote initial and propagation phase of the steamers, respectively.

In case of positive pulse, a positive streamer is generally formed close to the electrode at initial stage denoted as I in Figure 8.20 (a). High energy photons from the initial avalanche or the streamer-head deliver seed electrons for secondary avalanches, which build space-charge electric field (E). Then, these secondary avalanches are drawn into the positive streamer head, neutralize it, form a quasi-neutral streamer channel, and leave behind a new positive space charge. In consequence of this repetitive process, the streamer propagates towards the space as like of a positive-guided ionization wave accelerated by the space-charge electric field denoted as II in Figure 8.20 (a).

In contrast, a negative streamer is usually formed close to the electrode when a negative pulse is applied across it, indicated as I in Figure 8.20 (b). The propagation process is slightly different than that of positive steamer, marked as II in Figure 8.20 (b). Secondary avalanches are again originated by photoionization due to high energy photons from the primary avalanche which also build space-charge electric field (E) but in opposite direction of propagation. The streamer propagation takes place as the neutralization of the positive tails of secondary avalanches by the negative- charged streamer head.

Therefore, it can be revealed that due to heavier ions compared to electrons take place in the plasma steamer or bullet head in case of positive pulse, they can be easily accumulated in space and build an enhanced electric field increasing the propagation speed of the plasma bullet and enhancing the discharges. Besides, in case of negative pulse operated plasma jet, the light electrons in plasma steamer/ bullet head are scattered in space, recombined with positive ions and introduced weaker electric field. It can be assumed that the dissimilarity of polarity-induced effects for APPJ are related mainly with the conditions of ionization wave formation and propagation. On the basis of literature reviews [29-32] and experimental results in this work, a comparative study of pulse polarity-induced properties for APPJ can be summarized in Table 8.1.

Table 8.1. Pulse polarity-induced properties for APPJ

Property	Positive Pulse	Negative pulse
Electric Field	Stronger	Weaker
Electron temperature	Higher	Lower
Electron density	Higher	Lower
Propagation speed	Higher	Lower
Ionization Rate	Enhanced	Reduced
Recombination rate	Smaller	Larger
Ionization profile	Focused	Lower
Pre-ionization effect	Major	Minor
Jet length	Longer	Shorter
Positive ions	Enhanced	Reduced
Negative ions	Reduced	Enhanced
Plasma bullet	Discrete	Continuous

Furthermore, as the plasma jet operated at positive and negative pulse performs different discharge characteristics, the effects of pulse polarity on the optical emission as well as on RONS production in PAW were investigated by positive and negative pulse while keeping other experimental conditions are same. Figure 8.21 shows the typical emission spectra of the positive and negative pulse driven APPJ. Major emission spectral lines from OH, N_2, N_2^+, He and O were observed in both polarities. However, in case of positive pulse, the relative intensity of

N_2+, He are much higher and N_2, O are lower than that of negative pulse. This result indicates that a higher number of positive excited species exists in plasma when driven by positive pulse, which is also correlated with the discharge model demonstrate above. Generally, the second positive band system (SPS) of N_2 around 337 nm can be excited by direct electron-impact excitation, whereas the first negative band system (FNS) of N_2+ is mainly occurred though the inelastic-collision reaction between electrons and nitrogen, and the penning ionization between metastable He and N_2 according to the equation as inset in Figure 8.21. Thus Penning ionization can play an important role in the generation of denser plasma in case of positive pulse operated APPJ.

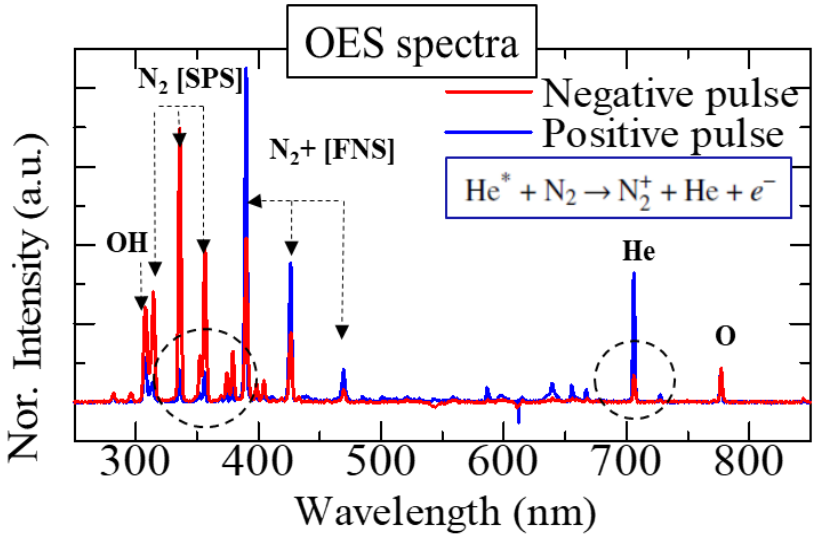

Figure 8.21. Optical emission spectra taken near the nozzle end of APPJ operated by positive and negative pulse of 8 kV at 50 kHz. The spectra were acquired at different exposure time in both polarities and were then normalized for comparison.

It can be stated that emission of these major spectra lines have similarly but different in intensities when the plasma jets are driven under positive and negative pulse. This may indicate that these plasma jets have similar ability to generate RONS in PAW even changing the pulse voltage polarity, but different in concentrations of RONS.

Figure 8.22. shows the concentrations of RONS in PAW by the plasma jets operated under positive and negative pulse. It shows that positive pulse driven plasma jet can produce a higher concentration of RONS in PAW compared to negative pulse driven plasma jet, while other experiment conditions are kept identical. Actually, the ionization rate in APPJ is mostly influenced by the induced electric field. In case of positive pulse operated plasma jet, the enhanced electric field leads to a higher speed of ionization rate, generates a higher density of excited species in plasma, accordingly a higher concentration of RONS is produced in PAW. In contrast, the negative pulse driven plasma jet introduces reduced electric field in localized

region, which leads a lower concentration of excited species in plasma as well as a lower concentration of RONS in PAW. Moreover, a variation of concentration ratio in ROS to RNS is also observed due to change of pulse polarity as indicated in inset of Figure 8.22.

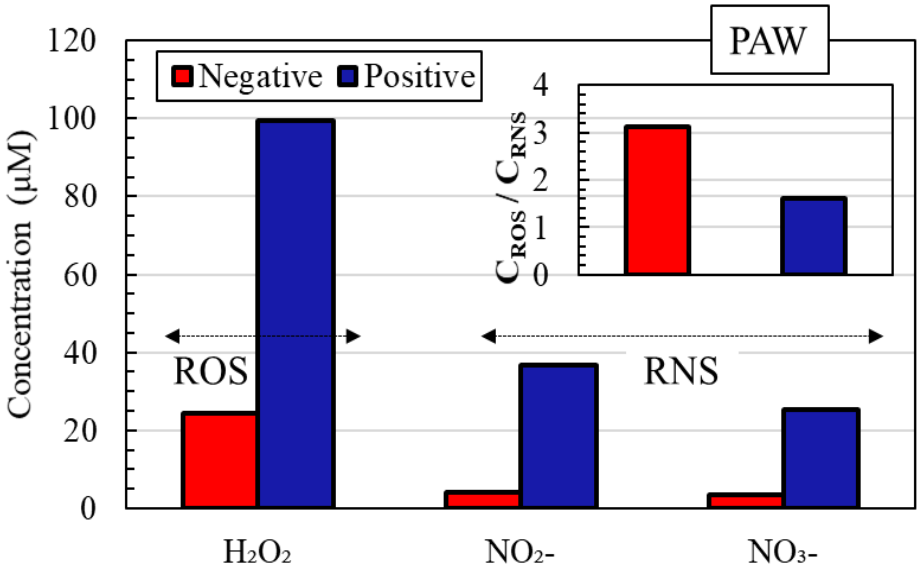

Figure 8.22. The concentrations of RONS in PAW by the plasma jets operated under positive and negative pulse. The operation conditions were as voltage amplitude of 8 kV (peak-peak), pulse frequency of 50 kHz, treatment time of 5 min, and treatment distance of 10 mm respectively.

However, the control of chemical reactions and the production of RONS by plasma jet are complex processes. As plasma introduces a variety of species in the aqueous phase, it is difficult to find out the role of a single species or to adjust single species. Therefore, further studies of the developed pulsed-APPJ system are still required to understand and control the discharge characteristics for the production of RONS in aqueous phase by changing discharge parameters such as working gas, gas flow rate, voltage amplitude, treatment time, treatment distance, and so on.

8.5. Conclusion

Atmospheric-pressure plasma jets designed as cylindrical configuration of DBD were investigated by means of electrical and optical characteristics using the developed DRPT-IG and He as working gas. Two types of single-electrode configurations such as strip-electrode and wire-electrode are employed for the generation of plasma jet with various experimental conditions. A strong influence of wire-electrode configuration on plasma jet were observed with the variation of frequency at a fixed voltage and gas flow rate. The analysis of OES for wire-electrode APPJ shows that the active species such as NO, N_2, N_2^+, He, O and OH exits in the plasma plume and their intensities increase with the increase of pulse operating frequency. Furthermore, the investigation of plasma jet characteristics and RONS production in PAW with

the variation of pulse operating frequency and polarity were also carried out. The results reveal that these both parameters have significant impact on the plasma jet characteristics and the production of RONS. A higher frequency operation of pulse enhances plasma jet density as well as the plasma-water interaction, which introduces to produce higher concentration of RONS and O_2 in PAW. The variation of pulse frequency also varies the concentration ratio of ROS and RNS. On the other hand, the positive pulse operated plasma jet shows the cylindrical shape and intense appearance, whereas negative pulse operated plasma jet displays conical and less intense. In addition, the plasma jet driven under positive pulse introduces higher electric field, leads to a higher speed of ionization rate, generates a higher density of excited species in plasma, accordingly a higher concentration of RONS production in PAW than that of negative pulse. Therefore, in the future, the developed pulsed-APPJ system can offer an effective and low cost method to control of RONS composition for specific biomedical applications.

References

[1] A. Schutze, J.Y. Jeong, S.E. Babayan, J. Park, G.S. Selwyn, R.F. Hicks, "The Atmospheric-Pressure Plasma Jet: A Review and Comparison to Other Plasma Sources", *IEEE Trans. Plasma Sci.* 26, 1685, (1998).

[2] M. Laroussi, T. Akan, "Arc-Free Atmospheric Pressure Cold Plasma Jets: A Review", *Plasma Process Polym.* 4, 777-788, (2007).

[3] C. Tendero et al. "Atmospheric pressure plasmas: A review", *Spectrochimica Acta Part B*, 61, 2-30, (2006).

[4] L. Chen, Y. Wei, X. Zuo, J. Cong, and Y. Meng, "The atmospheric pressure air plasma jet with a simple dielectric barrier," *Thin Solid Films*, 521, 226–228, (2012).

[5] N. Jiang, A. Ji, and Z. Cao, "Formation Mechanism of Atmospheric Pressure Plasma Jet," *Arxiv:0811.0130v1*, 1-4, (2008).

[6] M. T. Benabbas, S. Sahli, A. Benhamouda, and S. Rebiai, "Effects of the electrical excitation signal parameters on the geometry of an argon-based non-thermal atmospheric pressure plasma jet," *Nanoscale Res. Lett.*, 9,1–5, (2014).

[7] D. Maletić, N. Puač, G. Malović, A. Đorđević, and Z. L. Petrović, "The influence of electrode configuration on light emission profiles and electrical characteristics of an atmospheric-pressure plasma jet," *J. Phys. D. Appl. Phys.*, 50(14), 145202, (2017).

[8] N. Jiang, A. Ji, and Z. Cao, "Atmospheric pressure plasma jet: Effect of electrode configuration, discharge behavior, and its formation mechanism," *J. Appl. Phys.*, 106, 013308, 2009.

[9] X. Lu, Z. Jiang, Q. Xiong, Z. Tang, and Y. Pan, "A single electrode room temperature plasma jet device for biomedical applications," *Appl. Phys. Lett.* 92(15), 151504 (2008).

[10] C. Zhang, T. Shao, R. Wang, Z. Zhou, Y. Zhou, and P. Yan, "A comparison between characteristics of atmospheric-pressure plasma jets sustained by nanosecond- and microsecond-pulse generators in helium", *Phys. Plasmas*, 21, 103505, (2014).

[11] U.N. Pal, A.K. Sharma, J.S. Soni, K.R. Sonu, H. Khatun, M. Kumar, B.L. Meena, M.S. Tyagi, B.J. Lee, M. Iberler, J. Jacoby, K. Frank, "Electrical modelling approach for discharge analysis of a coaxial DBD tube filled with argon", *J. Phys. D Appl. Phys.*, 42, 045213, (2009).

[12] R. Zhang, R.J. Zhan, X.H. Wen, L. Wang, "Investigation of the characteristics of atmospheric pressure surface barrier discharges", *Plasma Sources Sci. Technol*.,12, 590, (2003).

[13] A. Yanguas-Gil, K. Focke, J. Benedikt, and A. von Keudell, "Optical and electrical characterization of an atmospheric pressure microplasma jet for Ar/CH4 and Ar/C2H2 mixtures" *J. Appl. Phys.* 101, 103307 (2007).

[14] L. Dong, J. Ran, and Z. Mao, "Direct measurement of electron density in microdischarge at atmospheric pressure by Stark broadening", *Appl. Phys. Lett.*, 86, 161501 (2005).

[15] Q. Wang, I. Koleva, V. M. Donnelly, and D. J. Economou, "Spatially resolved diagnostics of an atmospheric pressure direct current helium microplasma", *J. Phys. D. Appl. Phys.* 38, 1690 (2005).

[16] T. Tasaki, T. Ohshima, E. Usui, S. Ikawa, K. Kitano, N. Maeda, and Y.Momoi, " Plasma-treated water eliminates *Streptococcus mutans* in infected dentin model", *Dent. Mater. J.* 36, 422 (2017).

[17] J. Julák, V. Scholtz, S. Kotúčová, and O. Janoušková, "The persistent microbicidal effect in water exposed to the corona discharge", *Phys. Med.* 28, 230 (2012).

[18] M. Naïtali, G. Kamgang-Youbi, J.-M. Herry, M.-N. Bellon-Fontaine, and J.-L. Brisset, "Combined Effects of Long-Living Chemical Species during Microbial Inactivation Using Atmospheric Plasma-Treated Water", Appl. Environ. Microbiol. 76, 7662 (2010).

[19] H. Tanaka, M. Mizuno, K. Ishikawa, K. Nakamura, H. Kajiyama, H. Kano, F. Kikkawa, and M. Hori, "Plasma-Activated Medium Selectively Kills Glioblastoma Brain Tumor Cells by Down-Regulating a Survival Signaling Molecule, AKT Kinase" *Plasma Med.* 1, 265 (2011).

[20] S. Iseki, K. Nakamura, M. Hayashi, H. Tanaka, H. Kondo, H. Kajiyama, H. Kano, F. Kikkawa, and M. Hori, "Selective killing of ovarian cancer cells through induction of apoptosis by nonequilibrium atmospheric pressure plasma" *Appl. Phys. Lett.* 100, 113702 (2012).

[21] F. Utsumi, H. Kajiyama, K. Nakamura, H. Tanaka, M. Mizuno, K. Ishikawa, H. Kondo, H. Kano, M. Hori, and F. Kikkawa, "Effect of Indirect Nonequilibrium Atmospheric Pressure Plasma on Anti-Proliferative Activity against Chronic Chemo-Resistant Ovarian Cancer Cells *In Vitro* and *In Vivo*" *PLOS ONE* 8, e81576 (2013).

[22] D. B. Graves, "The emerging role of reactive oxygen and nitrogen species in redox biology and some implications for plasma applications to medicine and biology" *J. Phys. D* 45, 263001 (2012).

[23] K. Oehmigen, M. Hähnel, R. Brandenburg, Ch. Wilke, K.-D. Weltmann, and Th. von Woedtke, "The Role of Acidification for Antimicrobial Activity of Atmospheric Pressure Plasma in Liquids" *Plasma Processes Polym.* 7, 250 (2010).

[24] E. J. Szili, N. Gaur, S.-H. Hong, H. Kurita, J.-S. Oh, M. Ito, A. Mizuno, A. Hatta, A. J. Cowin, D. B. Graves, and R. D. Short, "The assessment of cold atmospheric plasma treatment of DNA in synthetic models of tissue fluid, tissue and cells", *J. Phys. D* 50, 274001(2017).

[25] J.-S. Oh, E. J. Szili, K. Ogawa, R. D. Short, M. Ito, H. Furuta, and A. Hatta, "UV–vis spectroscopy study of plasma-activated water: Dependence of the chemical composition on plasma exposure time and treatment distance," *Jpn. J. Appl. Phys.* 57, 0102B9 (2018).

[26] P. Lukes, E. Dolezalova, I. Sisrova, and M. Clupek, "Aqueous-phase chemistry and bactericidal effects from an air discharge plasma in contact with water: evidence for the formation of peroxynitrite through a pseudo-second-order post-discharge reaction of H_2O_2 and HNO_2", *Plasma Sources Sci. Technol.* 23, 015019 (2014).

[27] P. J. Bruggeman et al., "Plasma–liquid interactions: a review and roadmap", *Plasma Sources Sci. Technol.* 25, 053002 (2016).

[28] I. Adamovich et al., "The 2017 Plasma Roadmap: Low temperature plasma science and technology", *J. Phys. D: Appl. Phys.* 50, 323001 *(*2017).

[29] G. V. Naidis "Simulation of streamers propagating along helium jets in ambient air: Polarity-induced effects" *Appl. Phys. Lett.* 98, 141501 (2011).

[30] R. Talviste, "Atmospheric-pressure He plasma jet: effect of dielectric tube diameter", *Doctoral dissertation*, chap. 2, pp.15-17, 2016. (Retrieved from: https://dspace.ut.ee/bitstream/handle/10062/53497/talviste_rasmus.pdf?sequence=1&isAllowed=y).

[31] R. Wang, K. Zhang K, Y. Shen, C. Zhang, W. Zhu, T. Shao, "Effect of pulse polarity on the temporal and spatial emission of an atmospheric pressure helium plasma jet", *Plasma Sources Sci. Technol.* 25, 053002 (2016).

[32] Z. Liu at el. "Effects of the Pulse Polarity on Helium Plasma Jets: Discharge Characteristics, Key Reactive Species, and Inactivation of Myeloma Cell" *Plasma Chemistry and Plasma Processing* 38, 953 (2018).

Chapter 9

Summary

This chapter summarizes the main achievements drawn from the research and discusses future research recommendations, which could open new dimensions in the research of pulsed plasma discharge applications.

The main purpose of this study is to investigate the pulsed plasma discharge for low-pressure CVD of carbon thin films and atmospheric-pressure plasma jet (APPJ). A systematic analysis of the design of pulsed power generators are shown to develop an efficient pulsed plasma discharge method in both low-pressure and atmospheric-pressure.

In the first part of research, low-pressure pulse plasma discharge for the synthesis of carbon thin films was investigated. First of all, a pulsed DC plasma discharge technique including simply configured pulse power supply and chemical vapor deposition (CVD) apparatus was successfully developed. Deposition of diamond-like carbon (DLC) films were performed on silicon (Si) wafers by employing the pulsed DC plasma CVD system from acetylene (C_2H_2) and carbon mono-oxide (CO) source gas. A large number of graphite-like structures, oxygen content, C=O bond, and C≡C bond were observed in the film deposited from CO gas. DLC films from CO also exhibited low deposition rate and appeared as a soft graphitic conducting DLC. Besides, DLC films from C_2H_2 showed higher deposition rate and looked as mostly conventional hydrogenated amorphous carbon with insulating properties. Raman analyses suggested an enhanced graphitization of the DLC films at an increased temperature. The obtained results reveal that the developed pulsed DC plasma CVD system is useful for the deposition DLC films with wide variation of deposition conditions for alternative of conventional RF CVD.

To enhance the pulsed plasma discharge processes, a novel model for a pulsed DC generator (PDG) was designed and constructed using an LC half-resonant converter and a constant current controller with high-frequency solid-state switching to deliver high-voltage pulses for capacitive coupled plasma discharge in a vacuum chamber. Pulsed DC plasma discharge was operated using the prototype PDG for the monitoring of voltage and current waveforms, and evaluation of power conversion efficiency. In the order of microseconds, the voltage waveform was nearly rectangular and the current level was stable at the set value during the pulse on state. The generator can deliver maximum negative pulses of 1000 V with rise time less than 500 ns and fall time less than 800 ns, respectively. The controllable pulse duration is 1μs – ∞, and operating frequency range is 0 (DC) – 500 kHz. By recovering charge and energy from the capacitive load to the storage capacitor in the PDG, conversion efficiency from the

high-voltage (HV) DC input to the pulsed DC output at a repetition rate of 30 kHz was considerably improved approximately 12.2%, as expected from the design. The PDG can produce stable and uniform plasma suitable for material processing in a wide range of discharge conditions. It is our belief that this study will stimulate the further investigations on the development of high-frequency energy-efficient pulsed-DC generators for plasma discharge processes.

A new model of high frequency pulsed DC plasma CVD system has been developed for the deposition of hydrogenated amorphous carbon (a-C:H) films from C_2H_2 gas. This technique is employed by a developed novel pulsed DC generator (PDG) which can produce highly repetitive microsecond pulsed plasma glow discharge at considerably low pressure inside a customized vacuum chamber. The deposition of a-C:H films was carried out on Si substrates with a variation of pulse frequency up to 400 kHz at 50% duty cycle by keeping gas pressure of 15 Pa and negative pulse magnitude of 800 V. The impacts of increasing of pulse frequency on the plasma discharge characteristics, generated hydrocarbon species, deposition rate and structural properties of films were examined. The results show that the dissociation of C_2H_2 became higher with the increasing of pulse repetition rate as the electron excited energy increases. The growth rate slowly increases with pulse frequency until 200 kHz and after that a gradual reduction is observed. The hydrogen atoms in the films are mostly formed sp^3 hybridized bonds to the carbon atoms and it decreases with the increasing of pulse frequency. All the prepared films demonstrate highly insulating properties while the amorphization (sp^3 content) increases with the increase of pulse operating frequency. The results suggest that the proposed pulsed DC plasma CVD system driven by tiny high voltage pulses (few microseconds) with high repetition rate (several hundreds of kilohertz up to 400 kHz) can be considered as advantageous for the preparation of a-C:H films.

For the further investigation of pulsed plasma discharge processes by the developed novel pulsed-DC generator, Ar gas discharge experiments were examined by varying the discharge conditions, thus exhibiting significant flexibility to control the plasma discharge characteristics. The optical emission spectra of the Ar glow plasma were observed, and the electron excitation temperature (T_{exc}) was evaluated. It was confirmed that the electron excitation energy can be tuned by varying the precursor gas pressure and pulse parameters such as voltage, current, and duty cycle. Diamond-like carbon (DLC) films were deposited on Si substrates from C_2H_2 with a variation of gas pressure, applied voltage, and discharge current. The Raman spectra confirmed the DLC properties of the deposited carbon films. All DLC films demonstrated highly insulating properties, and the amorphization increased with a decrease in gas pressure, voltage, and discharge current. In addition, ultrathin pyrolytic carbon (PyC) films were

produced on glass substrates using nano-thickness metal catalysts from C_2H_2. The ultrathin PyC films exhibited conductive and semitransparent properties.

It can be suggested that the developed low-pressure pulsed-DC discharge system for plasma CVD is beneficial for the synthesis of insulating hard as well as soft-conducting carbon thin films with a broad variation of discharge conditions. It can also open new possibilities in etching, ion implanting, and sputtering applications for the material processing. However, the impact of pulsed plasma on CVD is relatively complex, and further investigation is required on the complex process of the gas phase to the surface and their relationship with the plasma parameters, ion energy distribution, and quantitative correlations to the resulting film.

In the second part of research, pulsed plasma discharge for atmospheric-pressure plasma jet (APPJ) was investigated. At first, a high-voltage impulse generator (IG) was designed and constructed using a step-up dual resonance pulse transformer (DRPT) and solid-state switches to drive atmospheric-pressure plasma jets. Dual resonance operation conditions were studied and achieved by optimizing the pulse transformer parameters. The developed generator is compact and has convenient control for voltage and frequency selection. It can deliver high-voltage impulses (peak to peak) of 0–11 kV with the pulse repetition rates of 0.5-100 kHz. The impulse rise-time and fall-time are almost 2 µs, and the pulse width is approximately 4 µs. The performance of DRPT-IG was evaluated and tested by generating a stable room-temperature atmospheric pressure plasma plume using He gas flow in a plasma jet device with single electrode configuration. It is expected that this study will stimulate the further investigations on the development of pulsed generators for atmospheric-plasma discharge processes.

Atmospheric-pressure plasma jets designed as cylindrical configuration of DBD were investigated by means of electrical and optical characteristics using the developed DRPT-IG and He as working gas. Two types of single-electrode configurations such as strip-electrode and wire-electrode are employed for the generation of plasma jet with various experimental conditions. A strong influence of wire-electrode configuration on plasma jet were observed with the variation of frequency at a fixed voltage and gas flow rate. The analysis of OES for wire-electrode APPJ shows that the active species such as NO, N_2, N_2^+, He, O and OH exits in the plasma plume and their intensities increase with the increase of pulse operating frequency. Furthermore, the investigation of plasma jet characteristics and RONS production in PAW with the variation of pulse operating frequency and polarity were also carried out. The results reveal that these both parameters have significant impact on the plasma jet characteristics and the production of RONS. A higher frequency operation of pulse enhances plasma jet density as well as the plasma-water interaction, which introduces to produce higher concentration of RONS and O_2 in PAW. The variation of pulse frequency also varies the concentration ratio of

ROS and RNS. On the other hand, the positive pulse operated plasma jet shows the cylindrical shape and intense appearance, whereas negative pulse operated plasma jet displays conical and less intense. In addition, the plasma jet driven under positive pulse introduces higher electric field, leads to a higher speed of ionization rate, generates a higher density of excited species in plasma, accordingly a higher concentration of RONS production in PAW than that of negative pulse. Therefore, in the future, the developed pulsed-APPJ system can offer an effective and low cost method to control of RONS composition for specific biomedical applications.

However, the control of chemical reactions and the production of RONS by plasma jet are complex processes. As plasma introduces a variety of species in the aqueous phase, it is difficult to find out the role of a single species or to adjust single species. Hence, further studies of the developed pulsed-APPJ system are still required to understand and control the discharge characteristics for the production of RONS in aqueous phase by changing discharge parameters such as working gas, gas flow rate, voltage amplitude, treatment time, treatment distance, and so on.